INFORMATION TO USERS

This manuscript has been reproduced from the microfilm master. UMI films the text directly from the original or copy submitted. Thus, some thesis and dissertation copies are in typewriter face, while others may be from any type of computer printer.

The quality of this reproduction is dependent upon the quality of the copy submitted. Broken or indistinct print, colored or poor quality illustrations and photographs, print bleedthrough, substandard margins, and improper alignment can adversely affect reproduction.

In the unlikely event that the author did not send UMI a complete manuscript and there are missing pages, these will be noted. Also, if unauthorized copyright material had to be removed, a note will indicate the deletion.

Oversize materials (e.g., maps, drawings, charts) are reproduced by sectioning the original, beginning at the upper left-hand corner and continuing from left to right in equal sections with small overlaps. Each original is also photographed in one exposure and is included in reduced form at the back of the book.

Photographs included in the original manuscript have been reproduced xerographically in this copy. Higher quality 6" x 9" black and white photographic prints are available for any photographs or illustrations appearing in this copy for an additional charge. Contact UMI directly to order.

UMI

A Bell & Howell Information Company
300 North Zeeb Road, Ann Arbor MI 48106-1346 USA
313/761-4700 800/521-0600

Université d'Ottawa · University of Ottawa

Behavior of High Strength Concrete Filled Circular Steel Tube Beam-Columns

by

© Farid Alfawakhiri

A thesis submitted to
the Faculty of Graduate Studies and Research
in partial fulfillment of the requirements
for the degree of
Master of Applied Sciences
in Civil Engineering *

Department of Civil Engineering
Faculty of Engineering
University of Ottawa
Ottawa, Ontario, Canada

August 1997

* The M.A.Sc. in Civil Engineering Program
is a joint program with Carleton University
administered by the Ottawa-Carleton
Institute for Civil Engineering

Abstract

High strength concrete filled tube (HSCFT) columns have been used in several high-rise building projects around the world in the last decade. With very few reported experimental results on the performance of such members, this is clearly an aspect of structural engineering where practice is far ahead of the research. A limited study on circular HSCFT beam-columns, presented in this thesis, was conducted to obtain additional experimental data on the behavior of these structural elements and assess recent design code provisions with regard to circular concrete filled tube (CFT) columns. Three long beam-columns ($L / D = 13.5$) were tested under constant axial compression and incrementally increasing lateral displacement reversals. The level of the axial load was the main parameter investigated in this experiment. In addition, one short column was tested in concentric compression. All specimens had the same cross-sectional geometry to allow for direct comparison. Both strength and deformability issues were addressed. Various aspects of concrete confinement in circular CFTs were analyzed. A comparative study of North American and European design code provisions was carried out. The experimental results were compared with theoretical predictions of strength.

Test results indicate that the use of high strength concrete for circular CFT members does not cause any dramatic changes in the behavior. General principles of structural analysis can be safely applied to circular HSCFTs. Beam-columns tested in this study exhibited ductile hysteresis behavior with no or little "pinching". Concrete confinement effects were found to contribute to the flexural strength, and this contribution increased with the increase of the axial load level. The local buckling of steel tubes did not cause any immediate changes in the behavior of beam-columns. Significant discrepancies were found between major codes in terms of design provisions for circular CFT columns, especially in predicting flexural strength. North American codes were shown to be more conservative than Eurocode 4, but all codes gave conservative predictions of strength compared to the experimental results. A less conservative design approach was recommended for CAN/CSA-S16.1-94.

Acknowledgements

I wish to express my appreciation to my thesis supervisor, Dr. N.J. Gardner, for his patience, advice, and for providing funding for the experiment. Appreciation is extended to the technical staff of the Civil Engineering Department for their assistance during the experimental part of this project. Thanks are also due to my fellow graduate students Luc Monette and Hakki Sharifi for their help in casting the specimens.

I am especially grateful to my sister, Suzanna Fawakhiri, whose financial and moral support throughout the years of my graduate studies was very important. And finally, I would like to thank my wife, Natalia, and my children, Dima and Nizar, for their patience and sacrifice.

Table of Contents

Abstract i

Acknowledgements ii

Table of Contents iii

List of Tables v

List of Figures vi

Notations xi

Chapter 1 - Introduction 1

1.1 Historical Review 2

1.2 Review of Previous Research 5

1.3 Summary of Literature Review 28

Chapter 2 - Experiment 30

2.1 Column Specimens 30

2.2 Materials 32

2.2.1 Steel Tubing 32

2.2.2 Concrete 34

2.3 Test Setup 35

2.3.1 Short Column 35

2.3.2 Beam-Columns 35

2.4 Instrumentation 37

2.4.1 Short Column 37

2.4.2 Beam-Columns 38

2.5 Loading 39

2.5.1 Short Column 39

2.5.2 Beam-Columns 40

Chapter 3 - Observed Behavior 62
3.1 Short Column 62
3.2 Beam-Columns 65
3.2.1 Column FA1 67
3.2.2 Column FA2 69
3.2.3 Column FA3 71

Chapter 4 - Discussion 112
4.1 Theory 112
4.1.1 Short CFTs under Axial Compression 112
4.1.2 CFT Sections under Combined Compression and Bending 117
4.2 Codes 119
4.3 Evaluation of Test Results 125
4.3.1 Short Column 125
4.3.2 Beam-Columns 127

Chapter 5 - Summary and Conclusions 142
5.1 Summary 142
5.2 Conclusions 142
5.3 Recommendations for Future Research 144

Appendix A - Strain Gauge Data 145
Appendix B - Fortran Code for Program CFTACI 181
Appendix C - Sample Calculations 186
Bibliography 188

List of Tables

Table 2.1 - Column Properties and Testing Conditions 41
Table 2.2 - Steel Coupon Tension Tests 42
Table 2.3 - Concrete Mix Proportions 43
Table 2.4 - Concrete Sample Cylinder Tests 43
Table 2.5 - Instrumentation of Beam-Column Specimens 44
Table 4.1 - Theoretically Predicted Axial Compression Capacities for Short Column ST1 131
Table 4.2 - Theoretically Predicted Bending Moment Capacities for Beam-Columns FA1-FA3 132
Table 4.3 - Experimental Ductility Factors for Beam- Column Specimens 133

List of Figures

Figure 2.1: Typical Column Cross-Section 45
Figure 2.2: Short Column Specimen ST1 45
Figure 2.3: Typical Beam-Column Specimen 46
Figure 2.4: Typical Steel Tension Test Specimen 47
Figure 2.5: Stress-Strain Curve for Steel Tension Test Specimen # 5 48
Figure 2.6: Stress-Strain Curves for Steel Tension Test Specimen # 6 49
Figure 2.7: Stress-Strain Curves for Steel Tension Test Specimen # 7 50
Figure 2.8: Stress-Strain Curves for Steel Tension Test Specimen # 8 51
Figure 2.9: Stress-Strain Curves for Steel Tension Test Specimen # 9 52
Figure 2.10: Views of Test Setup for Short Column Specimen ST1 53
Figure 2.11: Test Setup for a Beam-Column Specimen. Front View 54
Figure 2.12: Test Setup for a Beam-Column Specimen. Side View 55
Figure 2.13: General View of the Test Setup for Specimens FA1-FA3 56
Figure 2.14: Instrumentation of Short Column Specimen ST1 57
Figure 2.15: Scheme of LVDT Locations 58
Figure 2.16: Strain Gauges for Beam-Column Specimens 59
Figure 2.17: Instrumentation of Beam-Column Specimens FA1-FA3 60
Figure 2.18: The Path of Lateral Displacement Reversals 61

Figure 3.1: Specimen ST1 during Testing 73
Figure 3.2: Shape of Specimen ST1 after Failure (specimen is upside down) 74
Figure 3.3: Load-Displacement Relationship for Short Column Specimen ST1 75
Figure 3.4: Specimen ST1 - Data from Electric Resistance Strain Gauges 76
Figure 3.5: Comparison of Load-Strain Curves for Short Column Specimen ST! 77
Figure 3.6: Simplified and Exaggerated Illustration of the Waves Formed in Steel Tube Wall Along the Short Column Specimen ST1 78

Figure 3.7: Actual Forces Acting on a Typical Beam-Column Specimen 79
Figure 3.8: Assumed System of Forces Acting on a Beam-Column Specimen
"Lateral Load Includes Second Order Effects" 80
Figure 3.9: Assumed System of Forces Acting on a Beam-Column Specimen
"Lateral Load Does Not Include Second Order Effects" 81
Figure 3.10: Typical Plot of Steel Base Plate Rotation
Versus Lateral Displacement at the Point of Inflection 82
Figure 3.11: Specimen FA1 during the Test 83
Figure 3.12: Local Buckling of the Steel Tube of Specimen FA1 84
Figure 3.13: Load-Displacement Curve for Column FA1
(Lateral Load includes second order effects) 85
Figure 3.14: Load-Displacement Curve for Column FA1
(Lateral Load does not include second order effects) 86
Figure 3.15: Moment-Rotation Curve for Specimen FA1 87
Figure 3.16: Displacement-Rotation Curve for Specimen FA1 88
Figure 3.17: Transverse/Longitudinal Strain Ratios for Specimen FA1 89
Figure 3.18: Curvature of Specimen FA1 at 75 mm Above the Base Plate
(computed from data provided by strain gauges #3 and #13) 90
Figure 3.19: Specimen FA1 during Testing
(note the lateral displacement developed in the South direction) 91
Figure 3.20: Specimen FA2 after the Test 92
Figure 3.21: Load-Displacement Curve for Column FA2
(Lateral Load includes second order effects) 93
Figure 3.22: Load-Displacement Curve for Column FA2
(Lateral Load does not include second order effects) 94
Figure 3.23: Moment-Rotation Curve for Specimen FA2 95
Figure 3.24: Displacement-Rotation Curve for Specimen FA2 96
Figure 3.25: Rotation at the Top of Specimen FA2
(plotted versus Base Moment) 97
Figure 3.26: Rotation at the Top of Specimen FA2
(plotted versus Lateral Displacement) 98
Figure 3.27: Transverse/Longitudinal Strain Ratios for Specimen FA2 99

Figure 3.28: Curvature of Specimen FA2 at 75 mm Above the Base Plate (computed from data provided by strain gauges #3 and #13) 100
Figure 3.29: Curvature of Specimen FA2 at 125 mm Above the Base Plate (computed from data provided by strain gauges #1 and #11) 101
Figure 3.30: Specimen FA3 during Testing 102
Figure 3.31: The Shape of Specimen FA2 after the Test 103
Figure 3.32: Load-Displacement Curve for Column FA3 (Lateral Load includes second order effects) 104
Figure 3.33: Load-Displacement Curve for Column FA3 (Lateral Load does not include second order effects) 105
Figure 3.34: Moment-Rotation Curve for Specimen FA3 106
Figure 3.35: Displacement-Rotation Curve for Specimen FA3 107
Figure 3.36: Rotation at the Top of Specimen FA3 (plotted versus Base Moment) 108
Figure 3.37: Rotation at the Top of Specimen FA3 (plotted versus Lateral Displacement) 109
Figure 3.38: Transverse/Longitudinal Strain Ratios for Specimen FA3 110
Figure 3.39: Curvature of Specimen FA3 at 75 mm Above the Base Plate (computed from data provided by strain gauges #3 and #13) 111

Figure 4.1: Plot of Eqs. 4.5 and 4.7 134
Figure 4.2: Lateral Pressure in a Circular CFT under Axial Compression 134
Figure 4.3: Equations 4.12 and 4.14 ($k \geq 2/k_g$) 135
Figure 4.4: Equations 4.14 and 4.18 for the case of Specimen ST1 ($k_m = 1$) 135
Figure 4.5: Lateral Confinement Pressure in a Circular CFT under Combined Compression and Bending 136
Figure 4.6: Construction of Polygonal *M-P* Interaction Curve (Eurocode 4) 136
Figure 4.7: Lateral Load-Displacement Envelope Curves for Beam-Column Specimens FA1-FA3 137
Figure 4.8: *P-M* Interaction Curves for Specimen FA1 138
Figure 4.9: *P-M* Interaction Curves for Specimen FA2 139
Figure 4.10: *P-M* Interaction Curves for Specimen FA3 140
Figure 4.11: Experimental Definition of Yield Displacement 141

Figure A.1: Strain Gauge #3 of Beam-Column Specimen FA1 146
Figure A.2: Strain Gauge #4 of Beam-Column Specimen FA1 147
Figure A.3: Strain Gauge #10 of Beam-Column Specimen FA1 148
Figure A.4: Strain Gauge #13 of Beam-Column Specimen FA1 149
Figure A.5: Strain Gauge #14 of Beam-Column Specimen FA1 150
Figure A.6: Strain Gauge #15 of Beam-Column Specimen FA1 151
Figure A.7: Strain Gauge #16 of Beam-Column Specimen FA1 152
Figure A.8: Strain Gauge #20 of Beam-Column Specimen FA1 153
Figure A.9: Strain Gauge #1 of Beam-Column Specimen FA2 154
Figure A.10: Strain Gauge #2 of Beam-Column Specimen FA2 155
Figure A.11: Strain Gauge #3 of Beam-Column Specimen FA2 156
Figure A.12: Strain Gauge #4 of Beam-Column Specimen FA2 157
Figure A.13: Strain Gauge #5 of Beam-Column Specimen FA2 158
Figure A.14: Strain Gauge #6 of Beam-Column Specimen FA2 159
Figure A.15: Strain Gauge #7 of Beam-Column Specimen FA2 160
Figure A.16: Strain Gauge #8 of Beam-Column Specimen FA2 161
Figure A.17: Strain Gauge #10 of Beam-Column Specimen FA2 162
Figure A.18: Strain Gauge #11 of Beam-Column Specimen FA2 163
Figure A.19: Strain Gauge #12 of Beam-Column Specimen FA2 164
Figure A.20: Strain Gauge #13 of Beam-Column Specimen FA2 165
Figure A.21: Strain Gauge #14 of Beam-Column Specimen FA2 166
Figure A.22: Strain Gauge #17 of Beam-Column Specimen FA2 167
Figure A.23: Strain Gauge #18 of Beam-Column Specimen FA2 168
Figure A.24: Strain Gauge #20 of Beam-Column Specimen FA2 169
Figure A.25: Strain Gauge #1 of Beam-Column Specimen FA3 170
Figure A.26: Strain Gauge #2 of Beam-Column Specimen FA3 171
Figure A.27: Strain Gauge #3 of Beam-Column Specimen FA3 172
Figure A.28: Strain Gauge #4 of Beam-Column Specimen FA3 173
Figure A.29: Strain Gauge #7 of Beam-Column Specimen FA3 174
Figure A.30: Strain Gauge #8 of Beam-Column Specimen FA3 175
Figure A.31: Strain Gauge #10 of Beam-Column Specimen FA3 176
Figure A.32: Strain Gauge #12 of Beam-Column Specimen FA3 177

Figure A.33: Strain Gauge #13 of Beam-Column Specimen FA3 178
Figure A.34: Strain Gauge #14 of Beam-Column Specimen FA3 179
Figure A.35: Strain Gauge #20 of Beam-Column Specimen FA3 180

Notations

A_c	=	area of concrete core in column section
A_g	=	gross area of column section
A_s	=	area of steel tube section
D	=	outer diameter of circular steel tube
E_c	=	modulus of elasticity of concrete
E_s	=	modulus of elasticity of steel
e	=	eccentricity of axial force acting on column
F	=	lateral force acting on column
f'_c	=	compressive strength of concrete obtained from standard cylinder test
f'_{cc}	=	strength of confined concrete in column
f_k	=	parameter defined in Eq. 4.54
f_l	=	lateral confinement pressure
f_s	=	longitudinal stress in steel tube
f_{st}	=	circumferencial stress in circular steel tube
f_{my}	=	modified yield strength of steel tube, defined in Eq. 4.22
f_y	=	yield strength of steel tube
h_n	=	distance defined in Eq. 4.45
I_c	=	moment of inertia of concrete core in column section
I_s	=	moment of inertia of steel tube section
K	=	effective length factor
k	=	lateral confinement factor
k_g	=	factor defined in Eq. 4.11
k_m	=	modification factor for concrete
L	=	unbraced length of column, or shear span
M	=	bending moment acting on column
M_0	=	flexural strength of member in pure bending

M_u	=	flexural strength of beam-column
P	=	axial compressive force acting on column
P_0	=	nominal axial compression capacity of column, defined in Eq. 4.1
P_c	=	axial compression capacity of concrete core
P_s	=	axial compression capacity of steel tube
P_u	=	axial compression capacity of column
q	=	steel contribution factor, defined in Table 2.1
r	=	ratio of the lesser to the greater end moment in column
r_c	=	radius of gyration of concrete core in column section
r_s	=	radius of gyration of steel tube section
S_s	=	elastic modulus of steel tube section
t	=	wall thickness of steel tube
Z_c	=	plastic modulus of concrete core in column section
Z_s	=	plastic modulus of steel tube section
β	=	ratio defined in Eq. 4.15
χ	=	strength reduction coefficient, defined in Eq. 4.53
χ_d	=	parameter defined in Eq. 4.58
χ_n	=	parameter defined in Eq. 4.57
Δ	=	lateral displacement at point of inflection
Δ_y	=	yield displacement
Δ_{max}	=	maximum displacement
ε_s	=	longitudinal strain in steel tube wall
ε_{st}	=	circumferencial strain in steel tube wall
γ	=	parameter defined in Eq. 4.56
γ_d	=	parameter defined in Figure 4.6
γ_k	=	parameter defined in Figure 4.6
η_1	=	coefficient defined in Eq. 4.46
η_{10}	=	coefficient defined in Eq. 4.49
η_2	=	coefficient defined in Eq. 4.47
η_{20}	=	coefficient defined in Eq. 4.50
φ	=	average curvature in the hinging region
φ_y	=	yield curvature

φ_{max}	=	maximum curvature
λ	=	slenderness parameter defined in Eq. 4.51
λ_c	=	slenderness parameter defined in Eq. 4.33
λ_{ms}	=	slenderness parameter defined in Eq. 4.21
λ_s	=	slenderness parameter defined in Eq. 4.34
μ	=	displacement ductility factor
ρ	=	parameter defined in Eq. 4.32
τ	=	coefficient defined in Eq. 4.30
τ'	=	coefficient defined in Eq. 4.31

Chapter 1

Introduction

Structural engineers aim to efficiently utilize the available construction materials. Composite structures, made of concrete and steel, take advantage of the strength characteristics of both materials. In this context, a column made of a circular steel tube filled with concrete offers many advantages for economic design. The two materials are mutually beneficial: the steel tube confines the concrete core, effectively increasing its strength and ductility, preventing the spalling of the concrete and protecting it from accidental impact, while the concrete delays the local buckling and prevents the ovalization of the steel tube. Concrete-filled tube (CFT) columns offer technological advantages as well. Formwork and traditional reinforcement for columns are no longer required, which significantly reduces material and labor costs and speeds up the construction process. The use of steel tubes as erection columns, and filling them with concrete at a later construction stage, combines the speed of conventional steel erection with the cost effectiveness of reinforced concrete structures. There is evidence of increased fire resistance of CFT columns due to the concrete core, which reduces the thickness of required fire protection in many cases. For some applications, fireproofing can be eliminated altogether, which offers opportunities for exposed steel construction.

As high strength concrete gained acceptance in the construction industry, it was logical to use it in CFTs. High strength concrete filled tube (HSCFT) columns have been used in several high-rise buildings around the world in the last decade. With very few reported experimental results on the performance of such members, this is clearly an aspect of structural engineering where the practice is far ahead of the research. A limited study on circular HSCFT beam-columns, presented in this

thesis, was conducted to obtain additional experimental data on the behavior of these structural elements and assess recent design code provisions with regard to circular CFTs.

A short historical review, outlining major steps in how engineers gained knowledge and experience with circular CFT columns, is presented in the next section.

1.1 Historical Review

The earliest report to be found in the literature on the use of CFT columns is by Sewell (1902). He proposed that the danger of internal rusting, one of the past objections to the use of steel box columns, could be eliminated by filling the columns with concrete. Sewell reported that he had supervised the filling of columns with concrete in a new building, and later, when some of the columns for a traveling crane were accidentally overloaded, he concluded that the concrete filling increased the stiffness of the columns by at least 25%. He also predicted that a column filled with concrete would buckle much less easily in a fire than an empty column of the same size. However, for long time after that, the concrete filling was considered rather as an extra safety measure, and the contribution of concrete to the strength and stiffness of the tubular steel columns was usually ignored.

Publications of Vögeli (1948, 1950) indicate that circular CFTs were used in electrical transmission line towers in Switzerland. It might be concluded that similar practice was adopted in Germany, because Klöppel and Goder (1957) referred to German VDE 0210 "Regulations for the construction of overhead power transmission lines" as to contain a design formula for CFTs at that time. Circular CFTs also have been widely used as piles (Mason, 1950; Committee No. 30, 1954). Armco Drainage and Metal Products Ltd., which operated branch offices and plants all over the United Stated and Canada, sold millions of linear feet of circular CFT piles (Barnard, 1954). Lally Column Company Co. (1962) in USA specified "safe" working loads for CFT columns and suggested patented connection details for flat-slab and rigid-frame applications. Iengar (1977) reports that CFT columns were most often used for construction of one to four story buildings where smaller column sizes, exposed steel and repetitious use of standard off-the-shelf prefabricated components were primary design considerations. Simple, non-continuous beam-to-column connections either by a shear plate or a bearing cap plate were generally used.

Circular CFT columns were successfully used in projects where high vertical loads were combined with severe restrictions to the overall size of the cross-section, like the multilevel motorway interchange at Almondsbury in Great Britain (Kerensky and Dallard, 1968) and the annex to the city hall of Wuppertal in Germany (Roik and Bergmann, 1985).

Stelco Inc. as the only Canadian member of the International Committee for the Development of Tubular Structures (CIDECT) published a monograph (Stelco, 1981) providing a simple design method for CFT columns. It mentions that the Sunnybrooke Towers, a 15 story luxury apartment building in the Cote St. Luc district of Montreal, incorporated CFT columns. Another application of CFT columns in Canada was reported by Ghosh (1976). Pipe columns, 14 m long and about 330 mm in diameter, supporting the roof of the oil storage tanks in Lennox generating station were strengthened by filling them with concrete to enable them to resist limited horizontal loads. Pumping concrete was found to be an effective and economical way of filling, and once the crew on the job became familiar with the process, they were able to fill 35 columns in a single shift with one pump.

Gong et al (1994) described the application of circular CFT columns in three tall buildings, up to 30 stories high, constructed recently in earthquake areas of intensity 7 in China. These were the Quanzhou Post & Telecommunication Center, the Xiamen Jinyuan Building and the Xiamen Fukang Building. Steel tubes with diameter×thickness dimensions of up to 1000×10 mm were used in combination with 30-40 MPa concrete. Fire resistance was obtained by covering the steel tube with granite shell in the lobby or 30 mm thick ferro-cement coating on other floors. Apart from the increased floor area, savings of 10% in steel and 68% in concrete were achieved.

The use of circular CFT columns in Australia was pioneered by Connell Wagner in the 43 story building of Casselden Place in Melbourne which was completed in 1991 (Bridge and Webb, 1992). Apart from savings in materials, the major economy was achieved through the constructability of this type of column. Up to six floors of metal decks and concreted floors were designed to be supported by the bare steel tube. The concrete was then pumped into and up the steel tubes through a pump line connected to the bottom of the column section. With the use of a special 60-70 MPa concrete mix, neither the vibration of concrete nor the preparation of the interface between pours was required. Circular steel 950×8 mm tube sections (nominal yield strength - 250 MPa) were reported to be very light compared with the traditional steel columns. At

the bottom of Casselden Place, a two level column section weighed just over two tons, and no special lifting equipment or splice machining for erection was necessary. Uy and Patil (1996) reported circular CFT columns had been used with great success in many other tall building projects in Australia, including the Commonwealth Center in Melbourne, the Market City in Sydney, the Riverside Office and the Myer Center in Adelaide. Each of these buildings was over 30 stories high.

There had been many reports (Bauer, 1988; Gondfrey, 1987; Randall and Foot, 1989; Ralston and Korman, 1989) on the construction of the First Pacific Center and the Two Union Square office complex in Seattle, where the columns were made of large cylindrical steel shells filled with high-strength concrete of up to 19.000 psi (131 MPa) specified strength. The circular steel tubes had diameter×thickness dimensions of up to 10 ft × 0.625 in. (3048×15.9 mm) and had shear studs welded to their inner surfaces. Steel savings and other construction economies growing out of the structural system reportedly made for overall savings of 30% in construction costs. Another seven high-rise building projects in Seattle and San-Francisco, employing HSCFT columns were reported to be completed, under construction or in design at that time. The structural design of all these projects was conducted by Skilling Ward Magnusson Barkshire Inc., and some aspects of the design were discussed by Magnusson et al (1992).

It looks like the experimental research on CFTs always lagged behind practical applications. Early experiments with circular CFTs were reported by Swain and Holmes (1915) who conducted compression tests on concrete-filled "pipe columns". Lohr (1934) tested six short circular "encased concrete" columns by applying compressive loads to concrete core only. A publication of the Housing and Home Finance Agency (Russell, 1953) presented some experimental results on longer columns and established an allowable working load formula, which was adopted for some time in the United States and Canada. A very comprehensive program was carried out in Germany by Klöpel and Goder (1957) who tested a large number of circular CFT columns under short and long term axial loads. Extensive research on circular CFTs in many countries began in the 1960s. Most of the significant work conducted then and later is described in detail in the next section.

It is worth to note here, that extensive experimental work has been done recently on the fire resistance of CFT columns, but it is not described in this thesis. References for this particular area of research could be found in the publication of Hass (1991). It is well known, that the presence of

concrete core, which absorbs part of the heat, improves the fire resistance of CFT columns in comparison to hollow steel tubes. However, holes in the shell should be provided to prevent the accumulation of steam pressure from any moisture entrapped inside. The fire resistance could be further enhanced, when necessary, by providing internal reinforcement or by conventional methods of fire protection for steel structures.

The applicability of CFTs was officially recognized in 1936 when ACI "Standard Building Code" specified an allowable load for such sections. Later, many codes established special regulations for CFTs, which were gradually updated as more experimental information became available. For a long time, CFT sections along with other composite sections, were treated with suspicion, and the codes tended to underestimate their capacity, because it was not clear whether the different procedures developed for reinforced concrete or structural steel would be appropriate for the composite section. For example, the ACI-71 code, due to the introduced requirement of minimum eccentricity, was in many cases allowing loads on CFT columns less than those obtained from AISC provisions of that time for hollow sections alone. This fact was pointed out by Furlong (1974) and Iyengar (1977). The need for the reconciliation of various philosophies regarding composite columns was obvious. This issue was addressed by Furlong (1976, 1983) and Elnashai et al (1990). In this thesis, design procedures for circular CFT columns provided by several recent codes are discussed in Chapter 4.

1.2 Review of Previous Research

A summary of previous research on CFTs reported in the literature, arranged in chronological order, is presented in this section. Most of this research usually consisted of an experimental investigation complemented with an analytical assessment of results. The researchers addressed the issues of ultimate load capacity, ductility and seismic resistance, overall stability and local buckling of the tube, bond strength of concrete-steel interface and concrete confinement effects. Only experiments or analytical results regarding circular CFTs are described in some detail here.

H.J.Salani and J.R.Sims (1964)

The objective of this investigation, conducted at Rice University in Houston, Texas, was to examine the behavior of circular mortar-filled tubes in concentric compression. Seventeen mortar-

filled specimens, 60 in. (1524 mm) long, ranging from 1 to 3 in. (25-76 mm) in diameter, were tested. In addition, nine empty tubes of the same length and cross-section range were tested under similar conditions to provide a basis for comparison. Seamless cold drawn finish annealed tubing was used, with D/t ratios ranging from 14 to 56. The mortar strength varied within 2.6-4.0 ksi (18-28 MPa). Tensile tests were performed on full sections of tubing to determine the mechanical properties, and the same value of yield strength of 76 ksi (524 MPa) was established for all sections.

The 3 in. (76 mm) diameter empty tubes were reported to fail by local crumpling rather than by overall column buckling. No detailed description of the failure mode of other specimens were provided. Experimental values of the ultimate axial load capacities were compared to the theoretical values obtained from the tangent modulus formula, and limited agreement was found. The values of the tangent modulus of elasticity used in the computations of the theoretical loads were reported to be obtained from the stress-strain compression tests on short stubs of each individual tube, but no information about these tests was presented.

Both experimental and theoretical ultimate load capacities of the 1 and 1.5 in. (25 and 38 mm) diameter mortar-filled tubes were reported to be less than those of the corresponding empty tubes. The authors attributed that to the low ratio of the area of the mortar to the area of the steel. This remains the only case, when filling a steel tube was reported to produce a decrease in the load capacity.

N.J. Gardner and E.R. Jacobson (1967)

This paper describes a theoretical and experimental investigation into the behavior of circular CFTs under axial compression, and is based on the Master's thesis of Jacobson (1966). The experiment consisted of testing 10 long and 19 short columns. In addition, one short empty tube and two short tubes filled with compacted aggregate were tested in compression. To establish the repeatability of results, two long columns of each size were tested. For each long column, a short control stub column and concrete control cylinders were made from the same concrete. Seamless cold-drawn annealed tubing was used for all specimens. Outer diameters ranged from 3 to 6 in. (76 and 152 mm), wall thicknesses varied between 0.067 and 0.194 in.(1.7-4.9 mm) To ensure consistent steel properties, the tubing was purchased in lengths of 20 ft (6.1 m) as this allowed the

cutting of the long columns, short columns and tension test specimens from the same tube. The stress-strain characteristics of the steel tubes were determined from tension tests of complete section specimens with wall thickness reduced over a center length of 2 in.(51 mm) by machining the inside and outside surfaces. Considerable departure from the nominal yield strength of 49 ksi (338 MPa) was revealed. The measured yield strength for different tubes varied between 52.69 and 91.87 ksi (363 and 633 MPa). Concrete strengths ranged from 3 ksi to 6.3 ksi (21-43 MPa). For short columns, the length was taken to be twice the outer diameter. The length/diameter ratio of long columns varied between 8 and 20.

The experimental ultimate loads were presented and compared to the theoretical values calculated using the ACI and NBC working stress design formulas of that time. The experimentally determined factors of safety ranged from 3.37 to 5.13 for long columns, and exceeded 4 for all short columns.

Theoretical axial load capacities of short columns, calculated as the sum of the failure loads of concrete and steel acting alone, were significantly lower than the measured maximum loads. Thus, it was evident, that steel-concrete interaction increased the capacity of the composite section.

The authors proposed a method to determine the tangent modulus of elasticity of concrete confined in a steel tube from a stub column test. By using this concrete characteristic and the usual tangent modulus of steel, determined from tension tests, the buckling loads for long columns were estimated by the tangent modulus formula. These estimates showed to be in reasonable agreement with test results.

The effects of column end loading conditions were investigated. All long and most of the short columns in this program were loaded through cement sulfur caps which extended over the whole section to ensure that both concrete and steel are loaded. Two of the 3 in. (76 mm) diameter short columns were loaded through a circular ram fitting inside the tube, so that the load was applied to concrete core only. These columns failed in a more pronounced "barrel shape" mode, but gave the same maximum loads as similar columns tested with caps. Another two specimens of the same size and properties were prepared with concrete recessed at one of the ends, so that only the steel was loaded. These columns failed by local buckling at the end where the concrete was recessed, and produced ultimate loads equal to the capacity of a similar empty steel tube.

Tubes filled with compacted aggregate showed surprisingly high maximum loads that exceeded those of similar tubes filled with concrete.

The authors recommended further research to investigate the phenomenon of local buckling of tubes and concrete confinement and creep effects associated with circular CFT steel sections.

N.J. Gardner (1968)

This experimental study addressed the use of spiral welded steel CFTs as axially loaded compression members. This kind of steel tubes is produced by bending a narrow steel strip into a helix and then welding up along the spiral joints. Eight long and eleven short composite columns and two long empty steel tubes were tested in concentric compression. All columns were 6.6 in. (168 mm) diameter with wall thicknesses varying between 0.103 and 0.197 in. (2.6 and 5 mm). The strength of concrete and the yield strength of steel were in the ranges of 2.6-5.3 ksi (18-37 MPa) and 28.6-48.3 ksi (197-333 MPa), respectively. The yield strength of the steel was determined in both longitudinal and hoop directions from full section compression tests and internal pressure tests. Tests to determine the manufacturing stresses were also undertaken and large elastic strains were found to exist in the hoop direction. In order to take account of the residual stresses, it was recommended full section compression tests be used to determine the stress-strain properties of spiral welded steel tubes.

The columns were tested and analyzed much in the same manner as the earlier work on seamless CFT columns (Gardner and Jacobson, 1967). All long columns exhibited ductile behavior. Maximum loads of all short columns were considerably greater than the theoretical capacities that neglect the confinement of concrete. The results presented showed that both spiral welded and seamless CFTs behave in a similar way under axial compression.

R.W. Furlong (1967, 1968)

These publications reported tests on 30 circular and 22 square steel CFT columns conducted in a research program at the University of Texas. Cold-rolled welded steel tubing was employed in this program. All specimens were 36 in. (914 mm) long, with outer dimensions varying between 4.5

and 6 in. (114-152 mm). For circular specimens, the yield strength of steel tubes was between 42 ksi and 60 ksi (290 and 414 MPa). The yield strength for the 4.5 in. (114 mm) diameter tubes was established from manufacturer's mill reports. For other circular tubes with diameters of 5 and 6 in. (127 and 152 mm), the yield strength was obtained by using the 0.002 strain offset from stress-strain curves of compression tests on plain tubing. The concrete strength ranged between 3.05 ksi and 4.2 ksi (21 and 29 MPa).

Eight circular columns were tested in concentric compression only. Another 22 were tested in an eccentric loading frame, which allowed the application of both concentric and eccentric axial forces. During each test, an initial concentric load was applied to a column. A second, eccentric load was then applied, and the concentric load reduced accordingly to maintain constant total axial load on the specimen, while the applied bending moment due to eccentric load was increased until failure occurred. Lateral deflections at midheight of specimens were measured during these tests, and the load-deflection component was added to the moment produced by the eccentric force to obtain the total moment.

Ultimate strength combinations of axial load and moment were presented and analyzed. On the basis of test observations and some analytical considerations, equations for stiffness and strength were developed. The equation proposed for the axial load capacity not only neglected any increase in concrete strength due to confinement, but limited the concrete core bearing capacity by the strain level required for the steel to yield. Moreover, it was suggested, that in columns with steel tubes of yield strength in excess of 60 ksi (414 MPa), the encased concrete will crush before the steel yield strength is developed, and a limiting value of about 50 ksi (345 MPa) yield strength for steel was established. However, this equation produced rather good agreement with concentric compression tests, probably due to the fact, that no account for slenderness or secondary moment effects was taken for these tests, although it was reported that axial load specimens showed slight transverse deformations at the midheight. Estimates of pure bending strength derived from the plastic moment capacity of the steel tube alone proved to be low. Consequently, the proposed thrust-moment interaction equation, in the form of an ellipse, was undesirably conservative for most of the data. More accurate estimates of beam-column strength were made by treating the CFTs as ordinary reinforced concrete sections.

The interaction between steel and concrete was observed indirectly by means of strain-gage rosettes on four faces of the specimens. For loads less than about 90% of the maximum loads

obtained, the measured ratio between lateral and longitudinal strains did not depart much from the value of Poisson ratio, measured for steel tubes alone in compression. Based on this observation, it was suggested that the steel and concrete carried their loads independent of each other. In order to prove this point, some of the tests were made on pairs of specimens identical in all respects except for a film of axle grease on the inside face of one steel tube for each pair of columns prior to the placement of concrete inside the tubes. These tests showed no significant difference in the behavior of specimens in the pairs, regardless of shape, concrete strength, steel wall thickness or loading combination. Since the investigators were confident that no bond could develop in the greased specimens, they concluded that any bond that may have existed in the ungreased specimens must have been broken to permit separation between the steel tube wall and the concrete core at relatively low loads.

Steel tubes in all column specimens, with outer diameter/thickness ratios of up to 98, were able to develop nominal yield strains without local buckling, indicating that the concrete core stabilized the thin-walled steel encasements.

Some creep effects, as indicated by reductions in load at almost fixed displacement, were observed during tests after longitudinal yielding of tube walls had occurred. Furlong expressed the feeling, that the ultimate loads reported could be as much as 10% higher if the tests were conducted in continuous manner, without frequent interruptions for strain and deflection gage readings. Similarly, some reduction in maximum loads could be anticipated, if they were sustained for days of weeks instead of minutes.

Furlong advocated further investigations into the behavior of CFT columns and the economic advantages to be gained through the use of concretes with f_c' in excess of 8 ksi (55 MPa).

P.K. Neogi, H.K. Sen and J.C. Chapman (1969)

These authors reported the results of a numerical and experimental study conducted at the Imperial College, University of London. This was the first reported study where finite fiber sectional analysis was applied to circular CFT columns, loaded eccentrically. It was assumed that complete interaction takes place between the steel and the concrete, but both concrete and steel are stressed in the axial direction only. The differential equation governing the bent equilibrium configuration

of an eccentrically loaded column was derived by equating the internal and external forces and moments at a displaced section. The "exact" deflection shape was then obtained by integrating numerically this equation along the length of the column. A computer program was developed to calculate the load-deflection curves of eccentrically loaded columns, where the lateral deflection and axial load values were calculated for a series of equilibrium shapes defined by increments of curvature at the central cross-section. Alternative procedure was also proposed by assuming the deflected shape to be part of a cosine wave. This simpler procedure was shown to give sufficiently accurate results with the maximum loads calculated always conservative but not more than 5% below the values given by the "exact" shape calculation.

Experiments were carried out on 18 circular CFT columns varying in overall length from 55.5 to 131 in. (1410-3327 mm). For ten of them hot-finished seamless mild steel tubes with nominal diameters of 6.63 in. and 5.5 in.(168 and 140 mm) were used. The other 8 columns consisted of cold drawn seamless mild steel tubes having 5 in. (127 mm) diameter. The wall thickness varied between 0.064 in. and 0.384 in.(1.6 and 9.7 mm). The loads were applied with end eccentricities ranging from 0.25 to 1.875 in. (6.3-47.6 mm) The steel properties were determined from tensile coupon tests and compression tests on hollow stubs. The yield strength of hot-finished tubes was about 17.5-20 tonf/in^2 (271-310 MPa), and various three-linear stress-strain relationships were adopted for the cold-drawn tubes. The concrete cube strength was between 3920 and 12100 lbf/in^2 (27 and 83 MPa).

All columns failed by overall buckling and the final deflected shape of columns was symmetrical. Longitudinal compressive and tensile strains in excess of 3.2% and curvatures in excess of 0.35 m^{-1} were observed at the central section, but no local buckling of steel tubes was observed. One of the tubes was cut open and the concrete was found to have retained cohesion.

Reasonable agreement was found between numerical and experimental results for columns having length/diameter ratio greater than 15. It was concluded that triaxial effects are not important for such columns. The authors also concluded that there could be some augmentation in the maximum load due to the triaxial effect for shorter columns, but this effect diminishes as the eccentricity increases.

R.B. Knowles and R. Park (1969,1970)

These two papers presented the results of experimental work on axially and eccentrically loaded CFT columns carried out at the University of Canterbury, New Zealand. In addition, hollow steel tubes were tested to provide means of comparison. A wide range of slenderness ratios was investigated. In addition to 3×0.133 in. (76×3.4 mm) square tubes, two circular sections with diameter×thickness dimensions of 3.5×0.23 in. (89×5.8 mm) and 3.25×0.055 in. (83×1.4 mm) were employed. The circular tubes were of hot-finished seamless mild steel, with yield strengths of 58 ksi and 70 ksi (400 and 483 MPa), respectively. The yield strength was determined at 0.002 strain offset from compression stress-strain curves obtained during tests on 10 in. (25 mm) long tubes.

The concrete properties were determined from 3.1×8 in. (79×203 mm) cylinder specimens, prepared under conditions as close as possible to those in the core of a tube. The moulds were made from steel tubes split along a diameter and clamped together to form concrete cylinders of the same length as the cores of column specimens. These were cut later by diamond saw into 8 in. (203 mm) lengths and tested. The average concrete strength of 5925 psi (41 MPa) was determined from cylinders cut from the midlength of the sample cores. It was also found that generally the concrete had a higher strength at the bottom of a column than at the top, probably due to water gain at the top during casting. This variation was reported to be considerable. However, despite this strength variation, all tested columns failed at midheight.

The stress-strain relationships established for short hollow steel tubes and concrete were used to estimate ultimate loads for longer column specimens by the tangent modulus formula. These were compared with the experimental results. Six hollow columns and six concrete-filled columns ranging in effective length from 9 in to 68 in. (229-1727 mm) were tested axially for each section employed. It was found that the tangent formula underestimates the ultimate load of shorter circular CFT columns due to the increase in concrete strength caused by confinement. This was in contrast to short square tubes that showed no evidence of concrete strength enhancement. It was concluded that longer circular CFTs fail by overall column buckling before the longitudinal compressive strain reaches the level when concrete starts to increase in volume, so that no confinement effects could be expected from columns with higher slenderness ratios. A method based on the observed stress-strain behavior of concrete was proposed for calculating the limits of

slenderness ratio, which determines whether an increase in concrete strength due to triaxial confinement is likely or not. From this method it was further concluded that only short columns made of high strength steel tubes, with at least 50 ksi (345 MPa) yield strength, are likely to show an increase in strength due to confinement of the concrete by the steel tube.

The authors proposed two design equations for long and very long ranges of CFTs subjected to axial compression. These equations were based on summing the separate tangent modulus buckling loads of the concrete core and the steel tube. Both of these equations neglected concrete confinement effects, and were supposed to give conservative results for short columns. They were shown to be conservative in most cases when compared to experimental axial capacities of CFTs tested by the authors and another 100 tube column test results reported by other investigators. The results of axial compression tests of this experimental investigation were also compared with other design equations, available at that time, and it was shown that they do not give a better prediction of the ultimate loads than the equations proposed by the authors.

Another 10 hollow tube and 10 CFT columns, 32 to 56 in. (813-1422 mm) long, were tested under compressive loads with initial eccentricities of 0.3 in. and 1.0 in. (7.6 and 25.4 mm). The results were compared with theoretical values obtained by simple straight line interaction formula. However, the scatter in the experimental results obtained was larger that could reasonably be expected, and that reflects the difficulty of measuring actual eccentricities at failure and the very approximate nature of the linear interaction.

The authors noted that the CFTs tested were able to undergo considerable inelastic strain after buckling without any sign of local failure of the steel tubes. They concluded that CFT columns have large energy absorption capacities, especially the short columns, although no quantitative results were obtained.

W.-F. Chen and C.H. Chen (1973)

This paper presented results of an analytical study on CFT columns loaded concentrically or eccentrically. Theoretical moment-curvature relationships at various levels of thrust were obtained for the sections considered. The circular section studied had 3.5 in. diameter, 0.23 in. steel wall thickness, 5.8 ksi steel yield strength and 5.925 ksi concrete cylinder strength. These parameters

were chosen in order to allow the analytical results to be checked against the experimental data reported by Knowles and Park (1969). In the development of moment-curvature relationships, it was assumed that plane sections remain plain after bending and concrete has no tensile strength. While uniaxial elastic-perfectly plastic stress-strain relationship for steel was adopted in all cases, three types of stress-strain relationship for concrete were studied:

1) uniaxial state of stress, with the maximum concrete strength of $0.85 f_c'$;

2) triaxial state of stress, assumed to increase the ductility of concrete only;

3) triaxial state of stress, assumed to increase both the ductility and the strength of concrete (the maximum strength increased from $0.85 f_c'$ to f_c').

By using the sectional moment-curvature-thrust relationships and the column curvature curve (CCC) method (Chen and Atsuta, 1976), axial load-moment interaction curves were numerically obtained for a wide range of length/diameter ratios and different column end eccentricity conditions. In the analysis of concentrically loaded columns, an initial eccentricity of 0.1% of the column length was assumed for the circular section to account for probable imperfections. The presented theoretical curves of axial capacity plotted versus length/diameter ratio showed that the effect of the triaxial state of stress in concrete on the column strength is unimportant when length/diameter ratio is greater than 15.

From the comparison with experimental results it was concluded, that the analysis based on uniaxial strength of concrete is sufficiently accurate for columns with length/diameter ratios of 15 and more. However, even the results based on the triaxial state of stress in concrete underestimated the experimental capacities of shorter circular columns, probably due to the fact that the assumed increase in strength for confined concrete was very small.

M. Tomii, K. Yoshimura and Y. Morishita (1977)

The authors reported the results of a very comprehensive investigation carried out at Kyushu University in Japan. Tests were conducted on 268 CFT columns under concentrically axial loads. One hundred and forty eight columns were made of circular tubes, 60 were square and 60 octagonal. In order to establish repeatability of the results, three columns with identical properties were tested for each specimen type. Circular steel tubes had the diameters of 100 mm and 150 mm with wall thicknesses ranging between 2 and 5.4 mm. Hot-finished welded mild steel tubes

were used for all columns. All tubes were first cut into approximate lengths, then annealed to remove the residual stresses and machined in a lathe to insure parallel flat ends and accurate lengths. Steel properties were determined from tension coupon tests and full-section compression tests. The yield strength ranged between 260 and 348 MPa. Both normal and expansive concrete were used for tube filling. However, the type of concrete had very little or no effect on the behavior of CFT columns. Concrete strength was determined from 100 × 200 mm cylinders and varied between 11.7 and 37.1 MPa.

The column specimens were arranged in two series. The main purpose of the tests of Series I was to examine the effect of column length on the ultimate strength of CFTs. All columns tested were rather in the short range with length/diameter ratio not exceeding 7. Shorter columns failed by crushing, while in the case of longer columns general buckling was observed. All square columns showed deterioration of load after the ultimate level was reached. On the other hand, circular and octagonal columns exhibited elastoplastic type of load-deformation relationship, except the longest columns ,with length/diameter ratio of 5 and more, which failed in general buckling. Also, strain hardening phenomena were observed in the load-deformation relationships of shorter circular and octagonal columns with thicker steel walls. Ultimate loads of circular and octagonal CFT columns tended to decrease gradually with the increase of slenderness, but in all cases exceeded the "nominal squash load" computed as the sum of the strength of steel and concrete sections. On the other hand, there was no evidence of an increase in axial strength due to confinement for square columns even when the slenderness was low.

In the tests of Series II, the effects of diameter/thickness ratio and concrete strength were investigated. All columns of this group had length equal to about 3 times the diameter or the side length. From the results of tests of Series I, it was concluded that the inelastic behavior of columns with such dimensions are not affected by the end conditions. It was observed that circular and octagonal CFT columns had considerably large load and deformation capacity after local buckling had occurred, while square columns showed rapid deterioration of axial load capacity after the initiation of local buckling.

The authors found that the ultimate capacities of circular and octagonal CFT columns were considerably enhanced in many cases by strain hardening of the steel tube. The magnitudes of ultimate capacity increase due to this factor were widely scattered and remarkably affected by the slenderness ratio and wall thickness of the tube. In order to avoid complications associated with

taking into account strain hardening properties of steel tubes, the concept of yielding strength was proposed as the column strength instead of the ultimate strength. Yielding strength of a CFT column was taken as the axial load at longitudinal strain of about 1%, i.e. when strain hardening of the steel tube cannot be expected. The values of yielding strength divided by the nominal squash load showed to be almost not affected by the diameter/thickness ratio and compressive strength of concrete.

Linear relations between circumferencial strain and longitudinal strain were observed for circular and octagonal tubes through wide range of longitudinal strain. Slope of these linear relationships showed to decreased with an increase of steel contribution factor. It was further concluded that after steel tube has yielded initially, the true longitudinal stress carried out by the steel tube drops while the hoop stress increases due to concrete core lateral deformation, and both stresses converge to certain steady levels of stress when the longitudinal strain is 5-10 times as large as the longitudinal yield strain. These steady stress levels are affected by the steel contribution factor.

For circular CFT columns, from the experimentally obtained ratios of hoop/longitudinal strains in the plastic range, the true axial loads carried by the steel tubes were determined by applying the von Mises yield criterion. After that, the true axial strength of concrete core was determined by subtracting the estimated steel tube strength from the experimental yielding strength of CFT columns. As it could be expected, the true axial strength of concrete showed to increase with the increase of steel contribution factor. Finally, the values of lateral confinement factor for concrete were computed. These values showed rather large scatter between 1.4 and 4.8 with a mean of 2.6.

K.S. Virdi and P.J. Dowling (1980)

The purpose of this experimental investigation was to study the strength of bond between the concrete core and the steel tube in circular CFT members. Tests were carried out on 88 specimens made of seamless mild steel tubes 6 to 12 in. (152-305 mm) in diameter. The inside surfaces of the tubes were wire brushed to remove any rust and loose scale present, and any deposits of grease or oil were cleaned away. Polystyrene plugs 1.5 in. (38 mm) thick were fitted at the bottom of the specimens, and the tubes were filled with concrete flush to the top. The strength of core concrete, determined from tests on 6 in. (152 mm) cube samples, was in the range of 3.2-6.7 lbf/in^2 (22-46 MPa). The plugs at the bottom were removed before testing to create an air gap and allow the

concrete core to move.

The specimens were axially loaded through a 2 in. (51 mm) thick steel pad with a diameter about 0.5 in. (13 mm) smaller than the internal diameter of the steel tube being tested. The movement of the concrete core with respect to the steel tube was measured at the top end by means of three 2 in. (51 mm) travel electrical resistance gauge deflection transducers equally spaced around the periphery of the steel tube. An initial load of about 1 tonf (10 kN) was usually applied to eliminate any initial settlement effects due to irregularities on the concrete surface. This load was then released, and the zero reading were recorded. After that, the loading was continued in most cases until the concrete core ran out of the available travel of about 1.5 in. (38 mm).

The load-deflection response of all specimens showed a uniform pattern. Initially, the stiffness offered by the bond was high. Later, a marked reduction in stiffness was observed. The curves showed remarkably parallel slopes in the later stages of loading, suggesting that the resistance offered at these stages could be attributed entirely to friction. It was concluded that the resistance to push out loads in CFTs derives primarily from the interlocking of concrete in two types of imperfections in steel tubing. The first, microlocking, relates to the surface roughness of steel and the second, macrolocking, to the variations in cross-sectional dimensions along the length of the tube, away from the ideal cylindrical surface, due to manufacturing tolerances. Microlocking contributes to the initial stiffness of bond. It is broken when the concrete interface attains a local strain of 0.0035 associated with the compressive crushing. The macrolocking is related to the later stages of loading when primarily frictional movement occurs. These conclusions were supported by tests on specimens with specially treated steel surfaces. Three specimens had their inside surfaces machined to a smooth finish. An attempt was made to obtain good cylindrical surfaces from top to bottom. These specimens showed dramatically reduced resistance to movement. A sudden movement of concrete core accompanied by a sharp reduction in the load was observed after initially stiff response. The inner steel surfaces of another 3 specimens were treated with a lubricant in five coats. The response these specimens exhibited a near absence of the initial stiff region, and the resistance increased gradually almost up to the level of the normal specimens prepared without any special surface treatment.

The specimens were arranged in several groups to check the influence of various parameters separately. It was found that the ultimate bond strength is not affected to any appreciable degree by such parameters as the length of concrete-steel interface, age or strength of concrete, diameter

or thickness of the tube. On the other hand, test results indicated that by better compacting both microlocking and macrolocking were enhanced and higher values of bond strength were achieved. Three of the specimens were dry cured and, surprisingly, showed about 20% higher values of ultimate bond strength against similar wet cured specimens.

A characteristic ultimate bond strength was obtained by applying statistical corrections to the mean test value of all normal specimens. The authors recommended the value of 150-160 lbf/in^2 (about 1 MPa) for use in design.

R.J.T. Park, M.J.N. Priestley and W.R.Walpole (1983)

This paper is based on the post-graduate research project of Park carried out at the University of Canterbury, Christchurch, New Zealand. Six circular beam-columns were tested under fixed axial load and cyclic lateral load applied at the midheight through heavily reinforced central stub (giving shear span of 1600 mm). All test units consisted of 360 mm diameter mild steel cold-rolled welded tubes 5 mm thick and had the total height of 3.9 m. They were arranged in three pairs with one unit of each pair tested at the axial load level of $0.1 f'_c A_g$ and the other at $0.3 f'_c A_g$. The first pair of units, 1 and 2, consisted of continuous steel tubes, filled with plain concrete. Units 3 and 4 were additionally provided with longitudinal and spiral reinforcement. Units 5 and 6 were also reinforced, but they were constructed with a gap of 300 mm in the continuity of the steel tube at the midheight, so that the tube was embedded only 50 mm inside the central stub. The concrete strength at the time of testing was 28-29 MPa, and the yield strength of the steel tube, determined from coupon tension tests, was 370 MPa.

Under constant vertical load, the units were initially loaded horizontally in forward and reverse directions to the level of 75% of their theoretical ultimate lateral load. From the resulting load-deflection plots, the experimental values of yield displacement were obtained by extrapolating a straight line from the origin through the peak load-deflection point obtained up to the level of the theoretical ultimate load. The later was computed based on strain compatibility, the ultimate concrete strain of 0.003 in compression, the measured steel yield strength and concrete unconfined strength. After this initial loading, cyclic horizontal loading to increasing displacement ductility levels was applied. All units were subjected to a minimum of 2 cycles at each of displacement

ductility levels of ± 2, 4, and 6. After that, dynamic testing at the frequency of 0.13 Hz and the amplitude of approximately ± 65 mm was carried out.

Local buckling of the steel tube at the critical sections of units 1-4 was observed during the first cycle to a ductility level of ±4. The bulging occurred over the 60 mm region immediately adjacent to the central stub block. It was initially formed at only the extreme compression fibers of the section and grew to a maximum outstand of about 15 mm by the end of second cycle to the ductility level of ±6. However, the local buckling of the steel tube appeared to influence only the strength of unit 1. This unit suffered strength degradation at the second cycle to ±6 when the buckling spread right around the perimeter of the critical section. Under dynamic loading, units 1 and 2 experienced horizontal fracturing of the steel tubes at the bulging positions. Removal of the steel casing after the test revealed that the concrete in the bulging region was crushed.

In general, it was concluded, that units 1-4 exhibited satisfactory seismic performance and showed ductility capacities exceeding the requirements for bridges and buildings in New Zealand at that time. The authors emphasized the significance of the steel tube casing to the structural performance of the beam-columns. According to their estimates for units 1-4, at the ductility level of 6 the steel tube was contributing about 70% of the flexural strength and 95% of the shear strength. All four units showed ultimate capacities in excess of the ACI theoretical predictions. Units 1 and 2 (tested under axial load levels of $0.06\ P_0$ and $0.18\ P_0$, respectively) gave overstrength of 18% and 26%, respectively.

Units 5 and 6, with discontinuous casing, were loaded up to ductility levels of ±18 and performed extremely well. In the case of unit 6, which was more heavily reinforced, very little damage was inflicted even after dynamic testing consisting of 81 cycles to ductility level of ±21. Further slow cycle testing of this unit showed that it still had strength in excess of the theoretical prediction even at ductility levels as high as ±40. These extremely good results may be attributed in part to the method used in the calculation of the yield displacement. The theoretical ultimate lateral loads for units 5 and 6 largely underestimated the actual capacity because the steel tube, due to discontinuity, was neglected in the strength computations. This resulted in the experimental yield displacements, which depend on the values of the theoretical ultimate load, of only 3.2 mm for units 5 and 6 (experimental yield displacements of units 1-4 ranged between 12.6 and 14.5 mm).

This low value of yield displacement, which is only 1/5 of that for units 1-4, may be in part the reason for very high ductility levels, achieved for units 5 and 6.

R.J.T. Park, M.J.N. Priestley and J.B. Berrill (1987)

This paper summarized the main findings of the Ph.D. of the first author conducted at the University of Canterbury, New Zealand. Constitutuive models to describe the lateral interaction between the steel tube and the concrete core were developed for the cases of concentric longitudinal tension and compression of short circular CFTs.

To model the longitudinal tension behavior, it was assumed that after the tube has yielded the concrete is infinitely rigid in the radial direction. Lateral compatibility of the tube and concrete then implies that at this stage the steel hoop compressive strains cannot increase. It was then theoretically derived that the magnitude of the longitudinal stress in the yielded tube will increase by 15.5% in this case. This assumption was experimentally verified by testing one CFT specimen with outer diameter of 115 mm, wall thickness of 4.5 mm, steel yield strength of 308 MPa and concrete cylinder strength of 24 MPa. This was the only reported case when a circular CFT section was tested in tension.

The lateral interaction model for longitudinal compression was a modified form of that derived by Tomii et al (1977) from their extensive experimental data. The main difference between the two models is that the model of Tomii et al did not account for strain hardening of the steel tube, while the presented model followed the full stress-strain response of the tube. Empirical expressions were proposed to predict longitudinal and circumferencial stresses in the steel tube depending on the steel contribution factor.

Cyclic loading tests involving CFT beam-columns reinforced with traditional longitudinal and spiral reinforcement were reported briefly. These tests were conducted much in the same manner as the tests reported earlier by Park et al (1983). The range of tubes with diameter/thickness ratios between 34 and 214 was investigated. The test unit with the tube diameter/thickness ratio of 34 exhibited local buckling at the displacement ductility level of 4, while other units with $D/t \geq 60$ were reported to experience local buckling at ductility level of 2. This information is in conflict

with the earlier paper of Park et al (1983) where test units with diameter/thickness ratio of 72 were reported to buckle locally at ductility level of 4.

All test units, due to steel strain-hardening and concrete confinement, showed ultimate capacities in the range of 5-28% in excess of the theoretical strength computed on the basis of strain compatibility approach, uniaxial stress-strain properties of materials involved and the maximum concrete compression strain of 0.003. Despite the observed tube local buckling , strength, ductility and energy-dissipating characteristics of these units were similar or superior to those of conventionally designed reinforced concrete members. Hysteretic load-deflection curves were presented for two test units with the extreme tube diameter/thickness ratios of 34 and 214. Some pinching and loss of stiffness could be observed for the unit with the largest D/t ratio. However, in general, the unit exhibited excellent behavior, and the ductility level of 8 was achieved without any loss in strength.

H. Shakir-Khalil (1991b, 1991p, 1993p, 1993r)

The author reported tests on 106 rectangular, square and circular CFTs conducted at the Manchester University, Great Britain, to investigate the resistance of concrete core to pushout from the steel tube. The tubes were filled with 36-44 MPa cylinder strength concrete. An air gap was provided at the bottom of the specimens, so that the concrete-steel interface was about 50 mm shorter than the specimens' length. The pushout force was applied to the concrete core at the top of the specimens. Thirty eight circular specimens were tested in this investigation. They were arranged in several series to study the influence of various parameters and conditions.

Twelve circular 168.3×5 mm CFTs, 250,450 and 650 mm long were tested in series Y. In six of them, the inner steel surface had been oiled prior to casting of concrete core. Circular specimens of all other series were 450 mm long and had 168.3×5 mm steel sections, except for series F where 219.1×6.3 mm sections were used. Specimens of series Y, B and F were rested on the bottom of the tubes during testing, while brackets or sideplates welded to the tubes were used for support in series D and H. Various shear connector arrangements were provided in series B and F.

The test results were in agreement with the findings of Dowling and Virdy (1980). Strains measured along the outer surfaces of steel tubes of series Y showed to increase gradually from top

to bottom, clearly indicating load transfer from concrete core to steel through the bond along the interface. One circular specimen of this series was cut open, after being tested, and compared to similar square specimen. The friction marks on the concrete core indicated that, whereas the circular specimen resisted slip over all its perimeter, the square section was effective only near the corners. The tests clearly showed that circular sections are much more effective than rectangular in resisting pushout forces. Furthermore, the mechanical shear connectors were more effective when used in circular specimens.

Specimens supported through brackets or sideplates exhibited increased resistance to pushout forces due to the "constriction" effect of the lower end of the steel tubes which was subjected to longitudinal tensile stresses. Local "pinching" effect in specimens rested with brackets contributed to the increased steel-concrete bond capacity.

S. Sugano, T. Nagashima and T. Kei (1992)

A brief report was presented about results of seismic tests conducted in Japan on concrete-filled tubular columns. In total, 38 columns were tested, including 19 circular columns. However, sample results for only 6 columns (including 3 circular columns) were presented in two charts. Circular columns had an outer diameter of 300 mm and a shear span of 900 mm. The variable test parameters investigated were the level of axial force, D/t ratio and strength of component materials. Four of the circular columns were filled with high strength concrete, but the results of these tests were not reported.

Circular columns were reported to exhibit rich hysteresis curves and behave in a ductile manner even under high axial compression. The ultimate flexural strength of tested circular columns was 1.2-4.5 times the strength calculated according to Japanese standards. Three test results were presented in graphical format for a circular 300×8 mm CFT with $f_y = 400\ MPa$ and $f'_c = 37\ MPa$, tested under axial load levels P/P_0 of 0.3, 0.5 and 0.7. The flexural strength of these columns increased with the increase of axial load.

B.V. Rangan and M. Joyce (1992)

The results of tests performed in Australia on nine eccentrically loaded slender circular HSCFT columns were reported. The tubes had an outer diameter of 101.6 mm with a wall thickness of 1.6 mm. The average yield strength of steel was found to be 218 MPa from tension tests on sample strips of steel tubes conducted in accordance with relevant Australian standards. The average concrete cylinder strength at the age of 45 days, when the columns were tested, was 67.4 MPa. The effective length of the specimens varied between 807.5 mm and 2322.5 mm. Axial loads were applied with eccentricities of 10 and 30 mm.

After concrete placement, the columns and test cylinders were cured in a humidity controlled room for 7 days. The specimens were then left to air-dry until testing. About 1 mm longitudinal shrinkage of concrete was observed at top ends of columns, and a high-strength epoxy was used to fill this longitudinal gap.

All specimens were reported to fail at midheight "due to concrete crushing in the compression zone". The later reason was not supported by any arguments or observations. In specimens, subjected to 10 mm eccentricity of axial thrust, the extreme fiber tensile strains at failure did not reach the yield strain of steel. In other specimens, loaded with initial eccentricity of 30 mm, the steel at the extreme tensile fiber yielded at failure. Plots of ascending curves of axial thrust versus deflection at midheight were presented for all tested columns.

A method for calculating the strength of eccentrically loaded slender CFT columns was proposed based on the assumption that failure load is reached when the maximum moment at midheight is equal to ultimate bending strength of the cross section. The analysis of cross-sectional strength was based on the assumption of strain compatibility, Hognestad parabolic-strain relationship and maximum usable compressive stain of 0.003 for concrete. Simplifications were made by establishing assumed averaged stresses with resultants acting at compression and tension areas' centroids. The strengths calculated by the proposed method were compared with the obtained test results, and with the experimental data of Neogi et al (1969). The mean value of test/calculated strength ratio for these 27 columns was 1.17, with a coefficient of variation of 16%.

H.G.L. Prion and J. Boehme (1994)

The results of an experimental investigation into the behavior of thin-walled circular HSCFTs, conducted at the University of Toronto, were reported. In total, 26 specimens with a diameter of 152 mm and a wall thickness of 1.7 mm were tested. The yield strength of steel, ranging within 262-328 MPa, was determined from static tension tests, when strain in the sample coupon is held at a constant level while allowing the relaxation of fiber stresses to occur. The characteristic compressive strength of concrete was obtained from tests on 305×152 cylinders, and varied between 73 and 92 MPa. Shrinkage of the concrete resulting in a loss of steel-concrete bond was observed in some specimens before they were tested.

Ten specimens with lengths varying between 500 and 900 mm were tested under concentric axial load. Six of them were tested by applying the load on the steel and concrete simultaneously (Type A1), while the other four specimens had the load applied to the concrete core only by using loading plates that fitted within the tubes' inner diameter (Type A2). No appreciable difference in load-carrying capacity was found between the two types, or between longer and shorter specimens. All specimens failed within 5% of the predicted axial load capacity P_0.

Four 1100 mm long specimens (Type B1) were tested in bending. Constant moment region length varied between 0 and 600 mm. All beam specimens failed in a very ductile manner. The failure always occurred at the loading points and had the appearance of a concrete shear fracture followed by stretching and subsequent rupture of the steel casing. Local buckling of the tube was observed in the compression region at ultimate. Also, significant slippage between steel and concrete was observed at the ends of the beams, which was about 1-2 mm at ultimate and 10-13 mm at failure. No definite trend in bending moment capacity was detected for varying shear span. One beam specimen with effective length of 2120 mm and constant moment region length of 610 mm (Type B2) was subjected to cyclic loading at a ductility level of approximately two to three times the yield deformation. This was accomplished by loading and unloading the specimen in one orientation, then rotating the specimen about its longitudinal axis by 180° and repeating the loading sequence. Gradual pinching and decrease in strength was observed with every subsequent cycle. The specimen sustained four and half cycles of bending, after which it was loaded to failure. Analytical predictions of flexural strength, based on strain compatibility and variable

concrete stress block according to Hognestad equation, were compared with experimental bending moment capacities. The later showed overstrength between 27 and 56 %.

Eight specimens, with length dimensions arrangements similar to those of type B2 specimen, were subjected to various combinations of axial load and bending moment. Six of these specimens were tested monotonicaly (Type C1) and two were subjected to cyclic lateral loading (Type C2) in a manner similar to that applied to beam specimen of type B2. The axial load in each test was held at a predetermined level, which varied between 0.145 and 0.52 P_0 . All beam-column specimens failed in the center by rupture of the steel casing in the tension zone after substantial cracking of the concrete and buckling of the steel in the compression zone. Cyclic tests demonstrated ductile hysteretic curves, although some pinching and strength deterioration were observed. Experimental/theoretical flexural strength ratios varied between 0.921 and 1.153.

Three specimens, having effective length of 1071 mm, were tested under eccentric axial loads. The initial eccentricity varied between 11 and 15 mm. These specimens failed abruptly when overall buckling occurred. For the purpose of calculating experimental moments, which depended on the instantaneous eccentricity of the load, the lateral positions of the specimens and readings from strain gauges on the tube surface were used. Experimental loads did not achieve those predicted by the compatible strain model, which was attributed to imperfections such as out-of-straightness and end effects.

P.F. Boyd, W.F. Cofer and D.I. Mclean (1995)

These authors reported results of an experimental study on the flexural behavior of circular CFT columns conducted at Washington State University. Five columns were tested under reversed cyclic loads and a constant axial load of 40 kips (178 kN). All columns had an outer diameter of 8 in. (203 mm). Columns 1, 2 and 3 had tube wall thickness of 0.109 in. (2.8 mm) and steel yield strength of 50 ksi (345 MPa), columns 4 and 5 had 0.075 in. (1.9 mm) thick tubes with $f_y = 41$ ksi (283 MPa). All columns were filled with 4.6 ksi (32 MPa) concrete, except for column 5, which had concrete core of 7.0 ksi (48 MPa). Column 3 was provided with shear studs welded to the interior surface of the steel tube. The lateral loading pattern consisted of two cycles at each of the displacement ductility levels of $\mu = \pm 1, \pm 2, \pm 4, \pm 6$ and ± 8, unless actuator stroke limitations were

reached or failure occurred prior to reaching level 8. The yield displacement was determined experimentally in the same manner as described by Park et al (1983).

All tested columns exhibited ductile behavior with little strength degradation and some pinching in the hysteretic curves. Calculations of ultimate strength based on ACI methods underpredicted the measured lateral strengths by 11-26 %. The column with the studded steel tube showed slightly greater ultimate strength and less degradation in strength than the columns with nonstudded steel shells. It was pointed out that the ACI and AISC-LRFD minimum tube wall thickness requirement was unnecessarily restrictive for the tested columns.

C. Matsui, K. Tsuda and Y. Ishibashi (1995)

Results of a systematic and comprehensive study of CFT columns under concentric and eccentric compression in wide range of slenderness ratios, conducted at Kyushu University in Japan, were reported. Forty eight CFT specimens were tested, including 24 circular columns. The slenderness ratio KL/D varied between 4 and 30. The circular tubes were 165.2 mm in diameter and 4.5 mm thick. The initial eccentricity of applied axial load for circular specimens ranged from 0 to 105 mm. The average yield and ultimate strength of the steel, determined from coupon tension tests, was 4.22 t/cm^2 (414 MPa) and 5.03 t/cm^2 (493 MPa), respectively, for circular tubes. However, the mechanical properties of the steel, used for the evaluation of column test results, were taken from compression tests on short empty tubes. These were 3.6 t/cm^2 (353 MPa) and 4.1 t/cm^2 (402 MPa) for yield and ultimate strengths, respectively. The average compressive strength of concrete used for circular columns was 417 kg/cm^2 (41 MPa), obtained from sample cylinder tests.

The results were presented in plots of the axial load versus the deflection at the midspan. Experimental relationships between axial load and midspan moment were presented as well. It was observed that circular specimens with slenderness ratio of 12 and more were not able to attain the full plastic moment at the maximum load due to instability phenomenon, especially when the eccentricity was small. However, it could be observed from the descending branches of the presented P-M curves, that in most cases the specimens were attaining moments in excess of their full plastic moment capacities at lower P levels during unloading.

An elasto-plastic analysis, based on assumed sine wave shape of columns, was performed to predict load-deflection relationships for two wavelength cases of L and KL. Both degrading and nondegrading assumed stress-strain relationships for concrete were used in the analysis. For the maximum buckling load, good agreement was found between analytical models and experimental results. Assumed increased ductility of concrete showed to be not important for columns having slenderness ratio of 18 and higher.

The experimental results were compared with design strength predictions. AIJ (Architectural Institute of Japan), modified AIJ and CIDECT (International Committee for the Development of Tubular Structures) methods were examined. The AIJ method was shown to be too conservative. CIDECT method was found to agree well with the experimental results in the KL/D range from 12 to 30. The modified AIJ method gave conservative strength predictions for columns with the slenderness ratio of 4. For the rest of the slenderness range, it was shown to produce good agreement with the experimental results.

M.D. O'Shea and R.Q. Bridge (1995)

This paper describes the results from an experimental program on short circular HSCFTs carried out at the University of Sydney in Australia. The specimens had L/D ratio of about 3.5 and D/t ratios ranging from 55 to 200. Ten HSCFT columns and ten corresponding empty steel tubes were tested under concentric and eccentric loads. Tubes with D/t = 55 were commercial tubes with an outer diameter of 165 mm and wall thickness of 3 mm. Other tubes were manufactured using sheet steel metal fabricator to provide an outer diameter of 190 mm and had wall thicknesses ranging from 0.95 to 2 mm. These tubes were formed by cold rolling a steel sheet and then welding the longitudinal seam. The steel yield strength was determined from tension tests on sample coupons taken from representative steel tubes, and ranged between 184.8 and 364.3 MPa. Increase in the yield strength due to cold forming was observed for manufactured tubes compared to the original yield strength of the steel sheets. Two concrete mixes, A and B, with a target strength of 100 MPa were used in this investigation. Two sets of control 200×101 mm cylinders, labeled M and D, were prepared for each mix. The M cylinders were stored in a lime-bath in a fogroom at 100% humidity and 20°C. The D control cylinders were tightly wrapped in plastic to simulate conditions in the tube, and stored together with the HSCFT specimens under ambient

conditions. The M cylinders gave average strength of 113.5 and 115.8 MPa, while D cylinders gave 108.0 and 112.7 MPa, for mixes A and B respectively.

Results of bare steel tube tests were compared to predictions of AISC LRFD and Australian Standard AS 4100. It was concluded that the reduction in axial strength due to local buckling may be estimated with reasonable accuracy using the AISC LRFD, while AS 4100 was shown to give conservative results.

Results of HSCFT short column tests were compared with predictions based on Eurocode 4 formulas and a special method to account for the effect of local buckling in the thin-walled sections, and reasonable agreement was found. It was concluded that thin-walled tubes provided little or no confinement for the high strength concrete core.

1.3 Summary of Literature Review

During the survey of available English-language literature on circular CFT columns (see Bibliography) the following trends were observed:

- Most of the previous experimental research was concerned with short axially loaded columns.

- There was only one reported test result for a circular CFT in tension (Park et al, 1987).

- There was only one study (Prion and Boehme, 1994) that reported results of tests on circular CFTs in bending.

- Most of the data on flexural strength of circular CFTs under combined compression and bending comes from tests conducted on eccentrically loaded columns. All reported HSCFT columns, which were tested under eccentric loads (Rangan and Joyce, 1992; Prion and Boehme, 1994; O'Shea and Bridge, 1995) had D/t ratios of 55 or more.

- Very few tests have been done on circular CFT beam-columns under cyclic lateral loads. In almost all of these tests the axial load level did not exceed $0.2\,P_0$ and the shear span/diameter

ratio never exceeded 5. There was only two reported cyclic tests on HSCFT beam-columns (Prion and Boehme, 1992), and these were carried out with tubes having $D/t = 89.4$.

- There was no available experimental data on the behavior of circular HSCFT beam-columns with D/t ratios below 55.

The experiment of this study was intended to provide some data on the behavior of circular steel tubes with $D/t = 44.8$, filled with 70-90 MPa concrete and subjected to constant axial compression and cyclic lateral loading. It was also decided to employ a higher, than previously used in such tests, shear span/diameter ratio of 13.5 to find out whether the slenderness effects will be significant. The axial load level of up to $0.58\ P_0$ was the main variable parameter investigated in this experiment.

Chapter 2

Experiment

The experimental study consisted of design, construction and testing of three circular steel HSCFT cantilever beam-columns tested under various levels of constant axial compression and gradually increasing lateral displacement reversals. In addition, one short composite column was tested to failure under monotonicaly increasing concentric axial load. All column specimens had the same cross-sectional geometry to allow for direct comparison. The objective of this investigation was not only to determine experimentally the maximum load combinations for the specimens, but to study the behavior of the columns through the entire loading history up to and beyond the ultimate load. This chapter describes the details of tested columns, test setup, instrumentation and procedures. A summary of column properties and test conditions is presented in Table 2.1.

2.1 Column Specimens

One short column and three long beam-columns were designed, built and tested in this study. The short column was labeled ST1, and the three long beam-columns were labeled FA1 through FA3. Figure 2.1 shows the typical column cross-section. The column ST1 is illustrated in Figure 2.2. The geometry of a typical beam-column specimen is presented in Figure 2.3. The material properties are described in the next section.

All columns were cut from one circular hot-formed seamless steel tube with nominal diameter×thickness dimensions of 6 × 1/8 in. (152×3 mm). Cross-sectional dimensions of the steel tube were carefully measured to reveal any deviations from the nominal values. The tube

diameter varied within 152.07-152.68 mm. The average of 40 diameter measurements was calculated to be 152.426 mm. Tube thickness ranged between 3.16 and 3.67 mm, with the average of 3.393 mm for 84 measurements. Based on the measurements, the values of $D = 152.4\ mm$ and $t = 3.4\ mm$ were adopted for the purposes of this study. Consequently, the following cross-sectional geometry properties were common for all tested columns:

- $D / t = 44.8$;
- $A_g = 18\,241\ mm^2$;
- $A_c = 16\,650\ mm^2$;
- $I_c = 22\,060\,502\ mm^4$;
- $r_c = 36.4\ mm$;
- $Z_c = 514\,438\ mm^3$;
- $A_s = 1\,591\ mm^2$;
- $A_s / A_g = 8.72\ \%$;
- $I_s = 4\,418\,997\ mm4$;
- $r_s = 52.7\ mm$;
- $S_s = 57\,992\ mm^3$;
- $Z_s = 75\,497\ mm^3$.

The specimen ST1 was 380 mm long. This length was chosen to match the recommended effective length/diameter ratio between 3 and 3.5 for short composite columns tested in concentric compression (Shang-Tong, Ruo-Yu, 1987) in order to avoid significant end effects or lateral bending. The steel tube was carefully machined to ensure parallel ends.

The cantilever beam-column specimens FA1-FA3 were 1655 mm long. Each of them was attached to a steel base plate, 1100×400×25 mm in dimensions, by a full penetration groove weld along the perimeter of the steel tube. This type of connection proved to be sufficiently strong. Each base plate was additionally stiffened by two 660×75×25 mm steel strips welded to its upper surface in order to minimize bending deformations during testing and increase the rigidity of column fixity. Four 38 mm holes were drilled in each steel base plate to allow it to be fixed to the setup foundation by means of 32 mm threaded rods.

All columns were filled with high-strength concrete designed to attain the compressive strength of 70-90 MPa at the time of testing. Three batches were prepared for this purpose in a small mixer.

The columns were filled in vertical position. The concrete was placed into the steel tubes manually, in layers not exceeding 300 mm, and compacted with a small mechanical vibrator. Special care was given to insure proper filling.

Four 19 mm high-strength steel bolts were inserted in the fresh concrete at the top end of each long beam-column specimen. The bolts were fixed on plywood plates to facilitate proper positioning. After the concrete had hardened (next day), the plywood templates were removed. These embedded bolts were used later to connect the loading plate to the beam-column specimens.

All specimens were stored in normal room temperature conditions with the exposed ends wrapped by polyethylene sheets in order to seal the concrete inside the tubes. Contrary to observations of other researchers (Prion and Boehme, 1994), no loss of bond between steel and concrete due to shrinkage of concrete was observed during this investigation, although the specimens were stored for up to 310 days before they were tested.

At an early age, the concrete surface at each exposed end was roughened by chipping, washed with water, and then capped with a thin layer of fine cement-sand paste made flush with the tube end surface. This was done to achieve smooth end surfaces and ensure both steel and concrete being loaded together.

2.2 Materials

2.2.1 Steel Tubing

One circular seamless hot-formed steel tube, 5.8 meters long, was employed in the experiment. A short piece of tube, about 360 mm in length, taken from one of the ends of the original long tube, was used for the preparation of 9 longitudinal tension test specimens. All specimens were prepared and tested in accordance with ASTM A 370-92. The dimensions of a steel tension test specimen are shown in Figure 2.4. The results of steel coupon tension tests are summarized in Table 2.2.

Specimens #1-#4 were tested during the design stage in order to get a quick estimate of the steel properties. Strains were not recorded during these tests and only yield strength, ultimate strength

and elongation at fracture were determined. The yield strength was determined as the stress level at which the strain increase occurred without an increase in load. The elongation at fracture was determined by fitting the ends of a fractured specimen together carefully and measuring the distance between the gage marks.

For specimens #5-#9, loads versus corresponding strains (measured by an extensometer) were recorded up to the strain level of 10%, and the stress-strain curves were obtained. Each of the specimens #6 -#9 was also equipped with two electric resistance strain gauges (Showa Measuring Instruments Co., Type N11-FA-1-120), one measuring tensile strain in the longitudinal direction and the other measuring compressive strain in the transverse direction. Strain gauges were located at the middle of the specimens, at about 5 mm distance from each other. Strains measured by the longitudinal electric resistance gauges were used to verify the strains measured by the extensometer and the uniformity of strain distribution along the test specimens. Strains, measured by the transverse strain gauges were used to evaluate the Poisson's ratio in the elastic range. The stress-strain curves obtained for specimens #5-#9 are shown in Figs. 2.5-2.9.

Considerable differences in the shape of the stress-strain curves could be observed. The length of plastic plateau, and the strain level at which strain-hardening started, varied from one specimen to another. Specimen #9 showed linear stress-strain relation up to the ultimate stress level with no subsequent strain hardening. This specimen also had a remarkably small elongation at rupture. Specimens #5 and #6 did not exhibit a well-defined disproportionate increase in strain that characterizes a yield point, but showed rather gradual deviation from proportionality of stress to strain. For these two specimens, the yield strength was determined as the stress at 1% strain. This approach was considered more appropriate than the 0.2% offset method, because it reflects the stress level of the plastic plateau. The same approach was used for specimens #3 and #4, which exhibited similar behavior.

The variations in strength properties, especially the yield strength, were rather large, considering all tension test specimens were taken from adjacent positions. Similar differences in the mechanical properties of circular seamless steel tubes were revealed by other researchers (Klöppel and Goder, 1957). Such variations in yield strength, along with variations in tube thickness, should be kept in mind when column test results and theoretical calculations are compared.

Based on the results of the tension tests, the average values of the obtained mechanical properties were adopted for the steel tube for the purposes of this study. The yield strength and the ultimate strength were 330 and 390 MPa respectively. It was considered appropriate not to include the experimental result of specimen #9 in the calculation of the average yield strength. The established value of the Poisson's ratio in the elastic range was 0.258.

2.2.2 Concrete

Three different batches of concrete were prepared to fill the column specimens. The first and second batches were used to cast specimens FA1 and FA2 respectively. The third batch was used for columns FA3 and ST1. The three concrete mix designs used are shown in Table 2.3. The total water content and the amount of superplasticizer used (Conchem S.P.N.) were increased for the second and third batches to achieve better workability of concrete, because of concerns regarding the proper placement of concrete in the tubes. Type 10 Portland Cement (Lafarge SF) with 8% silica fume content and local aggregates were used for all batches. The 10 mm crushed lime stone coarse aggregate was carefully washed and dried before use in concrete. No retarding admixture was used, and the concrete was usually placed within 10 minutes after the batching was complete.

At least three standard 6×12 in. (152.4×304 mm) cylinders were cast with every batch. They were stored at room temperature wrapped in polyethylene sheets, without wet curing, in order to simulate conditions similar to those of concrete in the columns. Before testing, the cylinder ends were grinded to ensure smooth and parallel end surfaces. The concrete sample cylinders were tested at the same time (usually, the next day) as a corresponding column specimen was tested. The concrete cylinder tests were conducted in a Forney testing machine with 2200 kN capacity. All specimens failed in an abrupt and explosive manner reflecting the brittle nature of high-strength concrete. The results of cylinder tests are presented in Table 2.4.

The compressive strength of concrete for specimens FA1, FA2 and FA3 was established to be 89.4, 72.0 and 75.7 MPa respectively. Each of these values was determined as the average of the corresponding concrete sample cylinder test results. The concrete strength of 79.5 MPa for specimen ST1 was estimated from the assumption that it would be 5% more than the concrete strength of specimen FA3, because the same batch of concrete was used for both columns, but the age of ST1 at the time of testing was 143 days more.

2.3 Test Setup

2.3.1 Short Column

The specimen ST1 was tested at the structural laboratory of National Resources Canada. A five million pound capacity universal compression testing machine was used for this purpose. Figure 2.10 illustrates the overall view of the test setup for the short column.

The lower loading plate of the testing machine was rested on the strong laboratory floor and served as a foundation for the tested column. The upper loading plate had a spherical hinge which allowed it to rotate in any direction. Two smaller steel plates with diameter×thickness dimensions of 8×1.5 in. (203×38 mm) were inserted at the top and the bottom of the column specimen to protect the loading platens of the testing machine.

2.3.2 Beam-Columns

An existing testing facility at the structural laboratory of the University of Ottawa, previously used for simulated seismic loading of reinforced concrete columns, was adapted for the testing of composite beam-column specimens FA1-FA3. This facility allowed independent application of loads or displacements in both vertical and horizontal directions. Three hydraulic MTS actuators, a composite steel-reinforced concrete foundation and a heavy loading steel beam were the major components of the test setup. Sketches illustrating the configuration of setup components with some detail are presented in Figures 2.11 and 2.12. Photographs of Figure 2.13 show the general view of the setup.

The setup foundation consisted of four C-channels welded along the perimeter of a 75 mm thick bottom steel plate. The reinforced concrete portion of the foundation had a special H-shape (in plan) in order to provide support for the column base plate and accommodate the vertical MTS actuators, which were bolted down to the foundation bottom steel plate on both north and south sides of the tested column. The setup foundation was secured to the laboratory strong floor by means of four 64 mm diameter bolts, which were 1800 mm long in order to reach from the top of the foundation to the bottom of the thick floor. Another four bolts, 32 mm in diameter, 1000 mm

long, attached to the bottom plate, passed up through the reinforced concrete and protruded vertically out of the foundation. These were used to secure the beam-column specimens tightly to the foundation.

The loading beam was rigidly connected to the top of a beam-column specimen by 19 mm bolts. Specially manufactured 330×330×38 mm steel loading plate and two 270×77×38 mm spacer plates were employed in this connection in order to adjust to the spacing differences between the holes in the loading beam and the bolts embedded in the concrete core at the top of the specimen. The holes in the lowest flange of the loading beam were spaced at 100 mm distances in plan, and the cross-sectional dimensions of the beam-column specimens did not permit to use the same spacing for the four embedded bolts. The loading beam consisted of two major parts rigidly interconnected by eight 25 mm diameter bolts: The upper part box-section beam, oriented north-south, was built-up of thick steel plates welded together. Four 42 mm holes were provided in the bottom flange at each end of this upper part in order to facilitate the connection with the vertical actuators. The lower part of the loading beam had a built-up I-section with the web accommodating the connection to the horizontal actuator. This lower part was additionally stiffened by five steel plates (three on the east and two on the west side of the web) oriented in the direction of the horizontal force.

Two hydraulic MTS actuators were employed to apply a constant vertical compressive load. The third actuator was used to produce horizontal displacement reversals at the lower part or the loading beam above the beam-column specimen. Each actuator had a load capacity of 1000 kN in both tension and compression. All actuators were equipped with multi-directional swivels facilitating hinge connections at both ends. This arrangement minimized any moments at the connections and made the whole system of actuators very flexible allowing it to deform without damage during the tests. The vertical actuators were connected to the foundation steel plate at the bottom and the loading beam at the top. The horizontal actuator was attached at one end to a rigid steel frame secured to the strong laboratory floor. The other end was connected to the loading beam. All actuator connections were carried out with four 38 mm diameter, 400 mm long, bolts at each end. A single 33 GPM pump supplied the hydraulic pressure for all actuators, and MTS servo-valves maintained the desired pressure levels in each actuator.

The horizontal loads were applied 395 mm above the upper end or the beam-column specimens. This implies that the shear span of the tested cantilever beam-columns, measured from the steel

base plate to the point of inflection, was 2050 mm, which is representative of many columns used in practice. The horizontal actuator had a maximum stroke of 500 mm, which permitted the application of lateral displacement reversals of up to ±250 mm relative to the neutral position at the inflection point level.

Steel frames, about 3m high, made of hollow sections were provided at both north and south sides of the setup foundation. These could be observed in the photographs of Figure 2.13, but are not shown on the sketches of Figures 2.11 and 2.12. These frames were tied together at the top and secured to laboratory floor. They provided a sense of security against an unexpected out-of-plane column failure. Another small frame not shown on the sketches was located under the horizontal actuator ending about 20 cm below the later. It was secured to the rigid steel frame and served as a stopper against a sudden fall of the horizontal actuator from one end. All these frames were also necessary during the test preparation procedures as they provided the means of support for the actuators when the later were not connected to the loading beam.

The test preparation usually started with the attachment of the loading beam together with the steel loading and spacer plates to the top of the to-be-tested specimen. The whole assembly was then lowered onto the foundation and bolted into place. After that, the actuators were connected to the loading beam. The described operations were conducted with the aid the laboratory crane. Finally, the instrumentation, described in the next subsection, was complemented, connected and calibrated.

2.4 Instrumentation

2.4.1 Short Column

The instrumentation of specimen ST1 consisted of two dial gages and 12 electrical resistance strain gauges. The dial gages were placed on two opposite sides of the column at equal distances to measure the vertical displacement of the upper loading plate of the testing machine indicating the shortening of the specimen. Their readings were later reduced by the amount of vertical strain produced by the two smaller 203×38 mm loading plates. The electrical resistance strain gauges were placed in six different locations spaced at equal distances along the outer perimeter of the steel tube at the midheight of the specimen. They were arranged in pairs to measure the strains in

both the longitudinal and circumferential directions. They were numbered from 1 to 12, with each pair being assigned two consecutive numbers (1 & 2, 3 & 4, etc.). The longitudinal strain gauges were assigned odd numbers, while the gauges measuring transverse strains were numbered with even numbers. The readings from all measurement devices were recorded manually at each loading step. Figure 2.14 illustrates the instrumentation of the short column specimen ST1.

2.4.2 Beam-Columns

The beam-column specimens were each instrumented with up to six linear variable differential transducers (LVDTs) and up to 16 electrical resistance strain gauges. The locations of LVDTs and strain gages are shown schematically in Figures 2.15 and 2.16 respectively. Photographs of Figure 2.17 illustrate some instrumentation details. Table 2.5 lists the LVDTs and strain gages used for each of the beam-column specimens.

The LVDT #1 was of temposonic type with a usable stroke of ±250 mm. It was measuring the horizontal displacements at the point of inflection. The output from this LVDT, calibrated to be in mm, was provided directly to the MTS controller in order to manage the application of the horizontal displacement reversals. The MTS controller allowed continuous monitoring of these displacements in addition to the loads and strokes in the actuators. All data was recorded on a personal computer (PC).

The MTS controller was also connected to a Sciemetric System 200 Data Acquisition System supported by another PC. This data acquisition system automatically recorded the data from the MTS controller, the readings from all LVDTs and strain gauges every 5 seconds. This recorded raw data is the basis for the test results presented in the next chapter.

Temposonic LVDT #2 was used for columns FA2 and FA3. It measured the lateral displacements at the top of the beam-column specimens. It also allowed, in combination with the data from LVDT #1, to estimate the rotations at the top of the columns. Both temposonic LVDTs are illustrated in Figure 2.17. Each of them was used in combination with a string and a pulley roller. This arrangement allowed them to be positioned vertically, although for simplicity they are shown positioned horizontally in the scheme of Figure 2.15.

The rotations in the hinging region at the bottom of the beam-columns were measured by means of vertically positioned LVDTs ## 3 & 4 rigidly attached to the steel tube at 150 mm above the steel base plate. Each of these LVDTs had a 50 mm usable stroke and measured displacements against the upper surface of the foundation. The details of this arrangement are shown in Figure 2.17.

Vertically mounted LVDTs ## 5 & 6, each with a stroke of 50 mm, were used to measure the rotations of the steel base plate. In the case of column FA1, these LVDTs were of temposonic type, used in combination with strings and pulley rollers. LVDT #7, which was used only for column FA1, measured the horizontal slip of the steel base plate. All LVDTs, except for ## 3 & 4, were mounted on light steel frames rigidly attached to the foundation. This implies that all readings of displacements are relative to the position of the foundation.

Electrical resistance strain gauges were placed on the outer surface of the steel tube in the hinging region at the bottom of the beam-columns. They were arranged in four vertical rows spaced at equal distances around the perimeter of the tube. Two of the rows were located at the extreme cross-sectional fibers in the direction of the horizontal loading. Strain gauges oriented longitudinally were numbered with odd numbers, while those measuring circumferential strains were assigned even numbers. The intention was to obtain experimentally the ratio between the lateral and longitudinal strains at various segments of the steel tube at various stages of loading. It was also assumed that the strain gauge data obtained at different vertical levels would help to assess the lateral restraining effect provided by the steel base plate.

2.5 Loading

2.5.1 Short Column

The short column specimen ST1 was compressed concentrically up to failure. The load was applied slowly by increments of 20 kips (89 kN). It took about 15 seconds to apply each load increment. At each step, the load was held constant for at least 1 minute until the readings from all dial gages and electric resistance strain gauges had been recorded. When the axial load reached 460 kips (2048 kN) the increments were reduced to 10 kips (44 kN). The testing continued

without interruptions until the failure occurred. The total duration of this test was about 55 minutes.

2.5.2 Beam-Columns

The first loading step for each of the beam-column specimens was the application of the vertical axial compressive load up to the desired level, which was held then constant throughout the test. Specimens FA1, FA2 and FA3 were tested under axial loads of 400, 1000 and 700 kN respectively. At some stage during testing of specimen FA2, it was decided to decrease the axial load to the level 100 kN (this decrease is described in detail in the next chapter).

The horizontal loading always started in the West-bound direction, which was considered positive for both loads and displacements. The horizontal displacement reversals at the point of inflection were applied in the manner shown in Figure 2.18, while the required lateral loads were monitored. Three complete cycles were carried out at each of the displacement levels of ±20 mm, ±40 mm, ±60 mm, etc. These displacement levels roughly correspond to the lateral drift levels of ±1%, ±2%, ±3%, etc. Additional three initial cycles at the lateral drift level of ±0.5% and another three cycles at the level of ±1.5% were applied to specimen FA1. The testing usually proceeded at a slow rate, with each cycle taking about 5-10 minutes, until a considerable drop in the lateral load resistance was observed. The total duration of a typical beam-column test was about 3 hours.

Table 2.1 - Column Properties* and Testing Conditions

Specimen	Length of Column Specimen (mm)	Compressive Strength of Concrete f_c' (MPa)	Nominal Axial Capacity $P_o = A_s f_y + A_c f_c'$ (kN)	Steel Contribution Factor $q = A_s f_y / P_o$	Loading	Shear Span (mm)	Applied Axial Load P_{exp} (kN)	Axial Load Level P_{exp} / P_o
ST1	380	79.5	1849	0.284	increasing axial compression	-	2157	1.17
FA1	1655	89.4	2014	0.261	constant axial load + lateral reversals	2050	400	0.20
FA2	1655	72.0	1724	0.305	constant axial load + lateral reversals	2050	1000 & 100	0.58 & 0.06
FA3	1655	75.7	1786	0.294	constant axial load + lateral reversals	2050	700	0.39

* Common properties : D = 152.4 mm ; t = 3.4 mm ; f_y = 330 MPa ; A_s = 1591 mm^2 ; A_c = 16650 mm^2 ; D/t = 44.8 ; A_s/A_g = 8.7%

Table 2.2 - Steel Coupon Tension Tests

Specimen number	Yield Strength f_y (MPa)	Ultimate Strength f_u (MPa)	Elongation at rupture (%)	Poisson Ratio
1	352.0	391.4	19.3	-
2	360.1	397.2	18.6	-
3	304.5	395.1	23.8	-
4	311.2	401.3	23.2	-
5	322.3	381.9	21.8	-
6	321.8	374.6	21.3	0.240
7	337.2	385.2	19.2	0.276
8	331.3	376.3	21.1	0.262
9	400.7	403.8	9.7	0.253
Average	330.0 *	389.6	19.7	0.258

* Specimen # 9 was not included in the calculation of the average yield strength.

Table 2.3 - Concrete Mix Proportions

Column specimens	Cement (8% SF) (kg)	Slag (kg)	Coarse Aggregate (kg)	Sand (kg)	Total Water* (liters)	Super-plasticizer (liters)	Water/ Cement Ratio**
FA1	450	160	1120	740	151	24	0.248
FA2	450	160	1115	738	179	32	0.293
FA3 & ST1	450	164	1118	740	170	24	0.277

* Total water includes moisture content of aggregates and water portion of the superplasticizer.
** Water/Cementitious ratio accounts for all cementitious materials including slag and silica fume.

Table 2.4 - Concrete Sample Cylinder Tests

Column specimen	Age at the Time of Testing (days)	Results of Concrete Cylinder Tests (MPa)	Concrete Strength f_c' (MPa)
FA1	62	89.7 ; 89.9; 88.6	89.4
FA2	187	70.4 ; 70,8 ; 74.5 ; 72,5	72.0
FA3	178	76.4 ; 74.9 ; 75.8	75.7
ST1	310	-	79.5*

* Estimated to be 5% greater than the concrete compressive strength of specimen FA3.

Table 2.5 - Instrumentation of Beam-Column Specimens

Instrumentation Device	Column FA1	Column FA2	Column FA3
LVDT #1	×	×	×
LVDT #2		×	×
LVDT #3	×	×	×
LVDT #4	×	×	×
LVDT #5	×	×	×
LVDT #6	×	×	×
LVDT #7	×		
Strain Gauge #1		×	×
Strain Gauge #2		×	×
Strain Gauge #3	×	×	×
Strain Gauge #4	×	×	×
Strain Gauge #5		×	
Strain Gauge #6		×	
Strain Gauge #7		×	×
Strain Gauge #8		×	×
Strain Gauge #10	×	×	×
Strain Gauge #11		×	×
Strain Gauge #12		×	×
Strain Gauge #13	×	×	×
Strain Gauge #14	×	×	×
Strain Gauge #15	×		
Strain Gauge #16	×		
Strain Gauge #17		×	
Strain Gauge #18		×	
Strain Gauge #20	×	×	×

$D / t = 44.8$

$A_s = 1\,591\ mm^2$

$A_c = 16\,650\ mm^2$

$A_s / A_c = 8.7\ \%$

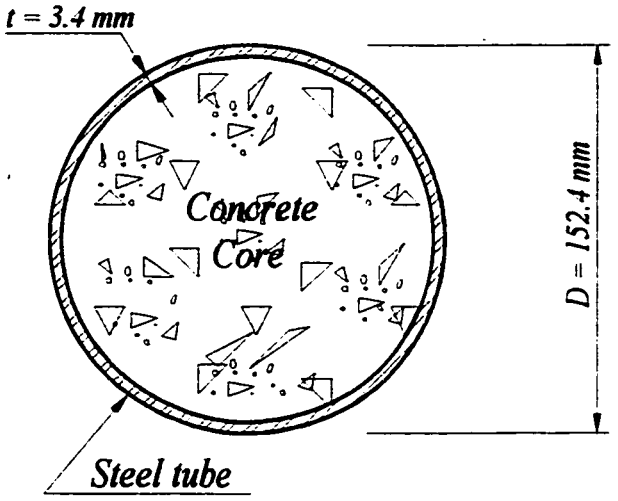

Figure 2.1 : Typical Column Cross-Section

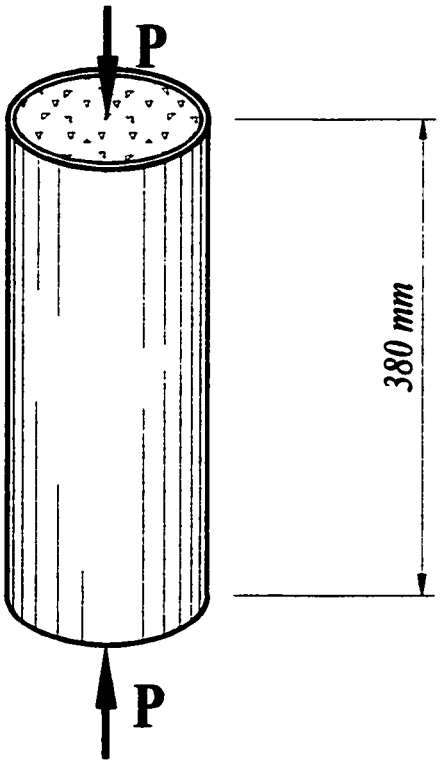

Figure 2.2 : Short Column Specimen ST1

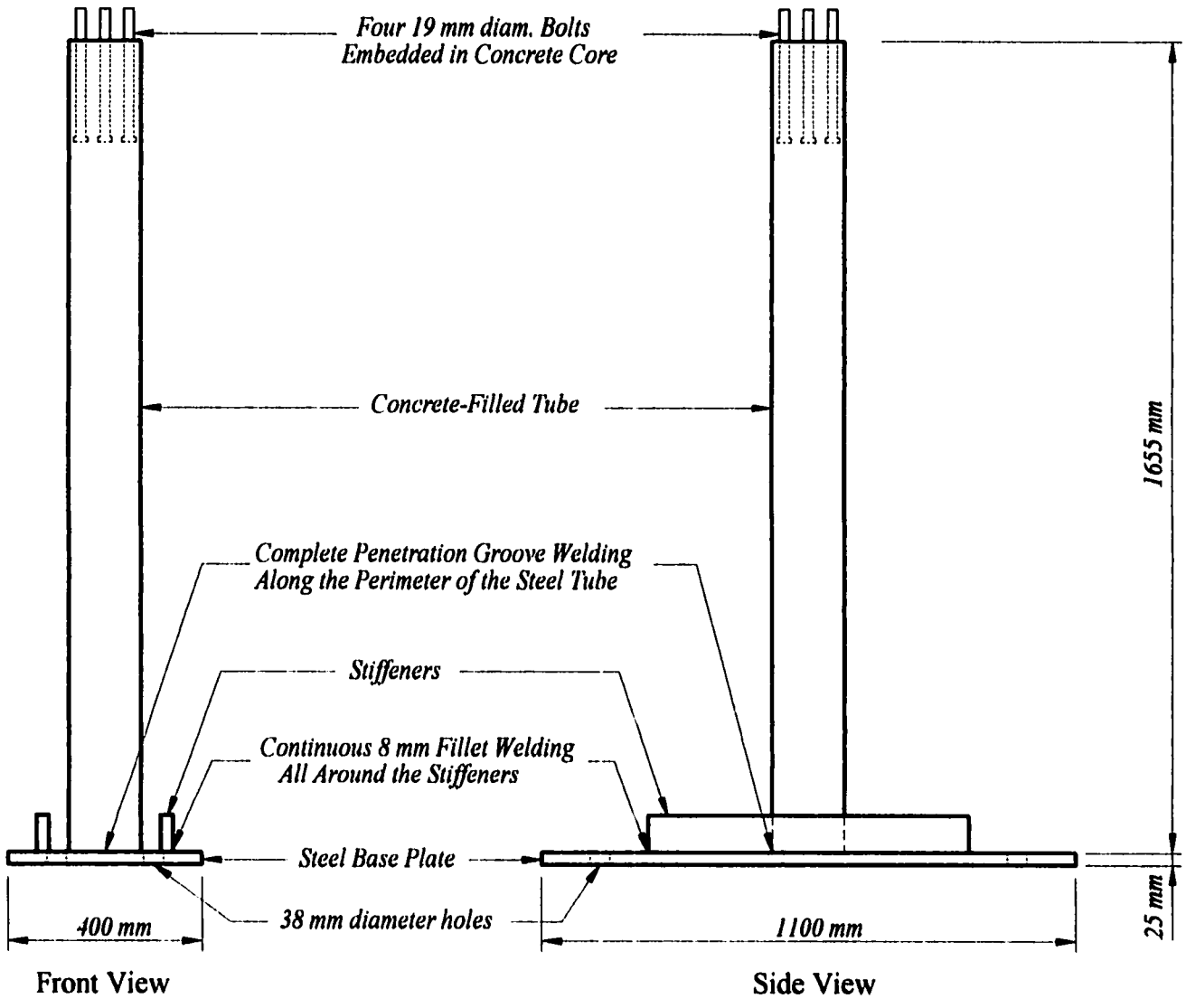

Figure 2.3 : Typical Beam-Column Specimen

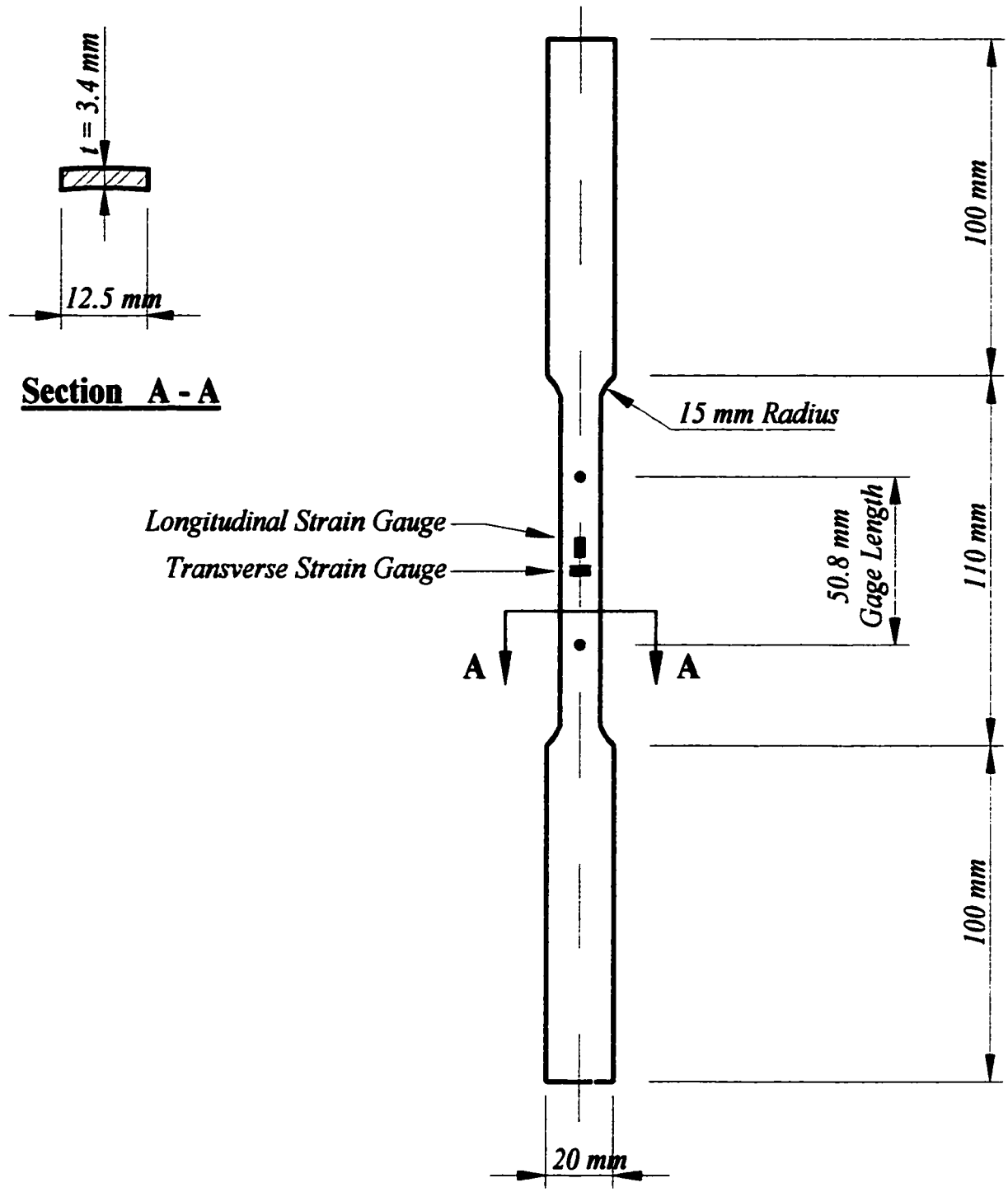

Figure 2.4 : Typical Steel Tension Test Specimen

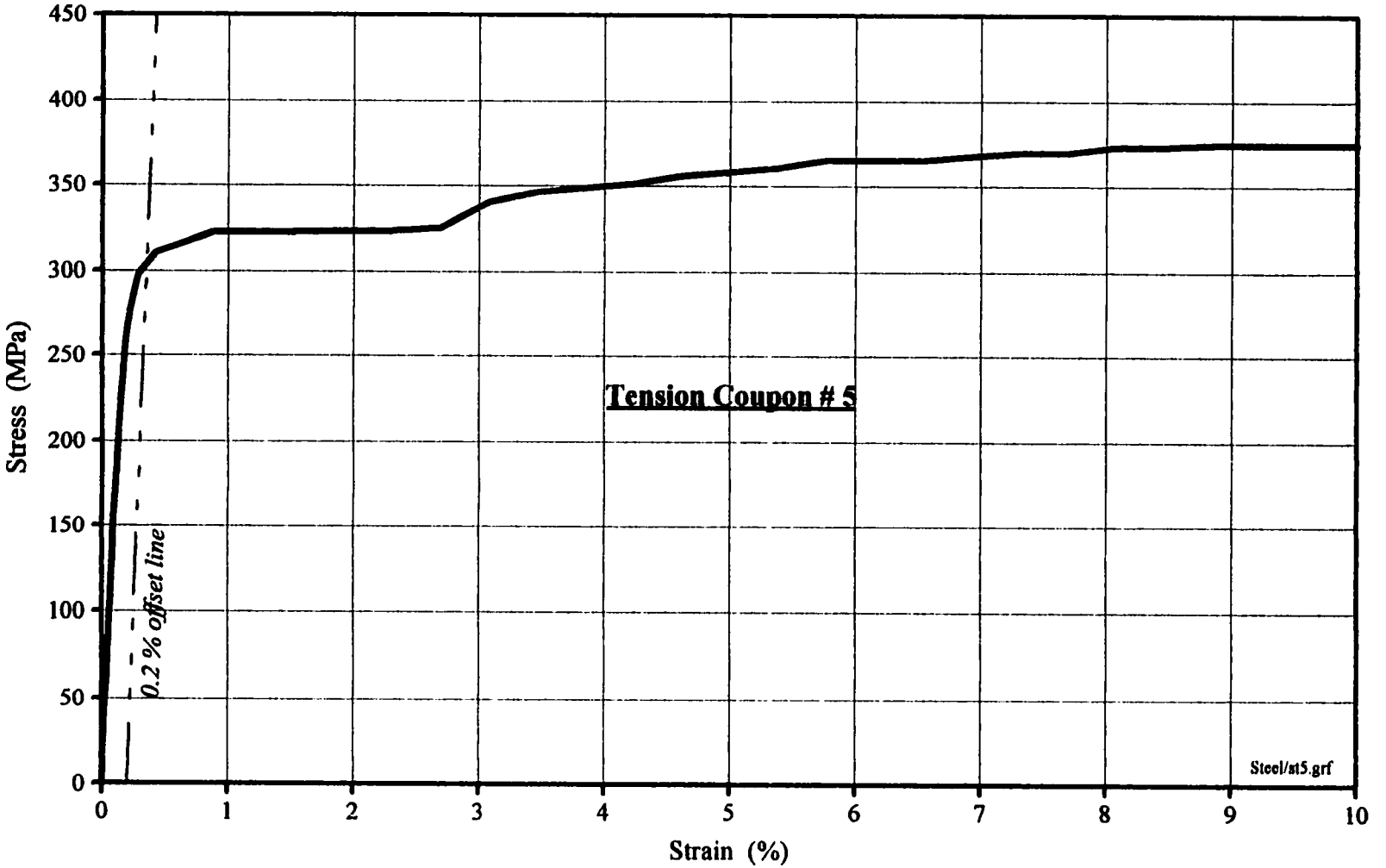

Figure 2.5 : Stress-Strain Curve for Steel Tension Test Specimen # 5

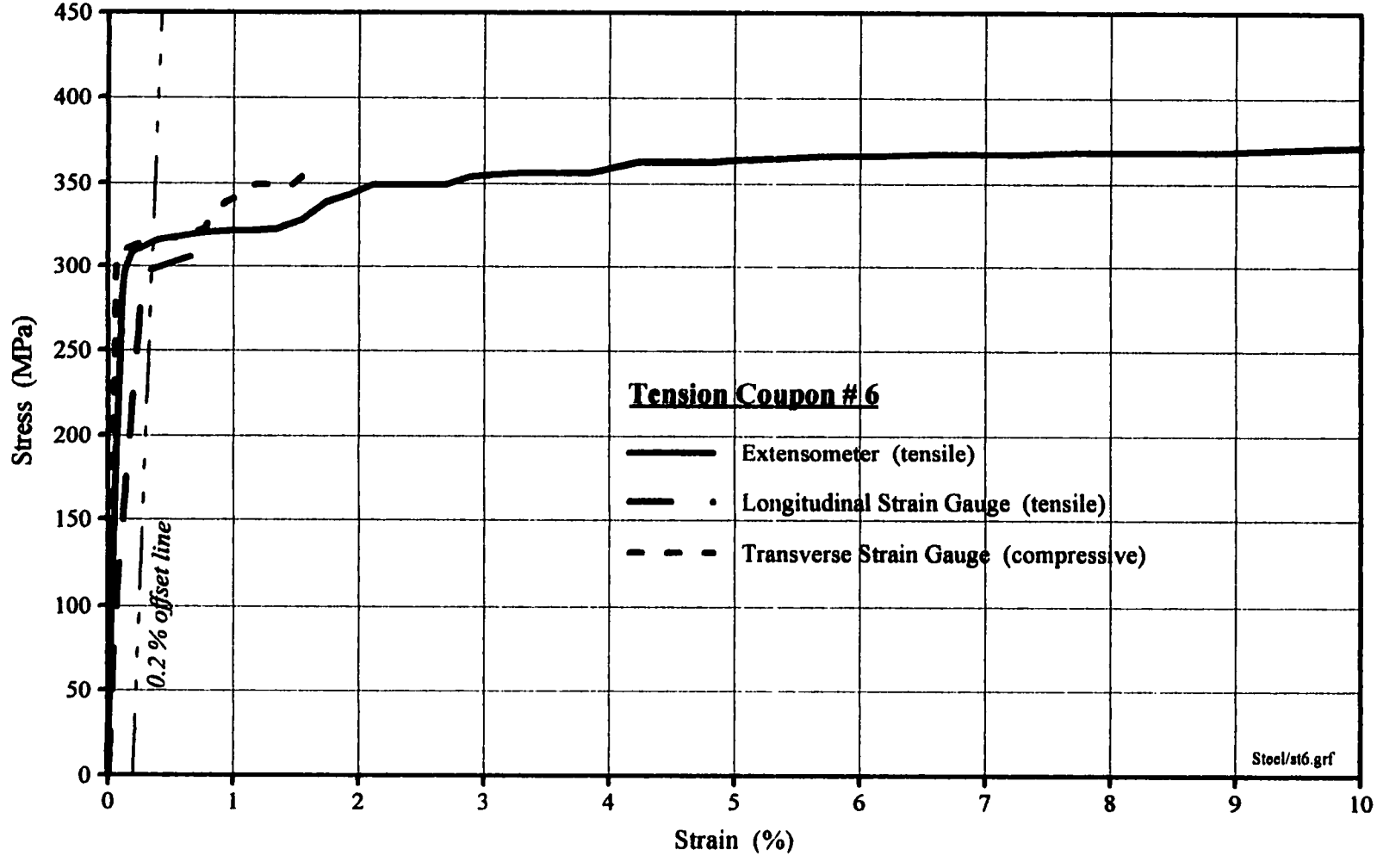

Figure 2.6 : Stress-Strain Curves for Steel Tension Test Specimen # 6

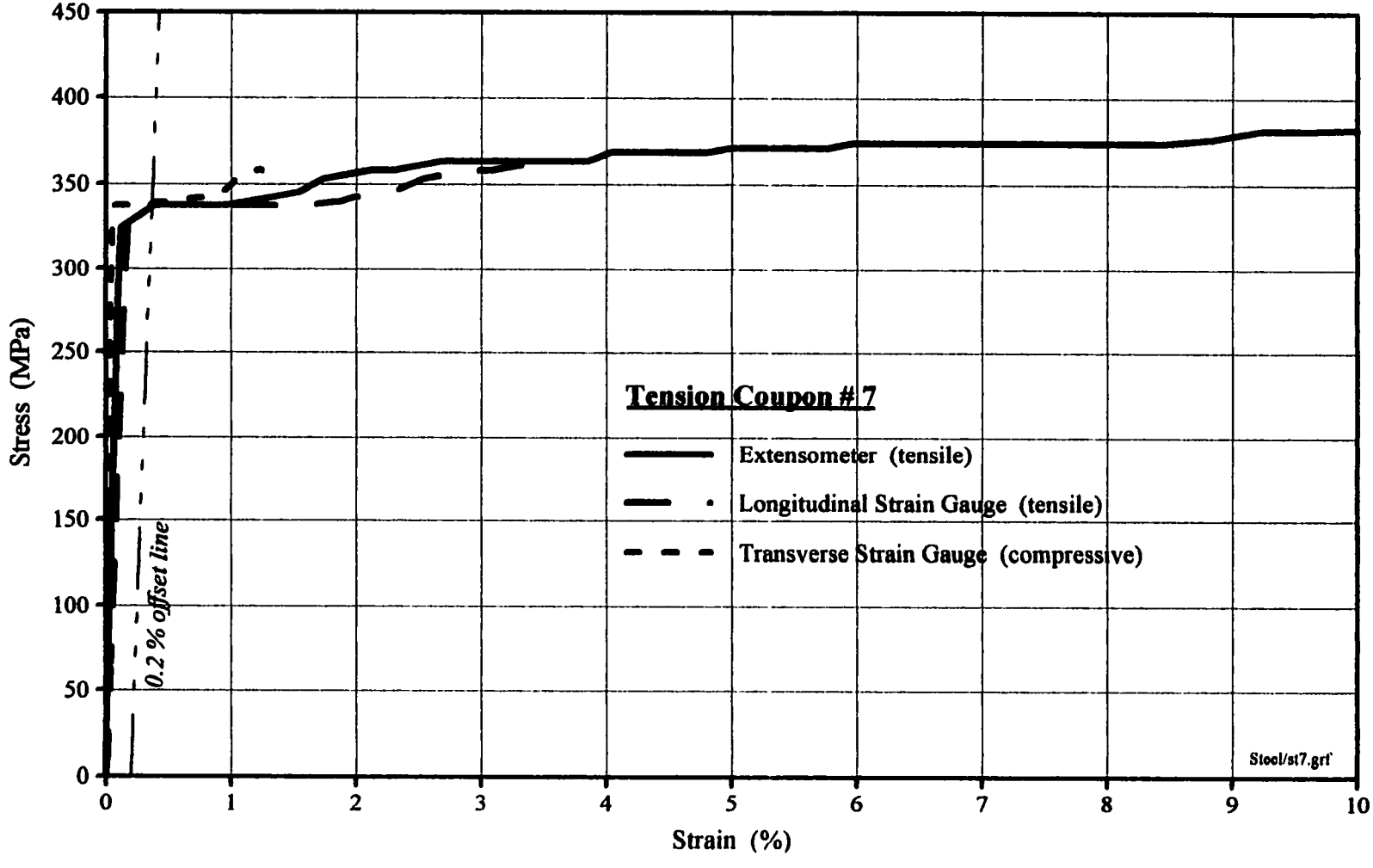

Figure 2.7 : Stress-Strain Curves for Steel Tension Test Specimen # 7

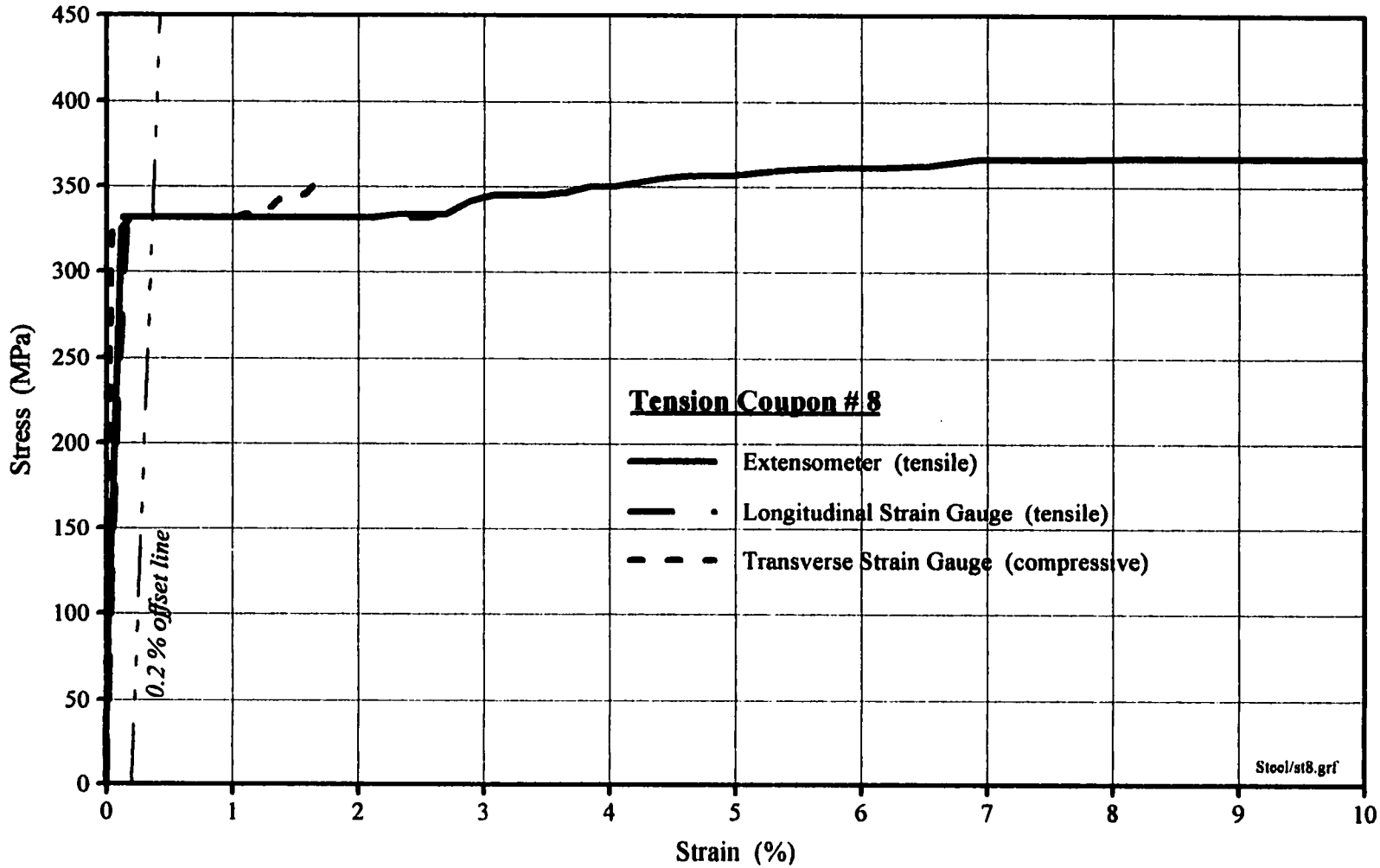

Figure 2.8 : Stress-Strain Curves for Steel Tension Test Specimen # 8

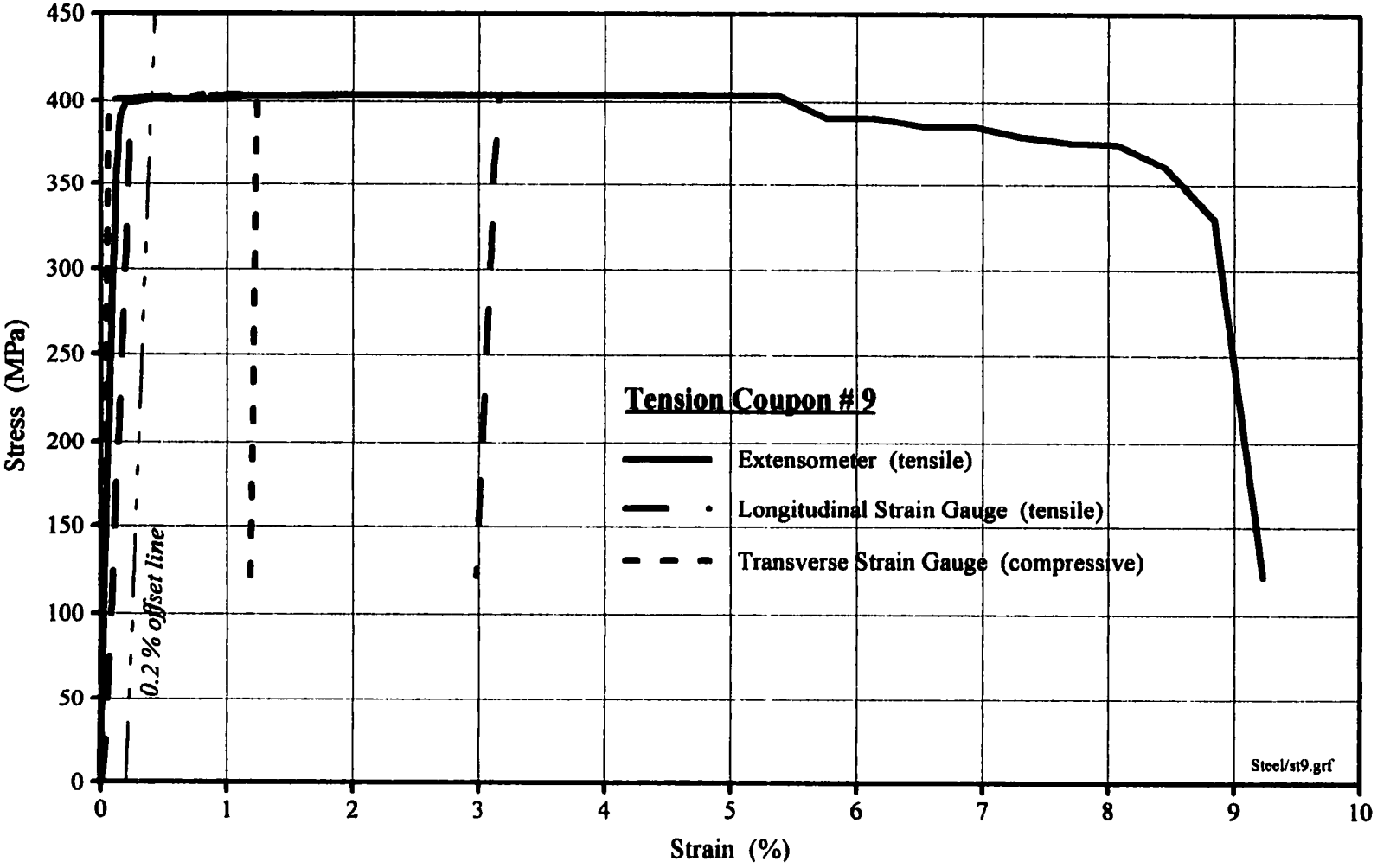

Figure 2.9 : Stress-Strain Curves for Steel Tension Test Specimen # 9

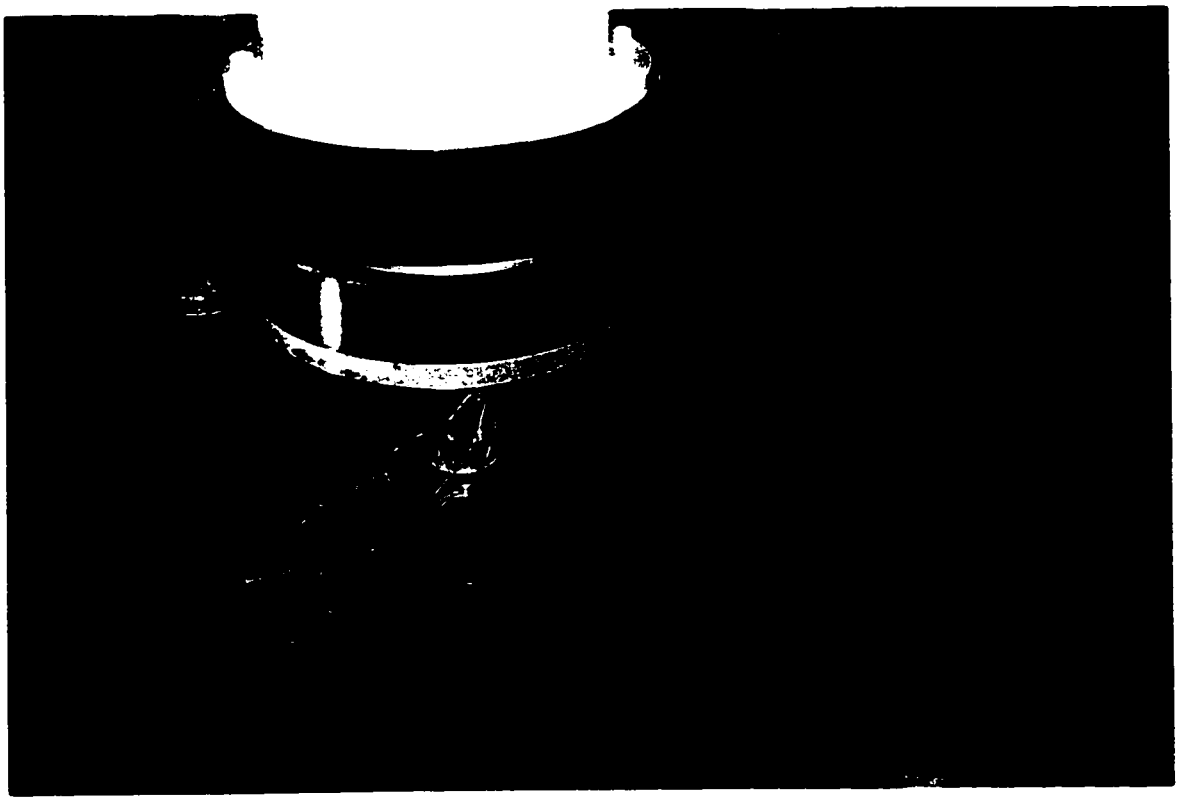

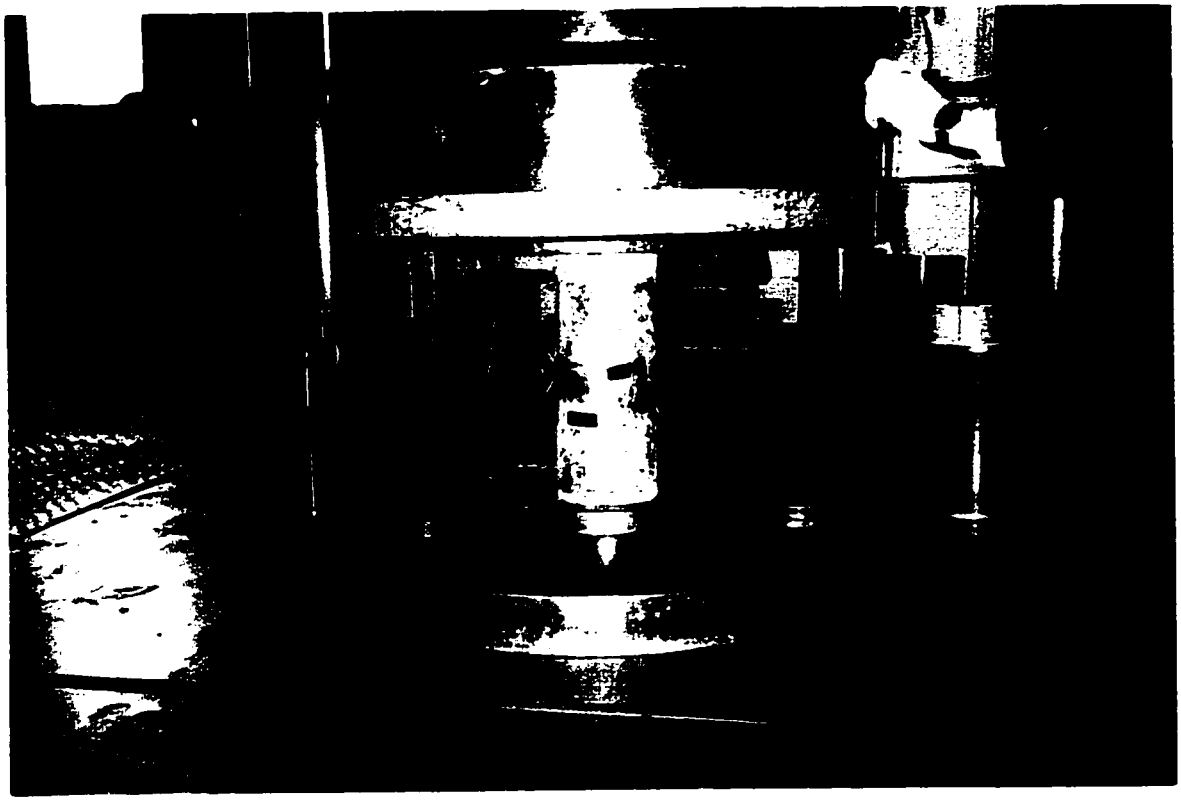

Figure 2.10 : Views of Test Setup for Short Column Specimen ST1

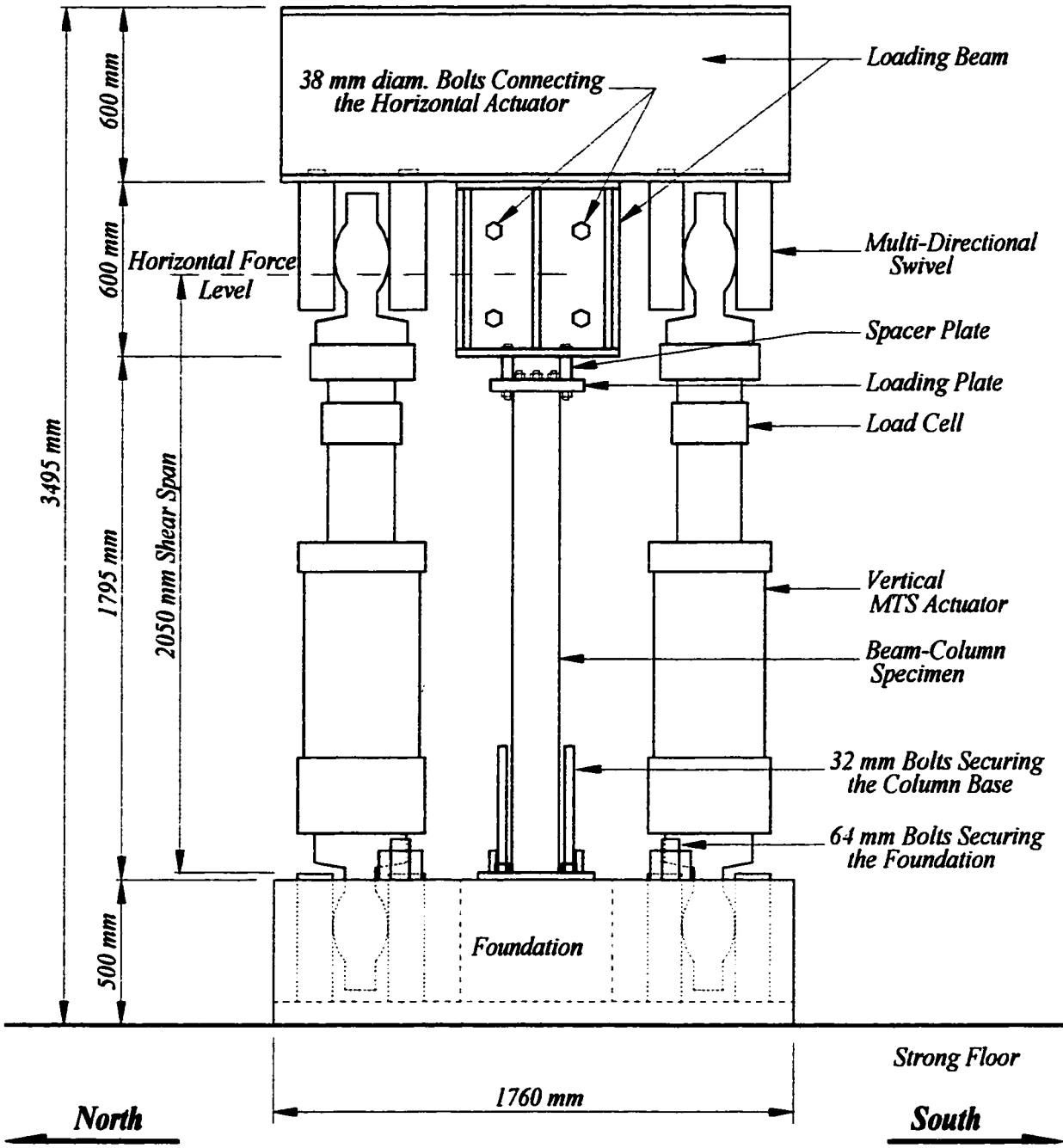

Figure 2.11 : Test Setup for a Beam-Column Specimen
Front View

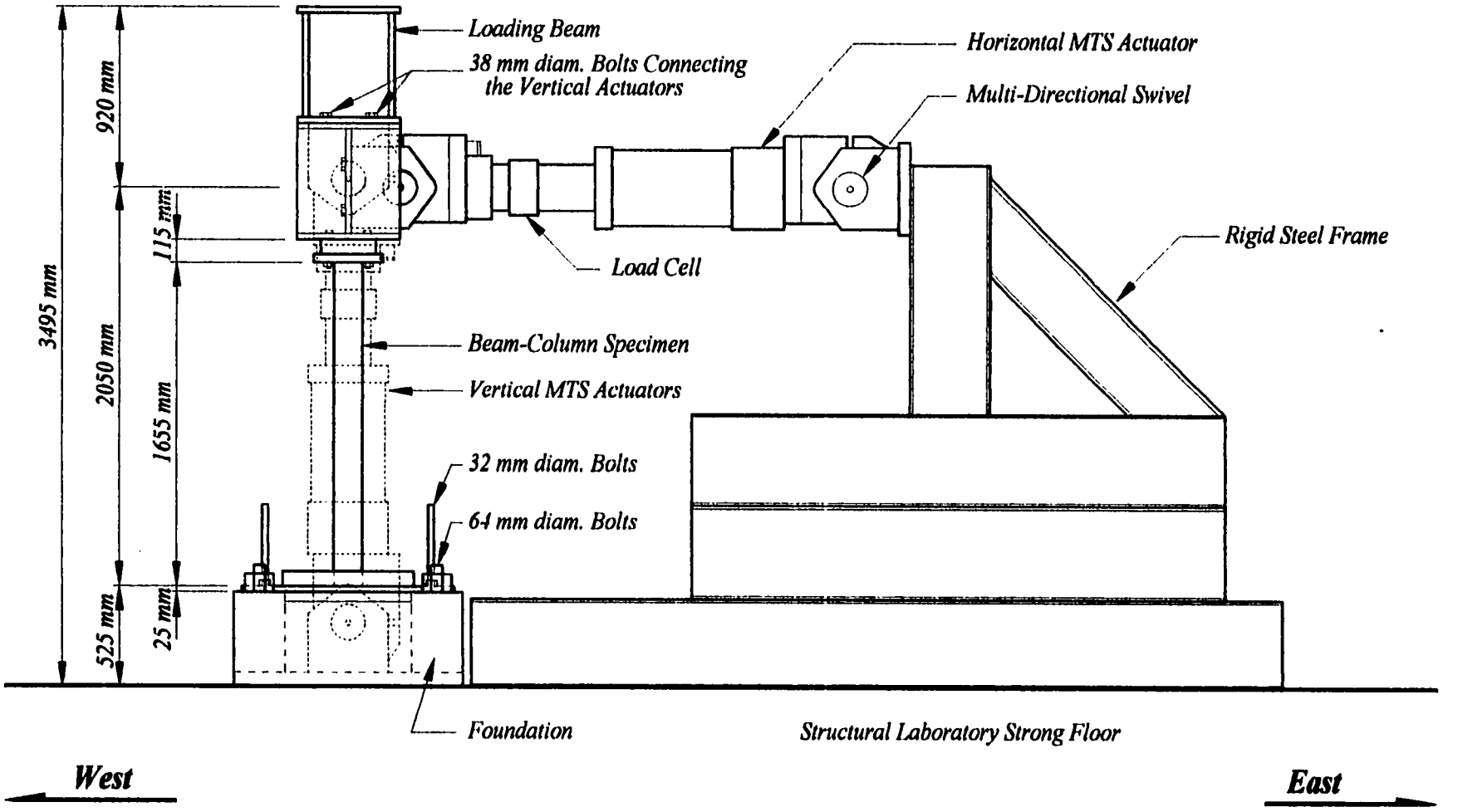

Figure 2.12 : Test Setup for a Beam-Column Specimen
Side View

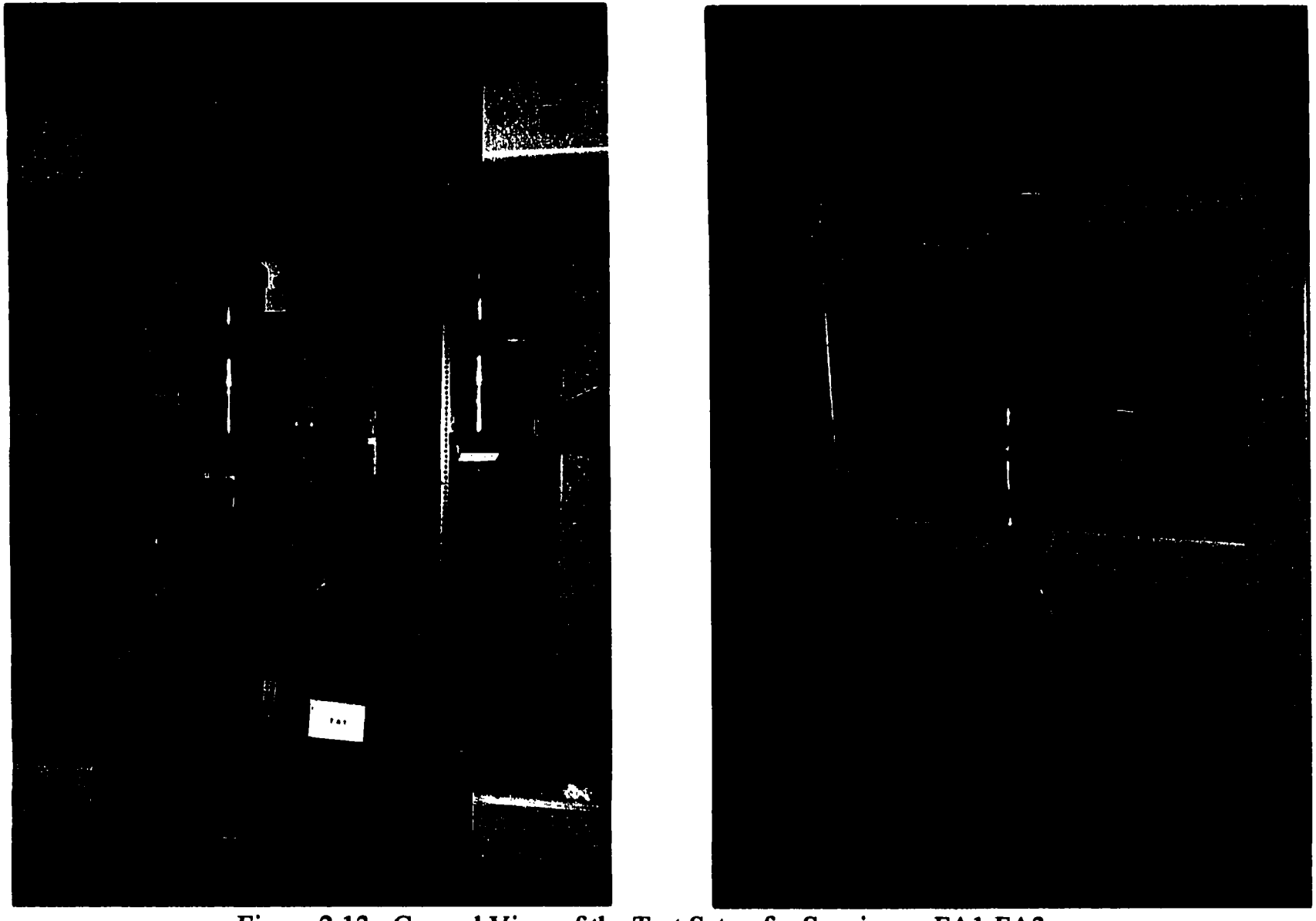

Figure 2.13 : General View of the Test Setup for Specimens FA1-FA3

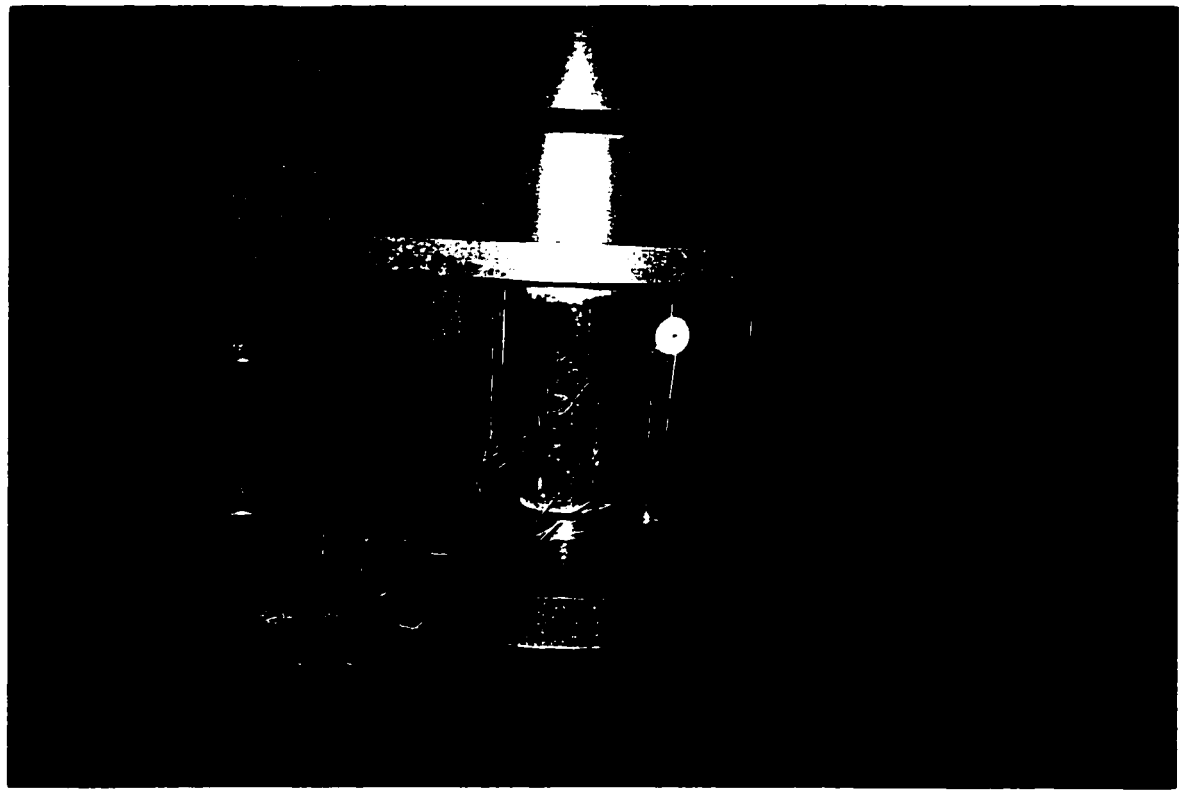

Figure 2.14 : Instrumentation of Short Column Specimen ST1

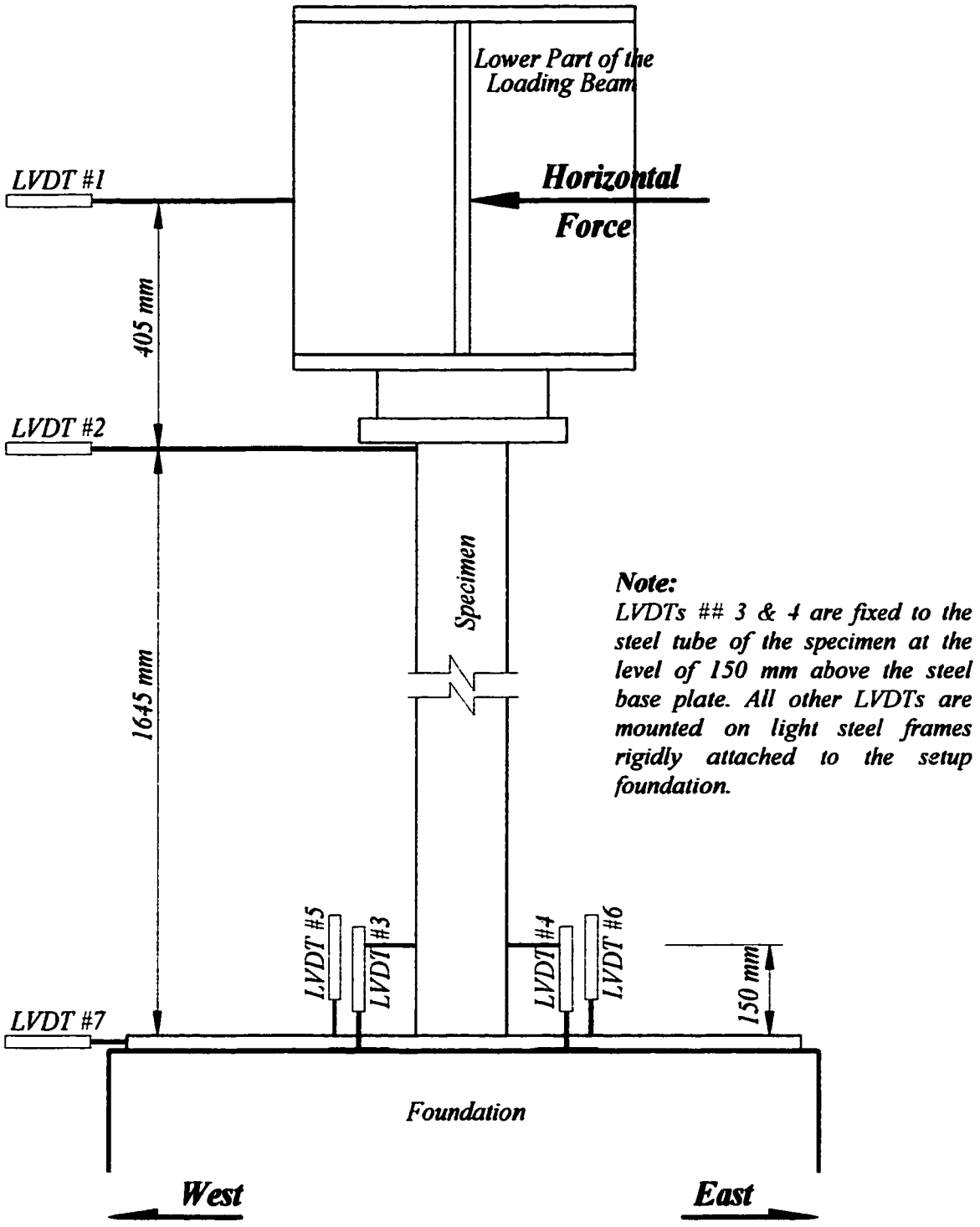

Figure 2.15 : Scheme of LVDT Locations

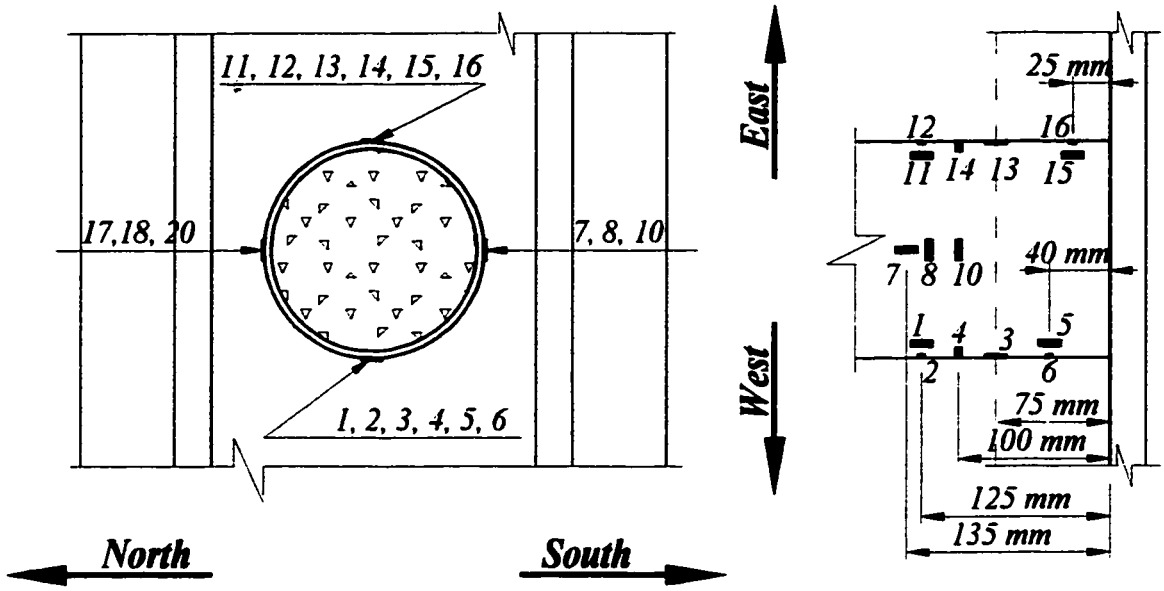

Plan View

South Side View

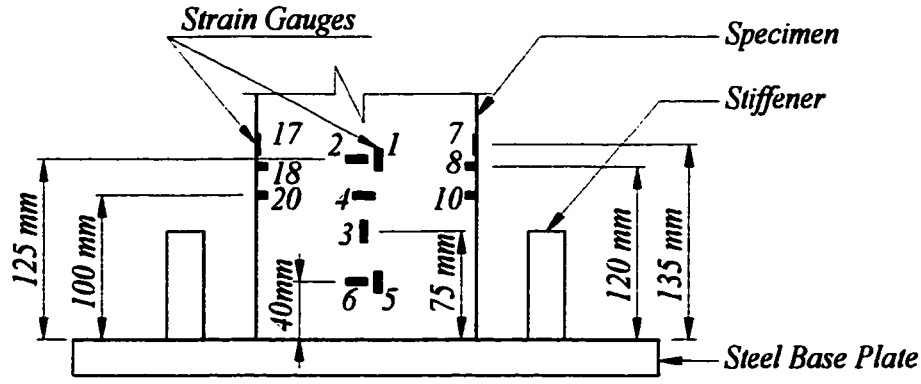

West Side View

Figure 2.16 : Strain Gauges for Beam-Column Specimens

Figure 2.17 : Instrumentation of Beam-Column Specimens FA1-FA3

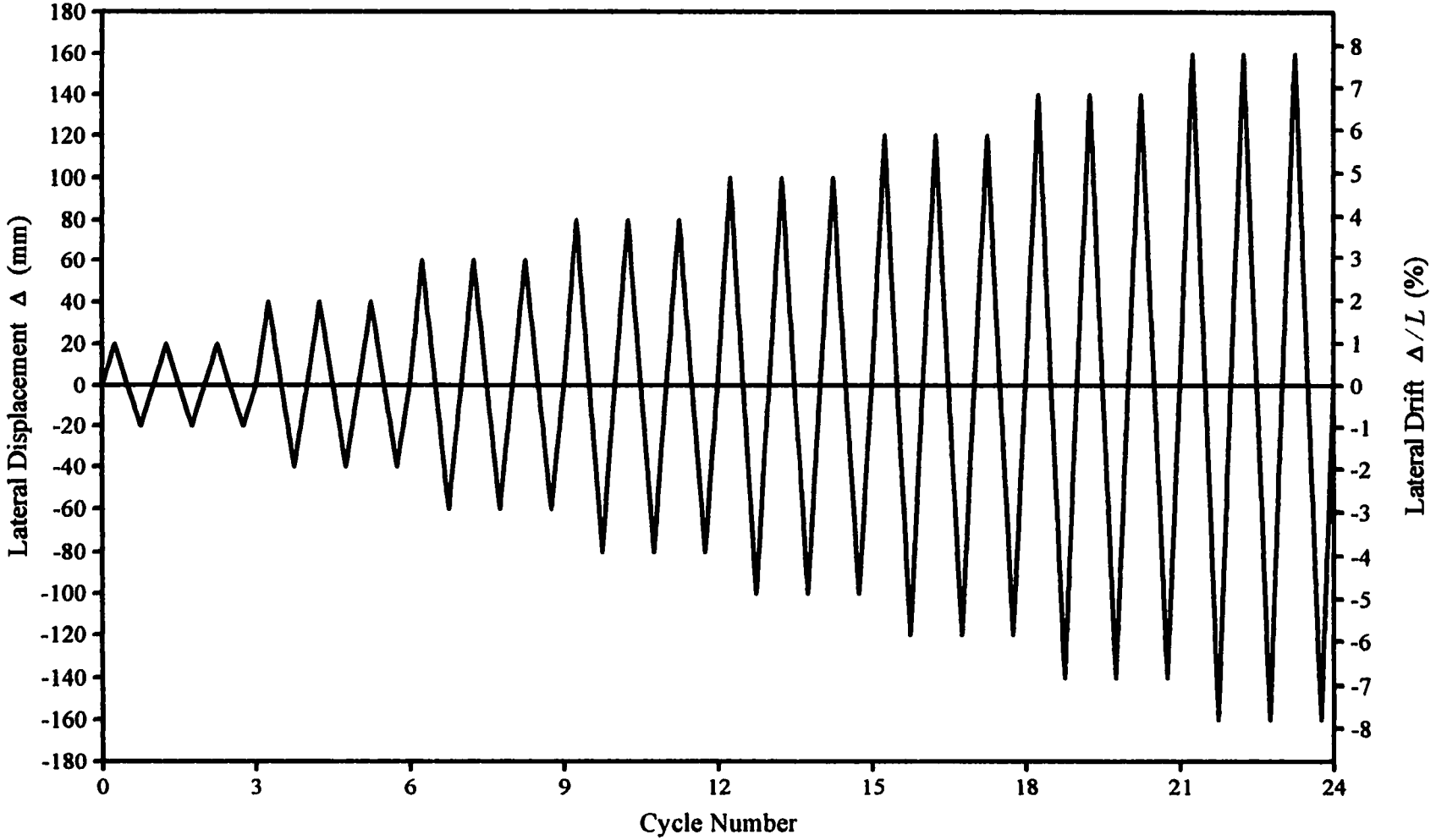

Figure 2.18 : The Path of Lateral Displacement Reversals

Chapter 3

Observed Behavior

The data recorded during column tests is presented in this chapter in several graphical formats. Load-displacement plots illustrate the strength and deformation characteristics of the columns. Moment-rotation and displacement-rotation relationships for beam-column specimens are presented as well. Longitudinal and transverse strains in the steel tube, or strain ratios, are plotted against applied forces or displacements. Experimental visual observations are described and illustrated with photographs. Some behavior patterns are discussed shortly.

The sign convention for strains throughout this chapter is positive for compression and negative in tension. However, when strain ratios are introduced, analogous to Poisson's ratio, both compressive strains in the longitudinal direction and tensile strains in the transverse direction are treated as positive. For beam-column specimens, lateral forces and lateral displacements are positive in the West-bound direction and negative in the East-bound direction. Accordingly, the West side of beam-column specimens will be referred to as "positive side", and the East side will be referred to as the "negative side". Moments, rotations and curvatures, generally associated with positive lateral forces and displacements, are positive, and vice versa.

3.1 Short Column

Specimen ST1 failed at axial compressive load $P_{exp} = 2157\ kN$, which was 16.7% higher than the nominal axial capacity of the specimen $P_0 = A_s f_y + A_c f_c' = 1849\ kN$. The failure mode was brittle, triggered by shear failure of the concrete core. The shape of the specimen after the test,

illustrated in Figures 3.1 and 3.2, clearly indicates this shear failure mode. The concrete core separated into two main parts with the upper wedge sliding down along the failure surface. The axial load at this stage dropped to the level of 1068 kN, which is slightly below half of P_{exp}. This reduced load-carrying capacity level was maintained almost constant by the resistance mechanism supported, primarily, by the hoop tension in the steel tube and the friction between the two concrete wedges. When the sliding upper wedge reached the steel plate at the bottom, effectively increasing the area under compression, the axial load started to increase again. Similar behavior of short circular HSCFT specimens under concentric compressive loads was reported by Prion and Boehme (1994).

Figure 3.3 shows the vertical load-displacement relationship for the specimen ST1. The ascending curve plotted with a solid continuous line indicate the step-by-step loading when the displacement readings from the dial gages were taken at every loading step. The last column shortening measurements were taken at the load level of 2137 kN. The rest of the relationship is shown in a dotted line, indicating that only axial loads were monitored at that time. The column failure was very abrupt and the resulting unloading occurred in about 3 seconds. The testing continued for about 30 seconds after that. No readings from any of the instrumentation devices were taken during this period. The displacements at this stage were estimated from the deformed shape of the specimen after the test.

The analysis of the ascending curve plot of axial load versus specimen shortening reveals that the initial axial stiffness of the short column was somewhat smaller than its stiffness at intermediate load levels. This reflects in part the difficulty of achieving full proportional loading of both concrete and steel simultaneously from the start of loading, because of unavoidable imperfections at the end surfaces of the specimen. The axial stiffness increased gradually from the initial value of 15 500 MPa to a maximum of 29 700 MPa in the load range of 800-1400 kN. With increasing load after that, it gradually decreased to 5 600 MPa just prior to failure. The maximum, experimentally obtained, stiffness value for the composite section is about 20 % less than the modulus of elasticity that could reasonably be expected from the concrete core alone. This fact is difficult to explain. The reduced stiffness reflects the high level of average axial compressive strain achieved by the specimen. This strain, measured by the dial gages, exceeded 6000 με at failure (more than twice the strain level achieved by standard concrete cylinders). The strains measured by the electric resistance strain gauges on the outer surface of the steel tube at the

midheight of the specimen suggest that most of this shortening took place at the ends of the specimen.

The data recorded from the electric resistance strain gauges is presented in Figure 3.4 plotted versus the axial load. Two longitudinal strain gauges (#5 and #11) malfunctioned at the beginning of the test and their readings were not recorded. Load-strain curves reflecting the average longitudinal and transverse strains measured at the midheight of the steel tube are shown in Figure 3.5. To allow for comparison, both figures show the load-specimen shortening curve as well.

From the electric resistance strain gauge data, it could be observed that the average transverse tensile strain in the steel tube at the midheight of the column specimen first exceeded the average longitudinal compressive strain at the load level of 980 kN. Transverse strain gauges #2 and #12 (the shear failure line later passed between these two locations) measured tensile strains in excess of 2 000 με as early as at load level of 1603 kN, when the longitudinal compressive strains were only about 1 000 με. It looks like the steel tube at the midheight section was completely yielded at the load level of about 1950 kN (yielding in some separate locations probably occurred earlier). With greater loads, a sharp increase in the circumferencial tensile strain was observed at all measurement locations, suggesting that the steel tube is actively engaged in the passive lateral confinement of concrete core. Most of the longitudinal gauges at this stage showed decreases in compressive strain levels, indicating that the load was partially redistributed from the steel tube to the concrete core.

The general trend was that both longitudinal compressive and circumferencial tensile strains increased gradually at every particular point on the steel tube with the increase in the axial load. This trend would indicate that longitudinal compressive or circumferencial tensile stresses or both had increased. However, it could be clearly observed from the stain gauge data, that at many load steps an increase in the longitudinal compressive strain at certain locations (sometimes, at all locations at the midheight section) was accompanied by a decrease in the hoop tensile strain at these locations, or vice versa, with an increase in axial load longitudinal compressive strains decreased while the corresponding hoop tensile strains increased. One possible explanation for this inconsistency could be that the steel tube wall formed waves along the specimen. These waves are illustrated in Figure 3.6 in an exaggerated manner. The waves are probably caused by the irregularities in the geometrical dimensions of the tube and the material properties of the steel.

They have very small amplitudes and cannot be observed visually. The lengths and amplitudes of these waves change with the increase in axial load, causing the described inconsistencies in the strains at the outer surface of the steel tube. Of course, this hypothesis needs further verification. If it is true, however, it implies that the chemical bond between steel and concrete is lost at very early stage of loading, and the bond between steel and concrete depends entirely on the geometrical imperfections of the steel tube. The waves will tend to strengthen the bond because they magnify the imperfections and provide the points of concrete-steel interaction.

3.2 Beam-Columns

Specimens FA1-FA3 were tested under a system of vertical and horizontal loads acting with continuously changing eccentricities as the horizontal reversals were applied. The most significant eccentricity, associated with the action of the axial load, was accounted for in the calculations of the bending moments acting at the base of the beam-columns. This eccentricity reflected the vertical and horizontal misalignments between the positions of specimen cross-section at the steel base plate and the swivels at the bottom of the vertical actuators. The vertical misalignment was 210 mm, while the horizontal misalignment varied between specimens within 4-6 mm. Although the position of the multidirectional swivels at the top of the vertical actuators was 80 mm above the horizontal actuator level, the vertical load was assumed as acting at the point of inflection, and the associated additional eccentricity was considered negligible. All other misalignments and eccentricities were neglected as well. The scheme of forces, which acted on a typical beam-column specimen, is shown in Figure 3.7. The base moments were computed using the formula shown in this figure. The weight of the loading beam and the horizontal actuator, although not shown in the scheme for simplicity, was estimated $W = 10\ kN$, assumed acting at the point of inflection, and included in the calculation of the base moments.

The lateral load-displacement relationships are presented for two imaginary classical cases : "lateral load includes second order effects" and "lateral load does not include second order effects". In the first case, illustrated in Figure 3.8, the axial load is assumed acting always in the direction of the center of the column base, so that no P-Δ effect occurs. The lateral load in this case is calculated simply from the base moment divided by the shear span. In the second case, illustrated in Figure 3.9, the axial load always acts strictly vertically and produces the moment component P-Δ at the base of the column, so that the lateral load has to be reduced by a value

proportional to this component. The second format of lateral load-displacement relationships is presented in this thesis to illustrate and emphasize the fact, that tested beam-columns were slender and sensitive to second order effects. Columns having slenderness similar to that of the tested specimens cannot be used in practice, unless horizontal sway is prevented, or the axial load is very low.

The stiff steel base plates performed very well in all three beam-column tests. The groove weld connections of the specimens to their base plates also proved to be reliable. The rotations of the steel base plates, measured by LVDTs #5 and #6, were at least one order less than the rotations provided by the hinging regions of the beam-columns at all phases of loading. A typical curve of steel base plate rotation plotted versus lateral displacement at the point of inflection is presented in Figure 3.10. The rotations ranged within ±0.0008 rad in the case of specimen FA3. The base rotation range was larger for columns with lower axial loads. For specimen FA1, which was axially loaded with 400 kN, this range was ±0.002 rad. In the case of specimen FA2, the steel base rotations were within ±0.0007 rad when the axial load was held at 1000 kN. When the load was decreased to the level 100 kN, the range of base rotations increased to ±0.0025 rad. In all cases, the steel base plate rotations were considered negligible compared to the rotations generated by the flexure of the specimens in the hinging region. The horizontal slip of the steel base plate relative to the foundation in the direction of the applied lateral load was measured by LVDT #7 during testing of specimen FA1 only. The recorded displacements never exceeded 0.25 mm in either positive or negative direction and were considered not important, so that no measurement of horizontal slip was employed in subsequent tests.

The length of the hinging region for the tested beam-column specimens was assumed to be approximately equal to the diameter. The rotations of beam-column sections at 150 mm above the steel base plate were measured by LVDTs #3 and #4. These rotations (which include the earlier mentioned negligible rotations of the base plate) reflecting the amount of flexure in the hinging region are presented in this section plotted versus base moments and lateral deflections at the inflection point. Average curvatures (computed from these rotations) within the hinging region are verified against curvatures computed from the strain gauge data.

The strains recorded from the electric resistance strain gauges during beam-column tests are presented in Appendix A. Transverse/longitudinal strain ratios are presented in this section plotted

versus lateral displacements. The data used for these ratios reflects only the strains corresponding to extreme positive and negative lateral displacements in each loading cycle. Where possible, section curvatures are computed from the measured strain data to investigate the variation of flexure intensity along the assumed hinging region. For clarity, some loops in the moment-curvature plots are marked with figures indicating the lateral displacement reversals applied (e.g. the mark "-3/2" will indicate, that the marked part of the curve corresponds to the second travel to the lateral drift level of -3%).

The behavior of each tested beam-column specimen is described separately in the following subsections. The overall discussion of the test results is presented in Chapter 4.

3.2.1 Column FA1

Specimen FA1 was tested under axial compression of 400 kN. The horizontal displacement cycles were applied up to the lateral drift level of ±8% when the decrease in lateral load resistance slightly exceeded 20%. Figure 3.11 illustrates the specimen during testing at drift levels of +4% and +5%. Local buckling of the steel tube in the hinging zone of the specimen first occurred on the positive side during the second travel to the displacement level of +100 mm (+5% drift). The buckle was visually observed to start forming when the lateral displacement was about +30 mm. During the next reversal to the negative side (second travel to drift level of -5%) the tube buckled on the other side as well. Vertically, the buckles were located at about 70 mm from the steel base plate on the positive side and about 100 mm on the negative side. Figure 3.12 illustrates the hinging region of specimen FA1 after the test.

The hysteretic force-displacement relationships are presented in Figures 3.13 and 3.14. The maximum moment resistance in both directions was attained during the first cycle at the drift level of ±4 %. The experimental moments were +50.098 kNm and -48.394 kNm, with the average of $M_{exp} = 49.246\ kNm$. With further cycles the lateral strength gradually deteriorated to about 80% of the maximum capacity at the drift level of ±8%. It could be also observed from the case "lateral load does not include second order effects", that the P-Δ effects would be very significant for such a slender column even at this relatively low axial load level of $0.2\ P_0$.

Figures 3.15 and 3.16 show the moment-rotation and displacement-rotation curves. The average curvatures within the hinging region were about +125 rad/km and -100 rad/km when extreme positive and negative moments, respectively, were attained at the lateral drift level of ±4%. The flexure within the hinging region was providing about half of the rotation necessary for the drift at that time. Average curvatures in excess of 160 rad/km on both sides were attained before local buckling occurred. Column curvature at a section 75 mm above the base plate, computed from the strain gauge data, is presented in Figure 3.18 and agrees fairly well with the average curvature in the hinging zone. At the lateral drift level of ±8%, the average curvatures in both directions slightly exceeded 400 rad/km and the hinging region was supplying about 3/4 of the required rotations (or drift).

Electric resistance strain gauge data for column FA1 is presented in Figures A.1 through A.8. It indicates that the steel tube yielded both in compression and in tension on the positive and negative sides, respectively, during the first travel to the lateral drift level of +3%. North and South sides of the tube yielded in tension during the first travel to +4% drift, which suggests that the whole section was in plastic state at that time. Longitudinal strains of at least 8000 με in compression and 18000 με in tension were recorded on the positive and negative sides of the hinging region at 75 mm above base before local buckling occurred.

Strains recorded from gauges #15 and #16, which were located on the negative side only 25 mm above the base plate, suggest that the steel tube, practically, did not yield at any time in this location. The strains recorded there ranged from -3200 to +1400 με in the longitudinal direction and from -1000 to +500 με in the transverse direction. It means, the column curvature at 25 mm above base plate never exceeded 40 rad/km. This is consistent with the reinforcing effect of the steel base plate, which, by restraining circumferencial expansions or contractions of the neighboring part of the steel tube, applied passive compression or tension to tube walls in the transverse direction, thus increasing the yield strength of the tube in the longitudinal direction. The presence of the base plate also made the concrete core in the neighboring part of the column much better confined. As a result, the column sections adjacent to the base plate became much stronger and stiffer than the less affected upper sections. This implies that the 30-60 mm long zone at the bottom of the column was developing curvatures less than the average, while the rest of the hinging region needed to develop curvatures in excess of the average to compensate for the shortage. The reinforcing effect of the steel base plate also shifted the area of the extensive

column damage (local buckling zone) to at least 60 mm away from the plate. In contrast to that, similarly tested columns (Boyd et al, 1995), which were anchored into a reinforced concrete footing, exhibited local buckling just above the footing.

The development of circumferencial strains in the steel tube is illustrated in Figure 3.17 where strain ratios for pairs of neighboring transverse and longitudinal stain gauges are plotted. Strain gauge pairs #4/#3 and #14/#13, located in the area of the potential extensive damage, showed that the ratio of tensile transverse strain to compressive longitudinal strain in the steel tube wall in the compression zone of the column's section approached or exceeded unity at the drift level of ±4% when the maximum bending moment capacities were attained in both directions. This suggests that the concrete core confinement mechanism was indeed initiated. It also implies, that the magnitudes of tensile circumferencial stresses at the extreme steel fibers of the compression zone of the section were equal to or greater than the longitudinal compressive stresses at that time.

3.2.2 Column FA2

Specimen FA2 was initially tested under an axial load of 1000 kN. The lateral loading continued until the second travel to the lateral drift level of +3%. During this test considerable horizontal displacement (up to 40-50 mm) at the point of inflection gradually developed in the South-bound direction (perpendicular to the direction of the applied horizontal load). The main reasons for this deflection were the 7-10 mm eccentricity in the positioning of the four 19 mm diameter bolts embedded in the concrete core at the top of the specimen and the high level of axial load applied. Probably, other eccentricities present in the loading system contributed to this deflection as well. As a result of this deflection, as shown in Figure 3.19, the loading beam was about to touch the steel frame on the south side of the test setup. At this stage, it was decided to stop the test. From the shape of the experimental load-deflection curves, it was concluded that column FA2 had already attained its maximum lateral resistance capacity (at the mentioned axial load level of 1000 kN) at the drift level of ±3%. It was decided to continue the testing under a lower axial load level in order to minimize the effect of the eccentricity and prevent the undesirable displacements in the South-bound direction. The next day, the column was brought back to its original position, loaded axially with 100 kN, and the lateral loading was continued starting from the second travel to the drift level of -3%. Local buckling of the steel tube occurred on the positive side during the second travel to the lateral drift level of +5%, and on the negative side during the second travel to the drift

level -6%. The lateral reversals were applied up to the first cycle at the drift level of ±10%. The steel tube was observed to fracture on both sides along the contraflexure lines of the previously formed buckles during this last cycle. Figure 3.20 illustrates the buckles and fractures in the hinging region of column FA2 after the test. The buckles were vertically located about 90 mm above the base plate on the positive side and about 100 mm above the base on the negative side. The fractures in the steel tube suggest that decrease in lateral strength of the column, after local buckling had occurred, could be attributed in part to gradual fatigue deterioration of the tube wall in the zone of severe flexure associated with the buckle.

Figures 3.21 and 3.22 present the load-displacement hysteretic curves for specimen FA2. They show that the bending moment capacity of the column dropped with the decrease of the axial load level. The extreme moments, sustained while the axial load of 1000 kN was applied, were +65.951 kNm during the second travel to +3% drift and -35.552 kNm during the first travel to -3% drift, which make the average moment $M_{exp} = 50.751\ kNm$. After the axial load was decreased to the level of 100 kN, the experimental moment capacities of +43.497 kNm and - 31.093 kNm were obtained, and that the average moment capacity for the axial load level of 100 kN was only 37.294 kNm. In the plot where "lateral load does not include second order effects", the P-Δ effects appear to be much less significant at the axial load level $0.06\ P_0$.

Figures 3.23 and 3.24 show the rotation provided by the hinging region plotted versus base moment and later displacement, respectively. Rotation at the top of the column is presented in Figures 3.25 and 3.26. Average curvature within the hinging region was about 0 when the extreme negative moment was attained during the first travel to -3% drift. During the next reversal in the positive direction, when the maximum positive moment was attained, average curvature of +145 rad/km developed in the hinging region. At the same time, during the first cycle at drift level of ±3%, more rotation at the top developed in the negative direction than in the positive. Analysis of these rotations suggests that the specimen formed a double curvature shape at the bottom, with the most of the flexure in the positive direction provided by the hinging region, while the rotation in the negative direction was developing mostly at column sections above the hinging region. Curvatures computed from strain gauge data at column sections 75 mm and 125 mm above base plate, presented in Figures 3.28 and 3.29, respectively, also tend to confirm this point. After the axial load level was decreased to 100 kN, the hinging region was again providing rotations in both directions, with average curvatures exceeding 400 rad/km in both directions at the lateral drift

level of ±9%. Average curvatures of about +200 rad/km and -110 rad/km were attained in the hinging region before local buckling was observed.

Strain gauge data for specimen FA2 is presented in Figures A.9 through A.24. It shows that the steel tube in the hinging region had yielded in compression on both sides as early as during the first cycle at ±2% drift. The South side of the tube also yielded in compression at about that time. There are indications that yielding occurred even earlier at the location of strain gauges #3 and #4. Data from strain gauges #5 and #6, which were located on the positive side only 40 mm above the steel base plate, indicates that strains at this location were considerably less than the strains at higher locations up to the drift level of ±3%, which suggests that the reinforcing effect of the plate (described in the previous subsection) is still pronounce at this distance. Development of circumferencial tensile strains in the steel tube at longitudinally compressed sides of the column tube is illustrated in Figure 3.27. Most of the strain ratios approached or exceeded unity during the first cycle at ±3% drift.

3.2.3 Column FA3

Specimen FA3 was tested under axial load of 700 kN. The horizontal displacement cycles were applied up to the lateral drift level of ±7% when the lateral load resistance in the negative direction completely deteriorated. Figure 3.30 illustrates the specimen during testing at-6% drift. Local buckling on both sides of the steel tube in the hinging region was observed to form during the second cycle at lateral displacement level of ±100 mm (±5% drift). The buckle on the positive side was vertically located at about 100 mm from base plate, while the buckle on the negative side was about 15 mm lower. With further cycles, the buckle on the positive side grew gradually, while the buckle on the negative side straightened up almost completely, and another buckle on the negative side of the tube, at about 410 mm from base, was formed during the second travel to the lateral drift level of -6%. At that time, the double curvature shape of the lower part of the column was clear. Figure 3.31 illustrates the lower part of the specimen after the test.

The force-displacement curves are presented in Figures 3.32 and 3.33. The maximum moment resistances attained were +57.126 kNm and -41.035 kNm. These were obtained during the first travel to +4% drift and first travel to -3% drift, respectively. Higher moment resistance in the

positive direction, attained during the first travel to +7% drift, was considered not representative and neglected. The average experimental bending moment capacity was $M_{exp} = 49.081\ kNm$.

Figures 3.34 and 3.35 present the rotation provided by the hinging region. Figures 3.36 and 3.37 show the rotation measured at the top of specimen FA2. The tendency for the formation of double curvature shape could be traced down to the drift level of ±2% , as indicated by the higher rate of increase in the negative rotation at the top of the column compared to the positive rotation. The average curvature in the hinging region was about -75 rad/km at first travel to -3% drift when maximum moment in the negative direction was attained, and about +90 rad/km at +4% drift when the maximum positive moment was obtained. Starting with the first cycle at lateral drift level of ±6%, the hinging region was providing only positive rotations, while the rotation in the negative direction was developed by flexure of column portion above the hinging region. Average curvature of about +720 rad/km was attained during the first travel to +7% drift. Column curvature at 75 mm above base plate computed from the strain gauge data, and presented in Figure 3.39, show accumulation of positive curvature at this section starting with the first cycle at ±3% drift level.

Data recorded from electric resistance strain gauges of specimen FA3 is presented in Figures A.25 through A.35. Strain gauge #11 malfunctioned at the beginning of the test and its data is not presented. It looks like the steel tube yielded in compression at both sides during the first cycle at ±2% drift. Strains recorded from gauges #1 and #2 suggest that yield occurred at their location as early as during the first travel to +1% drift. On the South and North sides of the tube the steel yielded in compression at the lateral drift level of ±3%. The strain ratios for gauge pairs #1 & #2, #3 & #4, #13 & #14, is presented in Figure 3.38. All ratios approached or exceeded unity at the drift level of ±4% or earlier.

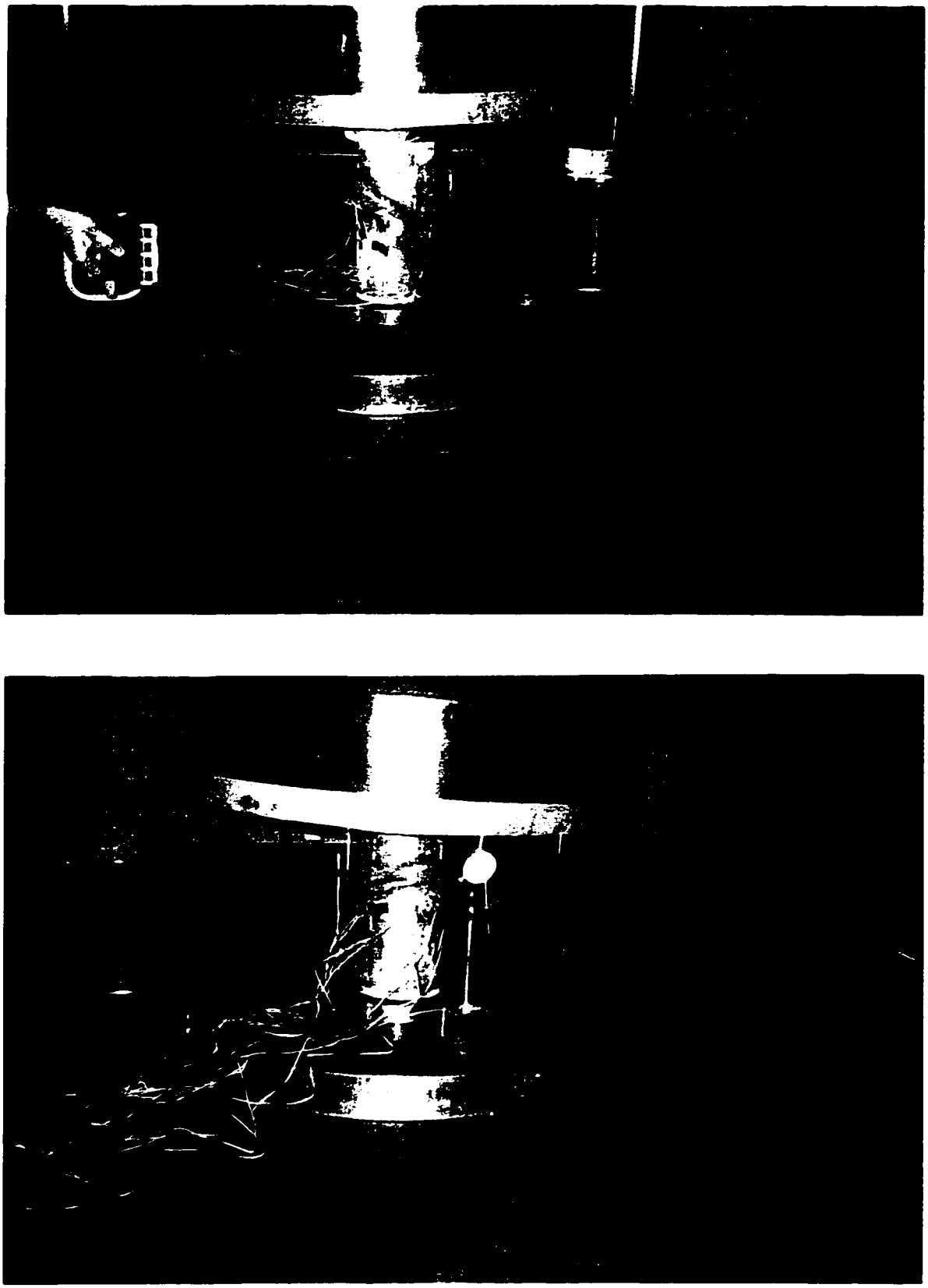

Figure 3.1 : Specimen ST1 during Testing

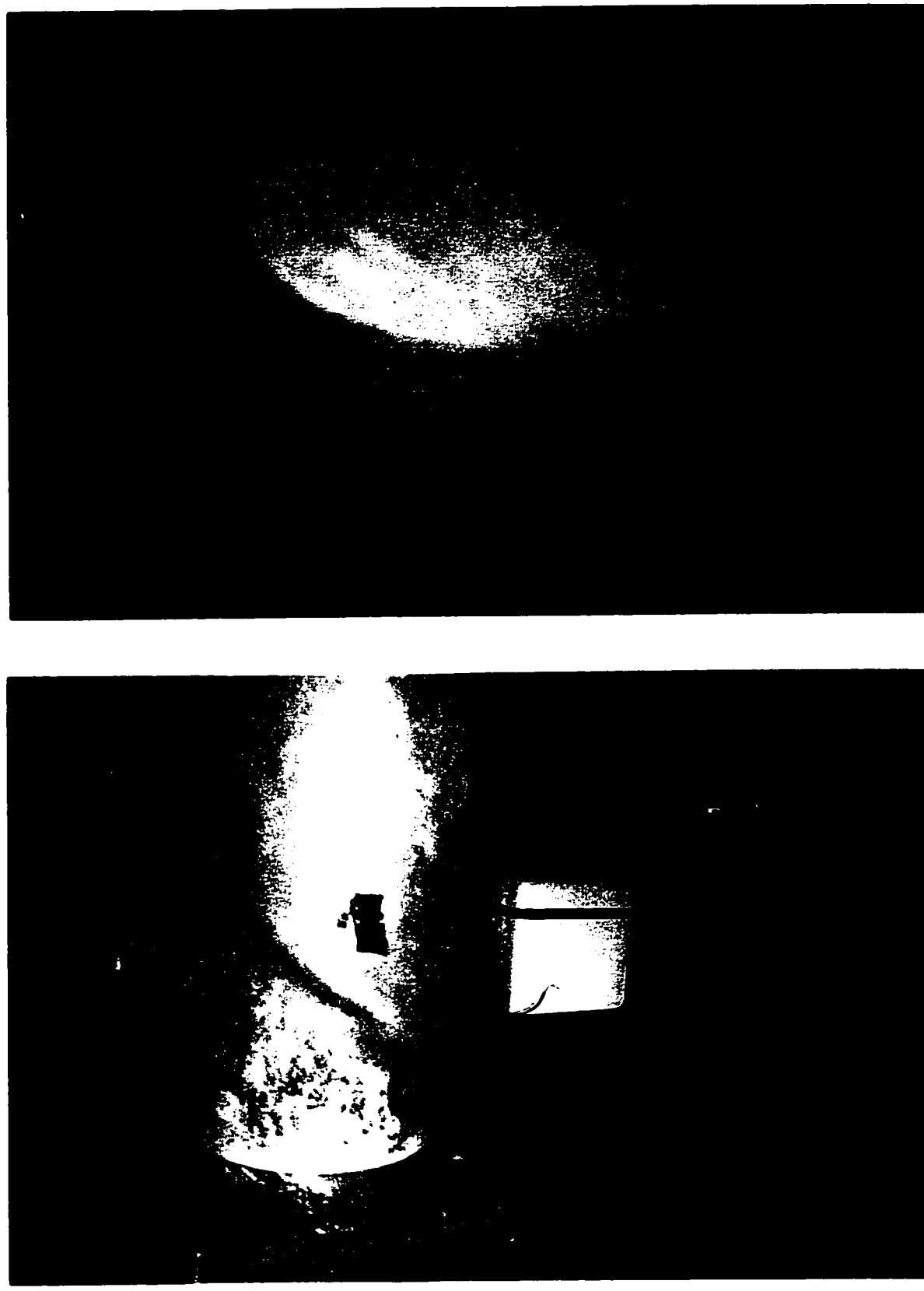

Figure 3.2 : Shape of Specimen ST1 after Failure (specimen is upside down)

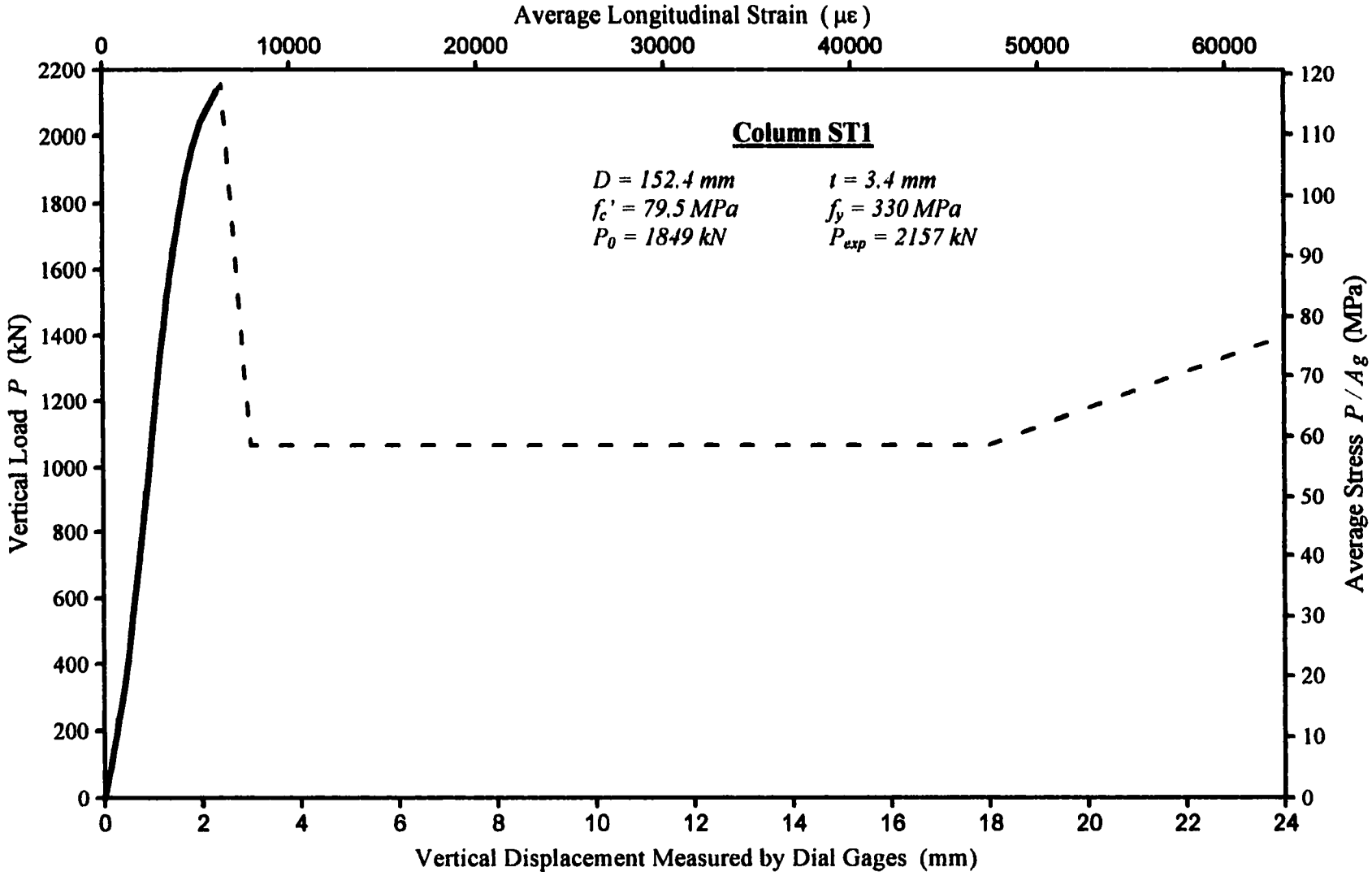

Figure 3.3 : Load-Displacement Relationship for Short Column Specimen ST1

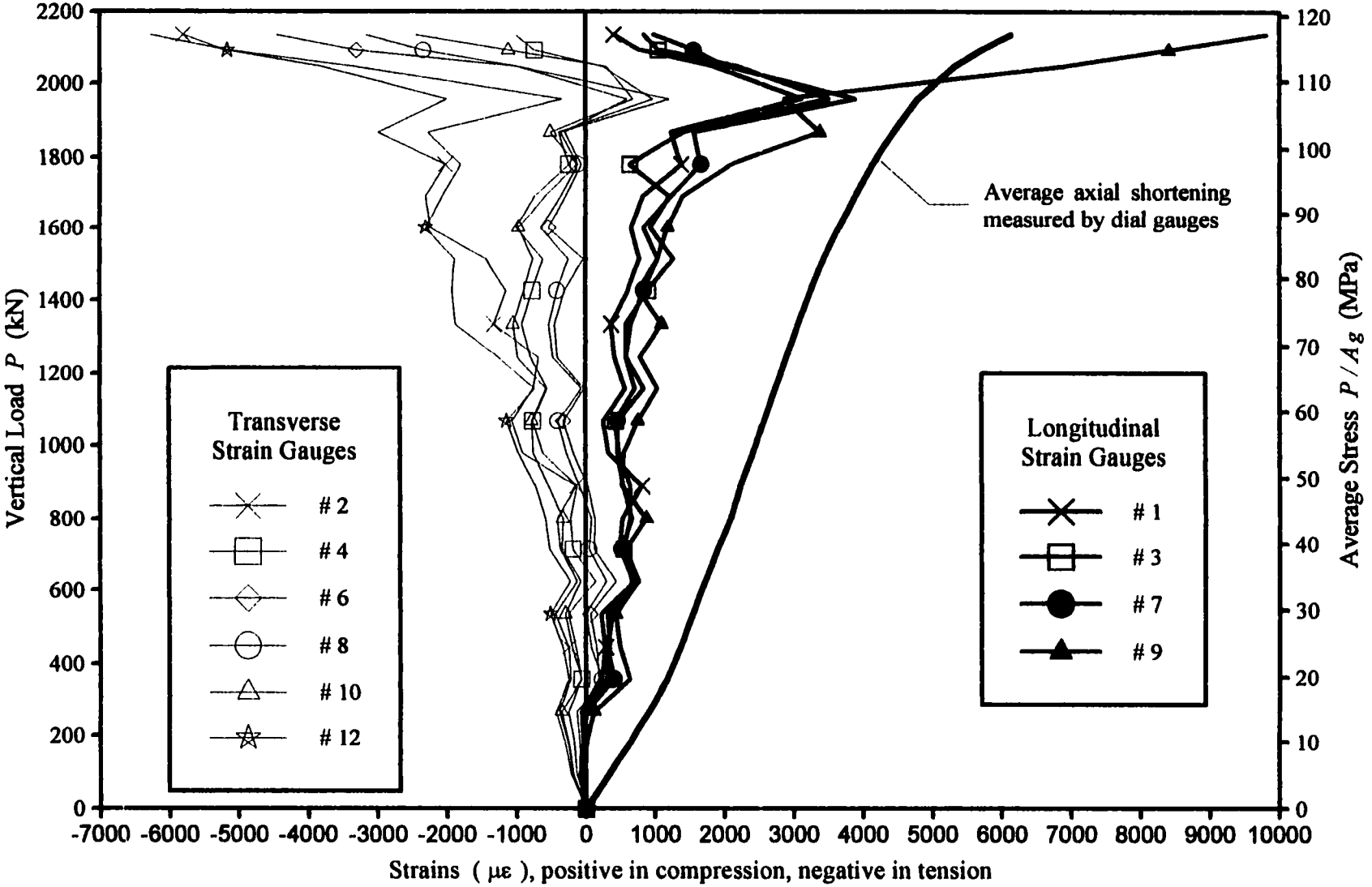

Figure 3.4 : Specimen ST1 - Data from Electric Resistance Strain Gauges

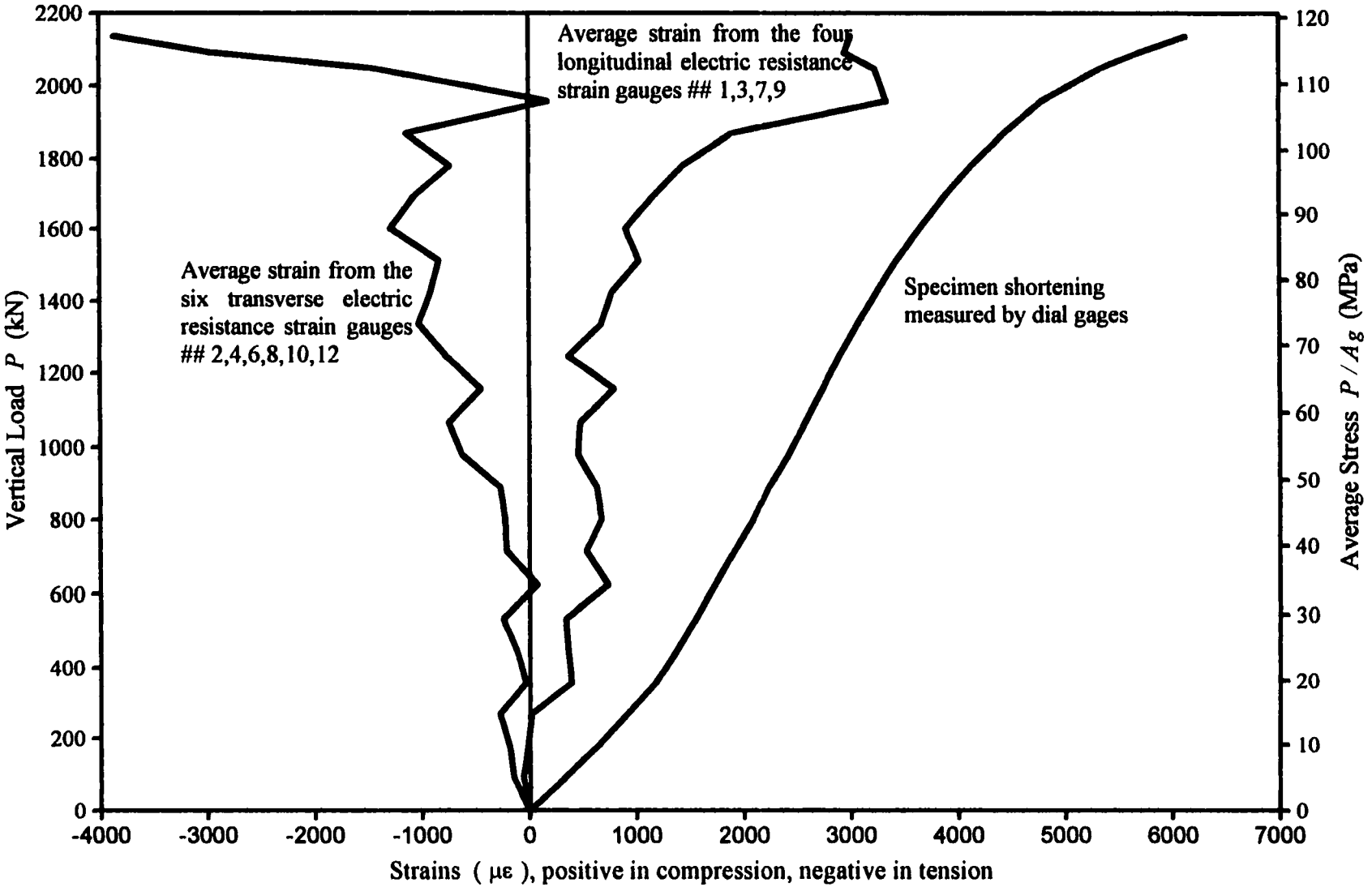

Figure 3.5 : Comparison of Load-Strain Curves for Short Column Specimen ST1

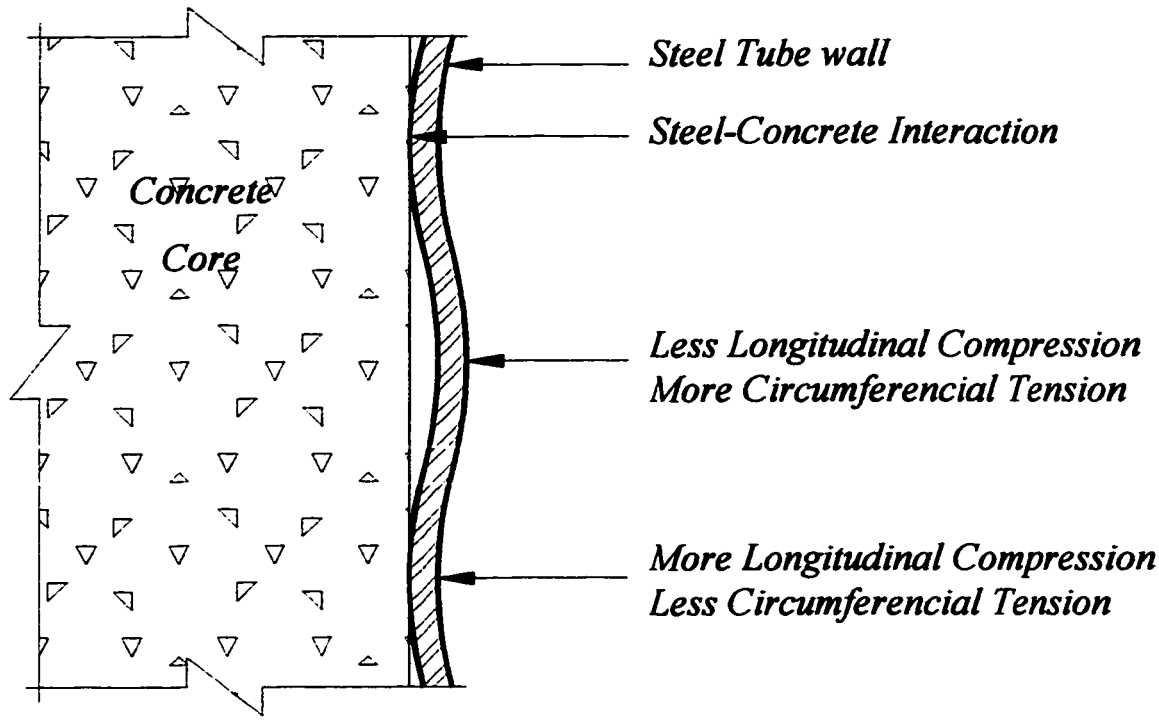

Figure 3.6 : Simplified and Exaggerated Illustration of the Waves Formed in Steel Tube Wall Along the Short Column Specimen ST1.

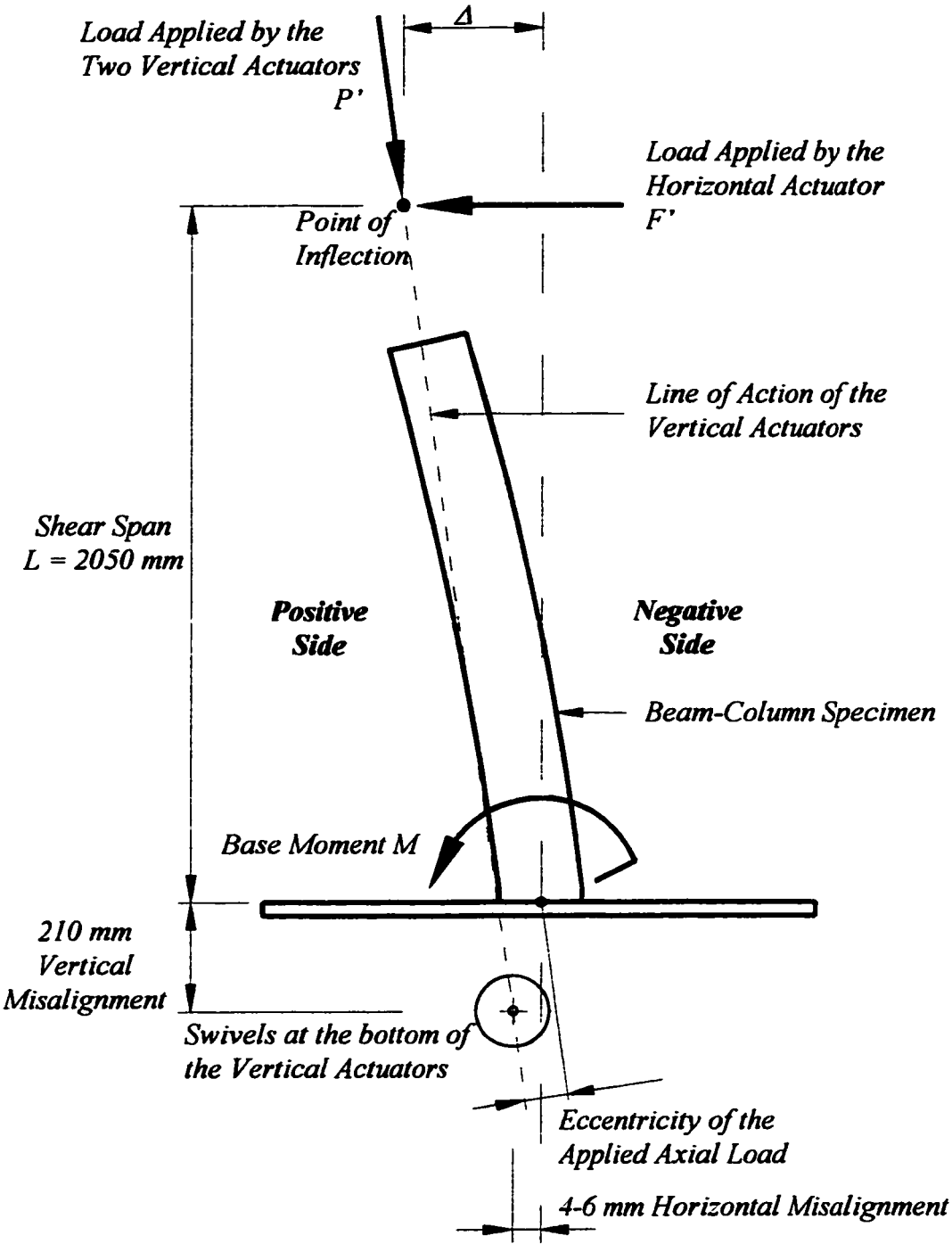

$$M = F' L + P' \Delta (L + 210) ((\Delta - 5)^2 + (L + 210)^2)^{-0.5} - P' L (\Delta - 5) ((\Delta - 5)^2 + (L + 210)^2)^{-0.5} + W \Delta$$

Figure 3.7: Actual Forces Acting on a Typical Beam-Column Specimen

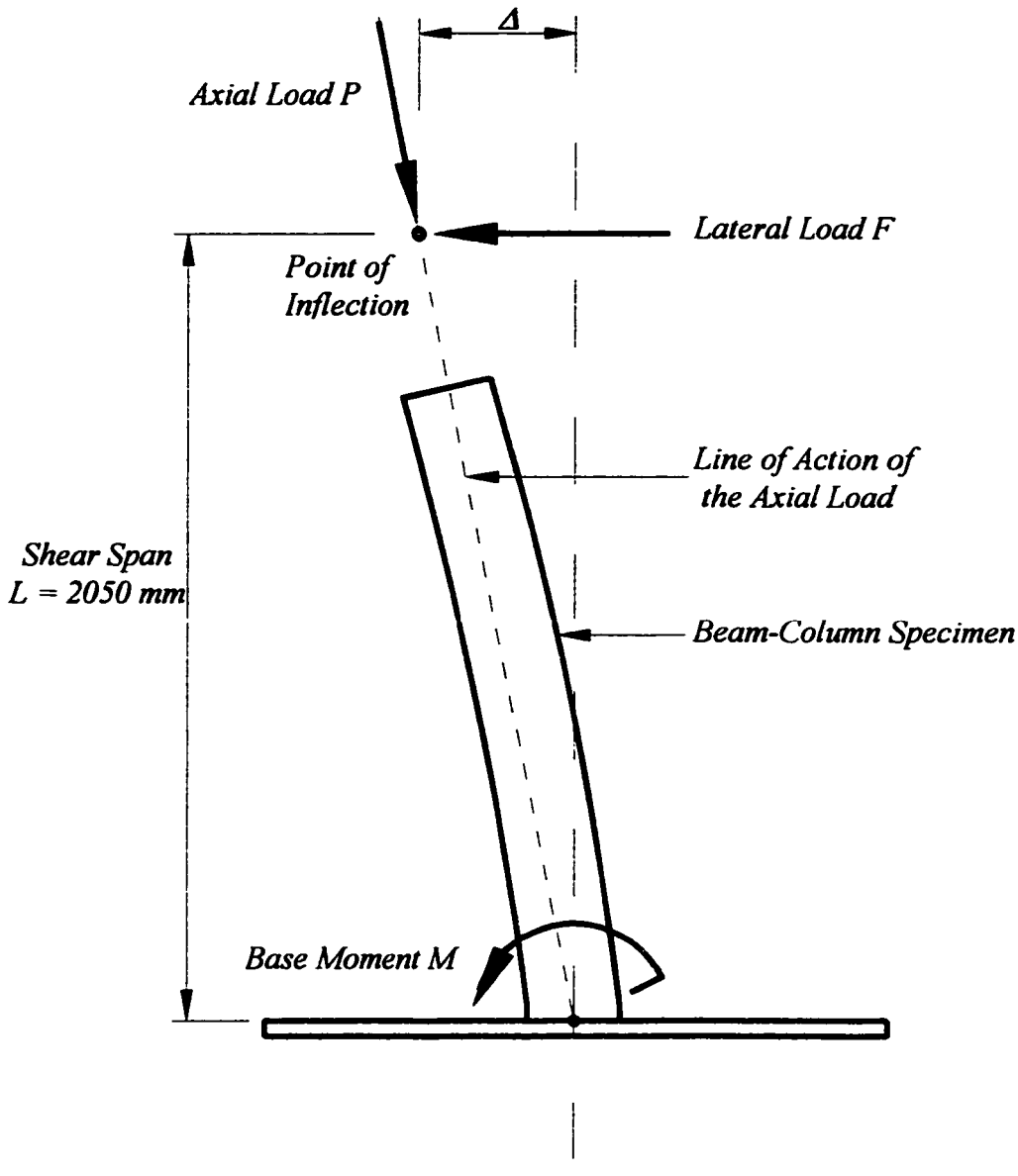

Figure 3.8: Assumed System of Forces Acting on a Beam-Column Specimen "Lateral Load Includes Second Order Effects"

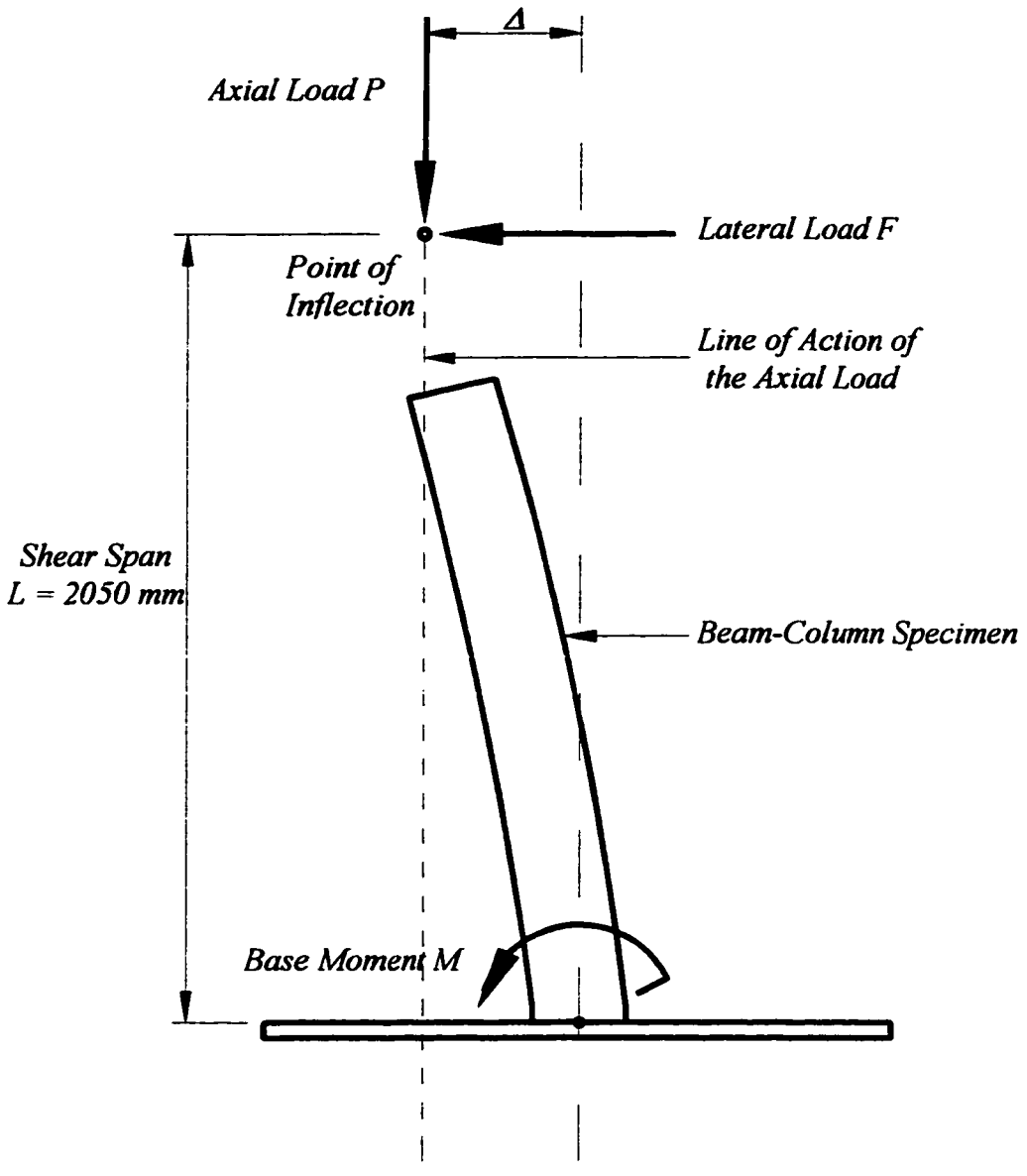

Figure 3.9: Assumed System of Forces Acting on a Beam-Column Specimen "Lateral Load Does Not Include Second Order Effects"

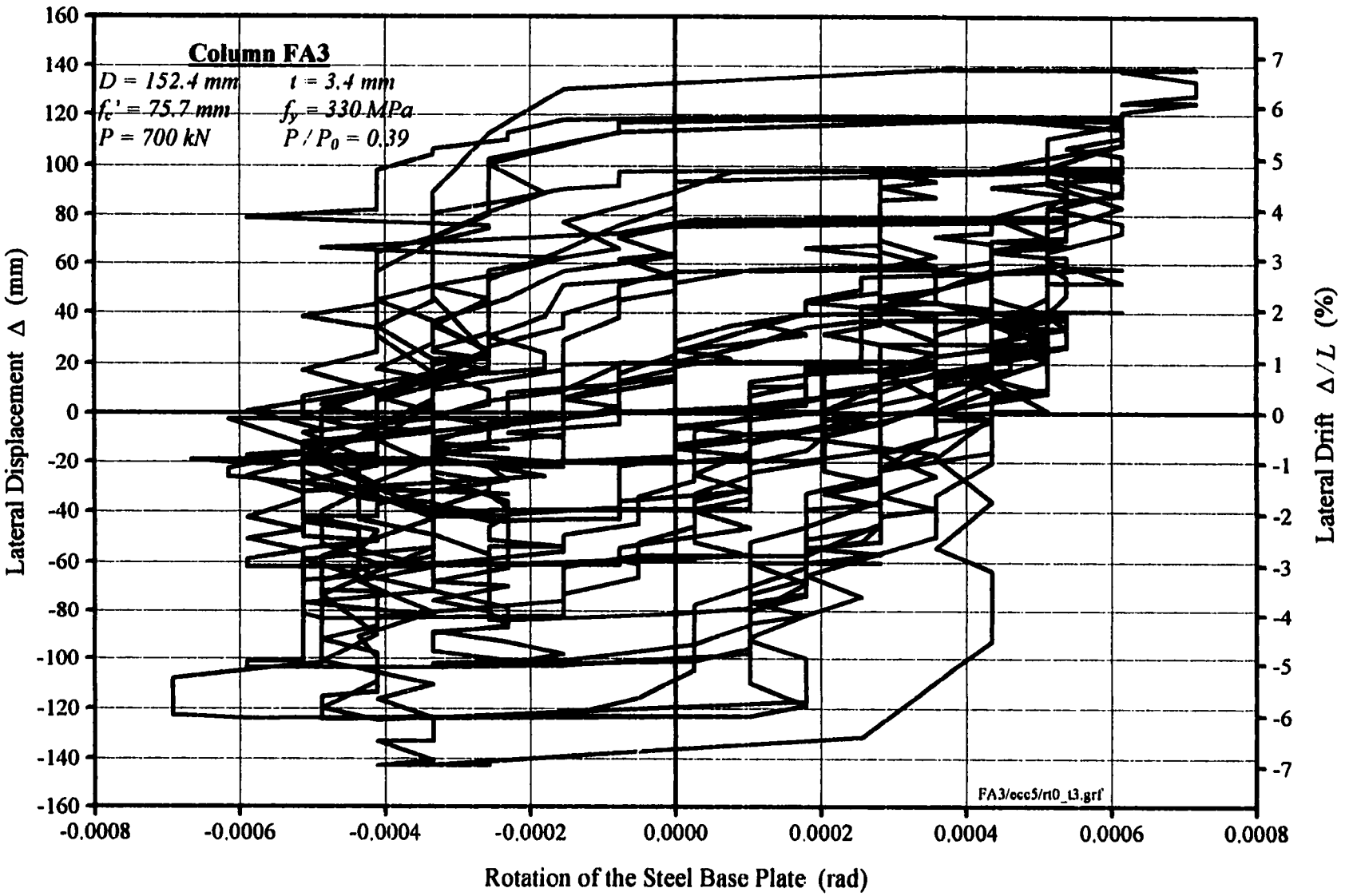

Figure 3.10 : Typical Plot of Steel Base Plate Rotation Versus Lateral Displacement at the Point of Inflection.

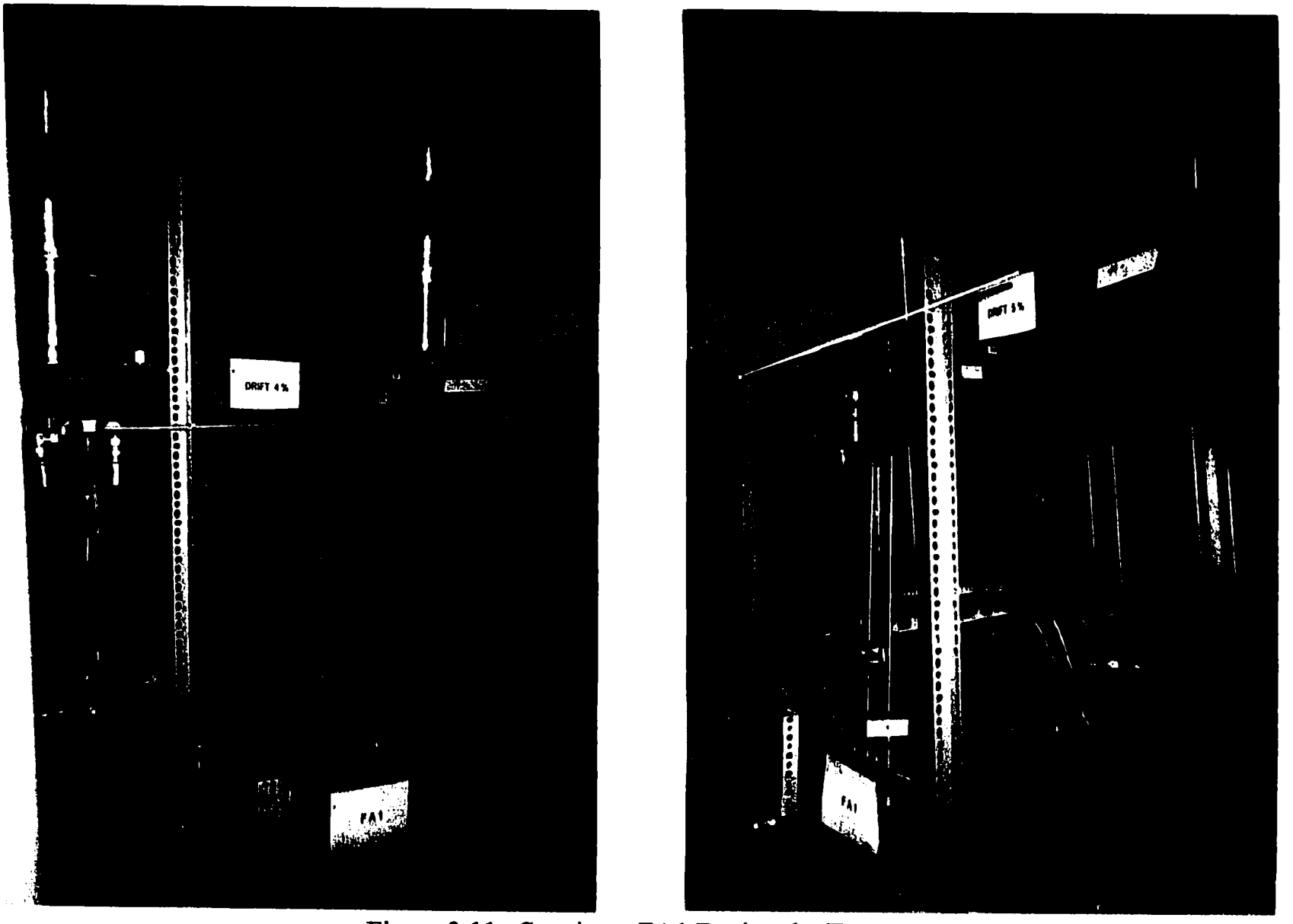

Figure 3.11 : Specimen FA1 During the Test

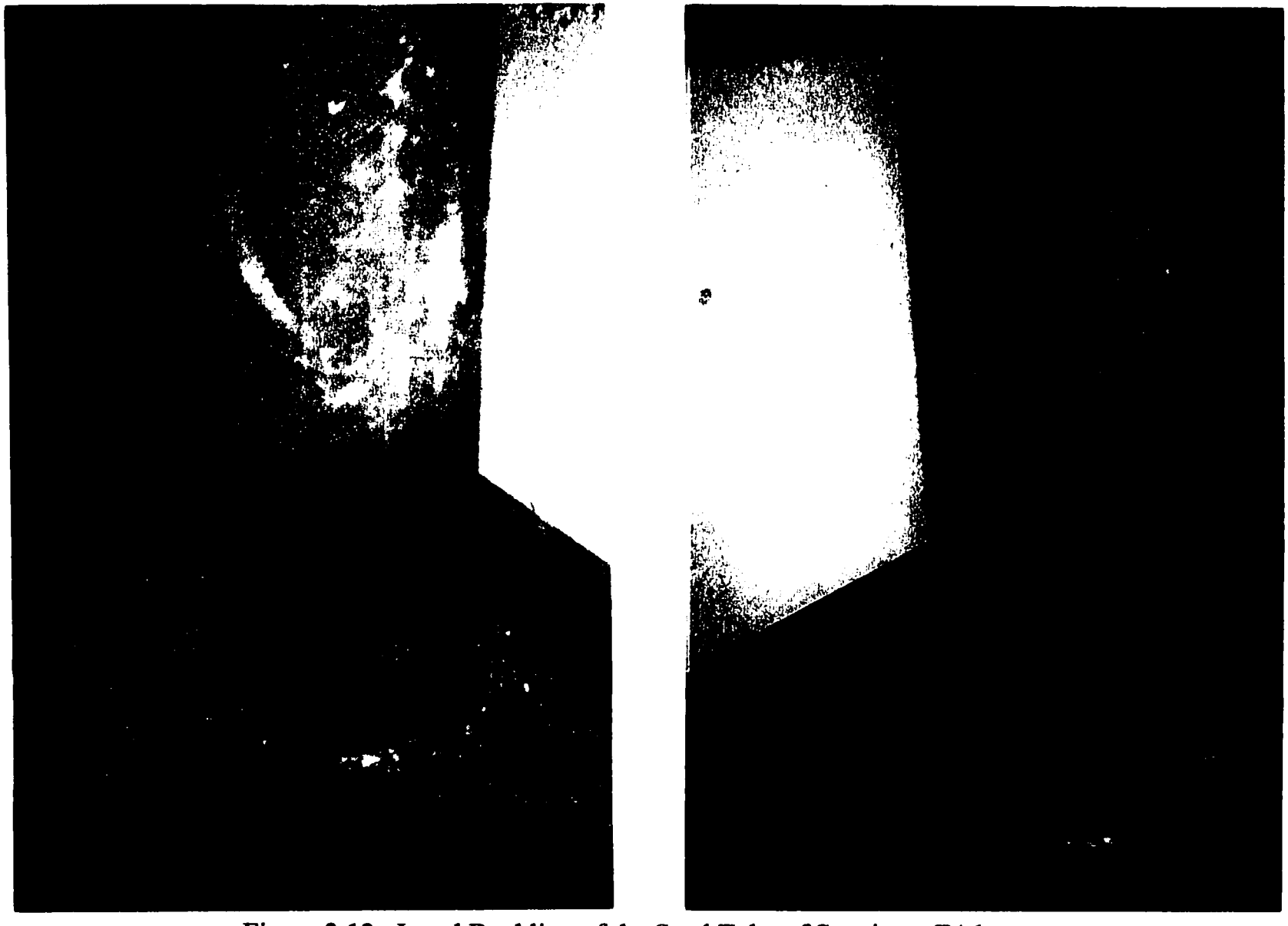

Figure 3.12 : Local Buckling of the Steel Tube of Specimen FA1

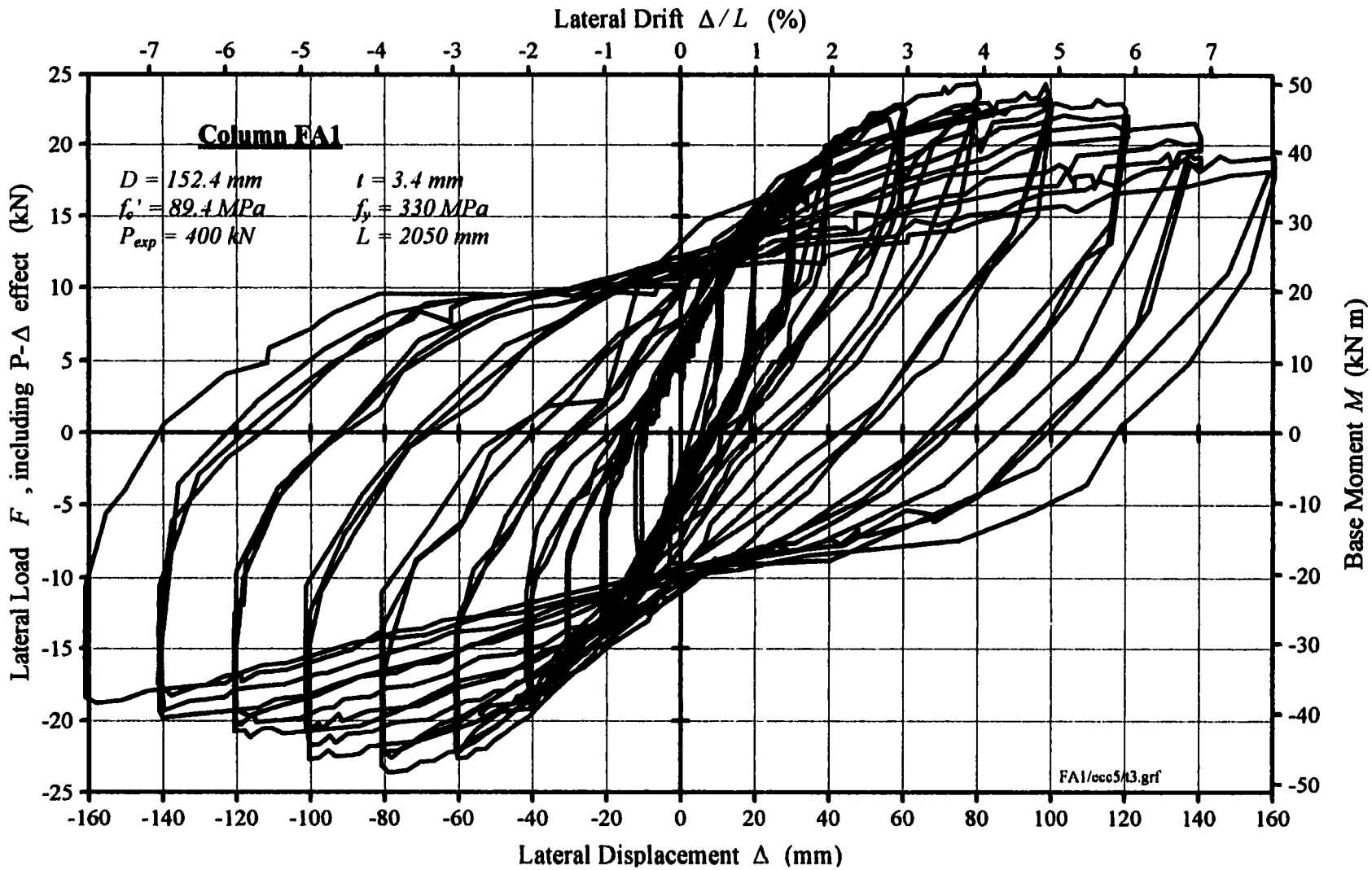

Figure 3.13 : Load-Displacement Curve for Column FA1 (Lateral Load includes second order effects)

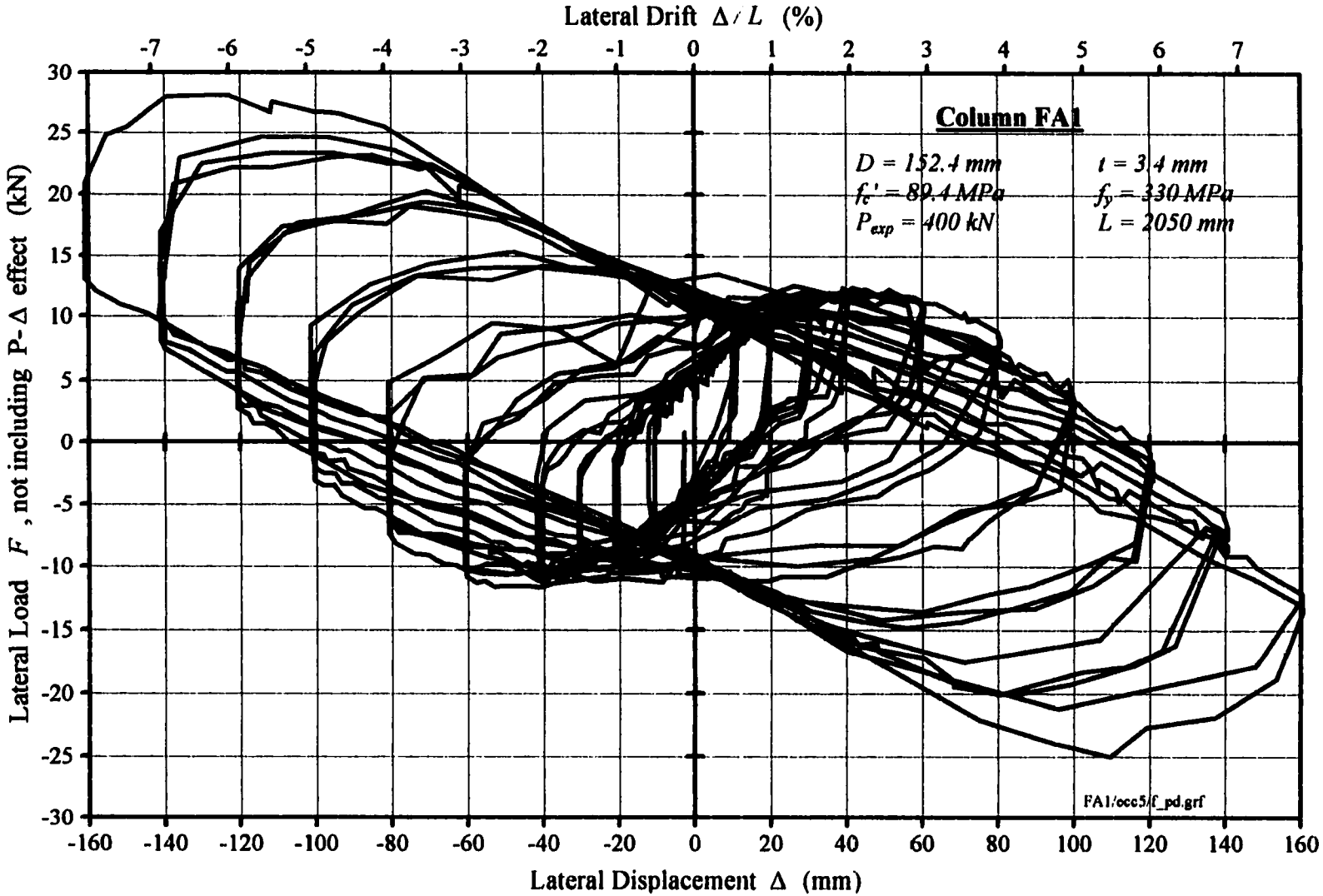

Figure 3.14 : Load-Displacement Curve for Column FA1 (Lateral Load does not include second order effects)

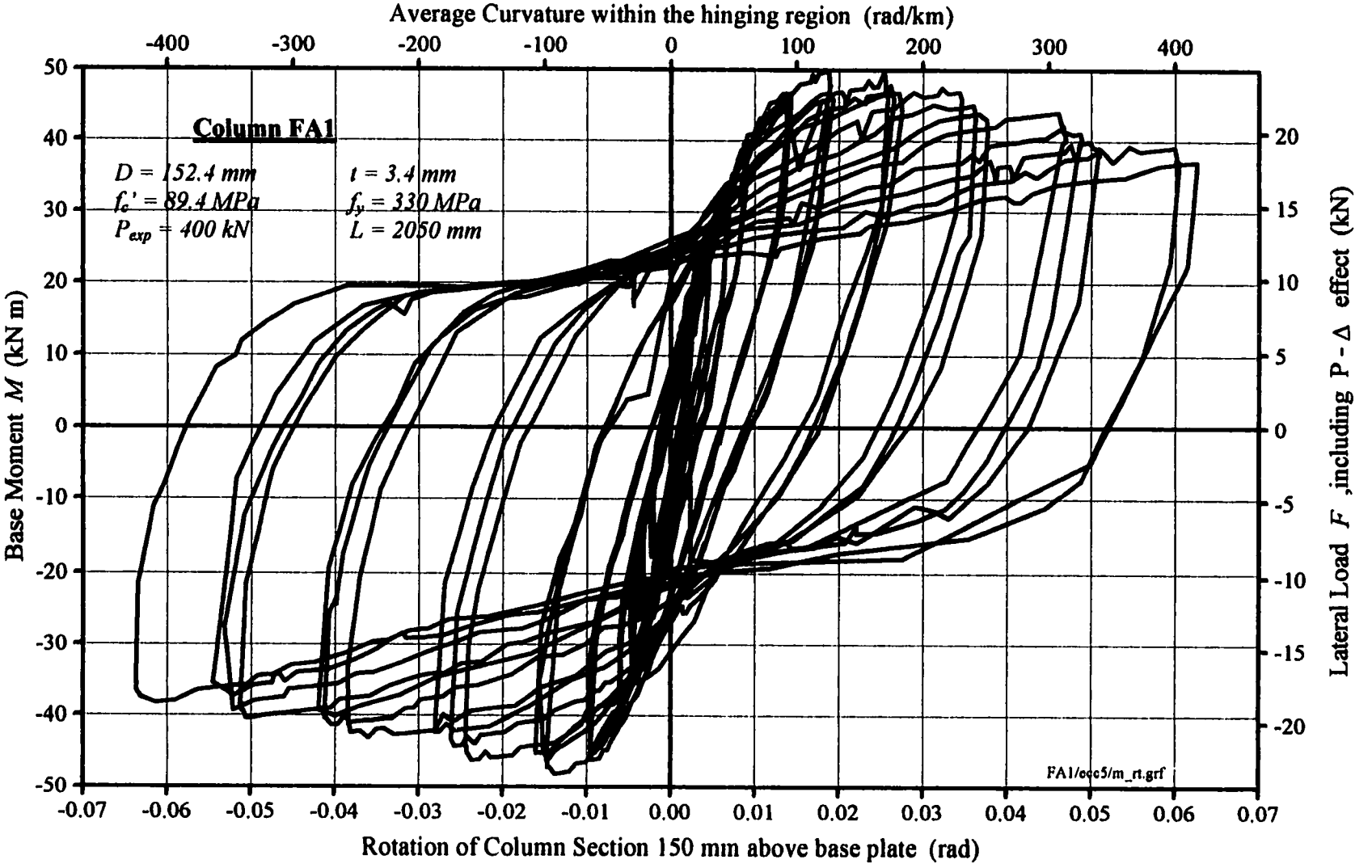

Figure 3.15 : Moment-Rotation Curve for Specimen FA1

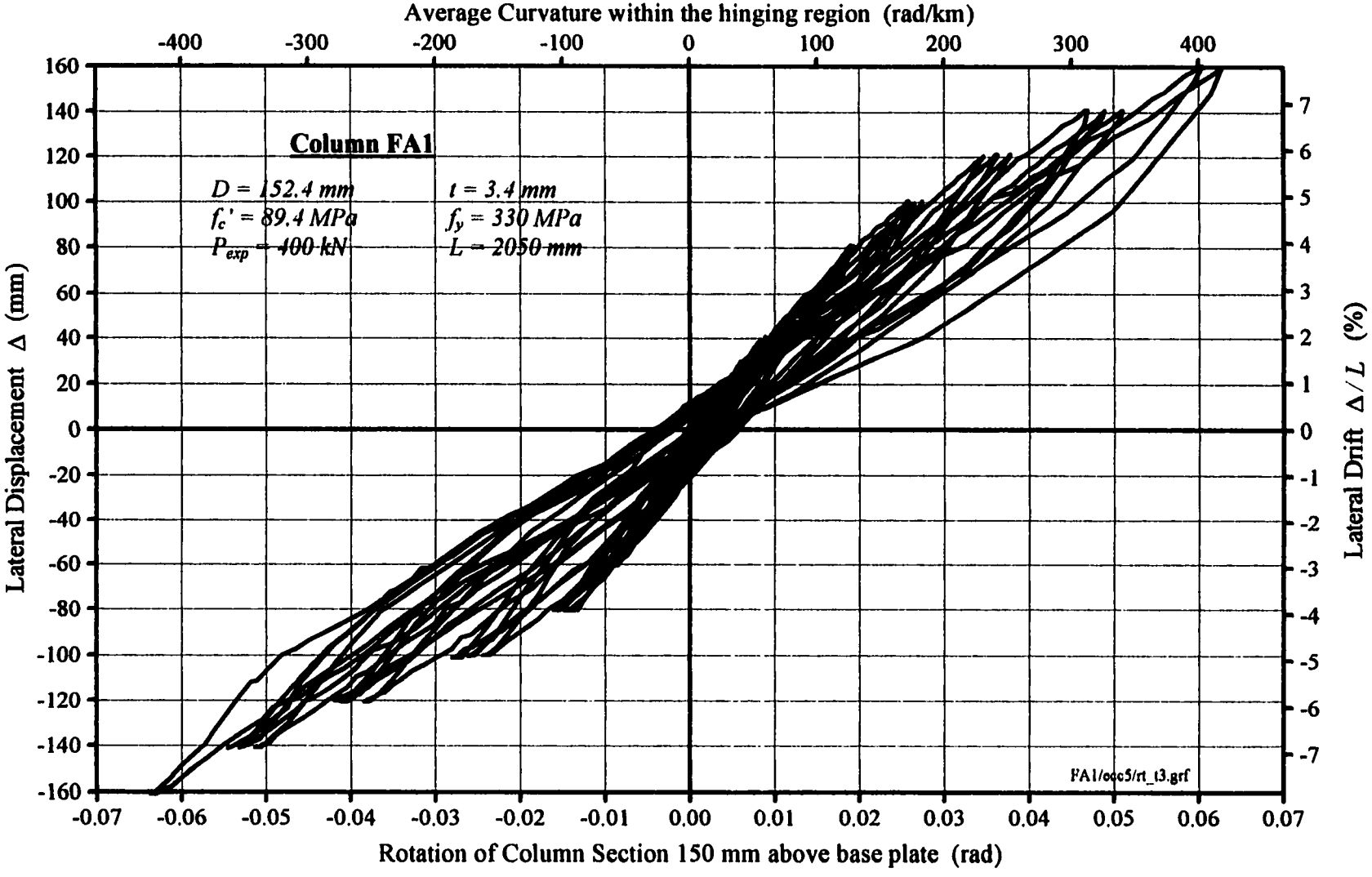

Figure 3.16 : Displacement-Rotation Curve for Specimen FA1

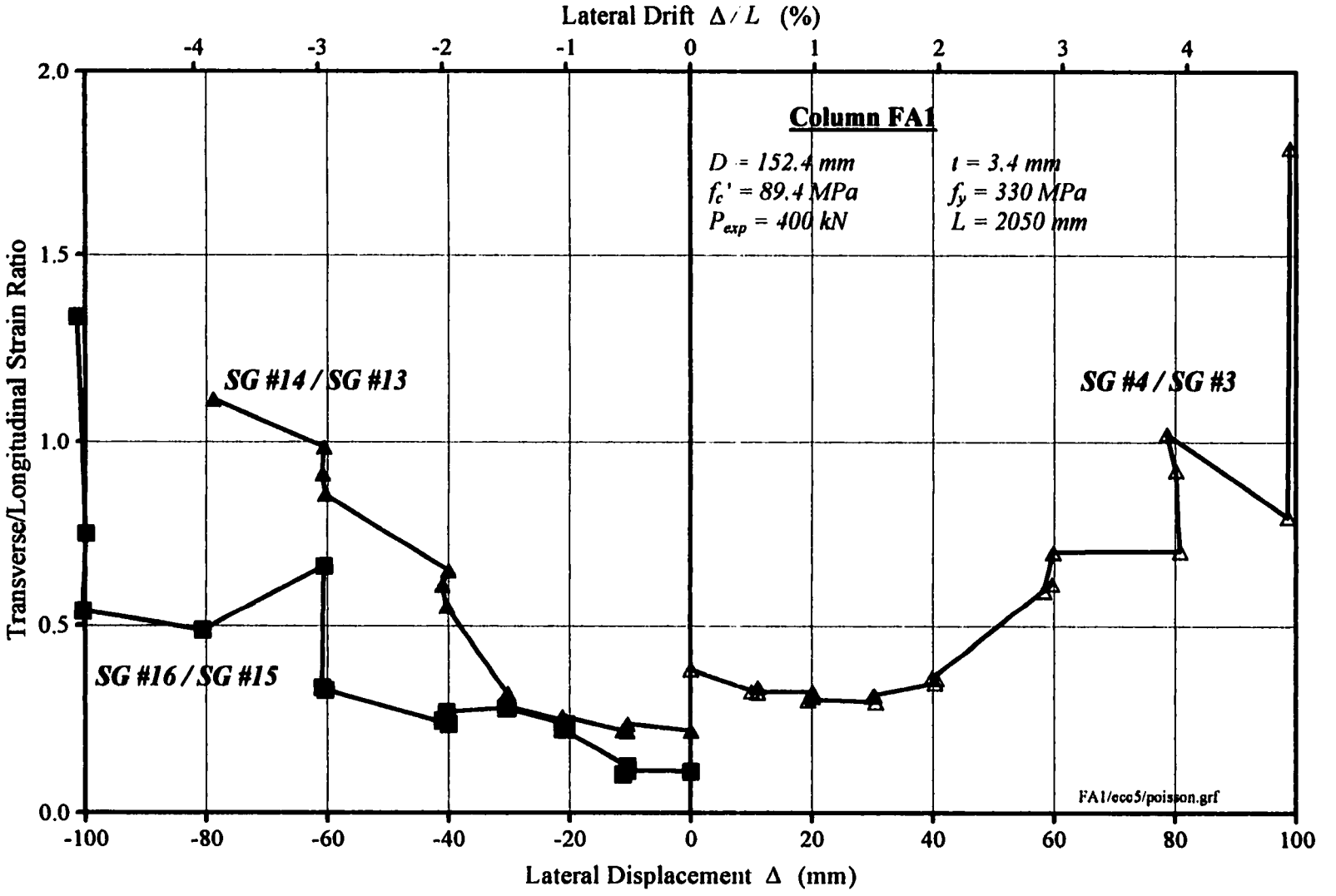

Figure 3.17 : Transverse/Longitudinal Strain Ratios for Specimen FA1

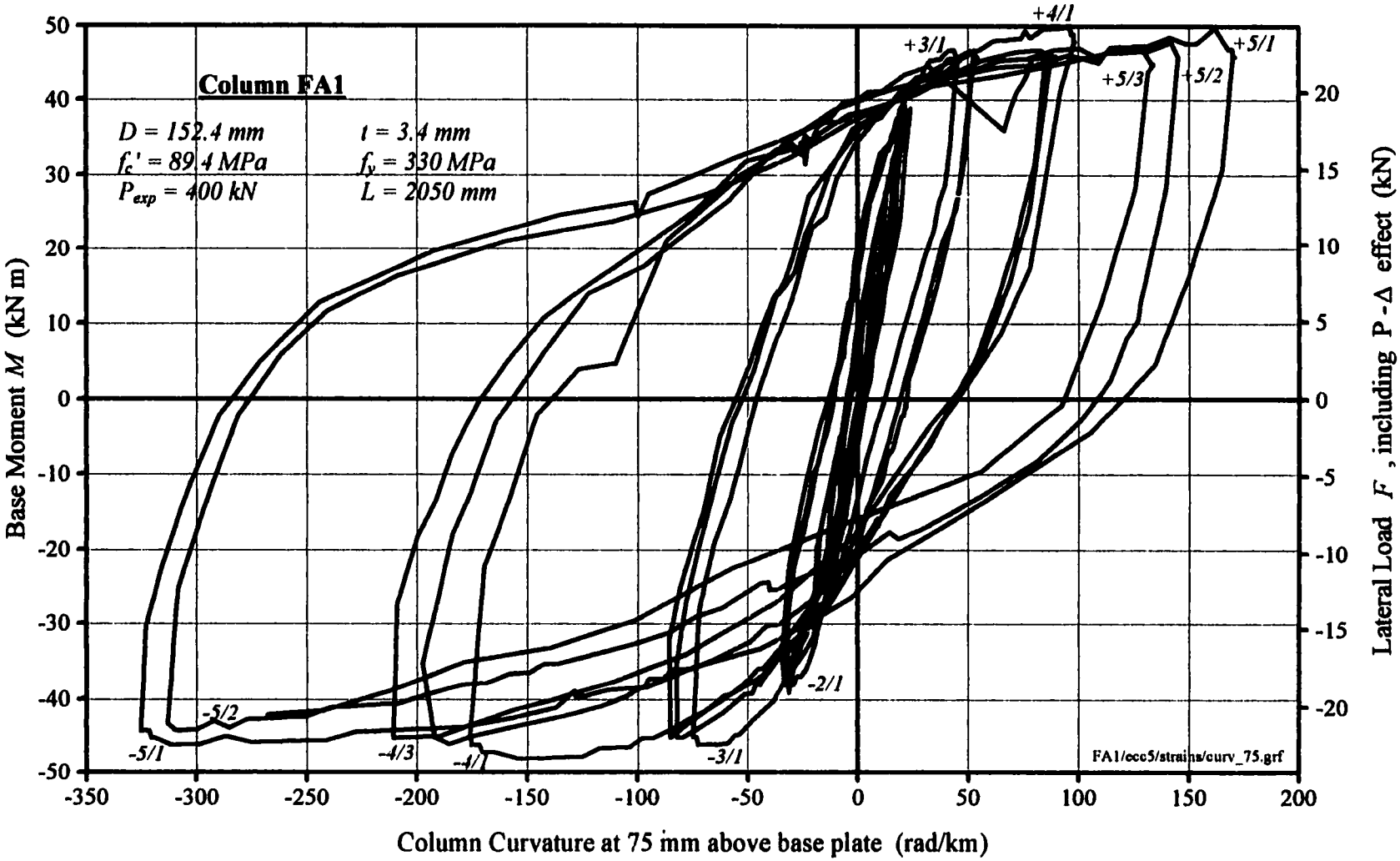

Figure 3.18 : Curvature of Specimen FA1 at 75 mm Above the Base Plate
(computed from data provided by strain gauges #3 and #13)

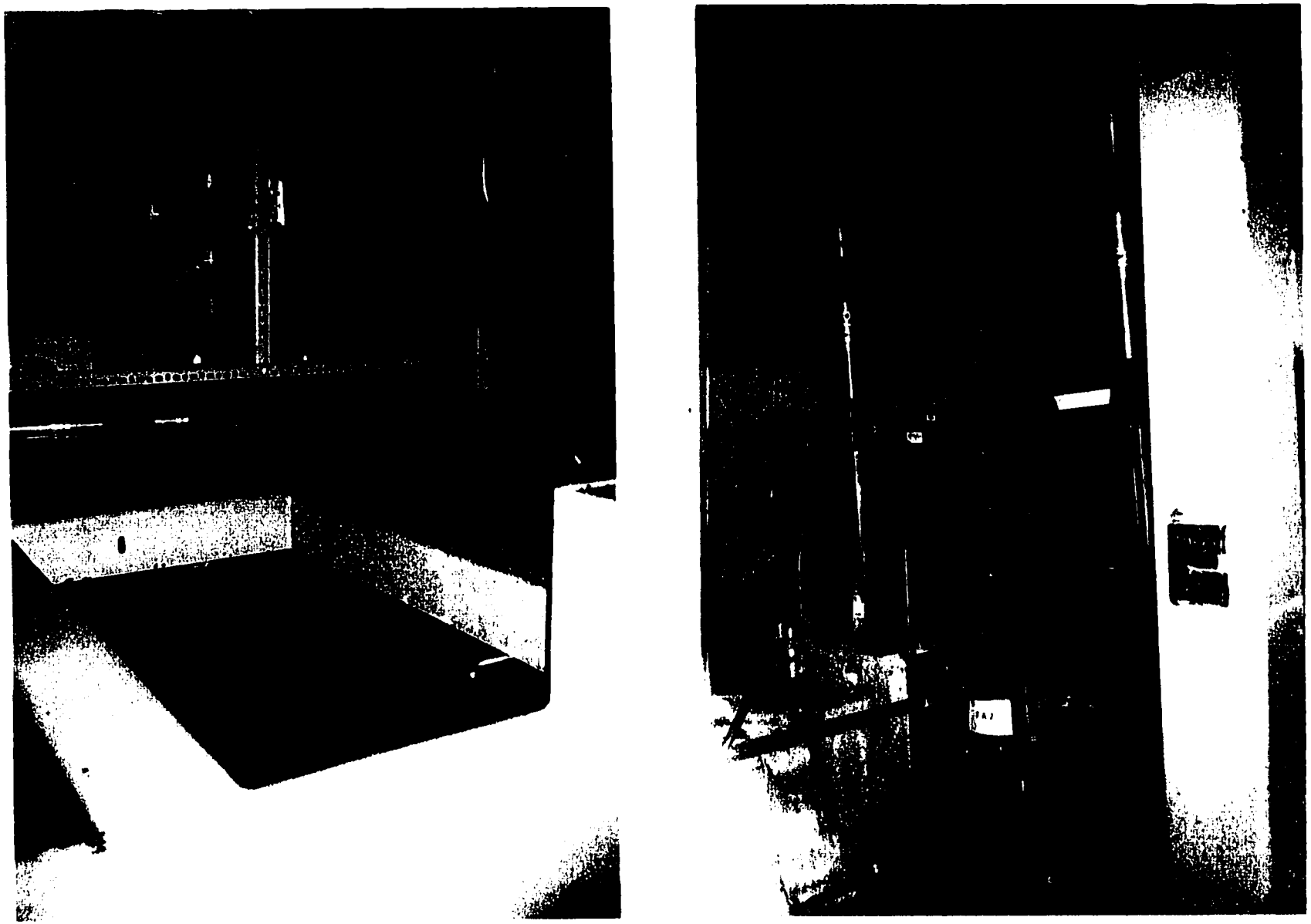

Figure 3.19 : Specimen FA2 During Testing (note the lateral displacement developed in the South direction)

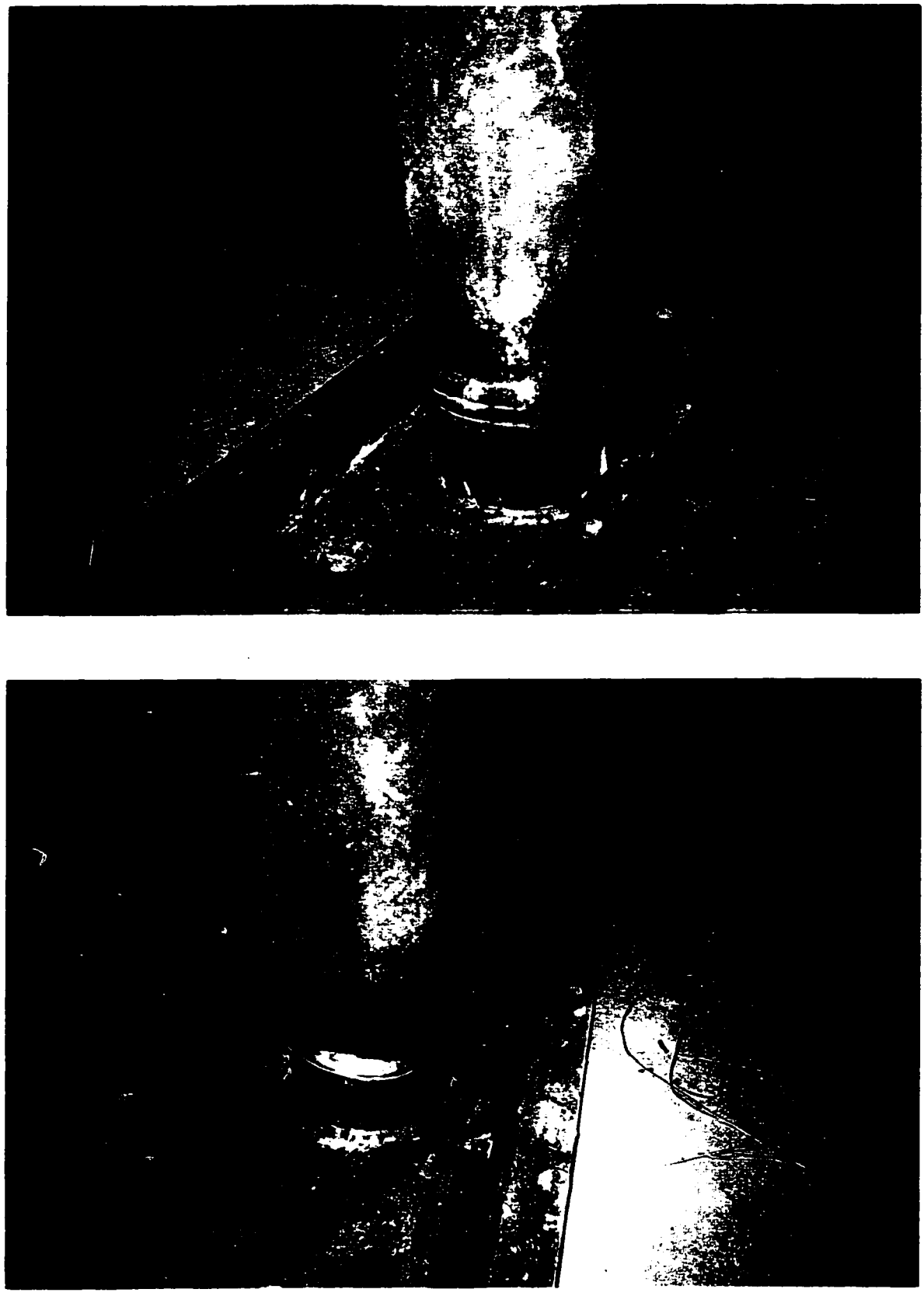

Figure 3.20 : Specimen FA2 after the Test

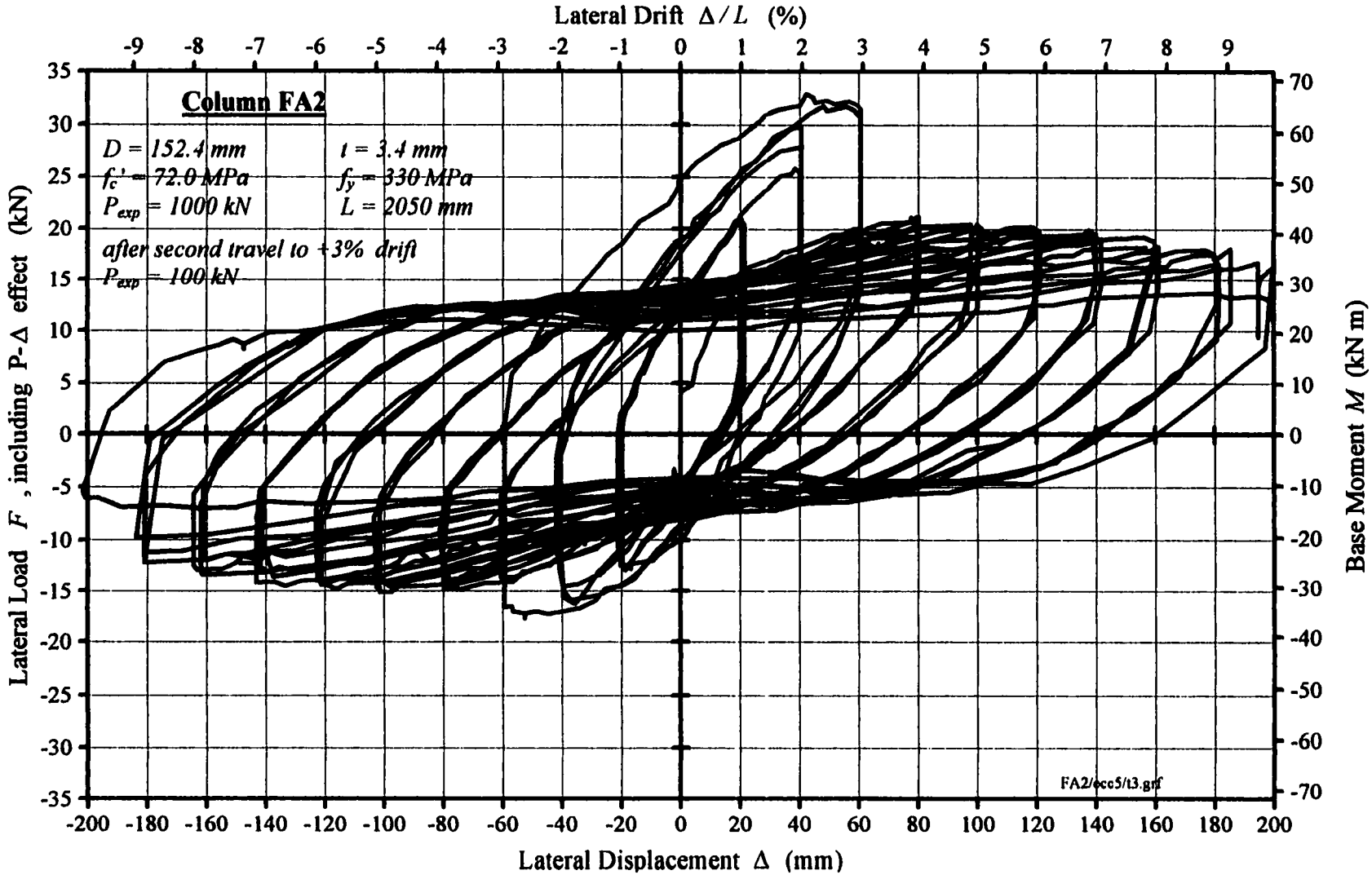

Figure 3.21 : Load-Displacement Curve for Column FA2 (Lateral Load includes second order effects)

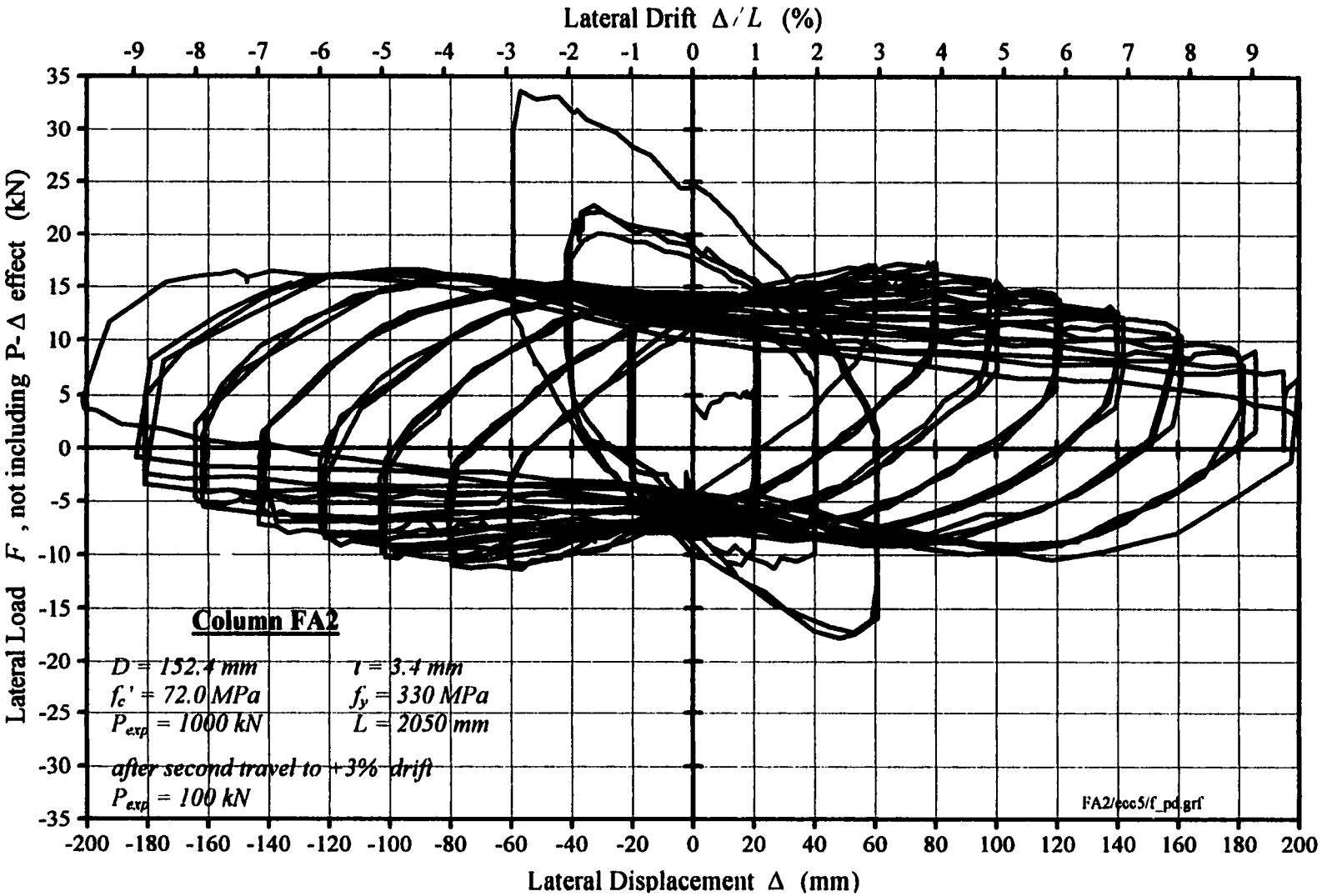

Figure 3.22 : Load-Displacement Curve for Column FA2 (Lateral Load does not include second order effects)

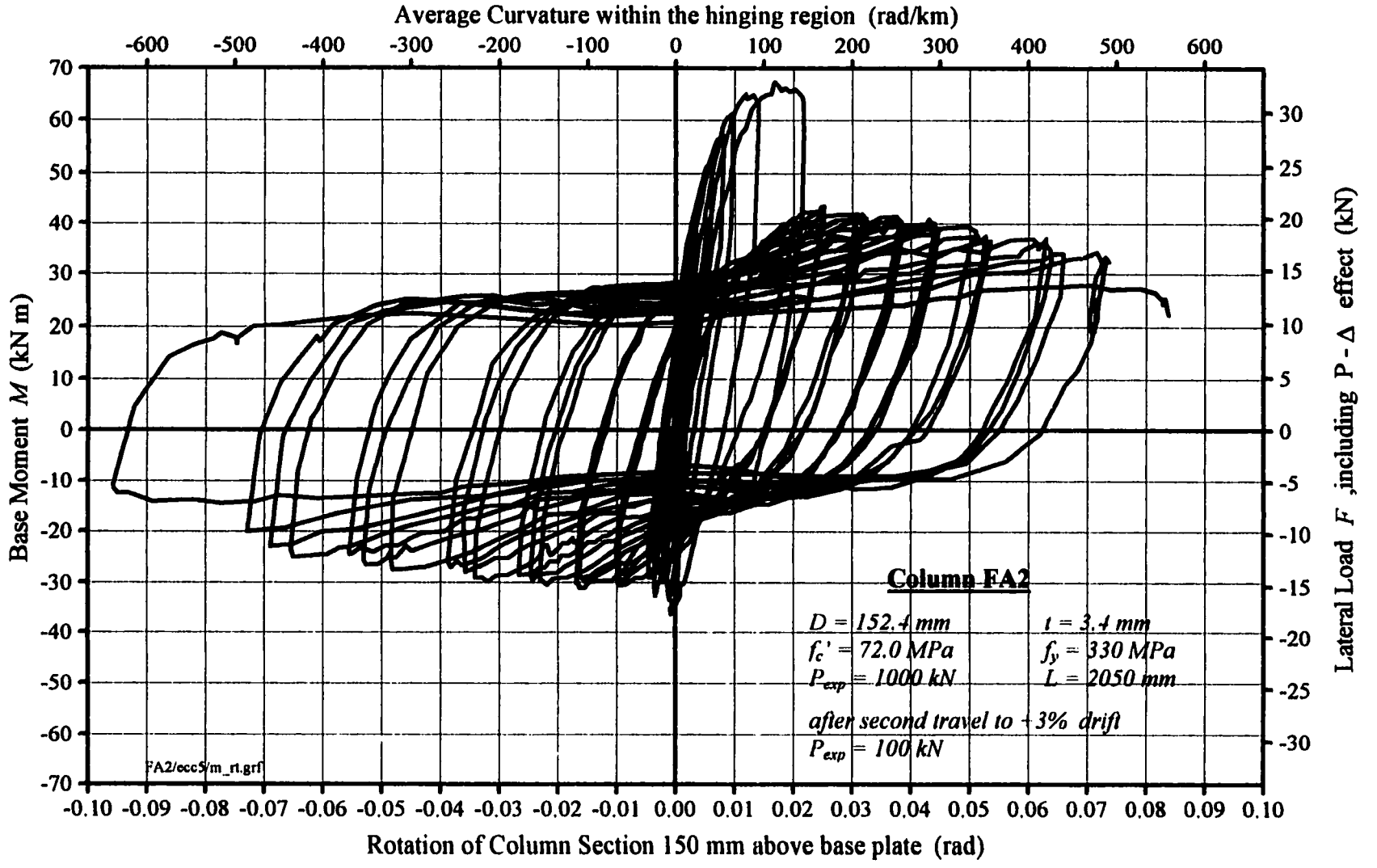

Figure 3.23 : Moment-Rotation Curve for Specimen FA2

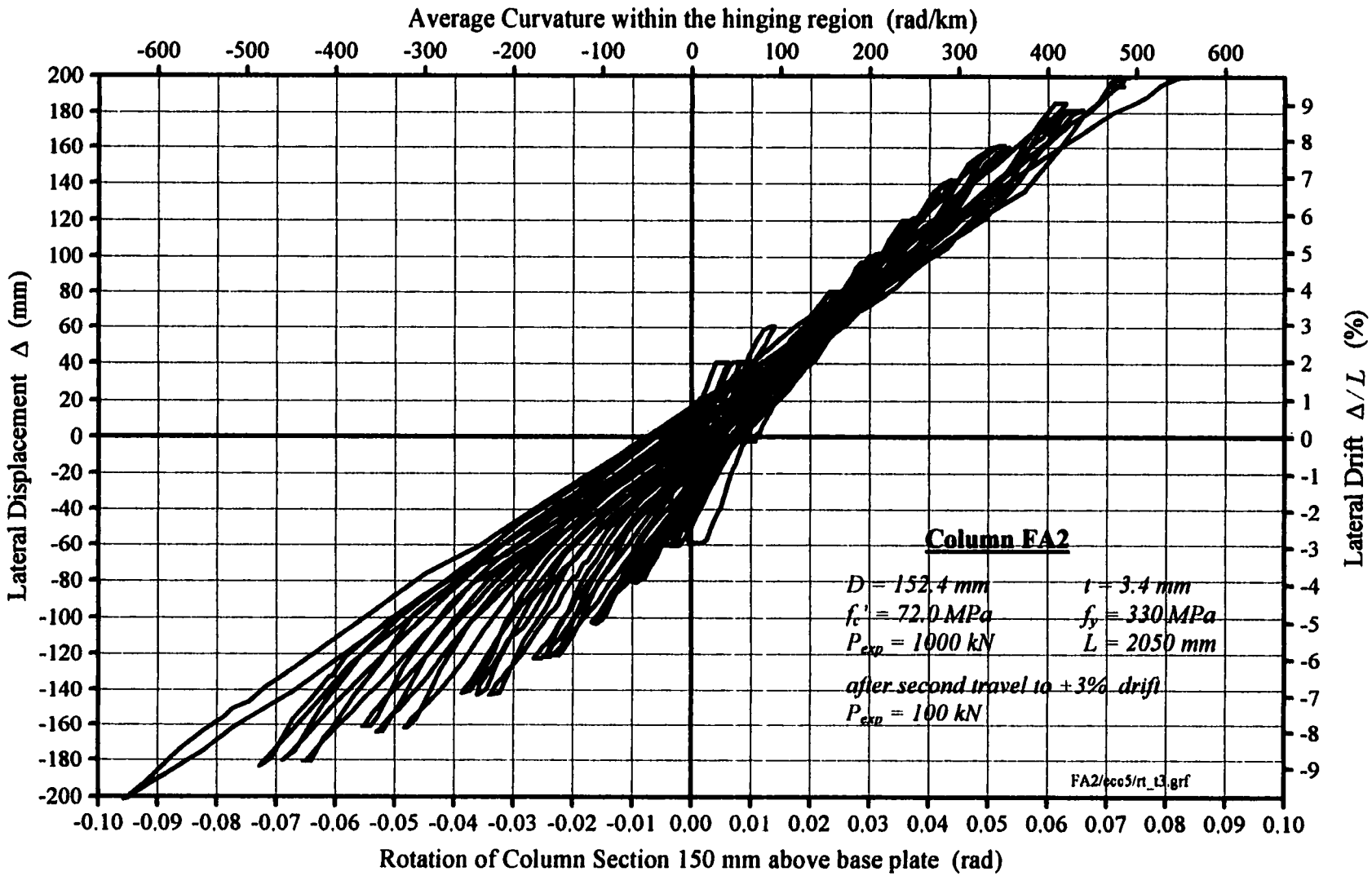

Figure 3.24 : Displacement-Rotation Curve for Specimen FA2

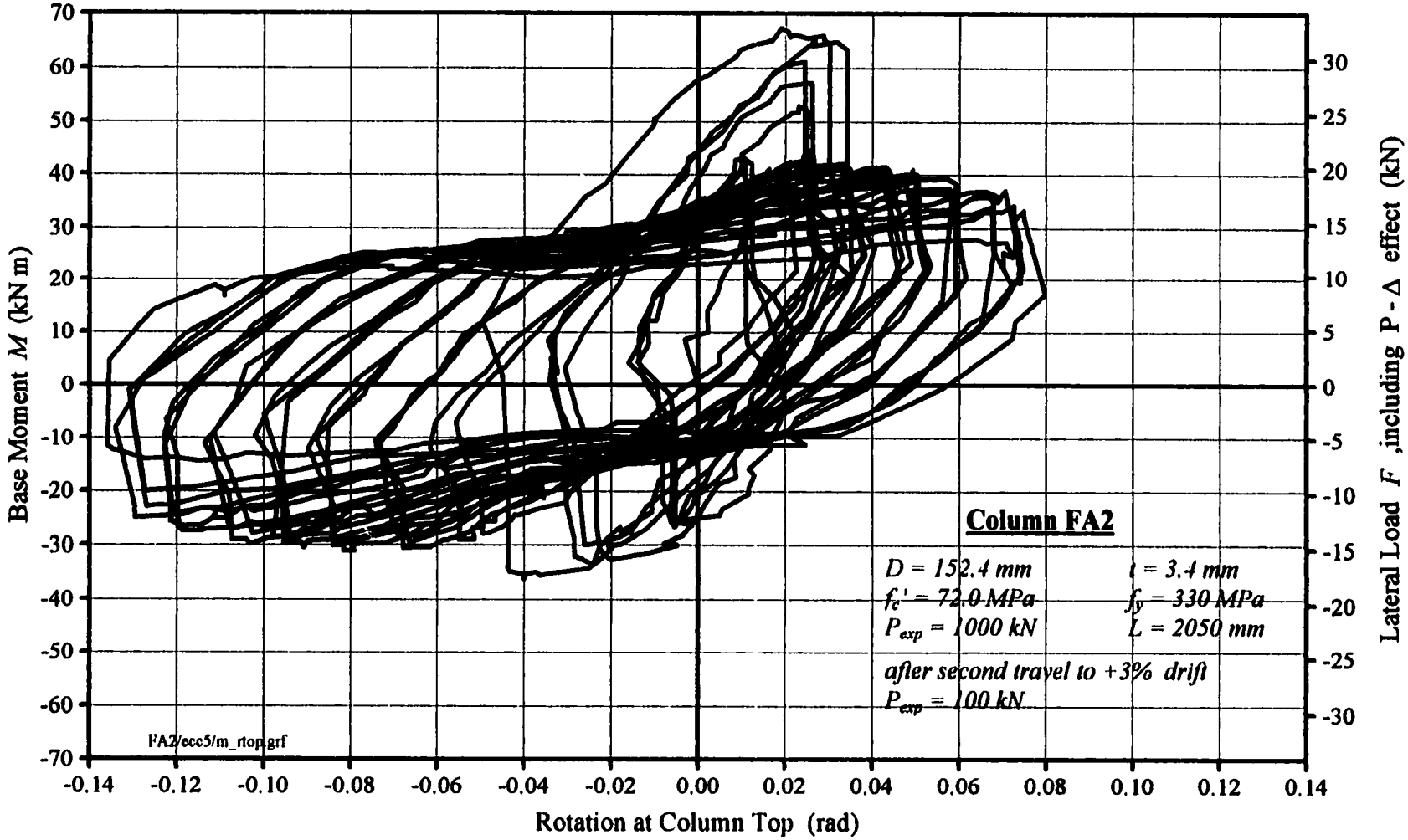

Figure 3.25 : Rotation at the Top of Specimen FA2 (plotted versus Base Moment)

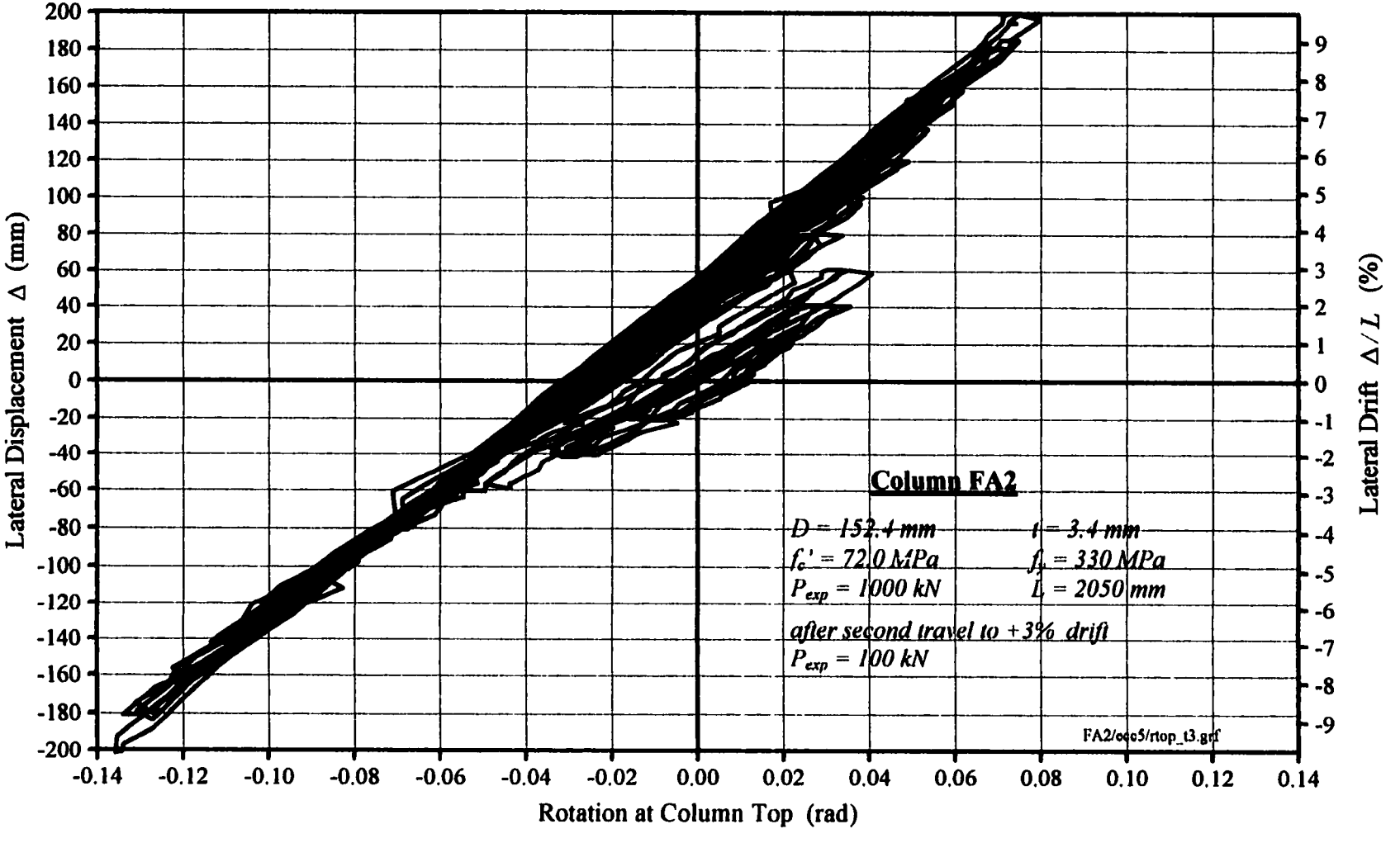

Figure 3.26 : Rotation at the Top of Specimen FA2 (plotted versus Lateral Displacement)

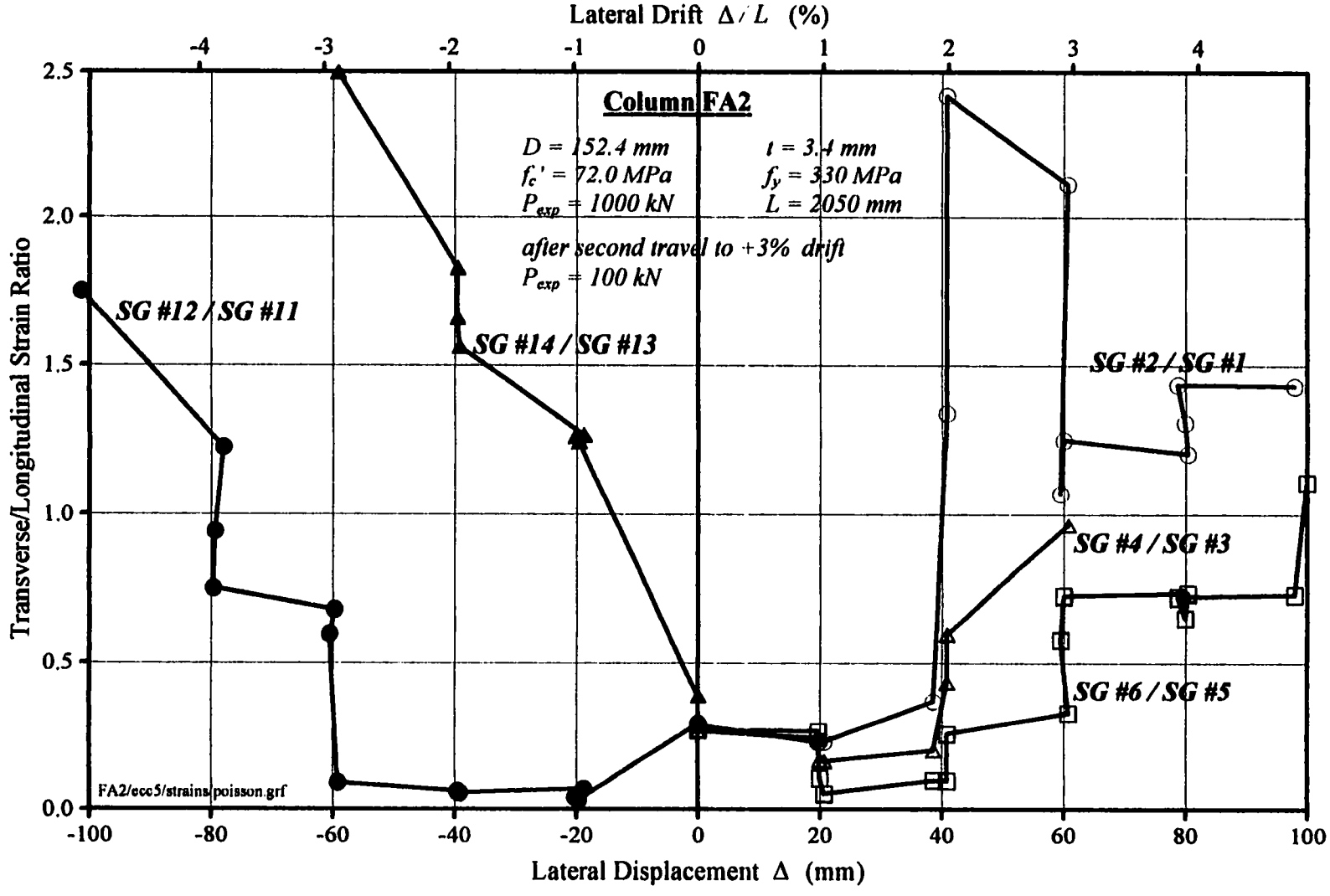

Figure 3.27 : Transverse/Longitudinal Strain Ratios for Specimen FA2

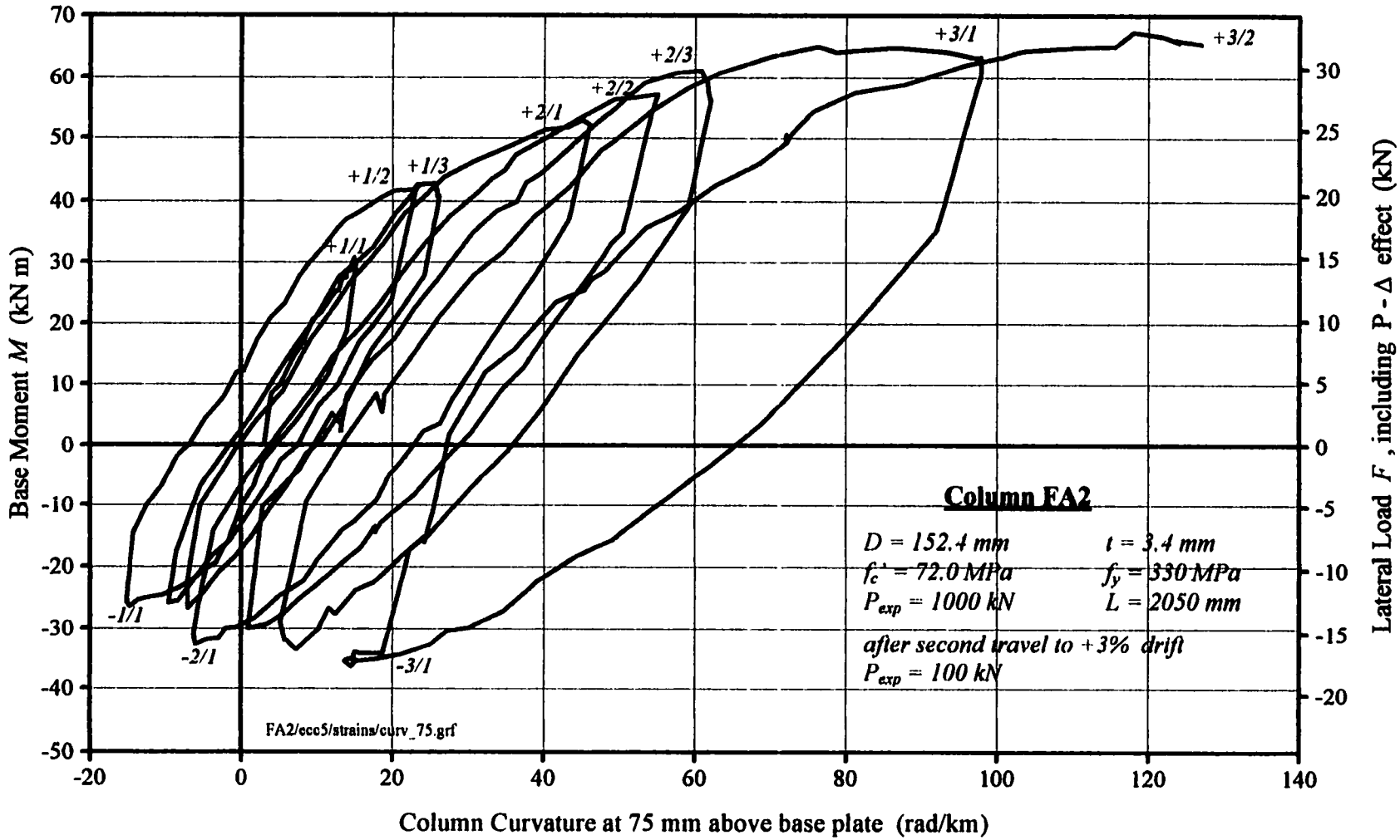

Figure 3.28 : Curvature of Specimen FA2 at 75 mm Above the Base Plate
(computed from data provided by strain gauges #3 and #13)

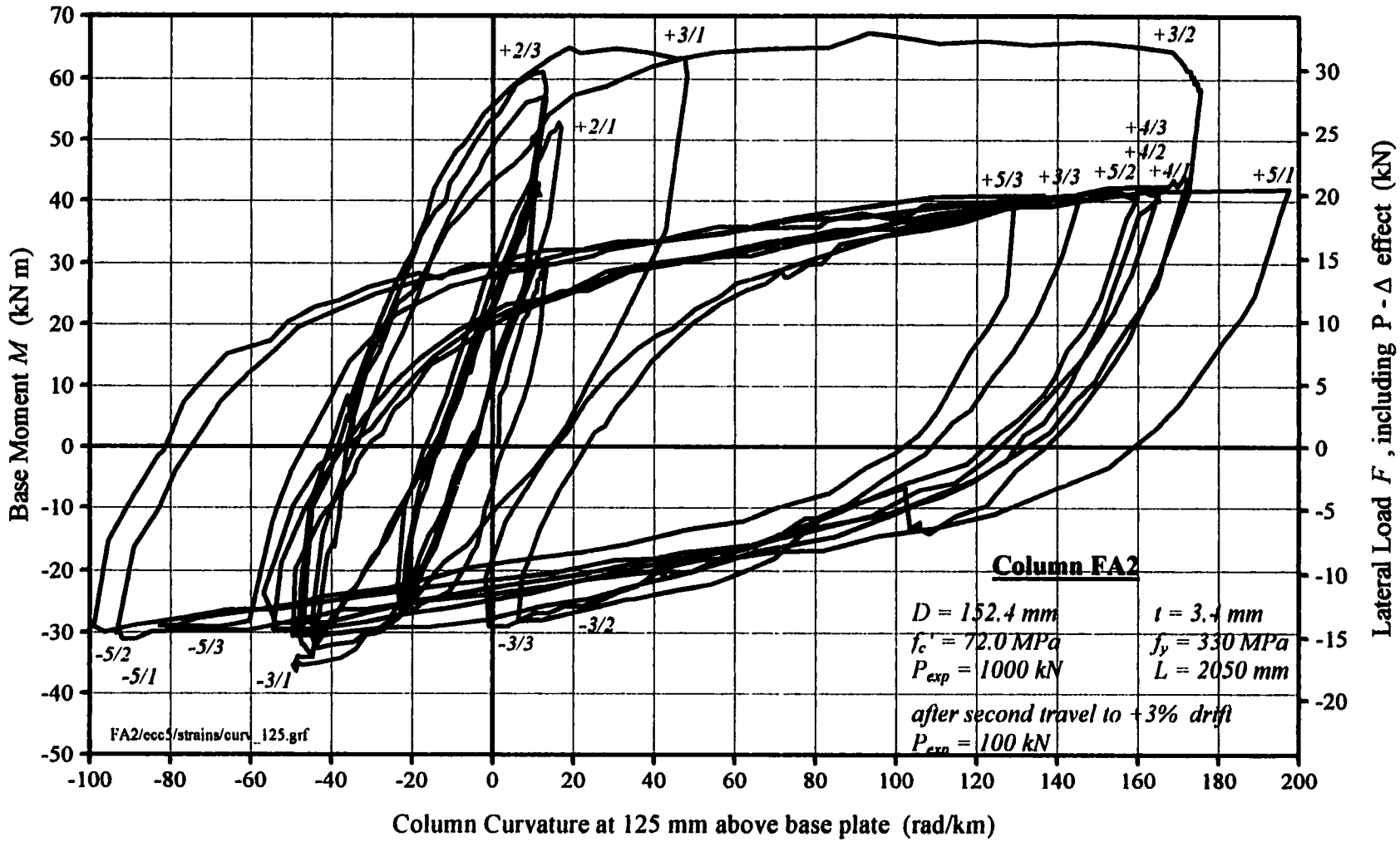

Figure 3.29 : Curvature of Specimen FA2 at 125 mm Above the Base Plate
(computed from data provided by strain gauges #1 and #11)

Figure 3.30 : Specimen FA3 During Testing

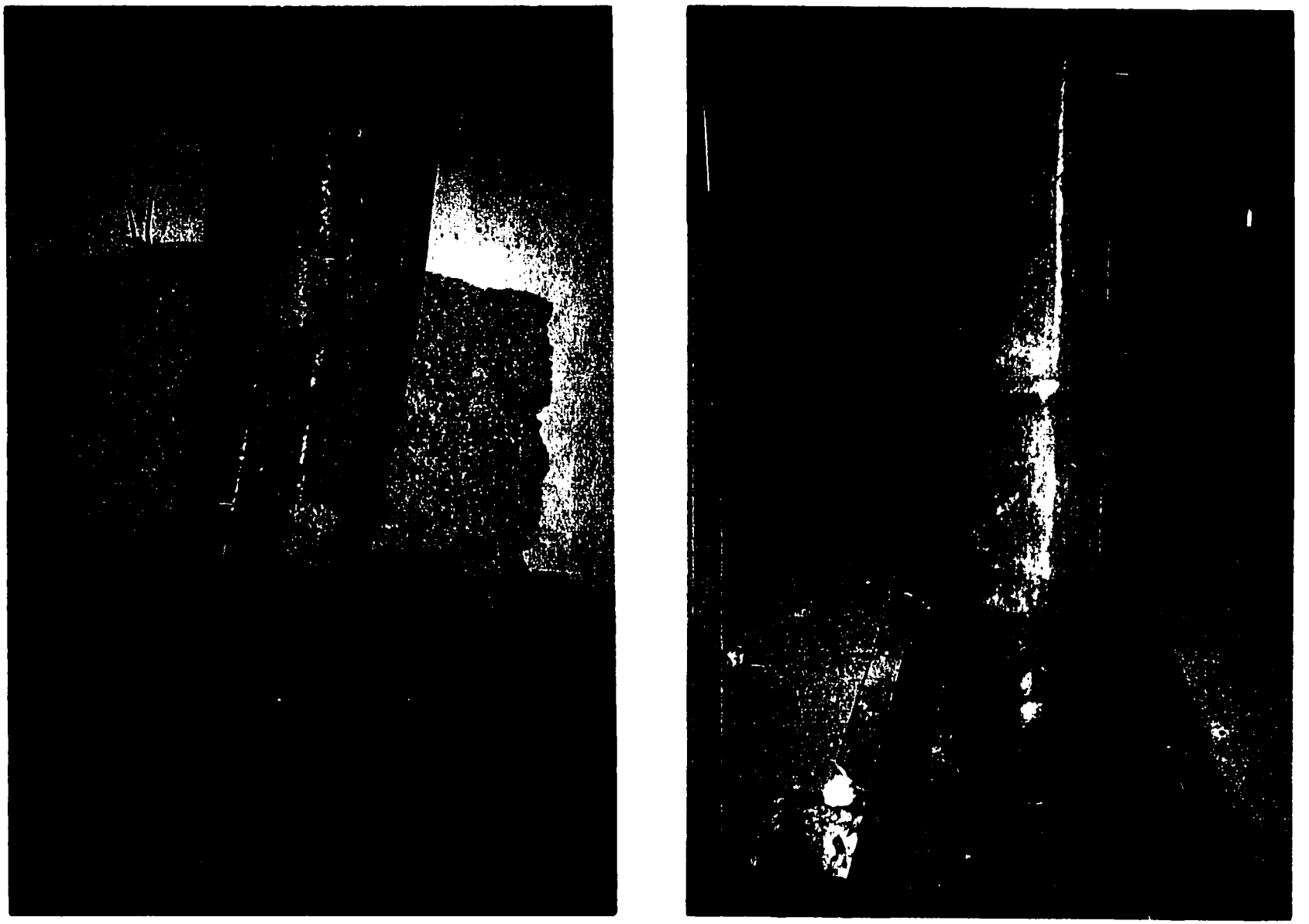

Figure 3.31 : The shape of Specimen FA3 after the Test

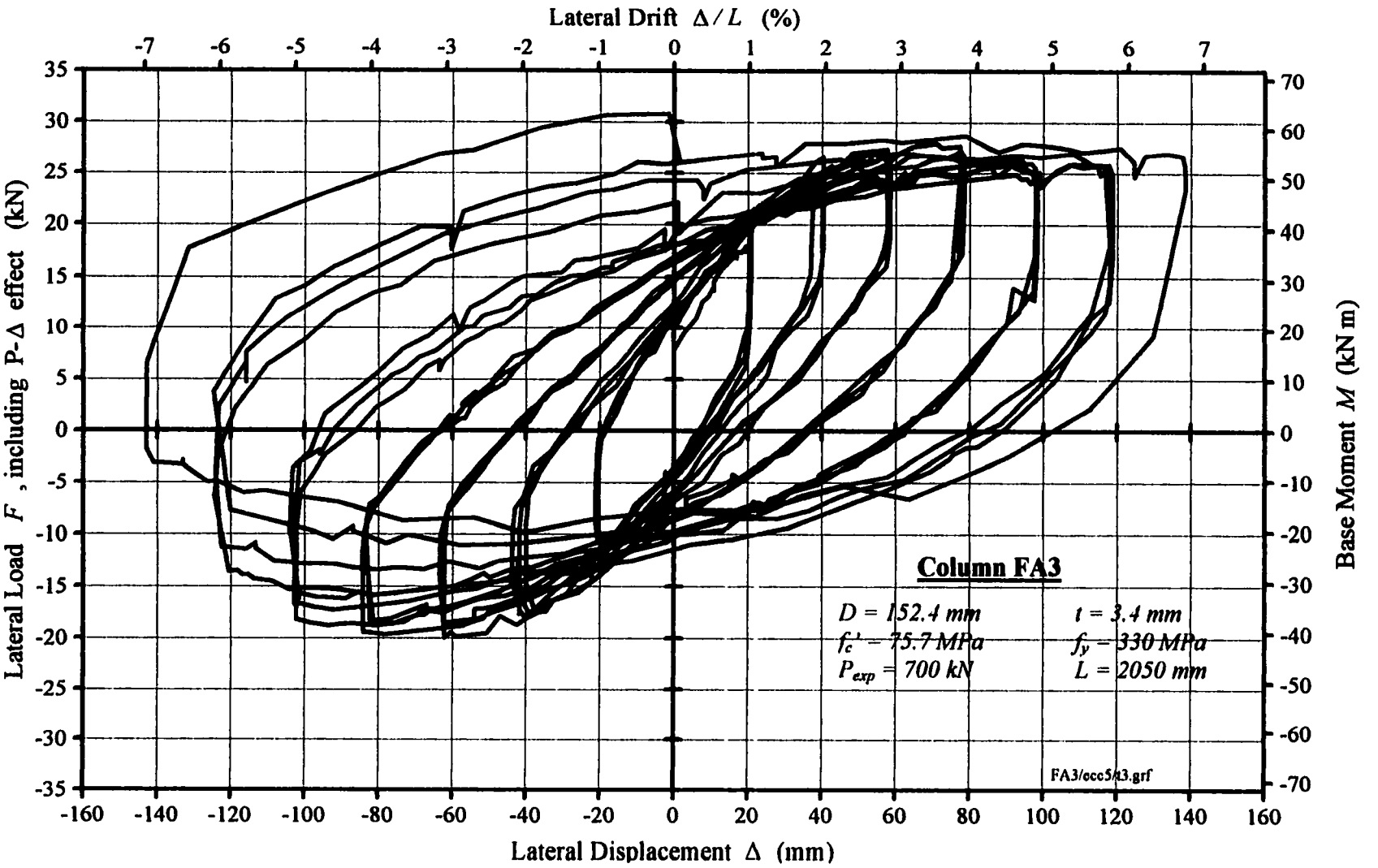

Figure 3.32 : Load-Displacement Curve for Column FA3 (Lateral Load includes second order effects)

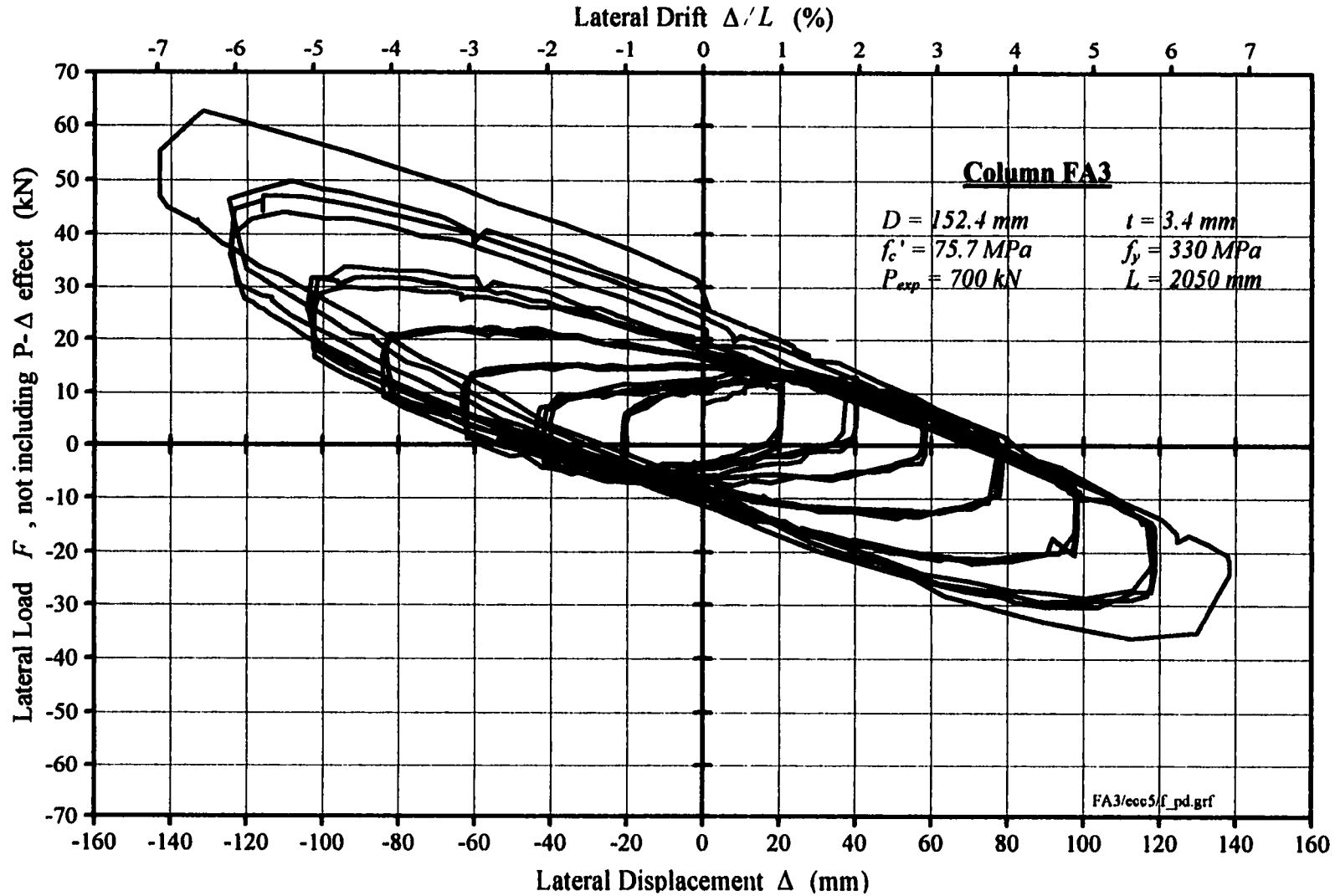

Figure 3.33 : Load-Displacement Curve for Column FA3 (Lateral Load does not include second order effects)

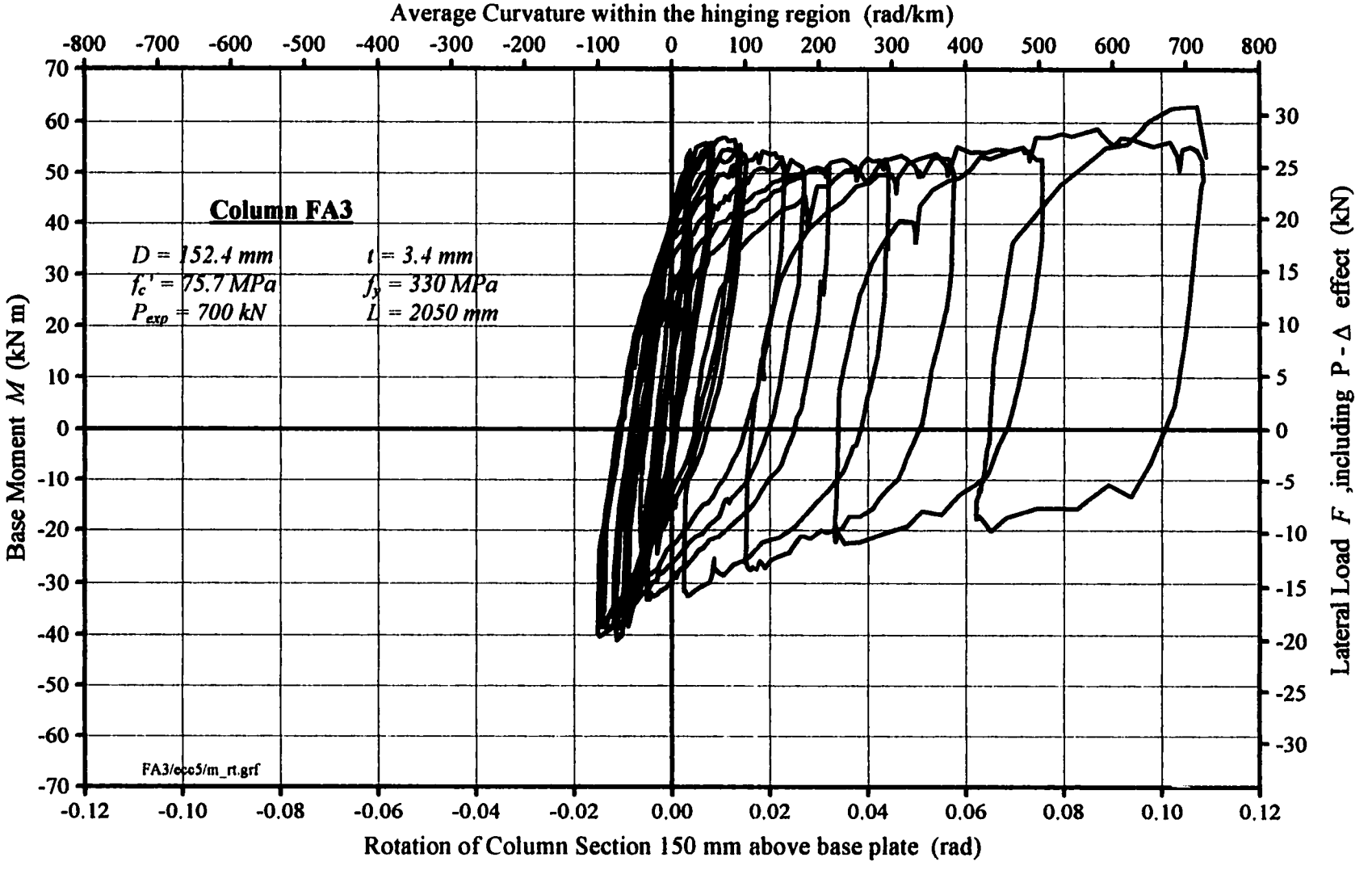

Figure 3.34 : Moment-Rotation Curve for Specimen FA3

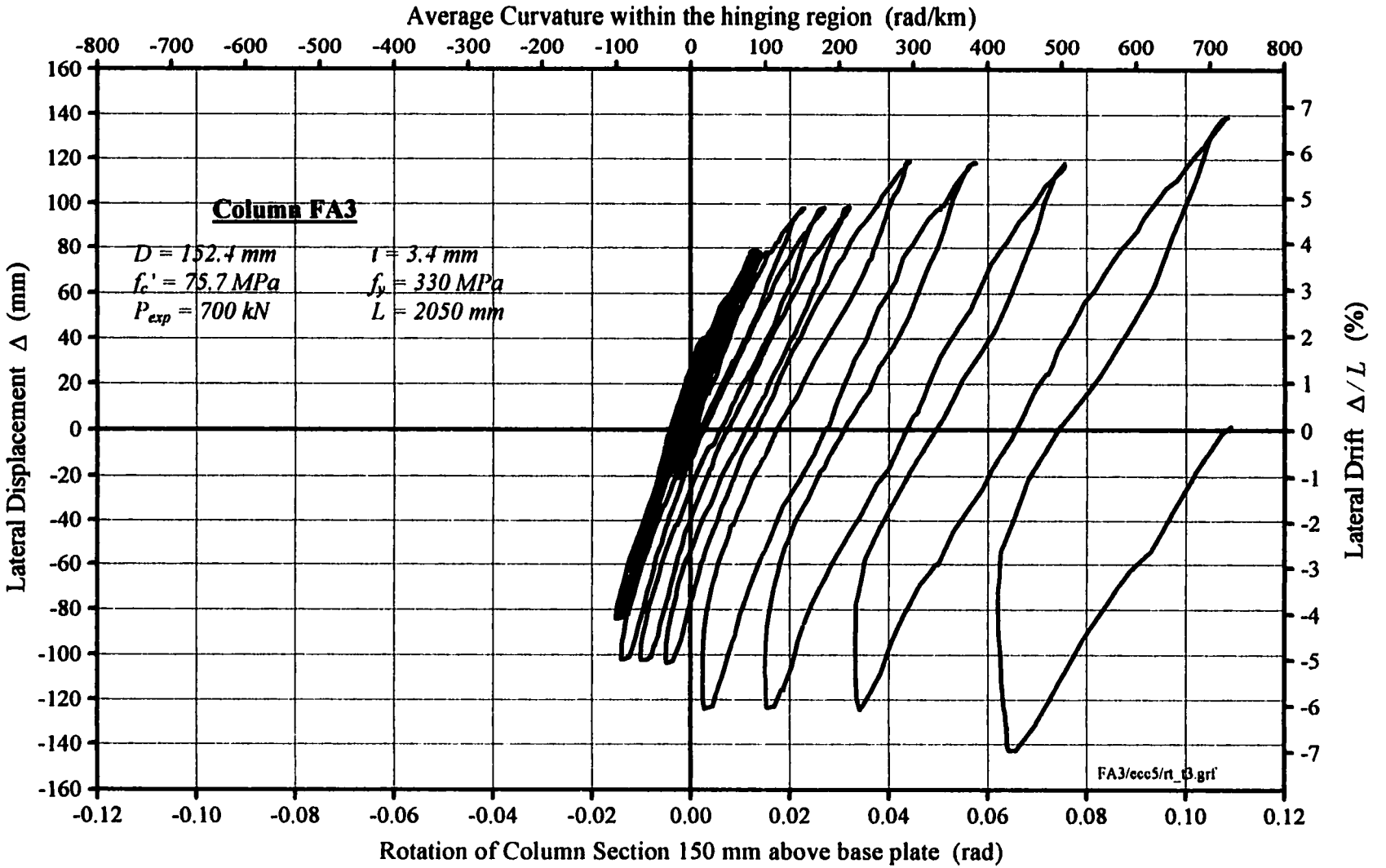

Figure 3.35 : Displacement-Rotation Curve for Specimen FA3

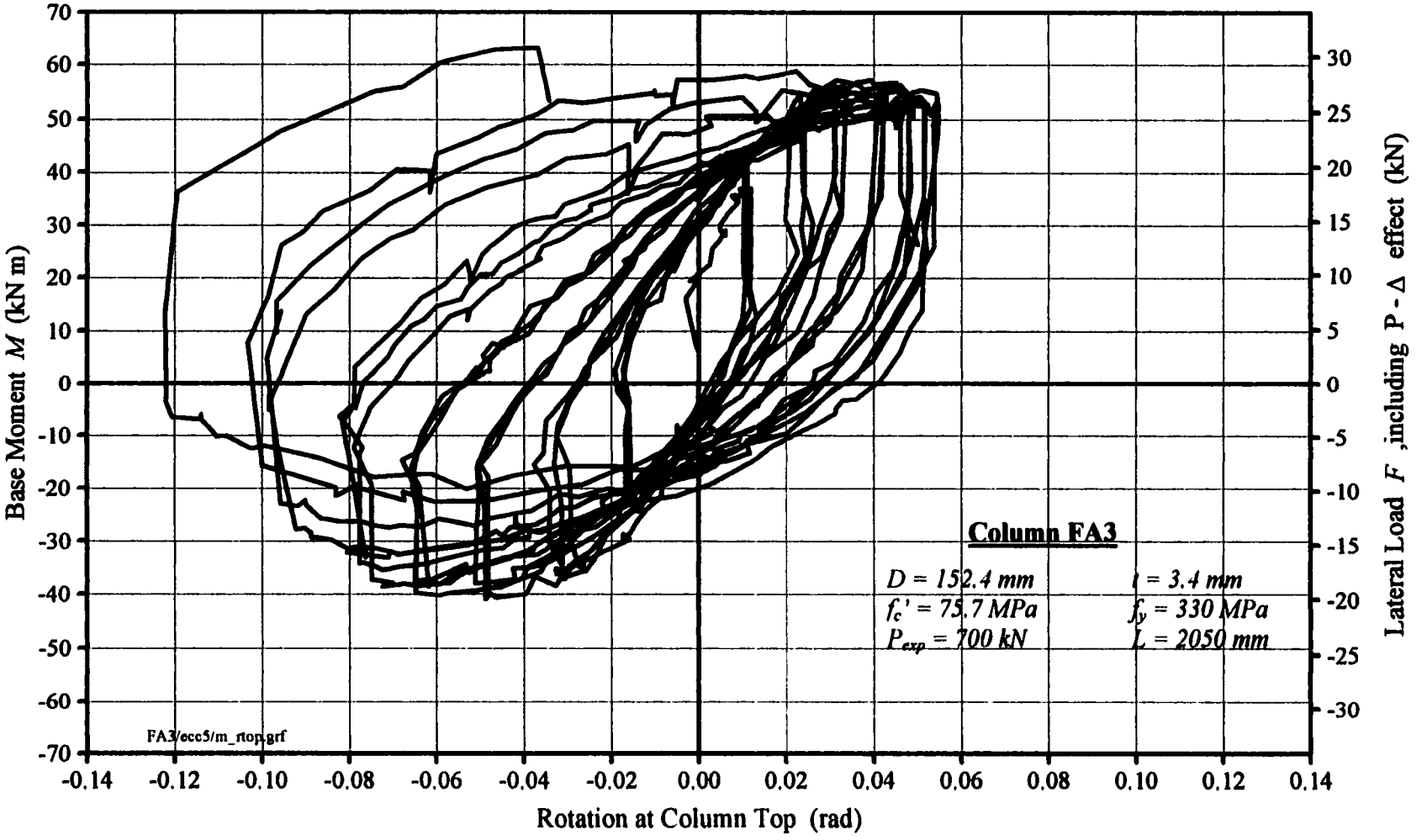

Figure 3.36 : Rotation at the Top of Specimen FA3 (plotted versus Base Moment)

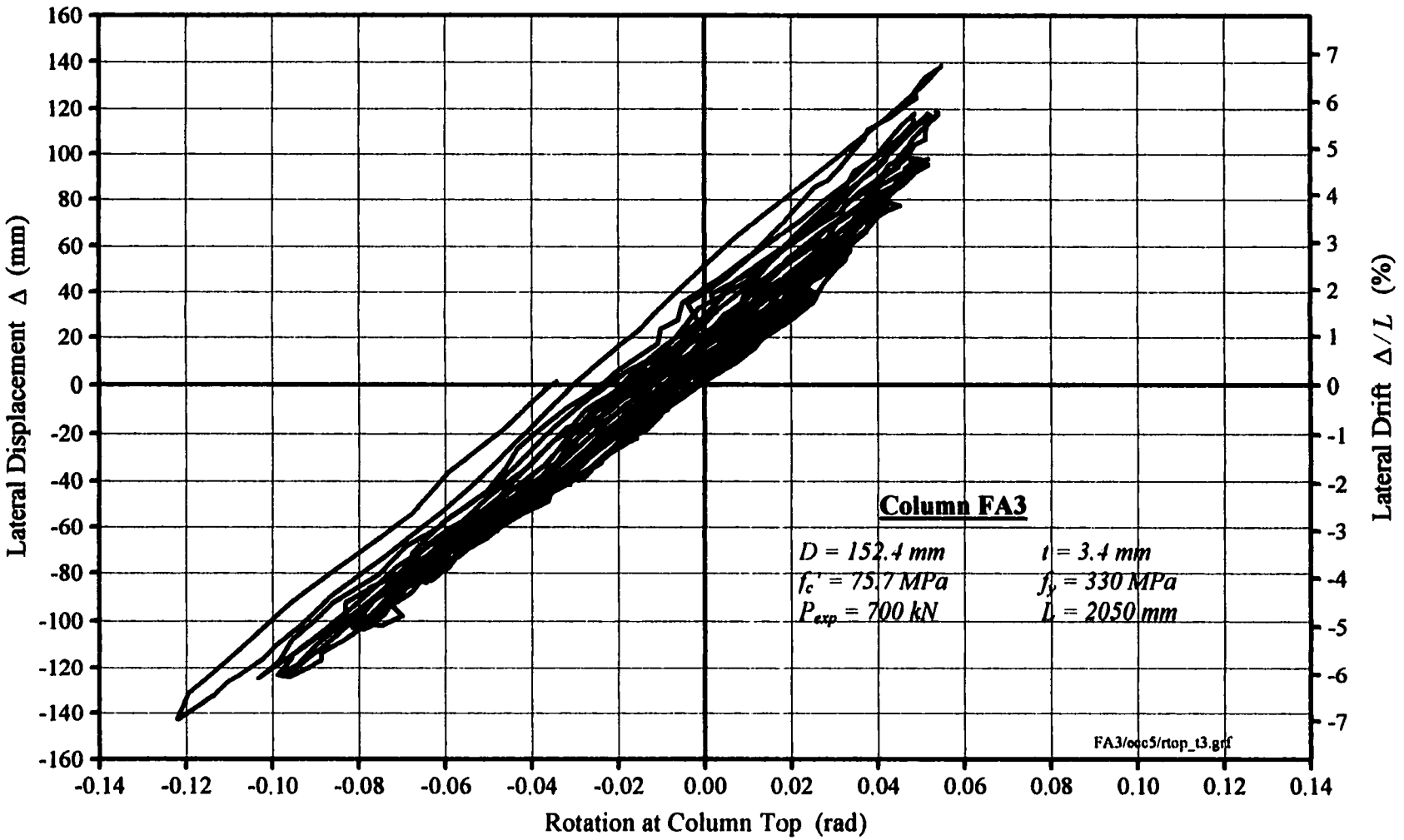

Figure 3.37 : Rotation at the Top of Specimen FA3 (plotted versus Lateral Displacement)

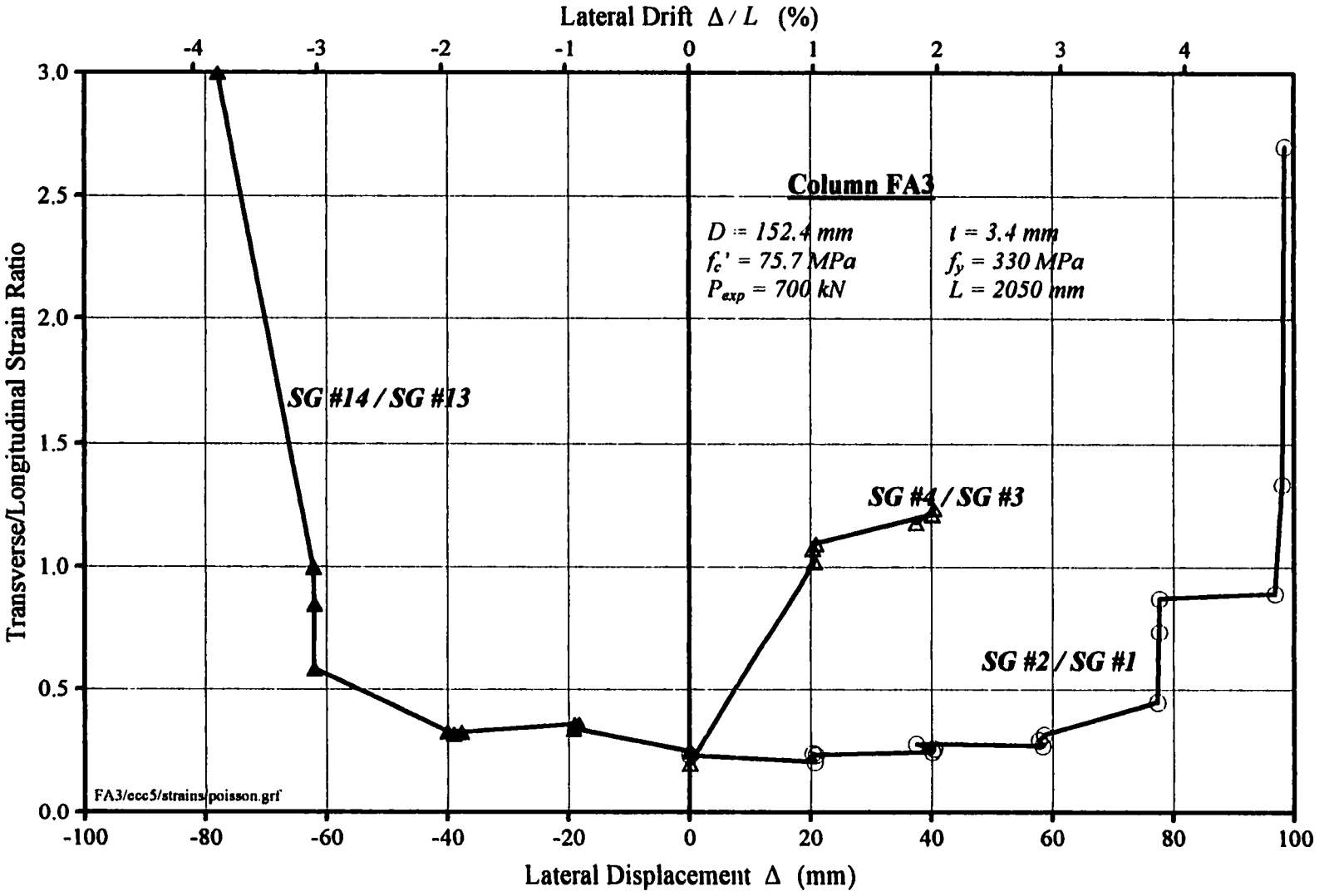

Figure 3.38 : Transverse/Longitudinal Strain Ratios for Specimen FA3

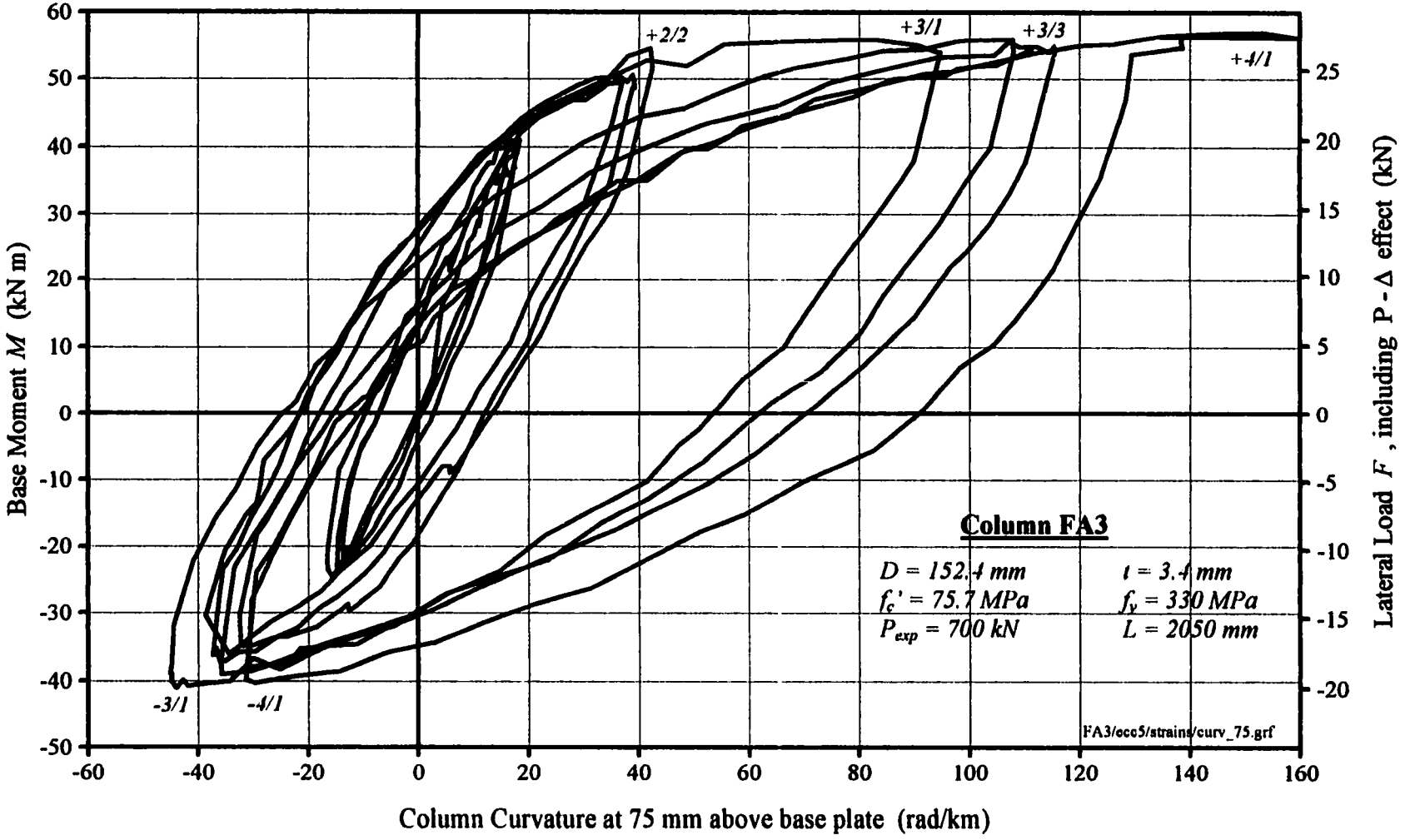

Figure 3.39 : Curvature of Specimen FA3 at 75 mm Above the Base Plate
(computed from data provided by strain gauges #3 and #13)

Chapter 4

Discussion

Analytical considerations pertaining to the effect of concrete confinement by the steel tube are presented. Various code provisions regarding the estimate of load bearing capacity of circular steel CFT columns are described shortly. Test results from Chapter 3 are then discussed. Experimental loads are compared with theoretical predictions. Conclusions and recommendations for future research are summarized in Chapter 5.

4.1 Theory

Some of the previous experimental research on circular CFTs (also, the results of this study) suggests that additional strength could be expected from such members due to the confinement of concrete by the steel tube. A method to evaluate this strength gain theoretically, based on previous analytical work of many researchers, is presented in this section.

4.1.1 Short CFTs under Axial Compression

The axial compression capacity of a circular CFT short column can be conservatively estimated by assuming that both component materials act independently:

$$P_0 = f_y A_s + k_m f'_c A_c \qquad (4.1)$$

where

k_m = modification factor, accounting for the difference between the specified concrete strength, obtained from standard cylinder tests, and the plain concrete strength in a member under concentric compression; modification factors ranging between 0.85 and 1.0 have been reported in the literature, depending on member shape, geometry, concrete casting practice and many other parameters.

Equation 4.1 assumes that the stress in the steel tube has reached the yield level. This is usually true, unless the tube wall is very thin compared to the diameter, so that local buckling of the wall may occur before the yield stress is attained. Data from tests on axially loaded hollow steel cylinders (Sherman, 1992) indicate that full yield capacity is usually achieved, if the diameter/thickness ratio of the tube does not exceed of $23\,000 / f_y$ (in MPa). This limiting value could be further relaxed if the steel tube is filled with concrete, which is known to delay the local buckling.

When a CFT short column is concentrically compressed, not much composite action between the steel tube and the concrete core can be expected during the initial stages of loading, because the Poisson ratio of the concrete is lower than that of the steel. However, as the concrete compressive strain approaches ε_0 (strain, corresponding to the peak stress of unconfined concrete $k_m f'_c$), the lateral expansion of the concrete core tends to become greater than that of the steel tube, and the confinement mechanism is activated. The concrete actively pushes in all lateral directions against the wall of the tube, while the steel passively confines the concrete core. In this situation, the concrete is placed into triaxial compression, while the steel in tube wall could be considered (with simplification) to be in a biaxial state of stress: compressed in the longitudinal direction, and under tension in the circumferencial direction. If the steel-concrete lateral interaction is taken into account, the ultimate axial compressive strength of a CFT column could be expressed as following:

$$P_u = f_s A_s + f'_{cc} A_c \qquad (4.2)$$

where

f_s = stress in steel tube wall in the longitudinal direction;

f'_{cc} = strength of confined concrete in the core.

Recent confinement model (Saatcioglu and Razvi, 1992), suitable for both normal strength and high strength concrete in traditionally reinforced columns, and based on large amount of experimental data, suggests that the strength gain due to confinement is independent of the original unconfined concrete strength. The triaxial strength of high strength concrete can be expressed in terms of its uniaxial strength and lateral confinement pressure by the following equation, originally proposed by Richart et al (1928):

$$f'_{cc} = k_m f'_c + k f_l \tag{4.3}$$

where

f_l = lateral confinement pressure;

k = lateral confinement factor, an empirical coefficient, determined from experimental data.

Richart et al (1929) reported that a constant value of $k = 4.1$ produced a good correlation for spirally reinforced test cylinders. Saatcioglu and Razvi (1992) proposed the following expression for k, obtained from regression analysis of test data::

$$k = 6.7 (f_l)^{-0.17} \tag{4.4}$$

It should be kept in mind, however, that the confinement models, developed for concrete in traditionally reinforced columns, may overestimate the strength and ductility of confined concrete in CFTs due to two major differences in the work of confinement mechanism:

- In reinforced concrete columns, the hoops or spirals restrict the lateral expansion of concrete from the start of axial load application. The lateral pressure gradually builds up. On the other hand, the confinement mechanism in CFTs is initiated only when concrete has already attained significant longitudinal strain.
- The hoops or spirals in reinforced concrete columns are stressed in lateral direction only. On the other hand, the tube wall of a CFT resist stresses in two directions. Both longitudinal compressive stress and circumferencial tensile stress contribute to the development of transverse tensile strain in the steel tube, which translates into a higher rate of lateral expansion for the steel tube (higher volume, lower strength for concrete).

Tomii et al (1977) reported k ranging between 1.4 and 4.8 for normal strength concrete confined by circular steel tubes, with the average $k = 2.6$.

The sign convention, adopted in this subsection for stresses and strains in the steel tube, is that both longitudinal compression and transverse tension are considered positive. Assuming von Mises yield criterion (and neglecting shear stress), the relation between longitudinal and transverse stresses in the steel tube wall after yield could be expressed as:

$$f_s^2 + f_{st}^2 + f_s f_{st} = f_y^2 \tag{4.5}$$

or

$$f_s = (f_y^2 - 0.75 f_{st}^2)^{0.5} - 0.5 f_{st} \tag{4.6}$$

where

f_{st} = transverse tensile stress in steel tube wall.

A simpler relationship could be obtained from Tresca yield condition:

$$f_s + f_{st} = f_y \tag{4.7}$$

or

$$f_s = f_y - f_{st} \tag{4.8}$$

Equations 4.5 and 4.7 are plotted in Figure 4.1. The maximum difference between the two conditions occur in the pure shear case ($f_s = f_{st}$), and it is about 15%. Results of combined biaxial stress tests on steel samples lie somewhere between the two lines (Chen and Atsuta, 1976). Von Mises yield condition is found to be closer to the test results, but Tresca condition gives the conservative limit.

As shown in Figure 4.2, from the condition of equilibrium of a CFT half-section, the lateral confinement pressure on concrete core can be expressed in terms of the transverse tensile stress in the steel tube wall:

$$f_l = f_{st} t / (0.5 D - t) \tag{4.9}$$

or

$$f_l = 0.5 k_g f_{st} A_s / A_c \tag{4.10}$$

where

k_g = a factor, depending only on the geometry of the circular steel tube cross-section; k_g approaches unity for large D/t ratios; its exact value can be calculated from:

$$k_g = 1 - ((D/t) - 1)^{-1} \tag{4.11}$$

Substituting Eqs. 4.3, 4.6 and 4.10 into Eq. 4.2, we obtain:

$$P_u = (f_y^2 - 0.75 f_{st}^2)^{0.5} A_s + k_m f'_c A_c + 0.5 (k_g k - 1) f_{st} A_s \tag{4.12}$$

If Eq. 4.8 is used instead of Eq. 4.6 in the substitution, then P_u can be expressed in a very convenient form:

$$P_u = f_y A_s + k_m f'_c A_c + (0.5 k_g k - 1) f_{st} A_s \tag{4.13}$$

or

$$P_u = P_0 + (0.5 k_g k - 1) f_{st} A_s \tag{4.14}$$

In Eqs. 4.12 and 4.14, P_u is a function of a single variable f_{st}, for a given CFT cross-section with defined material properties, if k is assumed constant (also, if k is assumed as a function of f_l). Both equations are plotted in Figure 4.3. It should be noted here, that the function $P_u(f_{st})$ does not have extremes at any point within the considered stress range of $0 \le f_{st} \le f_y$, and further simplifications from the condition of $dP_u / df_{st} = 0$ (or $dP_u / df_l = 0$) are not possible.

Equation 4.14 shows, that the increase in compressive strength of the concrete core more than compensates for the reduction in steel yield strength in vertical compression, as long as k is more than $2/k_g$. The second term on the right side of Eq. 4.14 represents the additional strength attained by a CFT short column due to concrete confinement effect. It is clear, that this strength gain depends primarily on f_{st}, i.e. the magnitude of transverse tensile stress developed in the tube before failure. Obviously, the tube will be best employed, if it is stressed only in the circumferencial direction, so that $f_{st} = f_y$ could be attained. However, it never happens, because longitudinal compressive stress is always present in the steel tube, due to the overall shortening of the column and axial load transfer from concrete core to steel tube through bond, even when concrete core is loaded alone (Gardner and Jacobson, 1967), or when the bond is weakened by artificial means (Orito et al, 1987).

It is not likely, that the strength of core concrete f'_c has any significant influence on f_{st} . It is reasonable to suggest that, for a given f_y , the magnitude of f_{st} will increase with the decrease of D/t ratio. Tests of Tomii et al (1977) showed that the distribution of stresses in longitudinal and transverse directions in the steel tube is affected by the steel contribution factor. The magnitude of tensile circumferencial stress f_{st} in a CFT, for every D/t and f_y combination, can be estimated with sufficient accuracy from experimentally determined ratio β of transverse/longitudinal strains in the steel tube at failure:

$$\varepsilon_{st} / \varepsilon_s = \beta \tag{4.15}$$

Also, from Tomii et al (1977):

$$\beta \cong d\varepsilon_{st} / d\varepsilon_s \cong (2 f_{st} + f_s) / (f_{st} + 2 f_s) \tag{4.16}$$

Combining Eqs. 4.8 and 4.16 and solving, we obtain:

$$f_{st} \cong \beta f_y / (\beta + 1) \tag{4.17}$$

If the lateral confinement factor is assumed not constant, the variation of k can be taken into account by substituting Eqs. 4.4 and 4.10 into Eq. 4.14:

$$P_u = P_0 + (3.77\, k_g^{0.83}\, (f_{st} A_s / A_c)^{-0.17} - 1)\, f_{st} A_s \tag{4.18}$$

Comparison of Eq. 4.14 (with constant $k = 4.1$) and Eq. 4.18 is presented in Figure 4.4 for the case of specimen ST1.

4.1.2 CFT Sections under Combined Compression and Bending

It is generally believed (Neogi et al, 1969; Chen and Chen, 1973), that concrete confinement is not important for slender CFT columns (with length/diameter ratio greater than 15). This is true, however, only in the context that confinement effect does not increase the buckling load, when increasing axial compressive (concentric or eccentric) load is applied, and instability dictates the

failure. Concrete has to attain considerable compressive strain before confinement is activated, and overall buckling in longer columns occurs before the concrete can expand sufficiently to result in any noticeable confinement effect.

When the axial load is held at a low or intermediate level, concrete confinement effect contributes to the bending moment resistance of CFT beam-columns. Test results of Matsui et al (1995) suggest that even long circular CFT beam-columns may resist moments exceeding their theoretical full plastic moment capacities.

The applicability of the theoretical approach, described in the previous subsection, to CFT sections subjected to combined compression and bending is severely complicated by the presence of the strain gradient. The lateral expansion of the concrete near the extreme compression fiber may be very significant, while concrete in the tension zone and near the neutral axis cannot be expected to expand laterally. This translates into nonuniform lateral confinement pressure, as shown in Figure 4.5. The combination of stresses in various directions is unique for every point in the concrete core cross-section. Consequently, concrete at every point will have its own unique stress-strain relationship. The analysis is further complicated by the variation of longitudinal and transverse stresses in the steel tube section. Due to the described difficulties, the sectional analysis for CFT beams or beam-columns is usually performed with uniaxial stress-strain relationships employed for both concrete and steel, and the beneficial effect of concrete confinement is either neglected or partially taken into account by assuming higher concrete ductility and $k_m = 1$ (Chen and Chen, 1973; Eurocode 4, 1994).

It is worth to note here, that the lateral shrinkage of the steel tube wall in the tension zone contributes to the lateral confinement pressure. On the other hand, the concrete core restricts the steel in the tension zone from contracting, causing the development of circumferencial tensile stress in the tube. This might translate into a slight increase of the yield strength of the steel in longitudinal tension. The most confined concrete is located far from the section centroid, so that any increase in concrete compressive resistance here efficiently contributes to the bending moment resistance of the CFT section. Another beneficial composite effect worth mentioning is that the concrete core restricts the ovalization (Sherman, 1986) of circular steel tubes in bending.

4.2 Codes

Recent provisions for circular CFT columns of three major North American design codes and Eurocode 4 are presented in this section. It was intended to maintain common notation, so that the original code notation is modified. The design equations are modified, where possible, to directly accommodate provisions pertaining to circular CFTs and exclude unrelated provisions, and simplify the expressions. All loading and safety factors are neglected. The design for shear is not discussed.

AISC LRFD 1993 (American Institute of Steel Construction, 1994)

The applicability of this code to circular CFTs is limited by the following conditions:

- $A_s \geq 0.04\, A_g$;
- $3\ ksi \leq f'_c \leq 8\ ksi\ (21\ MPa \leq f'_c \leq 55\ MPa)$;
- $f_y \leq 55\ ksi\ (379\ MPa)$ in calculating the strength;
- $t \geq D\,(f_y / 8\,E_s)^{0.5}$.

The third limitation, concerning the yield strength of the steel tube, was proven to be too concervative by Kenny et al (1994), who recommended this critrion to be revised for tubular members to allow for nominal yield stress values as high as 80 ksi (552 MPa).

The strength of axially loaded circular CFT columns is given by:

for $\lambda_{ms} \leq 1.5$ $$P_u = (0.568^{\lambda_{ms}^2})\, A_s f_{my} \tag{4.19}$$

for $\lambda_{ms} > 1.5$ $$P_u = (0.877 / \lambda_{ms}^2)\, A_s f_{my} \tag{4.20}$$

where

$$\lambda_{ms} = (K L / (r_s \pi))\, (f_{my} / E_{ms})^{0.5} \tag{4.21}$$

$$f_{my} = f_y + 0.85 f'_c A_c / A_s \tag{4.22}$$

$$E_{ms} = E_s + 0.4\, E_c A_c / A_s \qquad (4.23)$$

K = effective length factor;

L = laterally unbraced length of column.

Equations 4.19 through 4.23 take into account the contribution of the concrete core to the axial strength and stiffness of composite columns. The code, however, neglects any contribution of concrete to the flexural capacity of CFTs. In the case of combined compression and uniaxial bending, a simple bilinear interaction relationship is used for circular CFT beam-columns:

for $P / P_u \geq 0.2$ $\qquad P / P_u + 0.89\, M_u / M_0 \leq 1.0 \qquad (4.24)$

for $P / P_u < 0.2$ $\qquad 0.5\, P / P_u + M_u / M_0 \leq 1.0 \qquad (4.25)$

where

M_0 = the flexural strength of a CFT beam-column, when $P = 0$. Here M_0 is limited by the flexural strength of the steel section alone:

$$M_0 = Z_s f_y \leq 1.5\, S_s f_y \qquad (4.26)$$

CAN/CSA-S16.1-94 , Canadian Standards Association (Canadian Institute of Steel Construction, 1995)

This is the only national code that provides design guidance for circular CFTs in Canada. The code recognizes the superior performance of circular CFTs under axial compression, and accounts for triaxial effects by the introduction of special factors ($\tau' > 1.0$ and $\tau < 1.0$). In the 1994 standard, new provisions taking account of concrete core contribution to the flexural strength of rectangular CFTs were introduced, based on the research of Lu and Kennedy (1994). Consequently, bending moment resistance of rectangular CFTs under combined compression and bending was increased. However, the lower bound solution, assuming bending to be resisted by steel section alone, is retained for the design of circular CFTs, which is not very logical, since it is well known that circular CFTs perform better than the rectangular CFTs.

The code specifies the lower limit for the wall thickness of circular CFTs by $t \geq D f_y / 28\,000$.

The compressive resistance of circular CFT columns is specified as:

$$P_u = \tau' P_c + \tau P_s \tag{4.27}$$

where

$$P_c = 0.85 f'_c A_c \lambda_c^{-2} ((1 + 0.25 \lambda_c^{-1})^{0.5} - 0.5 \lambda_c^{-2}) \tag{4.28}$$

$$P_s = f_y A_s (1 + \lambda_s^{1.48})^{-0.446} \tag{4.29}$$

$$\tau = (1 + \rho + \rho^2)^{-0.5} \tag{4.30}$$

$$\tau' = 1 + (25 \rho^2 \tau t / D) (f_y / (0.85 f'_c)) \tag{4.31}$$

$$\rho = 0.02 (25 - (L / D)) \tag{4.32}$$

$$\lambda_c = (K L / (r_c \pi)) (f'_c / E_c)^{0.5} \tag{4.33}$$

$$\lambda_s = (K L / (r_s \pi)) (f_y / E_s)^{0.5} \tag{4.34}$$

$\tau = \tau' = 1.0$ for circular CFTs with $L / D \geq 25$ (and for all rectangular CFTs);
for circular CFTs in axial compression with $t < D f_y / 23\,000$, A_s must be taken as the effective area, determined in accordance with CSA Standard S136 (this condition does not apply for circular CFTs in flexural compression).

For circular CFT members required to resist both bending moment and axial compression, the concrete core is assumed to carry the axial load only, while the steel section must be proportioned to carry the total bending plus axial compression in excess of $\tau' P_c$. The introduction of $\tau < 1.0$ here makes the bending moment capacity of a CFT column at $P = 0$ even less than the moment resistance of hollow steel section alone in pure bending (and τ decreases for shorter beam-columns).

$$M_u \leq \tau M_0 \tag{4.35}$$

and if $P > \tau' P_c$ $$(P - \tau' P_c)/(\tau P_s) + U_l M_u / \tau M_0 \leq 1.0 \tag{4.36}$$

where

for $t \geq D f_y / 18000$ $$M_0 = Z_s f_y \tag{4.37}$$

for $D f_y / 18000 \geq t \geq D f_y / 28000$ $$M_0 = S_s f_y \tag{4.38}$$

U_l = parameter, accounting for second order effects due to the deformation of a member between its ends.

ACI 318-95 (ACI Committee 318, 1996)

The lower limit of tube wall thickness for circular CFTs is specified by $t \geq D\,(f_y / 8\,E_s)^{0.5}$.

The axial compression strength of CFT columns is limited to 85 % of the nominal section strength (with $k_m = 0.85$) to account for accidental eccentricities:

$$P_u = 0.85\,(0.85 f'_c A_c + f_y A_s) \tag{4.39}$$

The provisions for computing axial-flexural strength interaction curves for CFT sections are essentially the same as those for reinforced concrete. Linear strain gradient and full strain compatibility are assumed throughout the composite section, with the maximum usable strain at extreme concrete compression fiber equal to 0.003. Tensile strength of concrete is neglected. Rectangular stress block with a stress ordinate of $0.85 f'_c$ is assumed for concrete in compression, acting over an equivalent compression zone bounded by the edges of concrete cross section and a straight line located parallel to the neutral axis at a distance of $a = 0.65\,c$ from the concrete fiber of maximum compressive strain (coefficient of 0.65 is specified for $f'_c \geq 55$ MPa; c = distance from the concrete fiber of maximum compressive strain to the neutral axis). Stresses in steel tube fibers are determined from $f_s = E_s\,\varepsilon_s$ and $-f_y \leq f_s \leq f_y$.

The code requires slenderness effects to be taken into account by performing second-order analysis to determine design forces and moments. This analysis should consider material non-linearity and cracking, the effects of member curvature and lateral drift, duration of loads, shrinkage and creep, and interaction with the supporting foundation. Alternatively, slenderness effects may be analyzed in terms of specified moment magnifiers using a reduced Euler load and expressions for equivalent stiffness and radius of gyration, accounting for creep and cracking.

Eurocode 4 (European Committee for Standardization, 1994)

The minimum steel tube wall thickness for circular CFTs is limited to $t \geq D f_y / 21150$.

Favorable development of concrete strength in CFT columns is recognized by allowing the use of $k_m = 1.0$ (instead of $k_m = 0.85$ used for other composite columns). The code provides a simple method for the construction of composite cross-section interaction curve, approximated by a polygonal path, shown in Figure 4.6. The combinations of axial load and bending moment, that define the points A, B, C and D of the polygonal diagram, are calculated using full plastic rectangular stress blocks for both steel and concrete. The following expressions can be used circular CFT sections:

$$P_A = \eta_2 f_y A_s + f'_c A_c (1 + \eta_1 (t/D)(f_y/f'_c)) \quad (4.40)$$

$$P_C = f'_c A_c \quad (4.41)$$

$$P_D = 0.5 f'_c A_c \quad (4.42)$$

$$M_D = f_y Z_s + 0.5 f'_c Z_c \quad (4.43)$$

$$M_B = M_C = M_D - 2 t h_n^2 f_y - 0.5 ((D - 2t) h_n^2) f'_c \quad (4.44)$$

where

$$h_n = 0.5 f'_c A_c / (2 D f'_c + 4 t (2 f_y - f'_c)) \quad (4.45)$$

$$\eta_1 = \eta_{10} (1 - 10 e / D) \geq 0.0 \quad (4.46)$$

$$\eta_2 = \eta_{20} + (1 - \eta_{20}) (10 e / D) \leq 1.0 \quad (4.47)$$

$$e = M / N \quad (4.48)$$

$$\eta_{10} = 4.9 - 18.5 \lambda + 17 \lambda^2 \geq 0.0 \quad (4.49a)$$

but for $\lambda \geq 0.5$ $\eta_{10} = 0.0$ (4.49b)

$$\eta_{20} = 0.25 (3 + 2 \lambda) \leq 1.0 \quad (4.50)$$

$$\lambda = (K L / \pi) ((f_y A_s + f'_c A_c) / (E_s I_s + 0.8 E_c I_c))^{0.5} \quad (4.51)$$

The polygonal diagram in Figure 4.6 implies that $M_A = 0$ and $P_B = 0$. Equation 4.40 takes into account the increase in strength of concrete caused by confinement in shorter columns ($\lambda < 0.5$). This equation can be used (in combination with Eq. 4.52) to calculate the compressive resistance of eccentrically loaded ($0 < e \leq 0.1 D$) short circular CFT columns. However, for the interaction curve P_A is calculated with $e = 0$, and Eqs. 4.46 and 4.47 become $\eta_1 = \eta_{10}$ and $\eta_2 = \eta_{20}$, respectively. For longer columns, having relative slenderness $\lambda \geq 0.5$, the effect of confinement should not be taken into account, and the values of η_1 and η_2 become 0.0 and 1.0, respectively, according to Eqs. 4.46 through 4.50. The value of P_A in this case becomes equal to P_0 given by Eq. 4.1 (with $k_m = 1.0$). Also, it is worth mentioning here, that Eq. 4.51 takes into account the contribution of concrete core to the axial stiffness of the composite section.

The resistances derived for composite sections have to be reduced for real columns to take account of imperfections and slenderness effects. The resistance of members in axial compression is specified by:

$$P_u = \chi P_A \quad (4.52)$$

where

χ = reduction coefficient, depending on relative slenderness; for CFT columns χ is determined from buckling curve "a" of Eurocode 3 or calculated from:

$$\chi = f_k - (f_k^2 - \lambda^{-2})^{0.5} \leq 1.0 \tag{4.53}$$

with

$$f_k = 0.5\,\lambda^{-2}\,(1 + 0.21\,(\lambda - 0.2) + \lambda^2) \tag{4.54}$$

The bending moment capacity of CFT columns should be reduced according to:

$$M_u \leq 0.9\,\gamma\,M_B \tag{4.55}$$

where

$$\gamma = \gamma_d - \gamma_k\,(\chi_d - \chi_n)/(\chi - \chi_n) \tag{4.56}$$

$$\chi_n = 0.25\,\chi\,(1 - r) \tag{4.57}$$

$$\chi_d = P/P_A \tag{4.58}$$

γ_d and γ_k = parameters, shown in Figure 4.6;

r = ratio of the lesser to the greater end moment in the column; $-1.0 \leq r \leq 1.0$.

Smoother *P-M* interaction curves (and more accurate predictions) can be obtained by introducing a larger number of limiting combinations of axial load and bending moment, using the same underlying principles as for points A, B, C and D, i.e. full plastic section analysis with rectangular stress blocks of $\pm f_y$ for steel and f'_c for concrete in compression.

4.3 Evaluation of Test Results

4.3.1 Short Column

Table 4.1 provides the comparison of failure load P_{exp} of specimen ST1 with theoretical predictions of design codes, described in the previous section, and estimates, obtained by using Eqs. 4.1, 4.14 and 4.18. The values of $K = 1.0$ and $L = 380\ mm$ were used, where required by code specifications. The value of β was conservatively estimated to be equal to 1.0, based on the observed shear failure mode and measured strains. Consequently, $f_{st} = 0.5\, f_y$ was used in Eqs. 4.14 and 4.18. The value of k = 4.1 (Richart et al, 1929) was used for Eq. 4.14. Also, the assumption of $k_m = 1.0$ was considered appropriate for Eqs. 4.1, 4.14 and 4.18.

All considered design code predictions showed to be conservative compared to P_{exp}. Estimate by Eurocode 4 showed to be least conservative and very accurate. Compressive resistance obtained from CAN/CSA-S16.1-94 was also very close to the experimentally determined capacity. Both AISC LRFD 1994 and ACI 318-95 showed to seriously underestimate the resistance of short CFTs under axial compression, with ACI prediction being the most conservative and inaccurate.

Equations 4.14 and 4.18 gave accurate predictions. It seems that, with a broader base of available reliable experimental data on short HSCFTs under axial compression, the parameter β, involved in these equations, could be calibrated for a wide range of D/t ratios. Also, more experiments are needed to determine the variation of β for different levels of f_y and f'_c. Concrete confinement effects are present in short HSCFTs, and there is certain need to determine whether confinement models, developed for high strength concrete in traditionally reinforced columns, are applicable for CFTs. The result of this single test shows that the described confinement models can be indeed applied if appropriate value of β is chosen. Strains measured during the test indicate that β at various points of steel tube wall is far from uniform, and a reasonable approximation is required.

The estimate by Eq. 4.1 shows that P_{exp} exceeded the nominal axial compression capacity P_0 by only 16.7%. This result shows that, the relative increase in the overall compressive strength of a short HSCFT due to confinement effects is not that great, as it could be expected from CFTs with normal strength concrete. Since the increase in concrete strength due to triaxial effects does not depend (or depends very little) on its uniaxial strength, the relative increase in strength due to

confinement tends to decrease with higher f'_c , and would, probably, be negligible if concrete of $f'_c \geq 150\ MPa$ is used for standard structural steel CFTs. Greater levels of lateral confinement pressure are needed for high strength concrete in order to supply significant relative increase in strength due to triaxial effects. Apart of using thicker tubes, it is likely, that HSCFTs made of high strength steel (providing higher f_y, higher f_{st} and higher f_l) will be more efficient in terms of relative strength increase due to confinement. There is certain need for experimental research on circular CFTs that would incorporate high strength steel and high strength concrete.

4.3.2 Beam-Columns

In this subsection, the test results of specimens FA1-FA3 are discussed in terms of obtained experimental bending moment capacities and ductility levels. Theoretical predictions of flexural strength, calculated according to design code procedures, described in the previous section, are compared with experimental results. The effects of the axial load level, which was the main variable in this small series, are outlined.

Flexural Strength

Figure 4.7 shows the lateral load-displacement envelope curves for specimens FA1-FA3. The bending moment resistance of the beam-column specimens in the positive direction steadily increased with the increase of the axial load level. In the negative direction, the lateral load capacities of specimens FA2 and FA3 were less than that of specimen FA1. This was due to the development of the double curvature shape in specimens FA2 and FA3, described in section 3.2. Slenderness effects at axial load levels of 700 kN and 1000 kN caused the maximum bending moment to develop between the ends of the beam-columns. In both cases, this phenomenon was observed in the negative loading direction only, causing the lateral load resistance in that direction to be significantly less than in the positive direction. It looks like the cyclic loading promotes the slenderness to take effect in the direction of reversed loading. The ratios of measured extreme negative to positive base moments M^-_{exp} / M^+_{exp} for specimens FA1, FA2 ($P_{exp} = 1000\ kN$) and FA3 were 0.97, 0.54 and 0.72, respectively. In the case of specimen FA2 ($P_{exp} = 100\ kN$), this ratio was 0.71, which indicates that the specimen did not fully recover after the initial "shake" under axial load level of 1000 kN. It should be noted here, for specimens FA2 and FA3, that the maximum negative moments calculated at the base, probably, reflect only a part of the real

maximum negative moments experienced by the columns. The rotation measurements for these specimens and the final shape of beam-column FA3 support this suggestion. It is likely, that the bending moments measured in the positive direction are more representative of the real flexural strength of tested sections. Nevertheless, the values of M_{exp} used in the following comparison were taken as the average of maximum measured positive and negative base moments for each case. These values are conservative lower bound estimates of the experimental section capacity flexural strength of the tested columns.

The values of experimental bending moment strength M_{exp} of beam-columns FA1-FA3 are compared in Table 4.2 with the theoretical predictions of flexural capacity, based on the provisions of design codes, described in the previous section. Figures 4.8, 4.9 and 4.10 illustrate the theoretical *P-M* interaction curves for columns FA1-FA3, used in this comparison. A computer program, called CFTACI, was developed to compute the *P-M* combinations for the ACI 318-95 section capacity curves. Fortran code for this program is presented in Appendix B. Similar program was developed and used for the construction of Eurocode 4 full plastic section capacity curves. The CAN/CSA-S16.1.-94 and AISC LRFD 93 interaction curves were derived for $L = 0$. Because the procedure of CAN/CSA-S16.1.-94 leads to increase in flexural strength with the increase of L, it was found appropriate to include additional CAN/CSA-S16.1.-94 curve in the comparison, which was derived for $K = 0.7$ and $L = 2050\ mm$. Sample calculations for the derivation of CAN/CSA-S.16-94 and AISC LRFD 93 curves for column FA1 are presented in Appendix C.

Figures 4.8, 4.9 and 4.10 show, that significant discrepancies exist between design codes, and predictions of beam-column flexural strength are widely scattered. AISC LRFD 1994 gives the lowest estimates of M_u at intermediate and high axial load levels, while CAN/CSA-S16.1.-94 is the most conservative in the lower range of P. Both codes were developed for the design of steel structures, and seriously underestimate the contribution of concrete to the flexural strength of circular CFT beam-columns. These two codes also neglect any increase in flexural strength due to the concrete core in circular CFTs in the case of pure bending.

For all tested beam-columns, M_{exp} was higher than any of the considered predictions. Even the estimates using full plastic section analysis, which partially accounts for concrete confinement effects were less than the experimental results. Within the range of the axial load levels applied to

beam-column specimens during this experimental investigation $0.06 \leq P_{exp} / P_0 \leq 0.58$, both M_{exp} and the ratio M_{exp} / M_u steadily increased with the increase of the axial load, as shown in Table 4.2. It indicates, that the contribution of concrete core to the flexural strength and concrete confinement effects become greater as the area of the compression zone in the composite cross section increases with the increase of the axial load level. The obtained degrees of flexural strength enhancement M_{exp} / M_u (ACI 318-95) are similar to those reported by Priestley and Park (1987) for reinforced concrete beam-columns with high amounts of transverse reinforcement.

The method suggested by Eurocode 4 gave the least conservative and the most accurate predictions of flexural strength for circular CFT columns tested during this investigation. Also, the simplicity of this method makes it very attractive for practical use.

The local buckling in all three specimens occurred after the maximum moments had been attained. No immediate changes due to buckling could be observed in any of the obtained experimental data curves. Visual observations and strain measurements suggest that local buckling was associated with high amplitudes of strain cycles in the steel tube, rather than the crushing failure (or abrupt decrease in strength) of the concrete core, as it is generally believed. In circular CFT beam-columns under cyclic lateral load, crushing failure of concrete in the local buckling zone does not cause, accompany or immediately follow the local buckling of the steel tube. The observed final lengths of the bulges, not exceeding 35 mm, imply that the concrete core was well confined in the buckling zone up to the end of testing. The fatigue deterioration of steel tube wall along the lines of severe cyclic flexure, associated with the progress of local buckling under compression and subsequent straightening up under tension, certainly contributed to the gradual reduction in the lateral strength of CFT beam-columns after local buckling had occurred.

Ductility

Ductility is the ability of structures to undergo large deformations without significant loss in load bearing capacity. It is usually evaluated in terms of a ratio of the maximum deformation to the yield deformation. The latter is defined as the deformation at an assumed yield load (usually, estimated theoretically) reflecting the bilinear approximation of the load-deformation curve. The common procedure to experimentally determine the yield displacement Δ_y (Park et al, 1983) at the beginning of each test (and then apply increments of Δ_y for lateral reversals) was not adopted

in this experimental study because of the concern, that the theoretical ultimate lateral load predicted for CFT beam-columns will not be accurate. As it was mentioned in Chapter 1, if large difference occurs between this theoretical load and the obtained experimental ultimate lateral load, Δ_y determined based on the theoretical load will not be representative of the experimental hysteretic curve, and that will lead to errors in the assessment of the ductility levels achieved. Here, it was considered more appropriate to use lateral loading path based on lateral drift increments, and later calculate the attained displacement ductility levels using Δ_y, determined as shown in Figure 4.11. The presented method for the calculation of Δ_y is just a modification of the common procedure, but it does not depend on the theoretical ultimate lateral load.

On the experimentally obtained moment-displacement hysteretic curves, the points of first encountered $0.7\,M^{+}_{exp}$ and $0.7\,M^{-}_{exp}$ were found. The yield displacements in each direction were obtained by extrapolating straight lines from the origin through these points until they reached the levels of $0.9\,M^{+}_{exp}$ and $0.9\,M^{-}_{exp}$. The yield displacement Δ_y for each beam-column was taken as the average of yield displacements obtained for the positive and negative directions. The attained displacement ductility level in a direction was then calculated as $\mu = \Delta_{max} / \Delta_y$, where Δ_{max} represents the maximum lateral displacement achieved in that direction before the flexural resistance dropped below the level of 70% of the maximum experimental moment in that direction. The yield curvatures φ_y and maximum curvatures φ_{max} (reflecting average curvature in the hinging region) were obtained in the same manner from the moment-rotation relationships.

The computed ductility factors for specimens FA1, FA2 ($P_{exp} = 100\ kN$) and FA3 are presented in Table 4.3. In the case of specimen FA2 ($P_{exp} = 1000\ kN$), the testing was stopped, for reasons explained in section 3.2, just after the column attained a displacement ductility level slightly exceeding 2. The curvature ductility for the negative direction for specimen FA3 could not be established, because the negative rotations of the column were supplied by flexure outside the hinging region.

All specimens exhibited favourable ductile hysteresis behavior with no or little "pinching". Column FA1 gave the least ductility factors of $\mu = 4.0$ and $\phi_{max} / \phi_y = 8.3$. From the results of this investigation, it was not possible to establish the effects the axial load level might have on the ductility factors and parameters.

Table 4.1 - Theoretically Predicted Axial Compression Capacities for Short Column ST1

($P_{exp} = 2157\ kN$)

Theoretical Prediction Method Used	Predicted Capacity P_u or P_0 (kN)	P_{exp} / P_u or P_{exp} / P_0
AISC LRFD 1993	1641	1.314
CAN/CSA-S16.1-94	2009	1.074
ACI 318-95	1403	1.537
Eurocode 4	2093	1.031
Equation 4.1	1849	1.167
Equation 4.14	2112	1.021
Equation 4.18	2194	0.983

Table 4.2 - Theoretically Predicted Bending Moment Capacities for Beam-Columns FA1-FA3

Theoretical Prediction Method Used	Beam-Column FA2 P_{exp} = 100 kN M_{exp} = 37.294 kNm		Beam-Column FA1 P_{exp} = 400 kN M_{exp} = 49.246 kNm		Beam-Column FA3 P_{exp} = 700 kN M_{exp} = 49.081 kNm		Beam-Column FA2 P_{exp} = 1000 kN M_{exp} = 50.751 kNm	
	Predicted M_u (kNm)	M_{exp} / M_u	Predicted M_u (kNm)	M_{exp} / M_u	Predicted M_u (kNm)	M_{exp} / M_u	Predicted M_u (kNm)	M_{exp} / M_u
AISC LRFD 1993 *(KL = 0)*	24.11	1.547	21.77	2.263	15.74	3.119	9.86	5.145
CAN/CSA-S16.1-94 *(L = 0)*	18.84	1.980	18.84	2.614	18.84	2.605	18.84	2.694
CAN/CSA-S16.1-94 *(K = 0.7 ; L = 2050 mm)*	21.97	1.697	21.97	2.242	21.97	2.234	21.97	2.310
ACI 318-95 Section	33.12	1.126	40.08	1.229	33.94	1.446	25.28	2.008
Plastic Section (by EC4)	35.01	1.065	44.51	1.106	44.20	1.110	37.99	1.336

Table 4.3 - Experimental Ductility Factors for Beam-Column Specimens

Beam-Column Specimen	Δ_y (mm)	φ_y (rad/km)	Positive Direction				Negative Direction			
			Δ_{max} (mm)	μ	φ_{max} (rad/km)	φ_{max}/φ_y	Δ_{max} (mm)	μ	φ_{max} (rad/km)	φ_{max}/φ_y
FA1	40.3	50.3	160.5	4.0	418.0	8.3	161.0	4.0	424.5	8.4
FA2 (P_{exp} = *100 kN*)	32.5	37.3	199.7	6.2	491.3	13.2	181.2	5.6	459.2	12.3
FA3	26.7	43.1	138.5	5.2	724.2	16.8	113.6	4.3	-	-

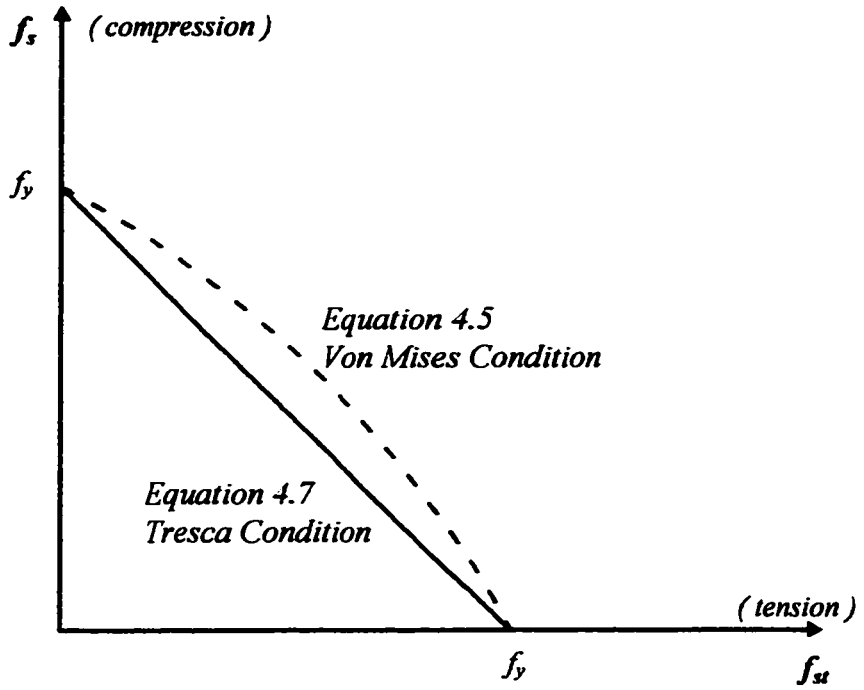

Figure 4.1 : Plot of Eqs. 4.5 and 4.7

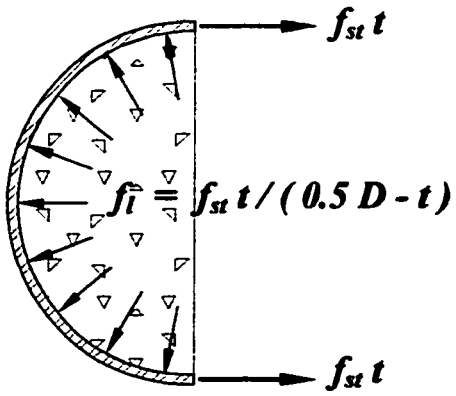

Figure 4.2 : Lateral Pressure in a Circular CFT under Axial Compression

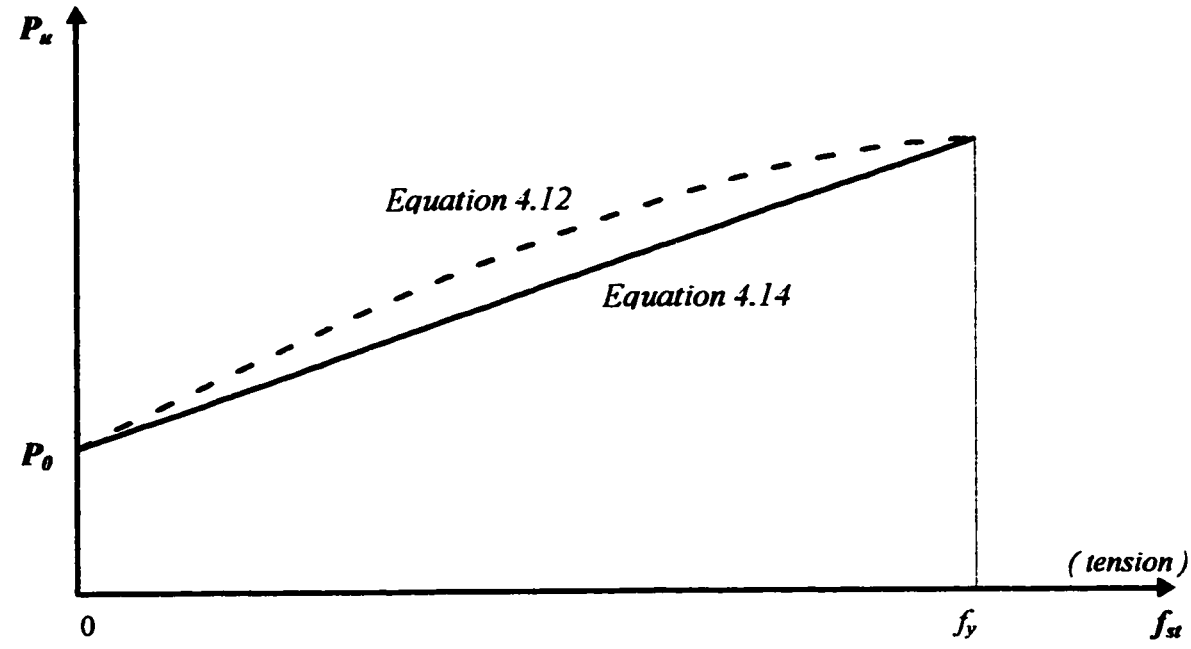

Figure 4.3 : Equations 4.12 and 4.14 ($k \geq 2/k_g$)

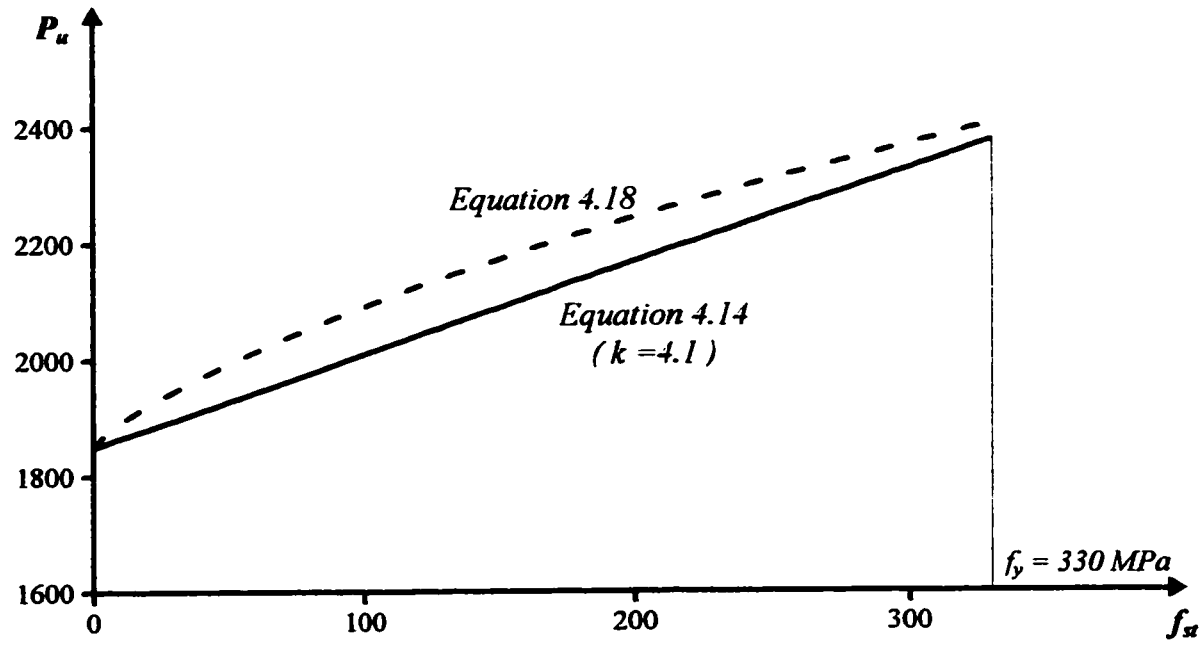

Figure 4.4 : Equations 4.14 and 4.18 for the Case of Specimen ST1 ($k_m = 1$)

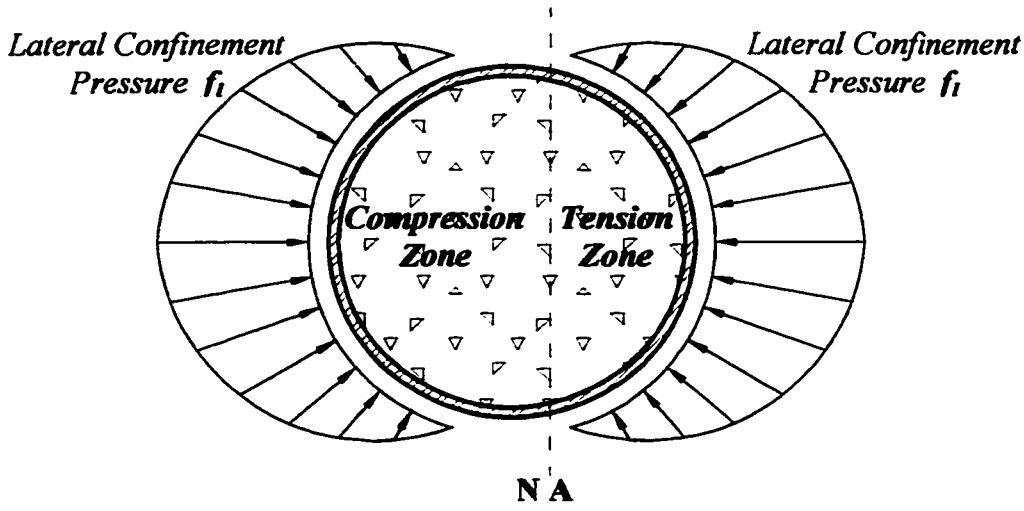

Figure 4.5: Lateral Confinement Pressure in a Circular CFT under Combined Compression and Bending

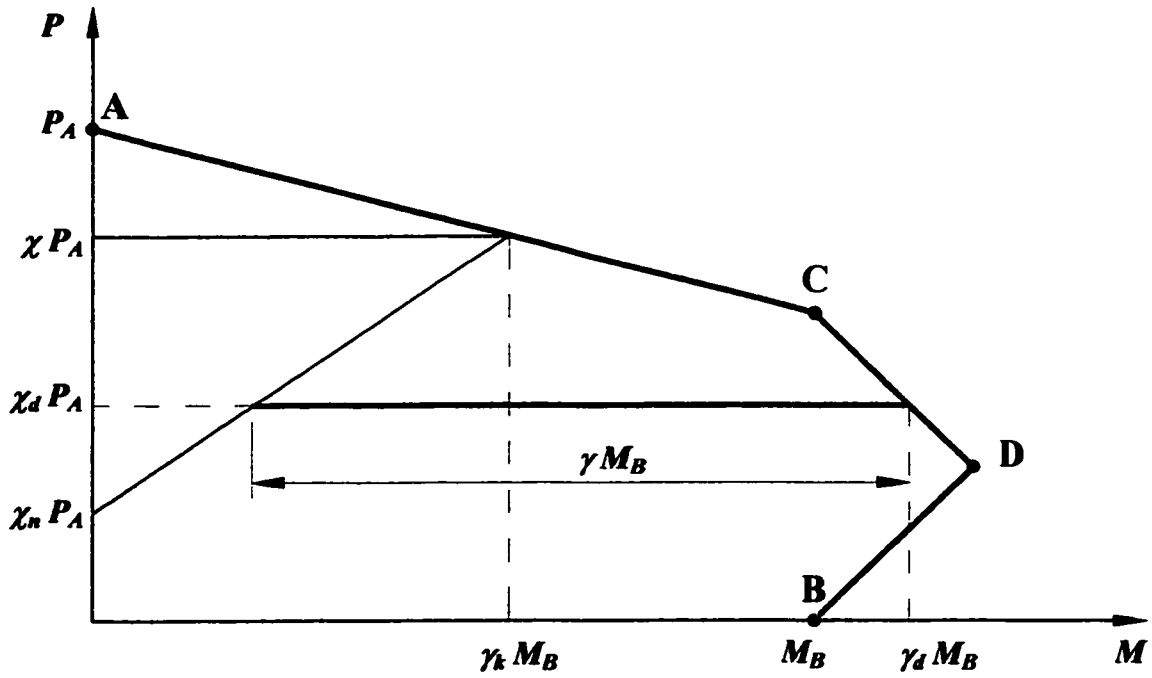

Figure 4.6 : Construction of Polygonal *M-P* Interaction Curve (Eurocode 4)

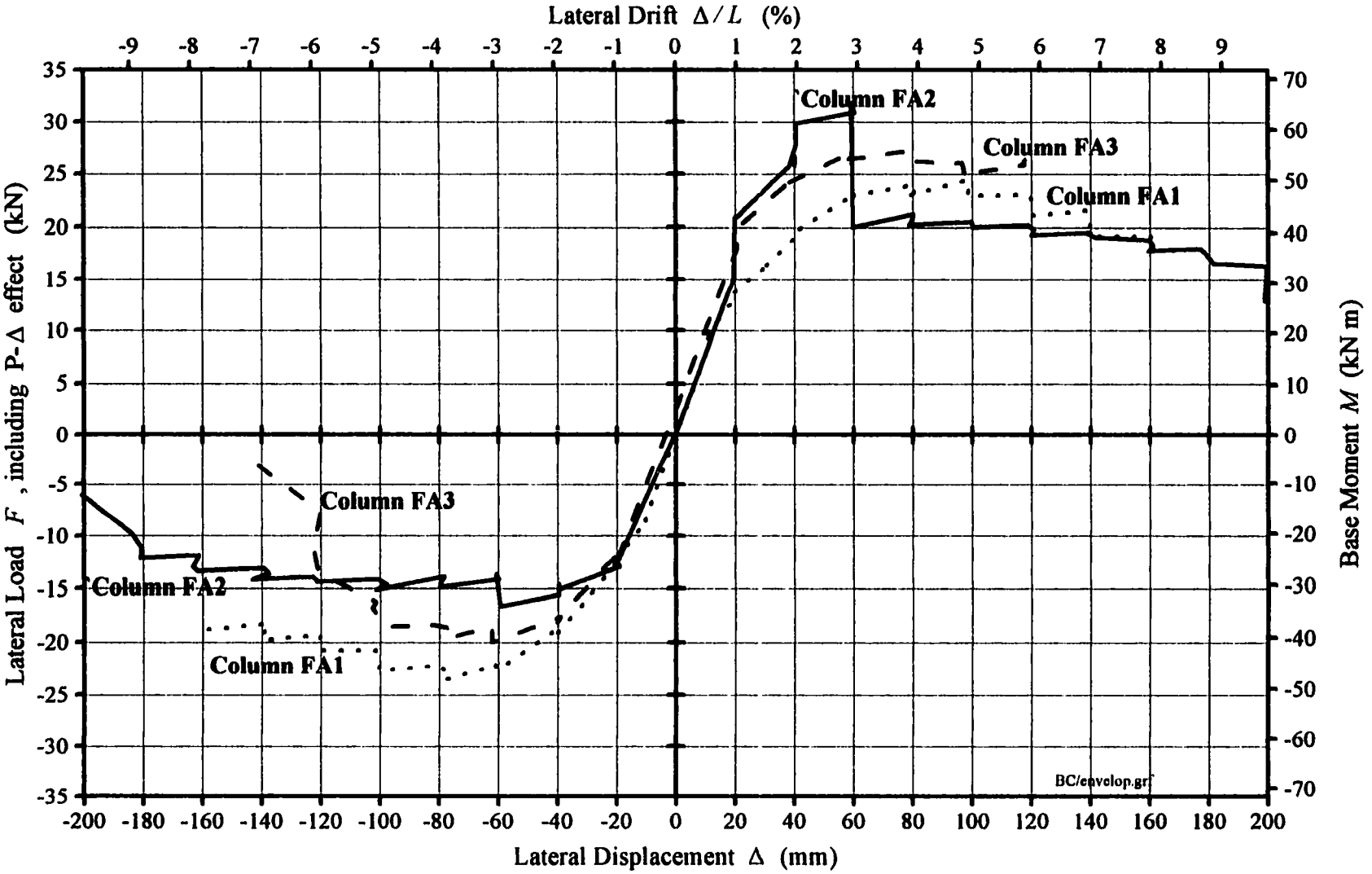

Figure 4.7 : Lateral Load-Displacement Envelope Curves for Beam-Column Specimens FA1-FA3

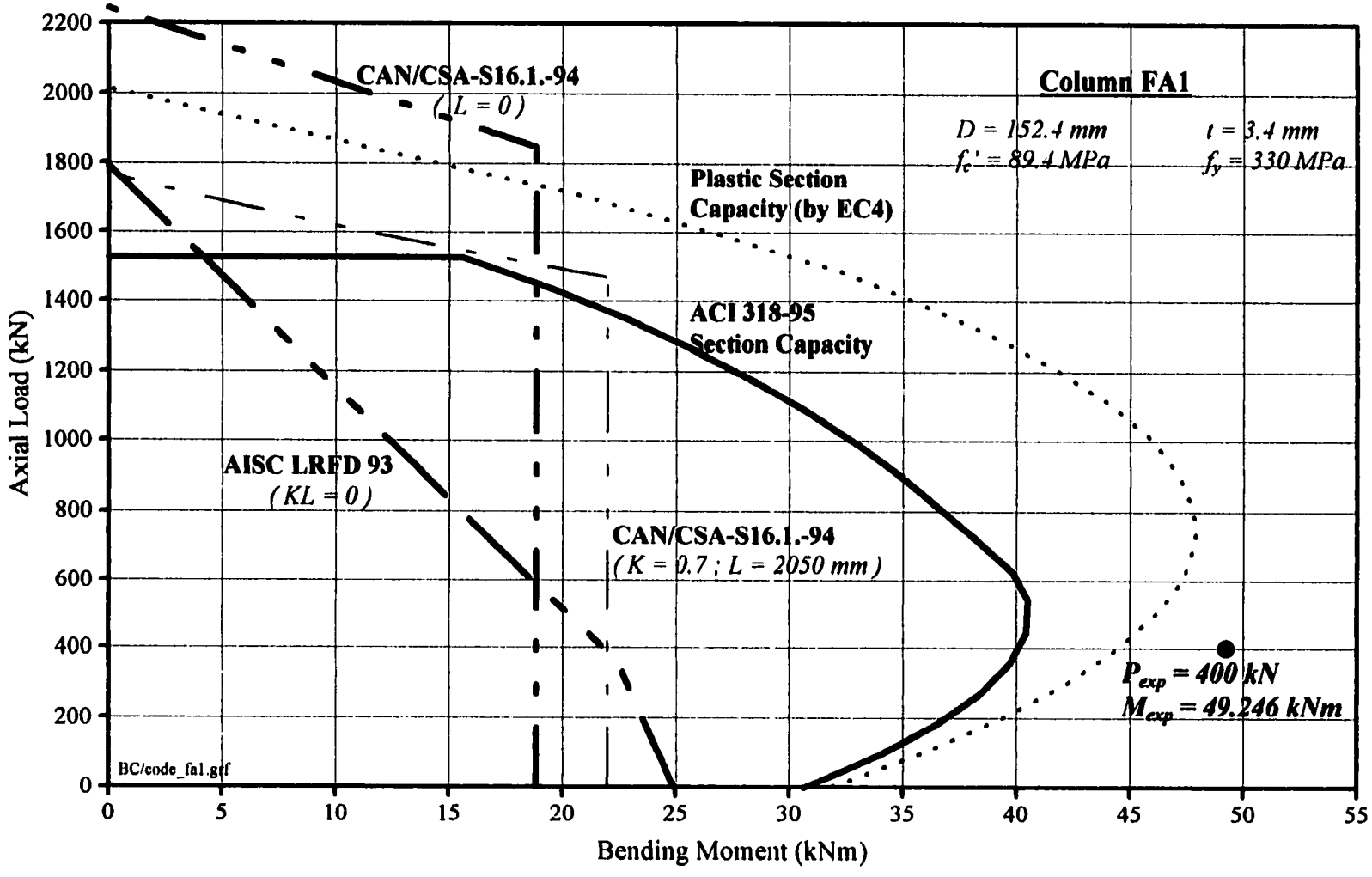

Figure 4.8 : *P* - *M* Interaction Curves for Specimen FA1

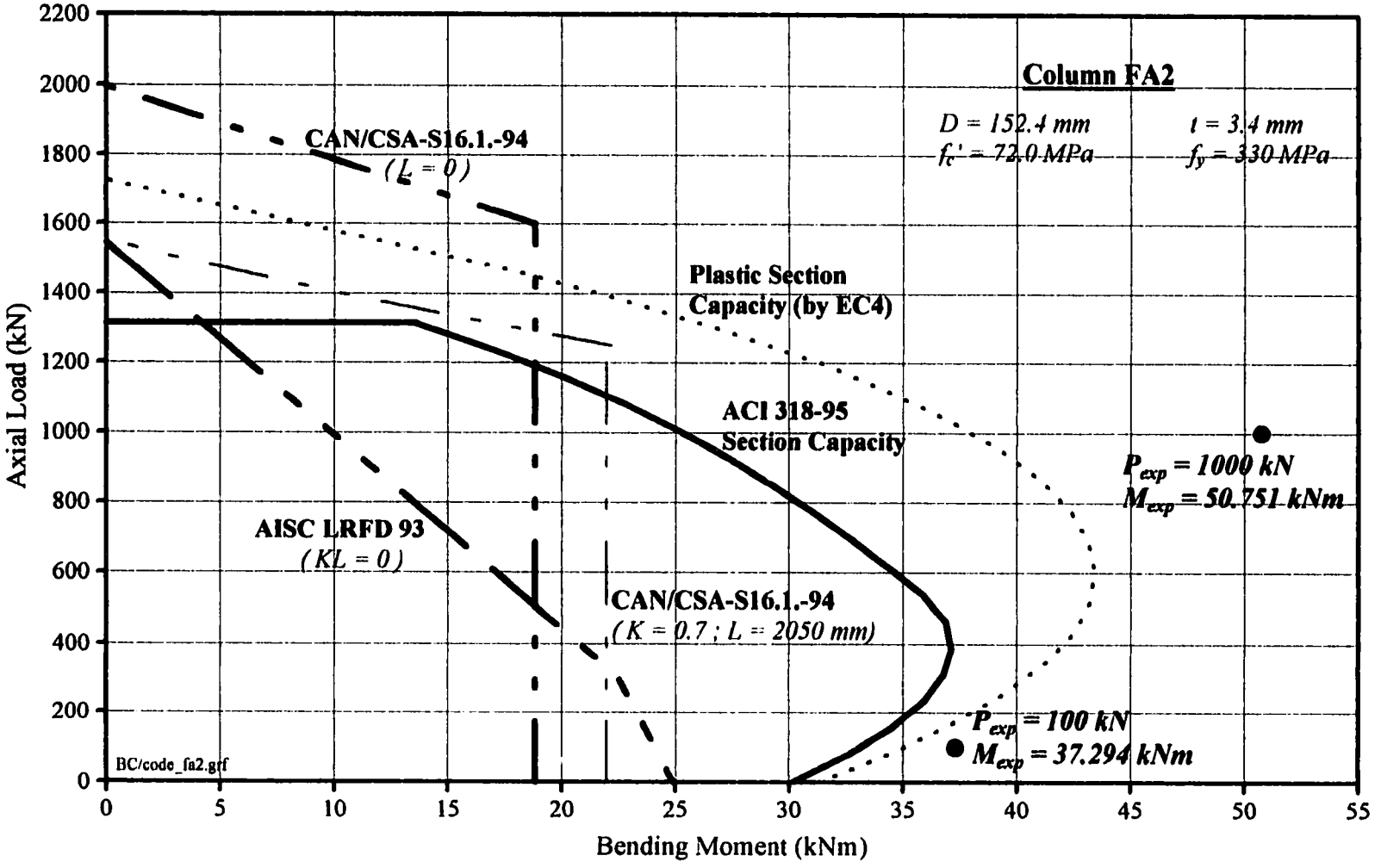

Figure 4.9 : *P* - *M* Interaction Curves for Specimen FA2

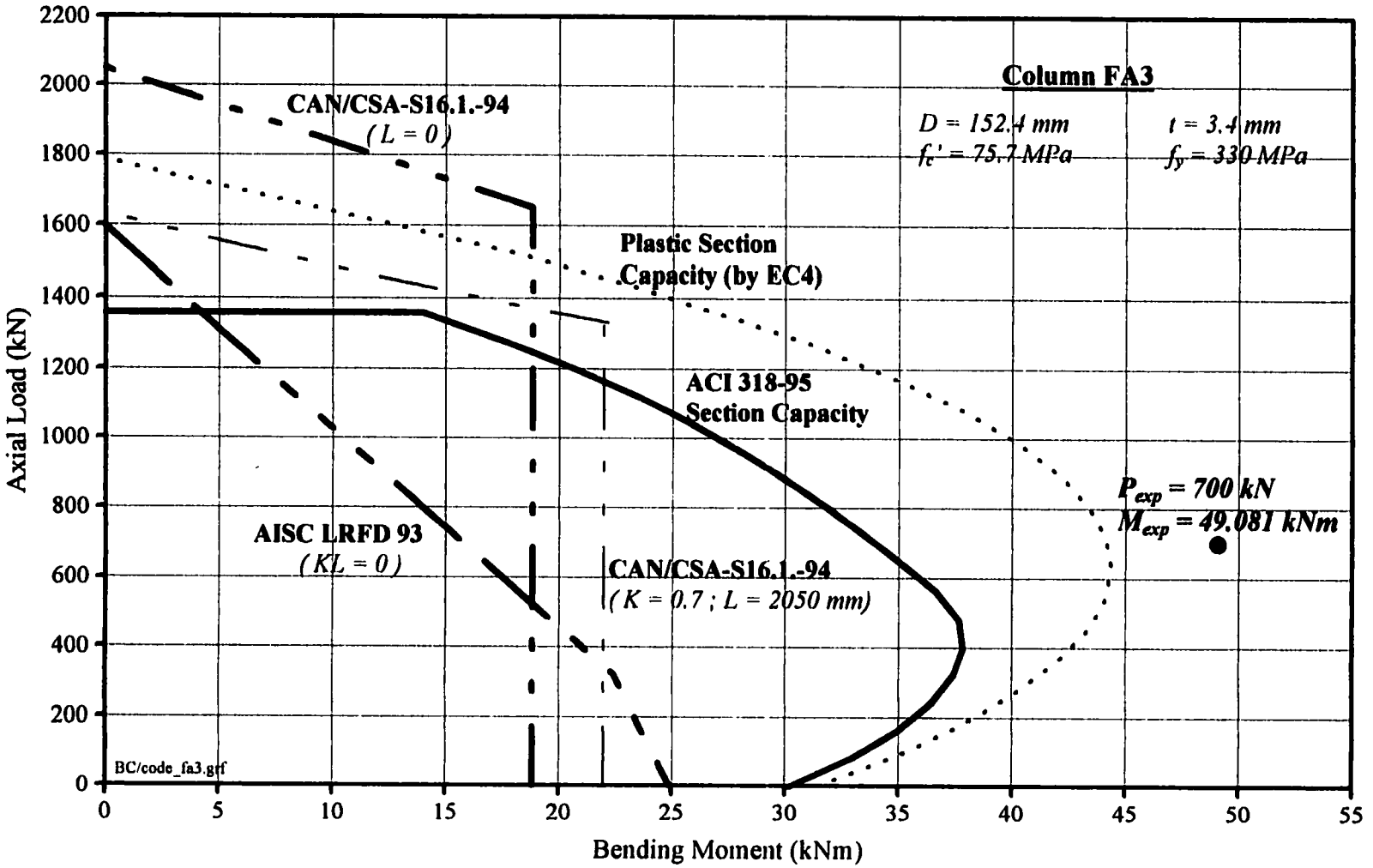

Figure 4.10 : *P* - *M* Interaction Curves for Specimen FA3

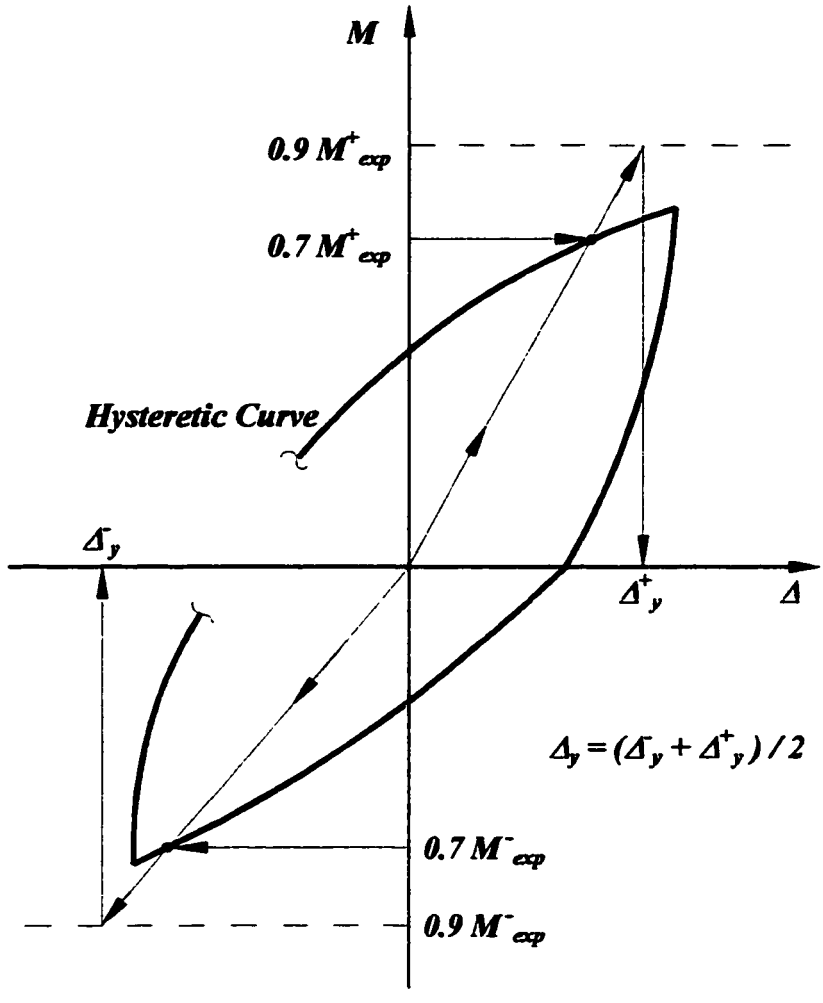

Figure 4.11 : Experimental Definition of Yield Displacement

Chapter 5

Summary and Conclusions

5.1 Summary

A combined analytical and experimental investigation was conducted to study the behavior of circular HSCFT beam-columns. An extensive literature review was done to evaluate the available data on CFTs. Three long beam-columns were tested under constant axial compression and incrementally increasing lateral displacement reversals. While the level of the axial load was the main variable parameter in this experiment, both strength and deformability issues were addressed. In addition, one short column was tested in concentric compression. A comparative study of North American and European design code provisions, with regard to circular CFTs, was carried out. Various aspects of concrete confinement in CFTs were analyzed. The experimental results were compared with theoretical predictions of strength.

5.2 Conclusions

The following conclusions can be drawn, with regard to circular HSCFTs with $D/t \leq 50$, from the research reported in this thesis:

- Use of high strength concrete of up to 90 MPa for circular CFT members does not cause any dramatic changes in the behavior. General principles of structural analysis can be safely applied to HSCFTs. It should be kept in mind, however, that the failure mechanism of short

concentrically loaded columns is triggered by shear failure of the concrete core, leading to a sudden decline in load-carrying capacity beyond ultimate.

- Circular HSCFT beam-columns possess good characteristics in terms of ductility. Tested specimens exhibited favorable hysteresis behavior with no or little "pinching" under cyclic loading.

- Concrete confinement effects contribute to the flexural strength of circular HSCFT beam-columns. This contribution increases with the increase of the axial load level within a certain range of P depending of columns' slenderness. For the beam-columns tested in this experiment, this range was about $0 \leq P / P_0 \leq 0.6$.

- Local buckling of the steel tube wall occurs after the maximum bending moment capacity is attained. It does not cause any immediate changes in the behavior of HSCFT beam-columns, and the concrete core remains well confined in the zone of the local buckling.

- Significant discrepancies exist between major codes in terms of design provisions for circular CFT columns. The discrepancies are especially large when predictions of flexural strength for CFT beam-columns, given by various codes, are compared.

- All considered codes can be safely used for the design of circular HSCFT columns.

- AISC LRFD 1994 interaction curves give the most conservative, if not to say poor, predictions of flexural resistance of CFT beam-columns for the most of the axial load range.

- CAN/CSA-S16.1-94 unfairly treats circular CFTs in bending and combined compression and bending, compared to rectangular CFTs. Limiting the flexural capacity of circular CFTs by the bending moment strength of steel section alone is unnecessarily restrictive. It also seems illogical to apply the biaxial steel reduction factor τ in the evaluation of the bending moment capacity. Still conservative to a significant degree, expressions similar to those adopted for rectangular sections can be easily developed and adopted for circular CFTs.

- The ACI procedure is the most complicated. It does not take any account for concrete confinement in circular CFTs, and is more conservative than the Eurocode 4 method.

- Eurocode 4 provides a simple, conservative and relatively accurate method to estimate the flexural strength of circular CFT beam-columns. Eurocode 4 gave an exceptionally accurate prediction of axial strength for the short circular HSCFT column tested in this investigation.

5.3 Recommendations for Future Research

- Results of this study suggest that concrete confinement models developed for traditionally reinforced concrete columns may be applied to circular CFTs, if lateral confinement pressure is properly estimated. More research is required to determine whether it is true, or modifications to these models are needed in order to account for different concrete confinement mechanism in circular CFTs. Still little is known about the development of circumferencial stresses in steel tubes and their correlation with the longitudinal stresses.

- More tests on circular HSCFTs are needed to establish a broader experimental data base. So far, very few tests had been conducted on circular CFTs containing concrete stronger than 70 MPa, and any additional data will be valuable, regardless of test parameters.

- Tests on circular CFTs incorporating high strength concrete and high strength steel are recommended.

- The flexural strength of circular CFT beam-columns is not well predicted. The benefits of concrete confinement are generally ignored. Numerical studies should be conducted that will take confinement effects into consideration.

- Further research is recommended to address the issue of creep in circular CFT columns.

Appendix A

Strain Gauge Data

Strains measured by the electric resistance strain gauges in the hinging zone of tested beam-column specimens FA1-FA3 are presented in this appendix. The recorded strains are plotted versus lateral force including second order effects. Where possible, the loops are marked with figures indicating the lateral displacement reversals applied (e.g. the mark "-3/2" will indicate, that the marked part of the curve corresponds to the second travel to the lateral drift level of -3%). With increasing lateral displacements, the strains in the steel tubes at almost all measurement locations exceeded the capacity of the strain gauges. Most of the gauges failed before the testing was over. For this reason, the data presented here, in many cases, reflects only a part of the loading history.

The sign convention for strains is positive for compression and negative for tension. Lateral forces are positive in the West-bound direction and negative in the East-bound direction. The locations of the strain gauges are shown in Figure 2.16.

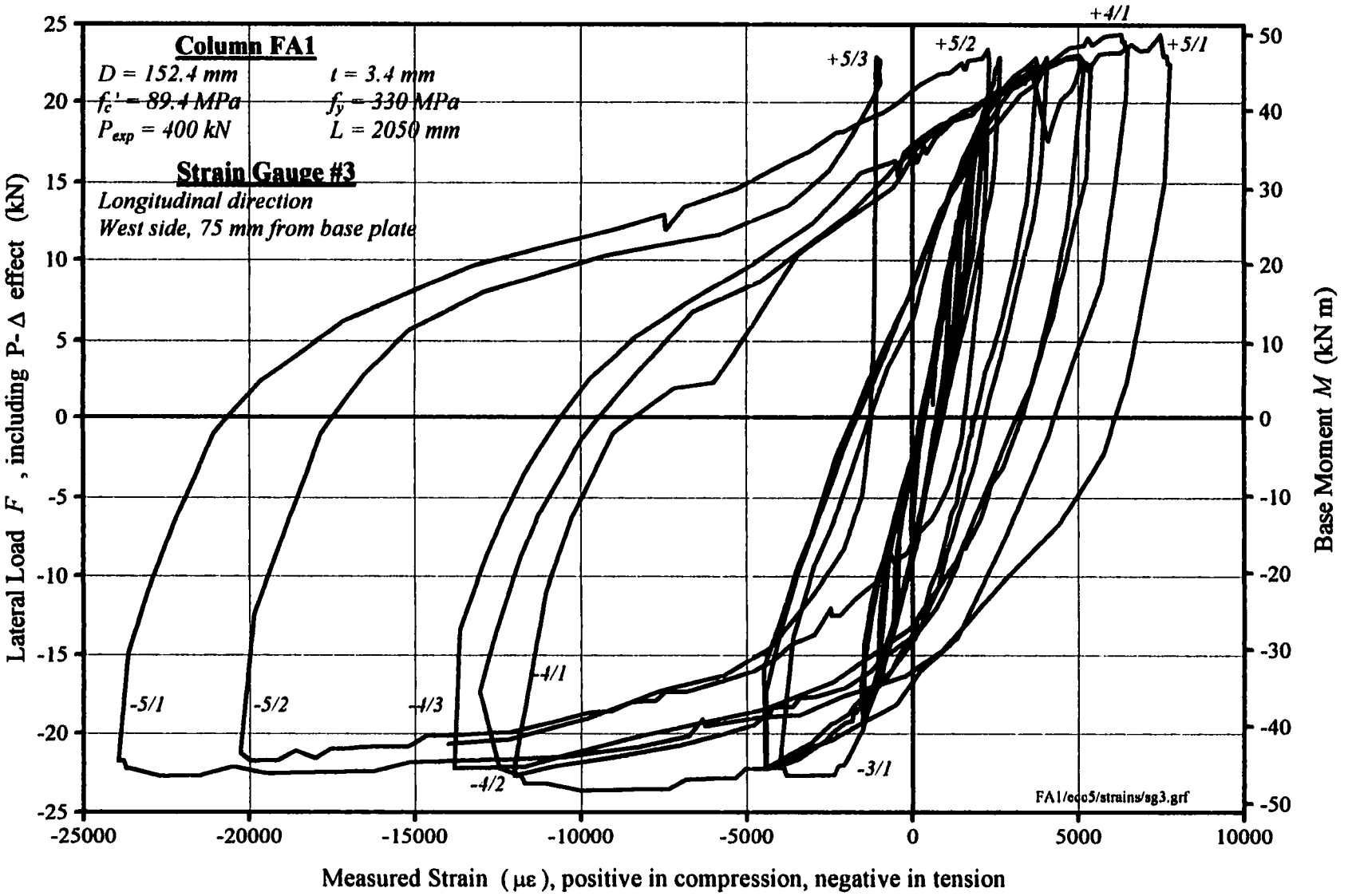

Figure A.1 : Strain Gauge #3 of Beam-Column Specimen FA1

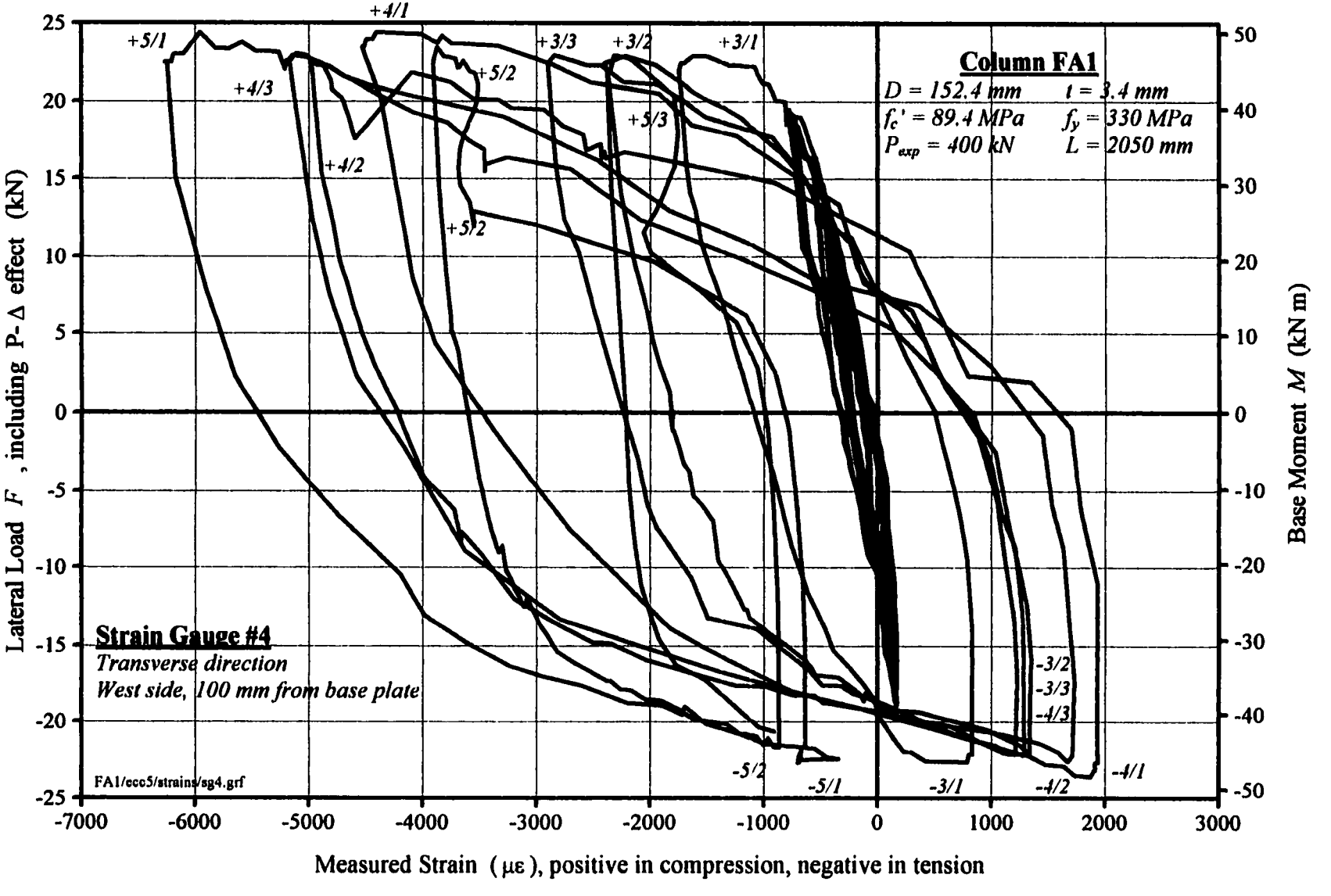

Figure A.2 : Strain Gauge #4 of Beam-Column Specimen FA1

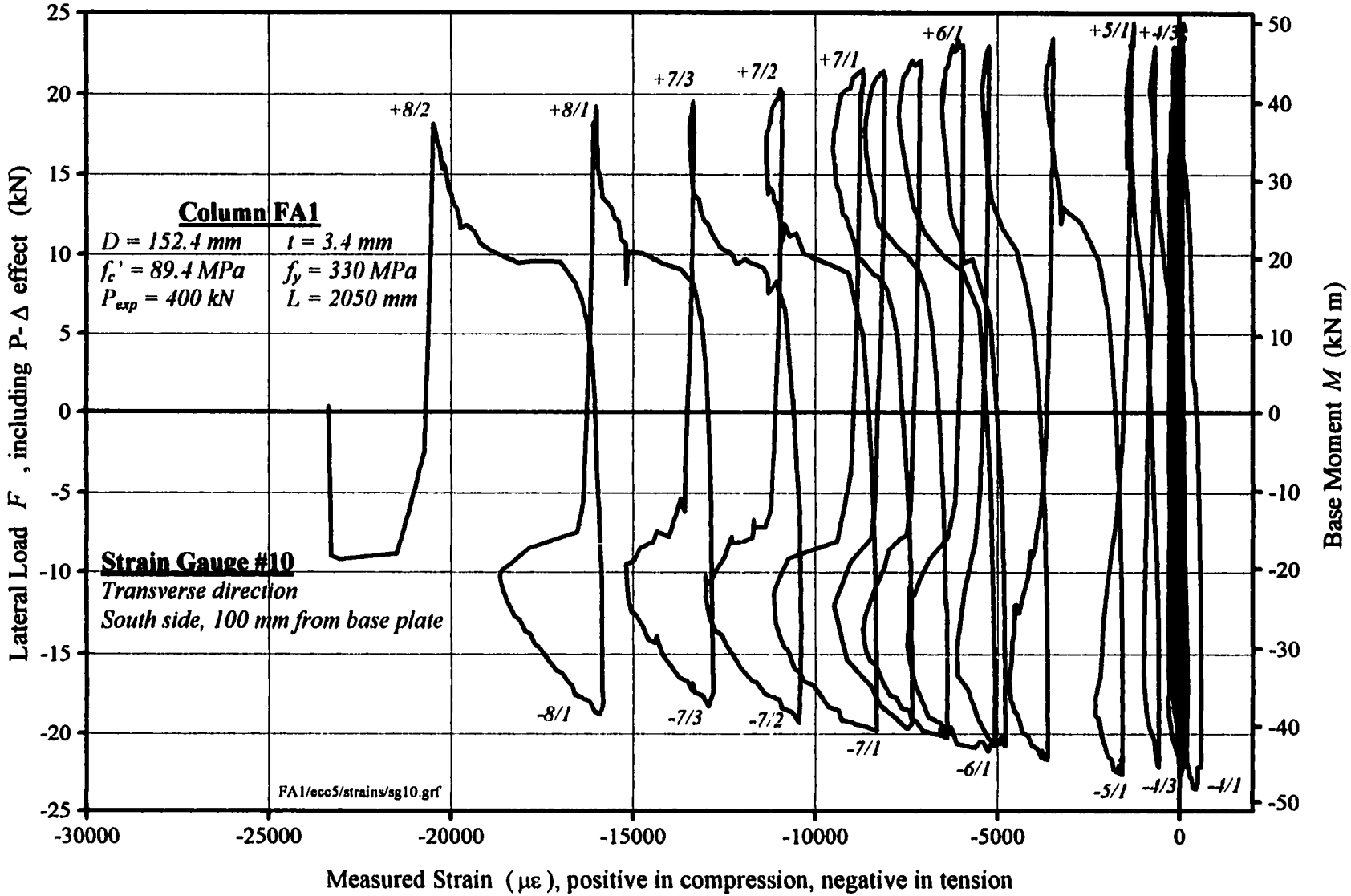

Figure A.3 : Strain Gauge #10 of Beam-Column Specimen FA1

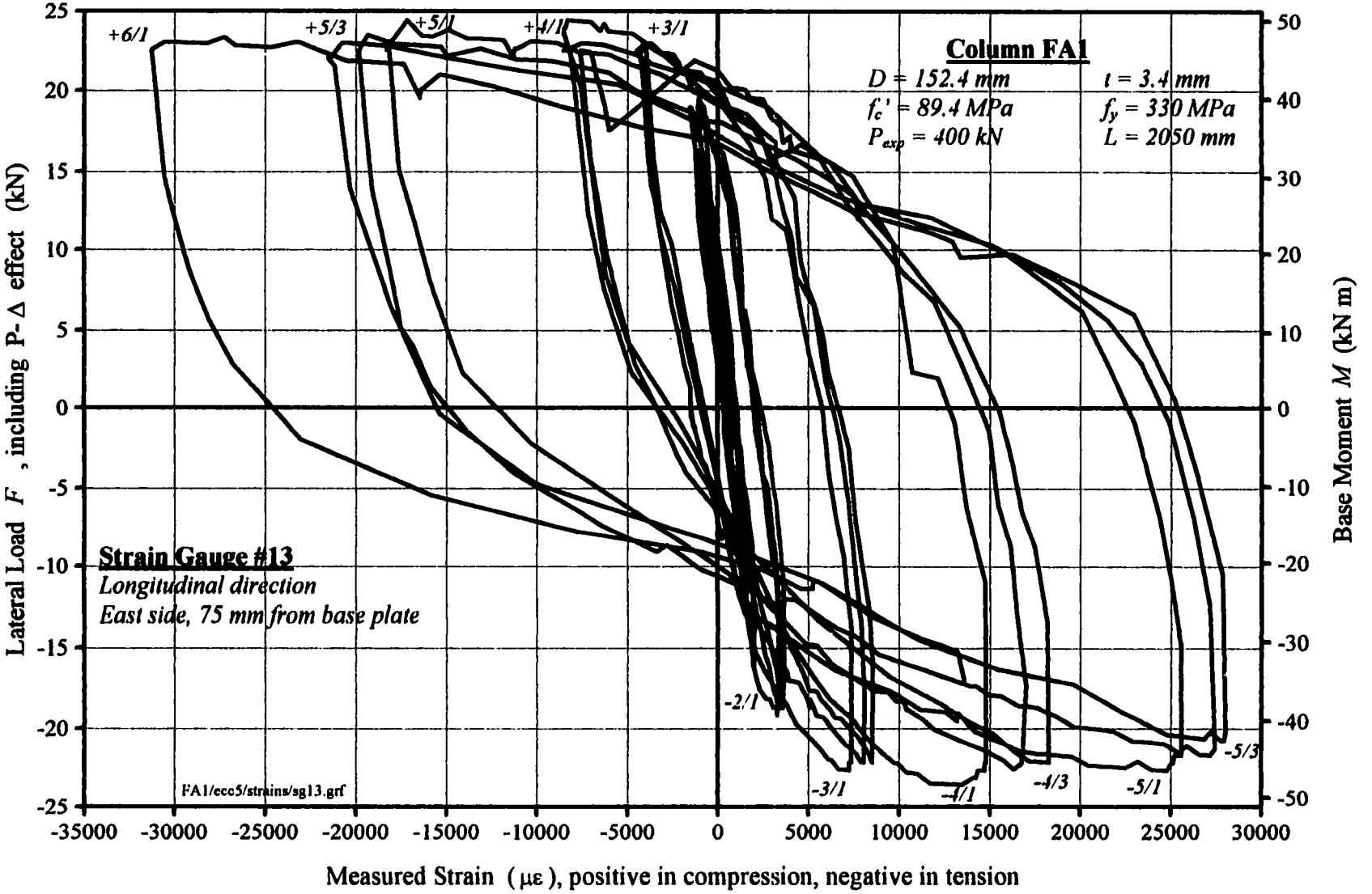

Figure A.4 : Strain Gauge #13 of Beam-Column Specimen FA1

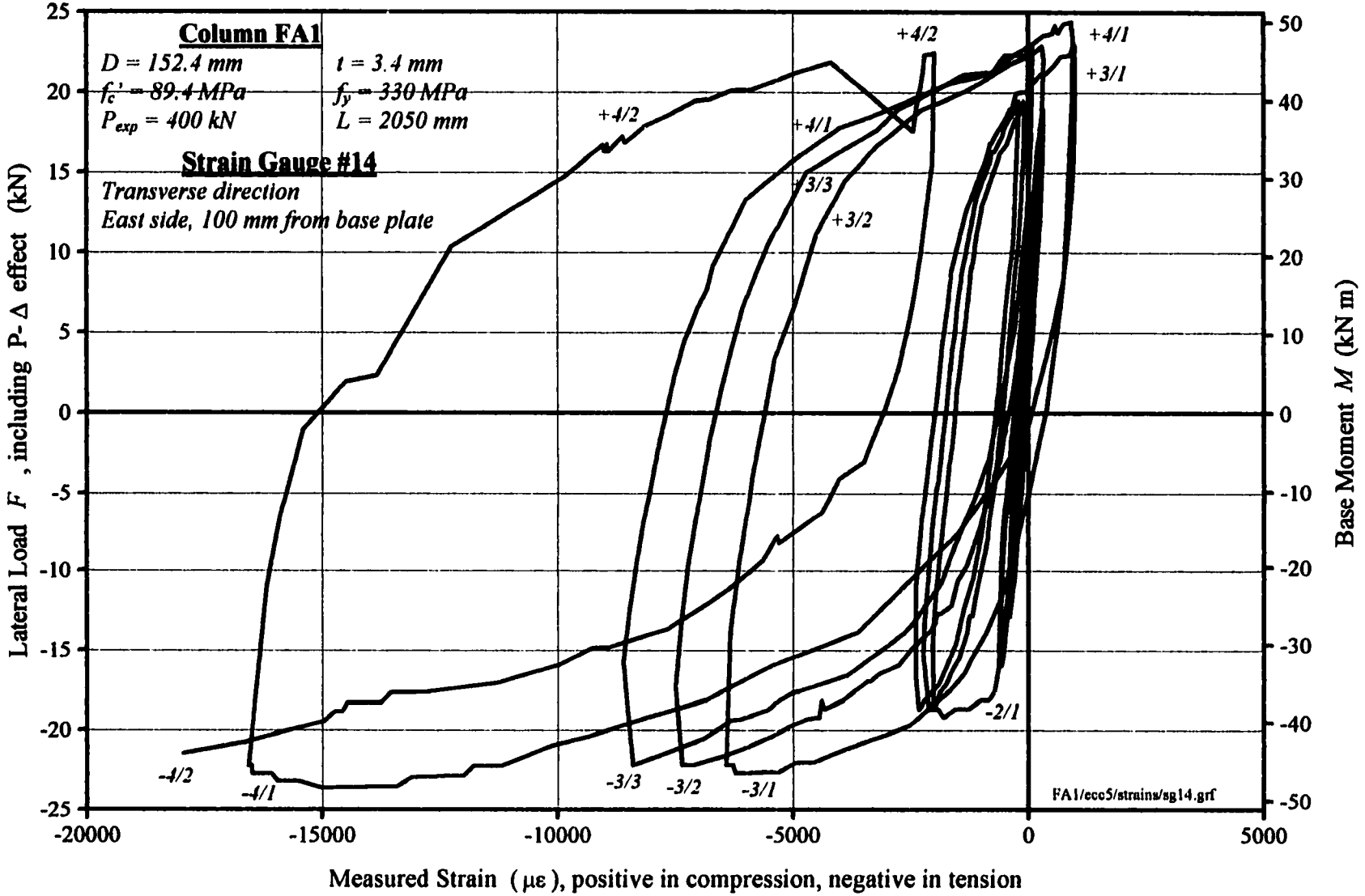

Figure A.5 : Strain Gauge #14 of Beam-Column Specimen FA1

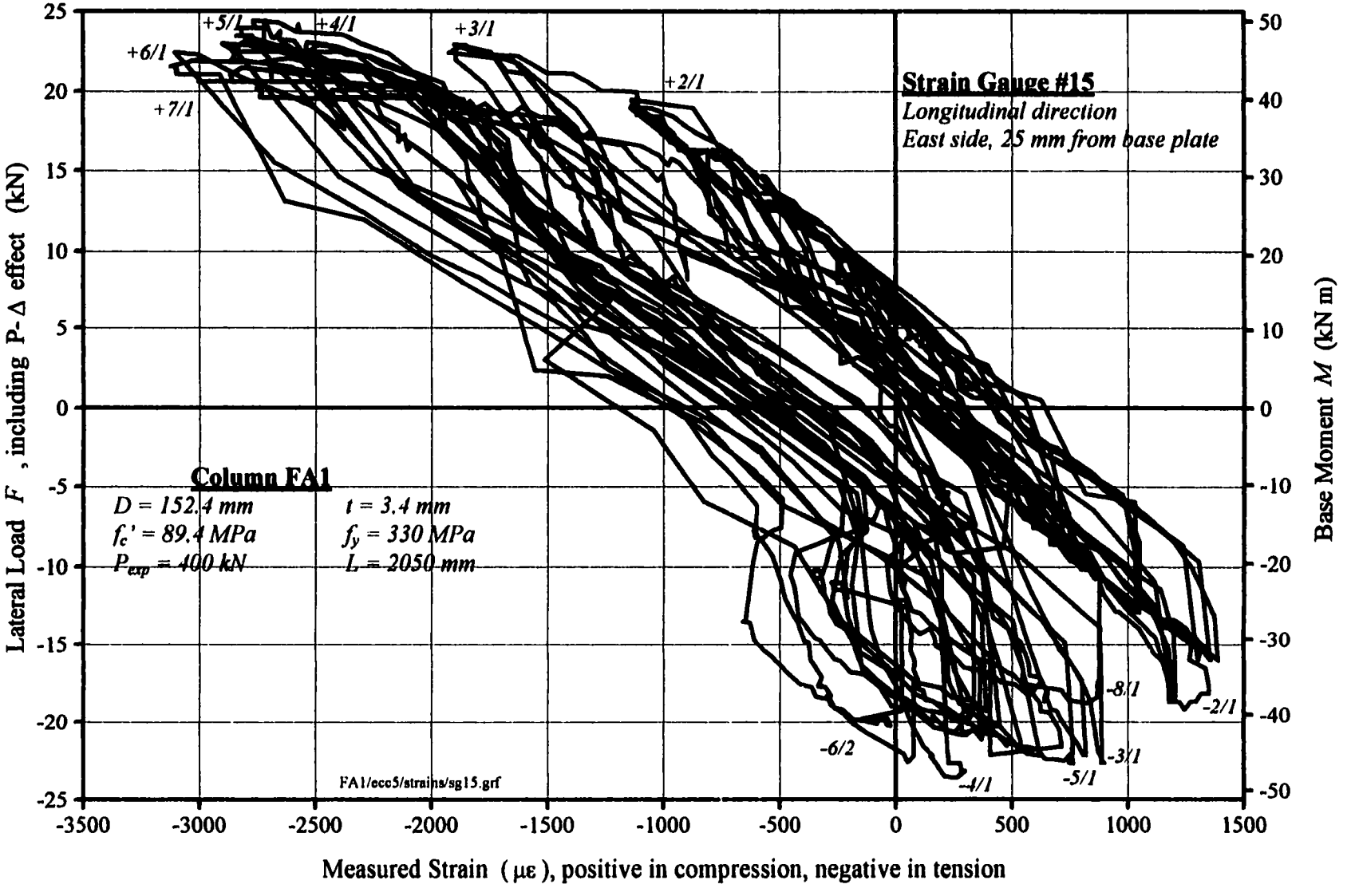

Figure A.6 : Strain Gauge #15 of Beam-Column Specimen FA1

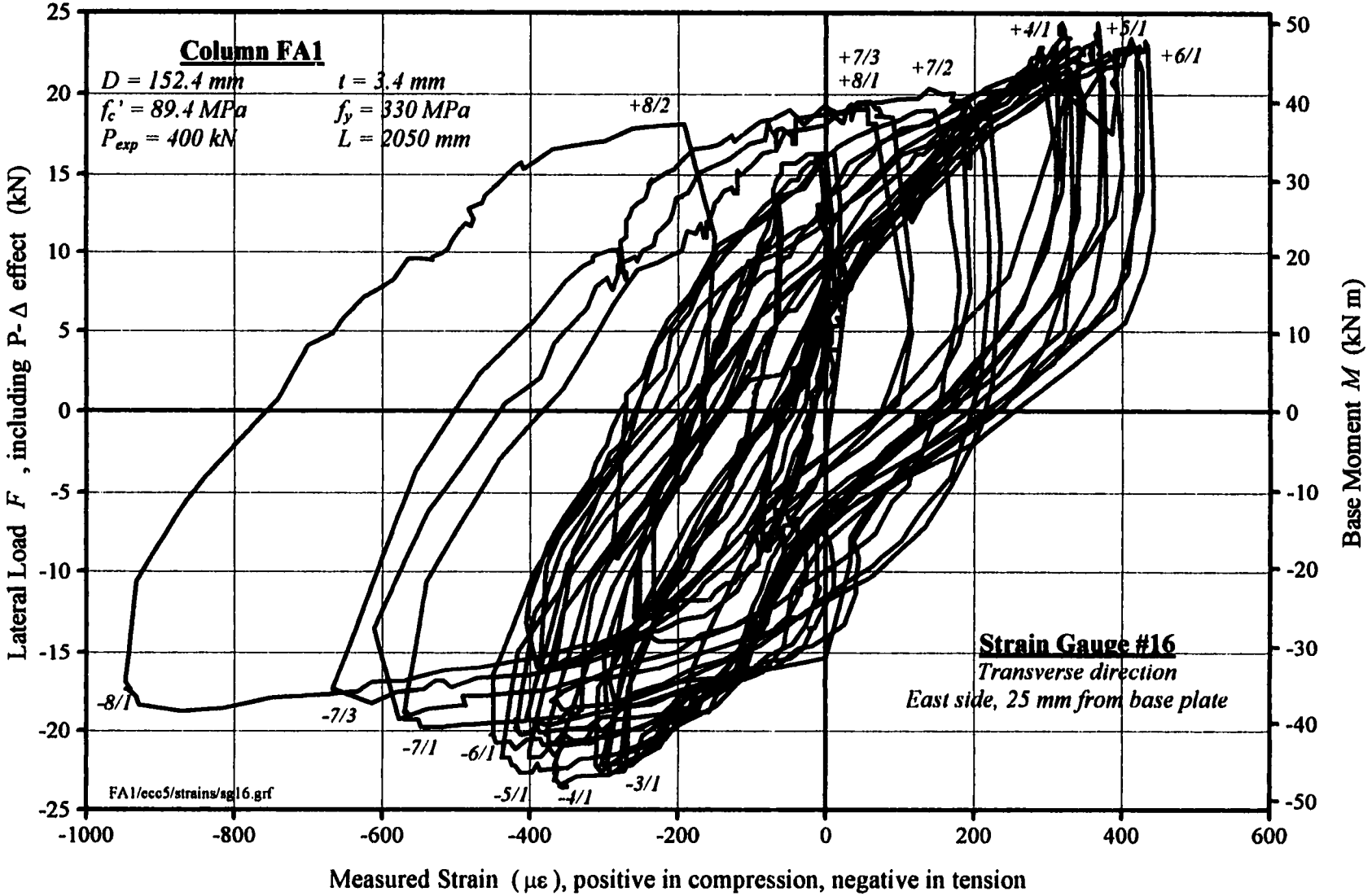

Figure A.7 : Strain Gauge #16 of Beam-Column Specimen FA1

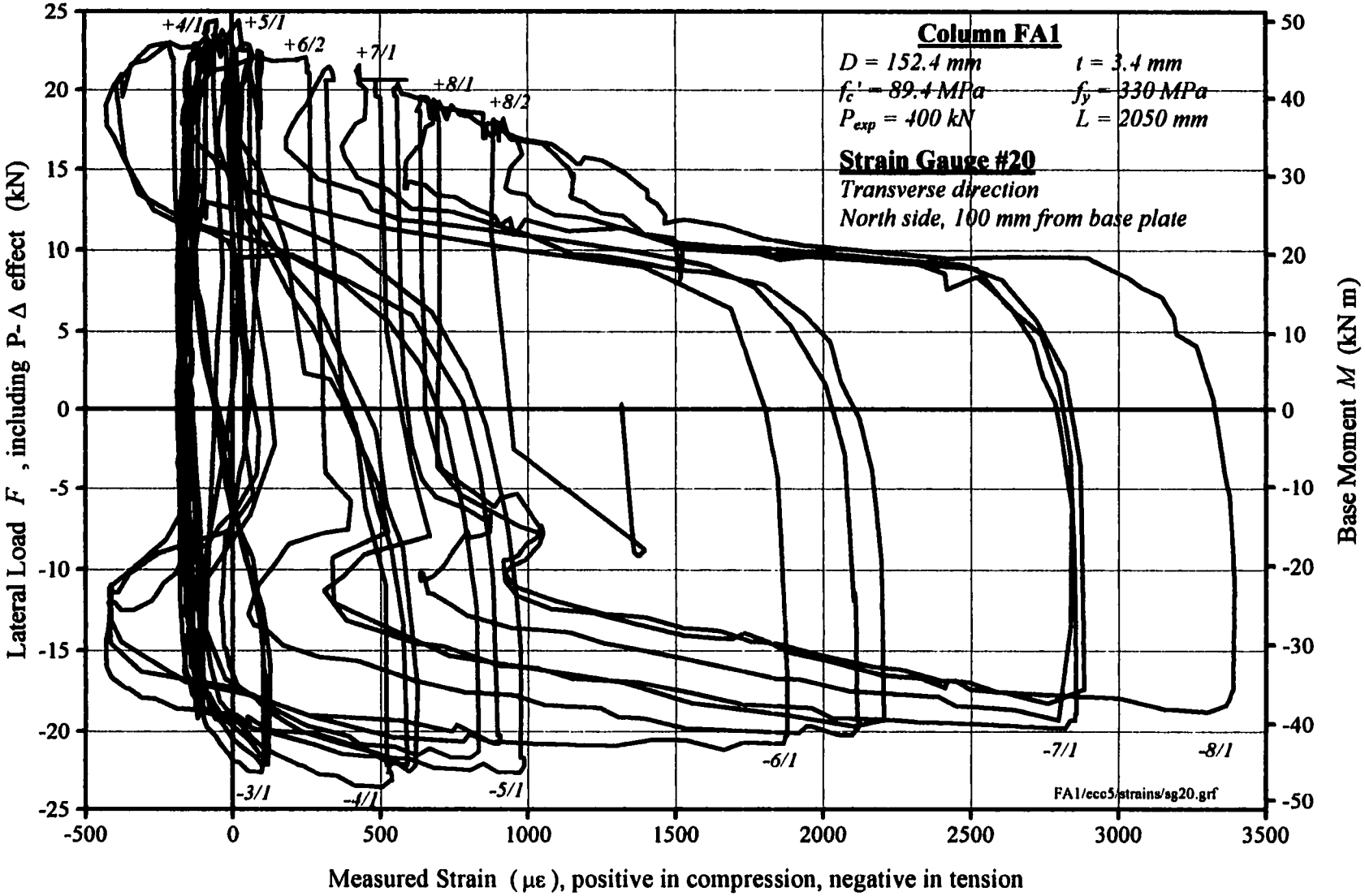

Figure A.8 : Strain Gauge #20 of Beam-Column Specimen FA1

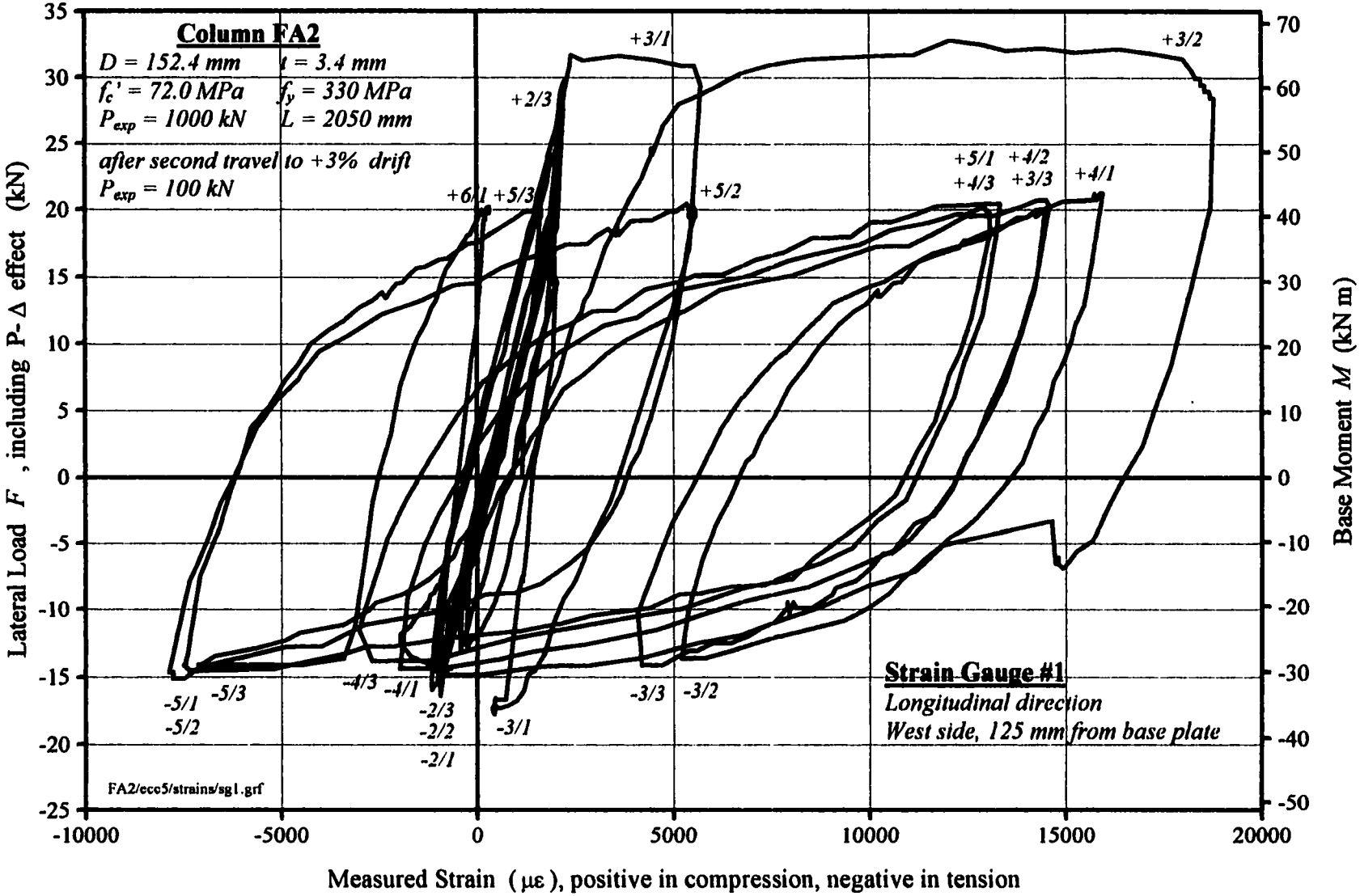

Figure A.9 : Strain Gauge #1 of Beam-Column Specimen FA2

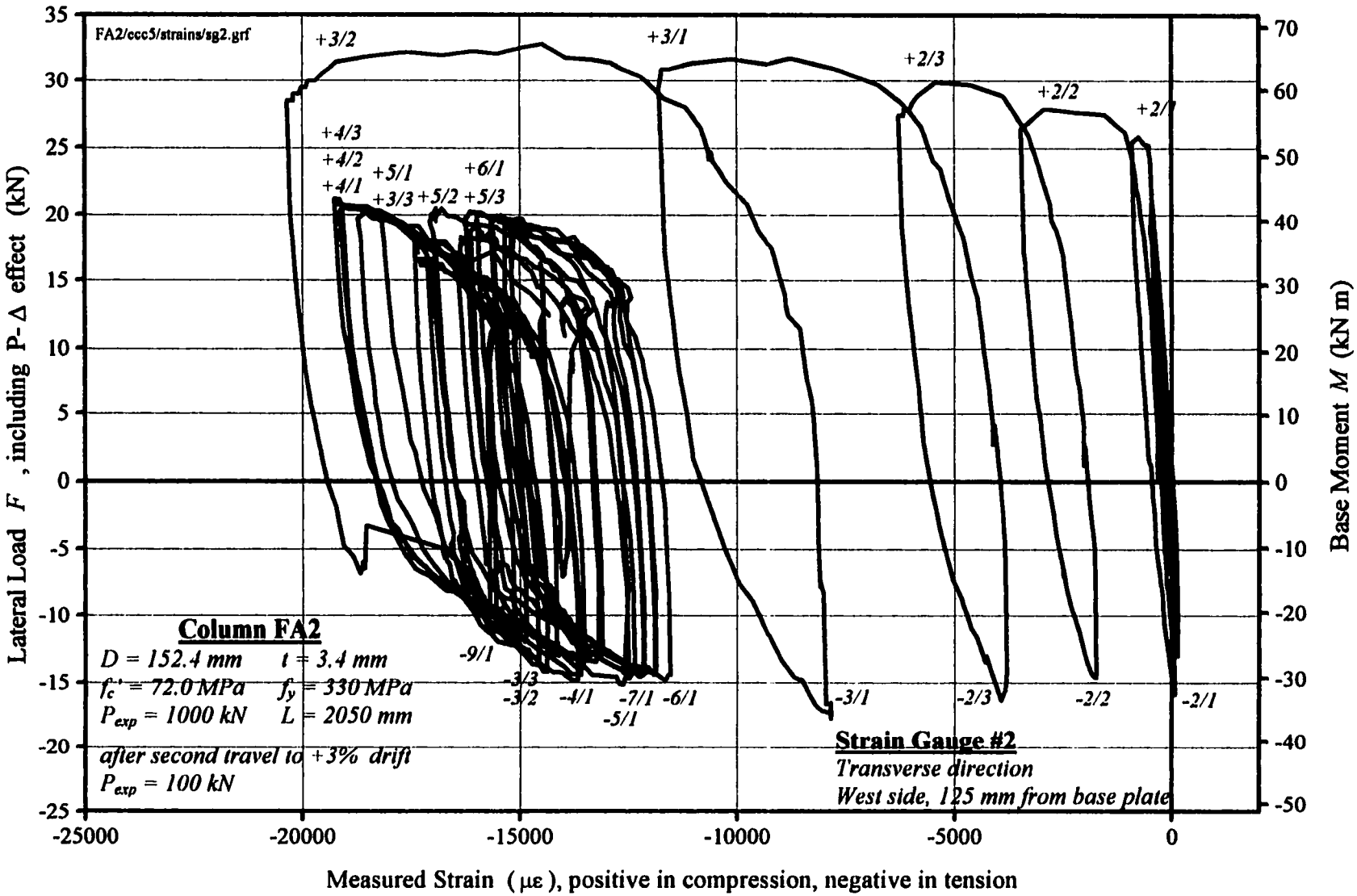

Figure A.10 : Strain Gauge #2 of Beam-Column Specimen FA2

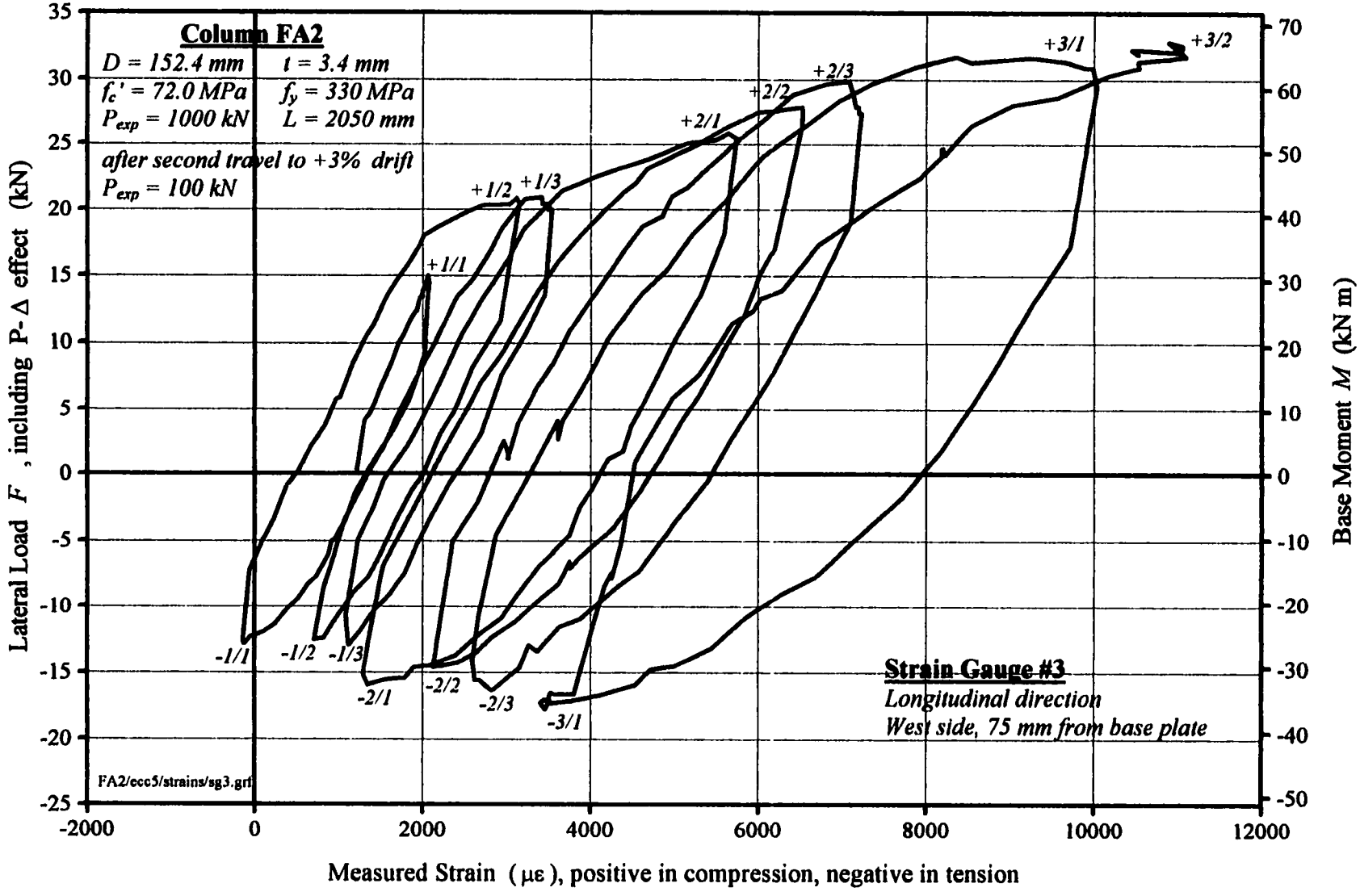

Figure A.11 : Strain Gauge #3 of Beam-Column Specimen FA2

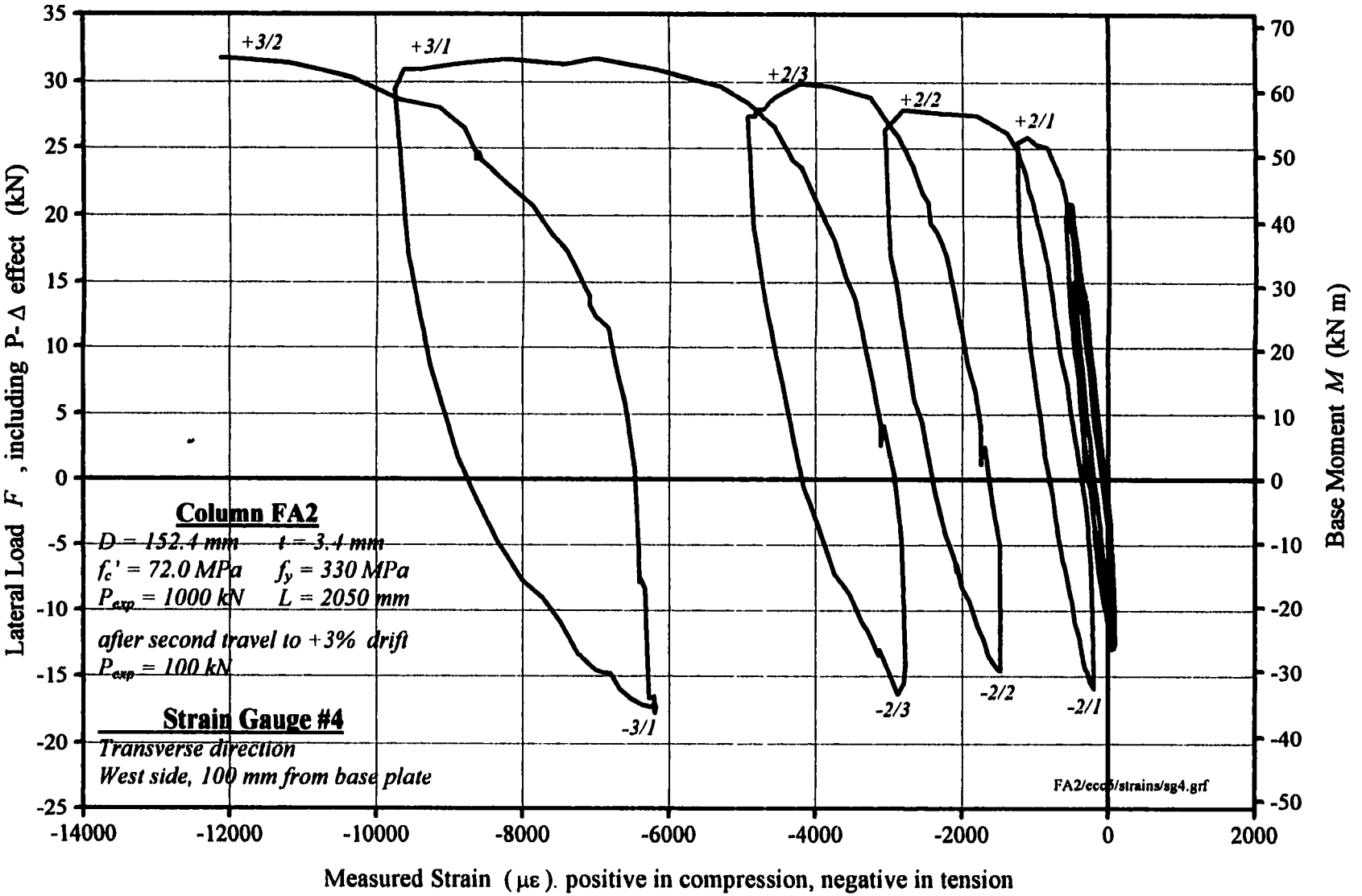

Figure A.12 : Strain Gauge #4 of Beam-Column Specimen FA2

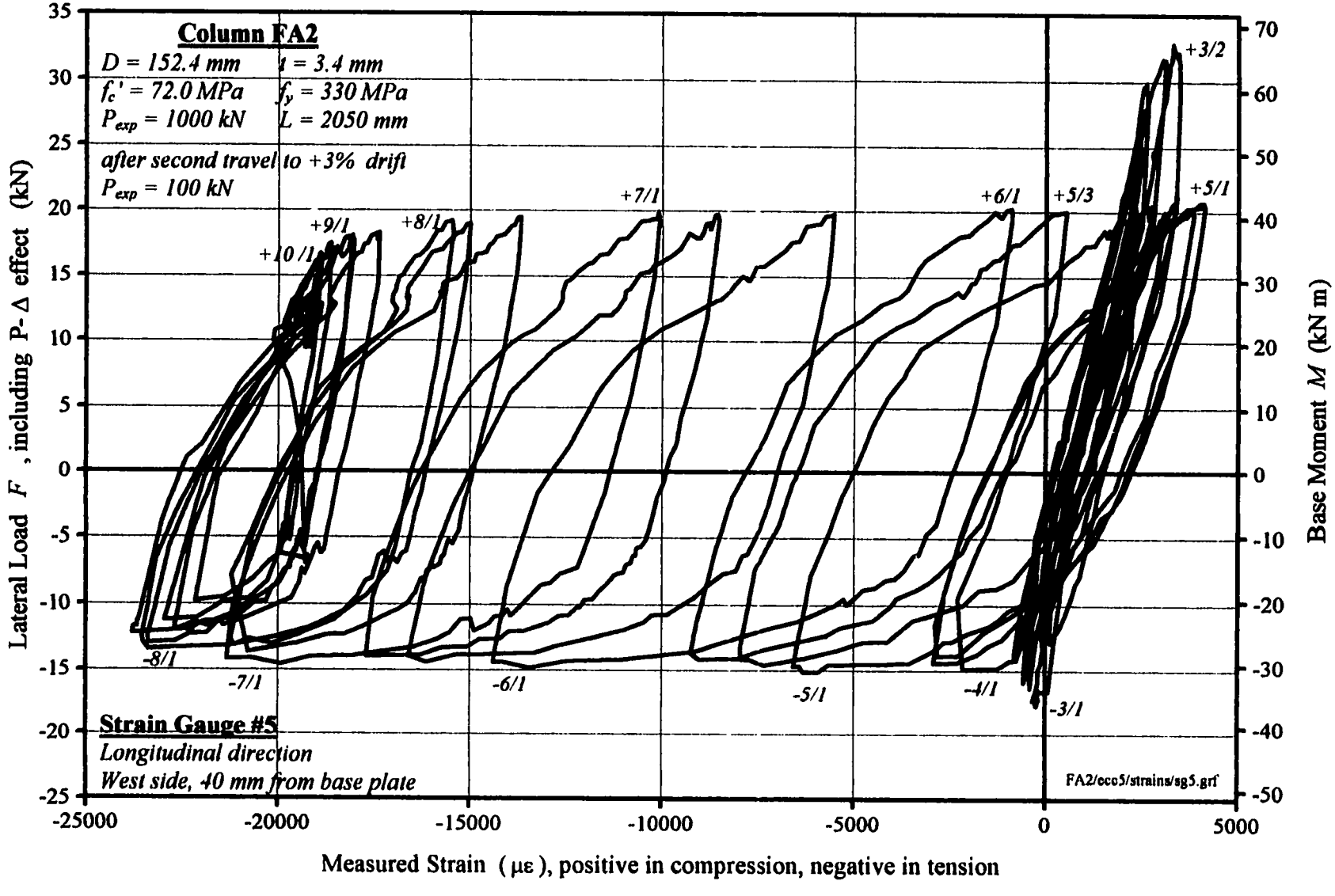

Figure A.13 : Strain Gauge #5 of Beam-Column Specimen FA2

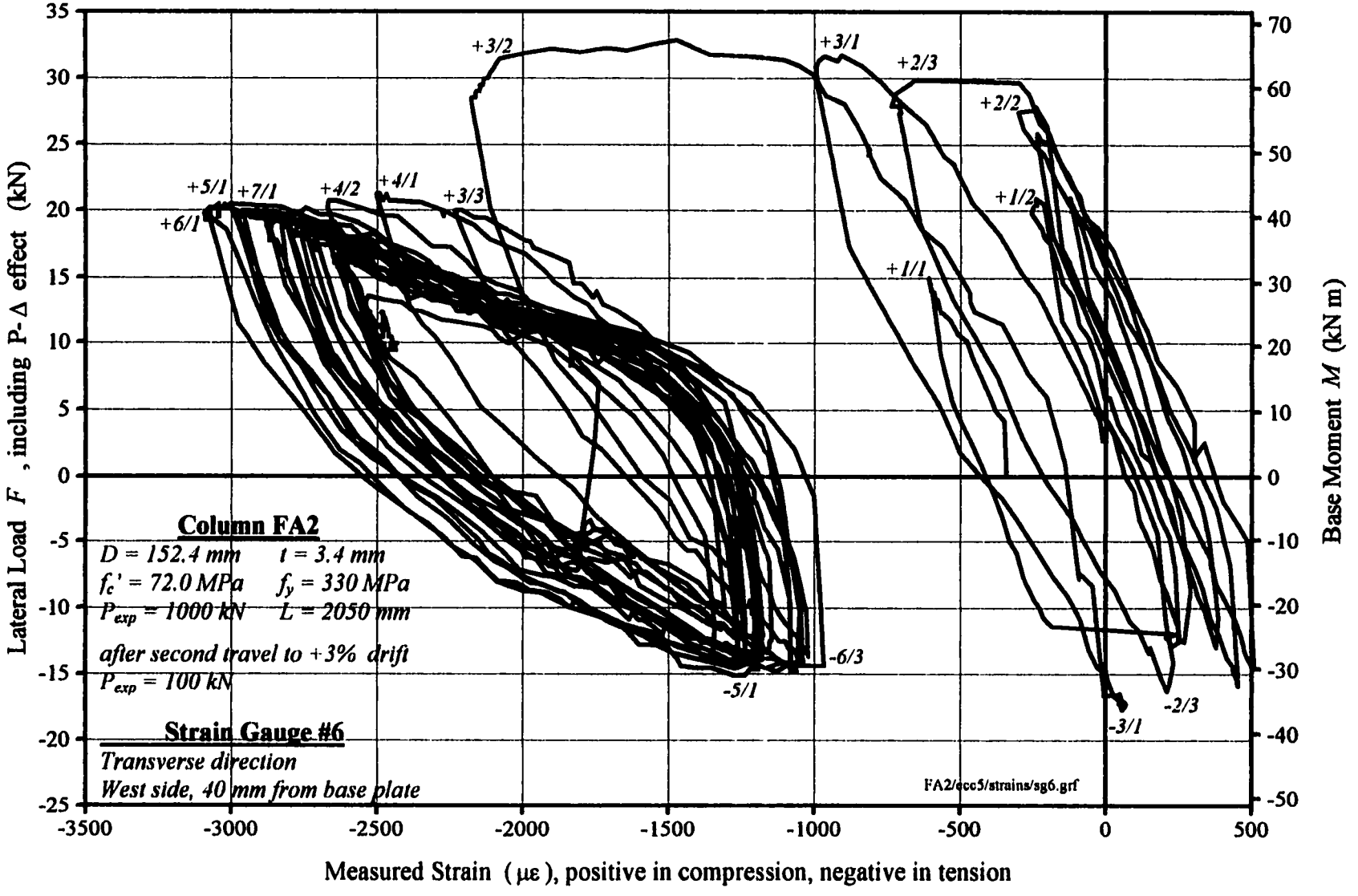

Figure A.14 : Strain Gauge #6 of Beam-Column Specimen FA2

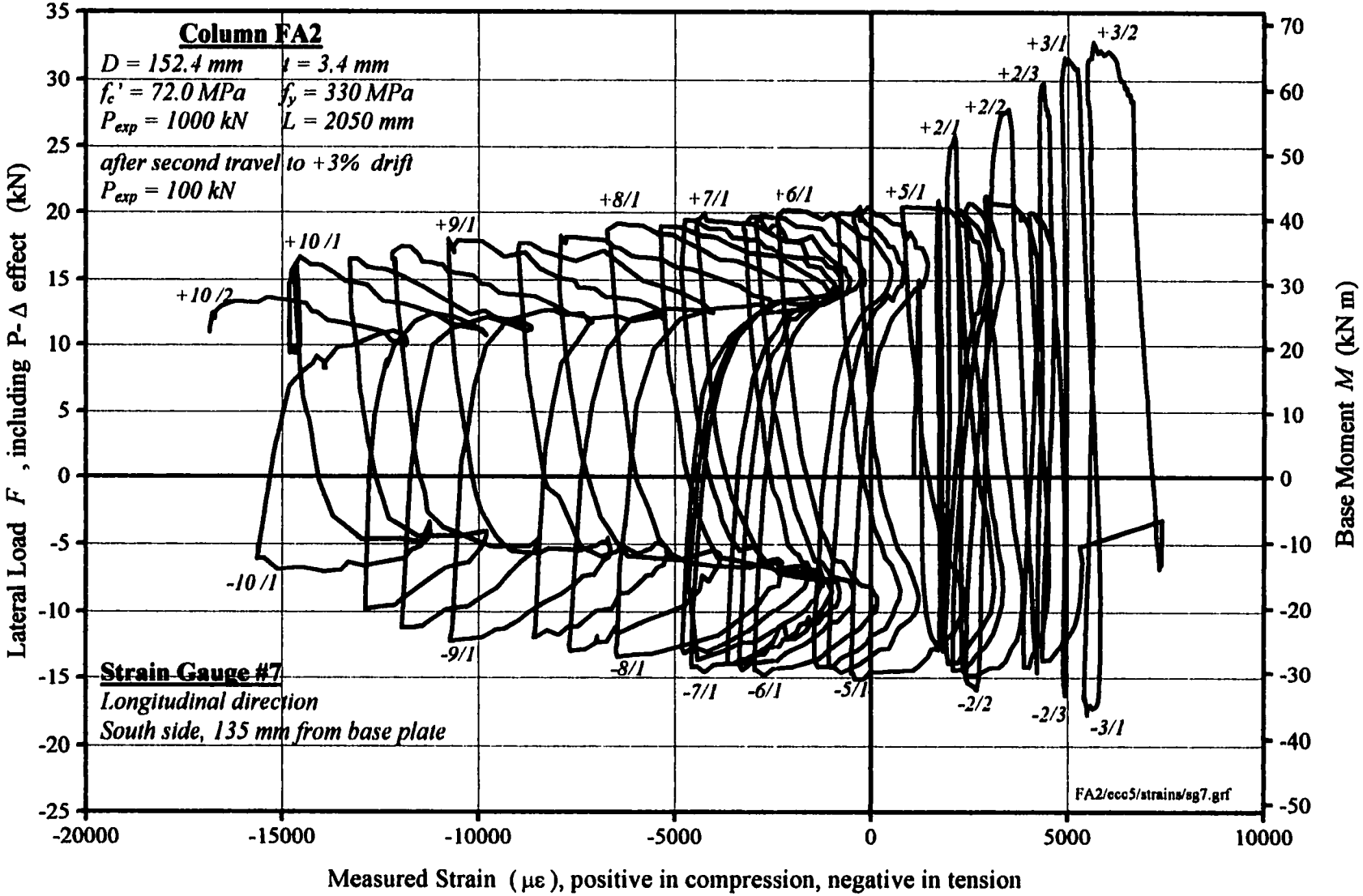

Figure A.15: Strain Gauge #7 of Beam-Column Specimen FA2

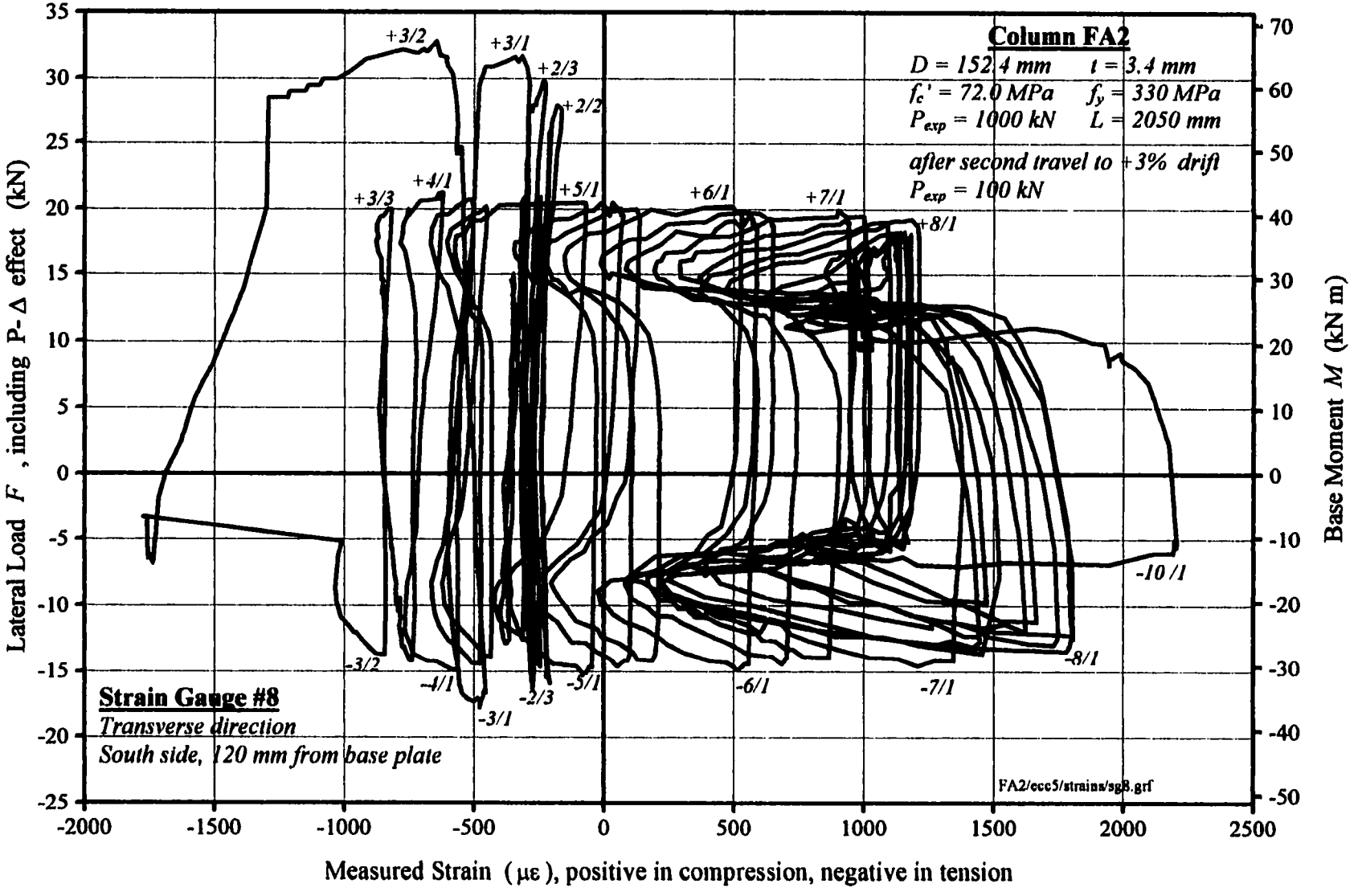

Figure A.16 : Strain Gauge #8 of Beam-Column Specimen FA2

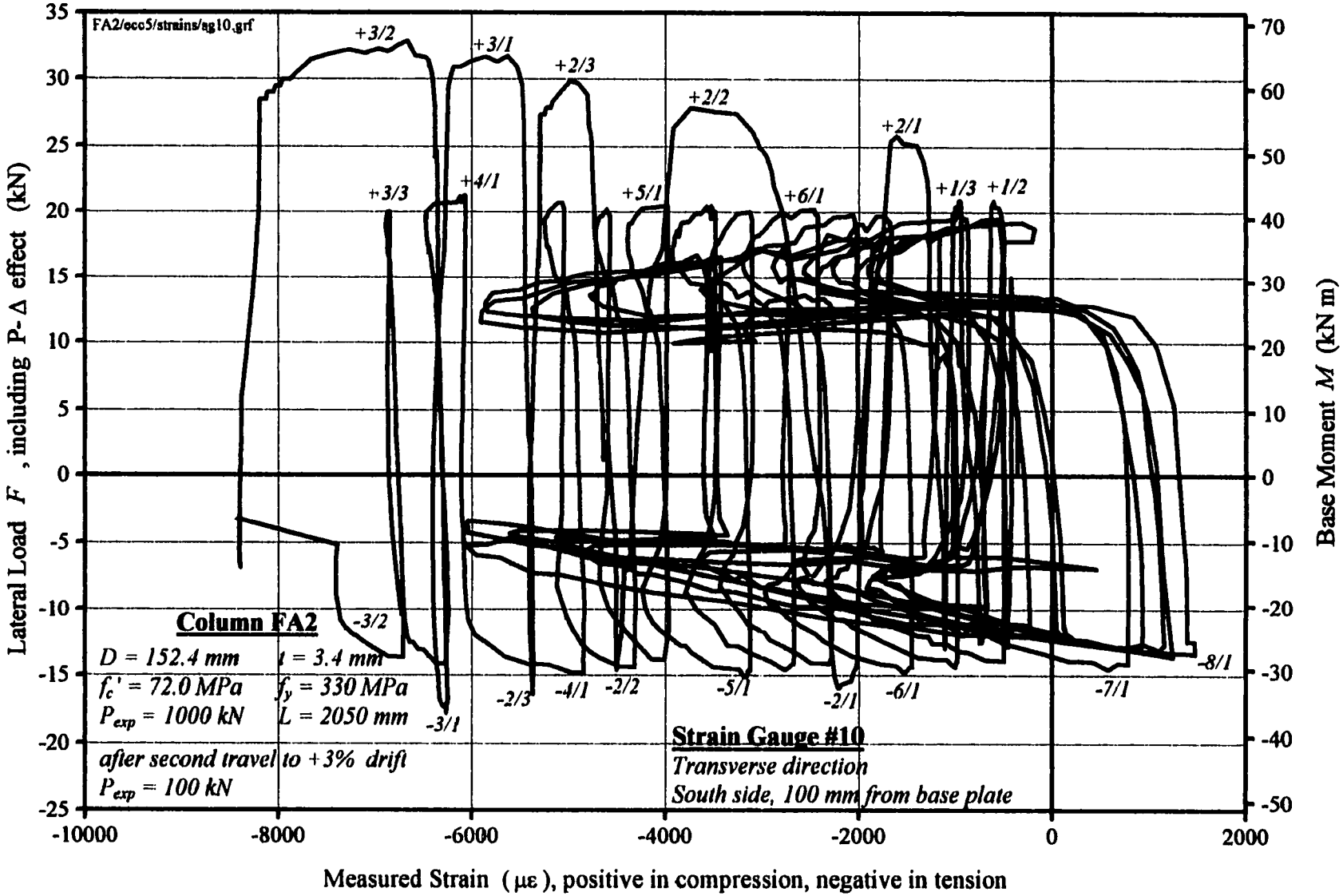

Figure A.17 : Strain Gauge #10 of Beam-Column Specimen FA2

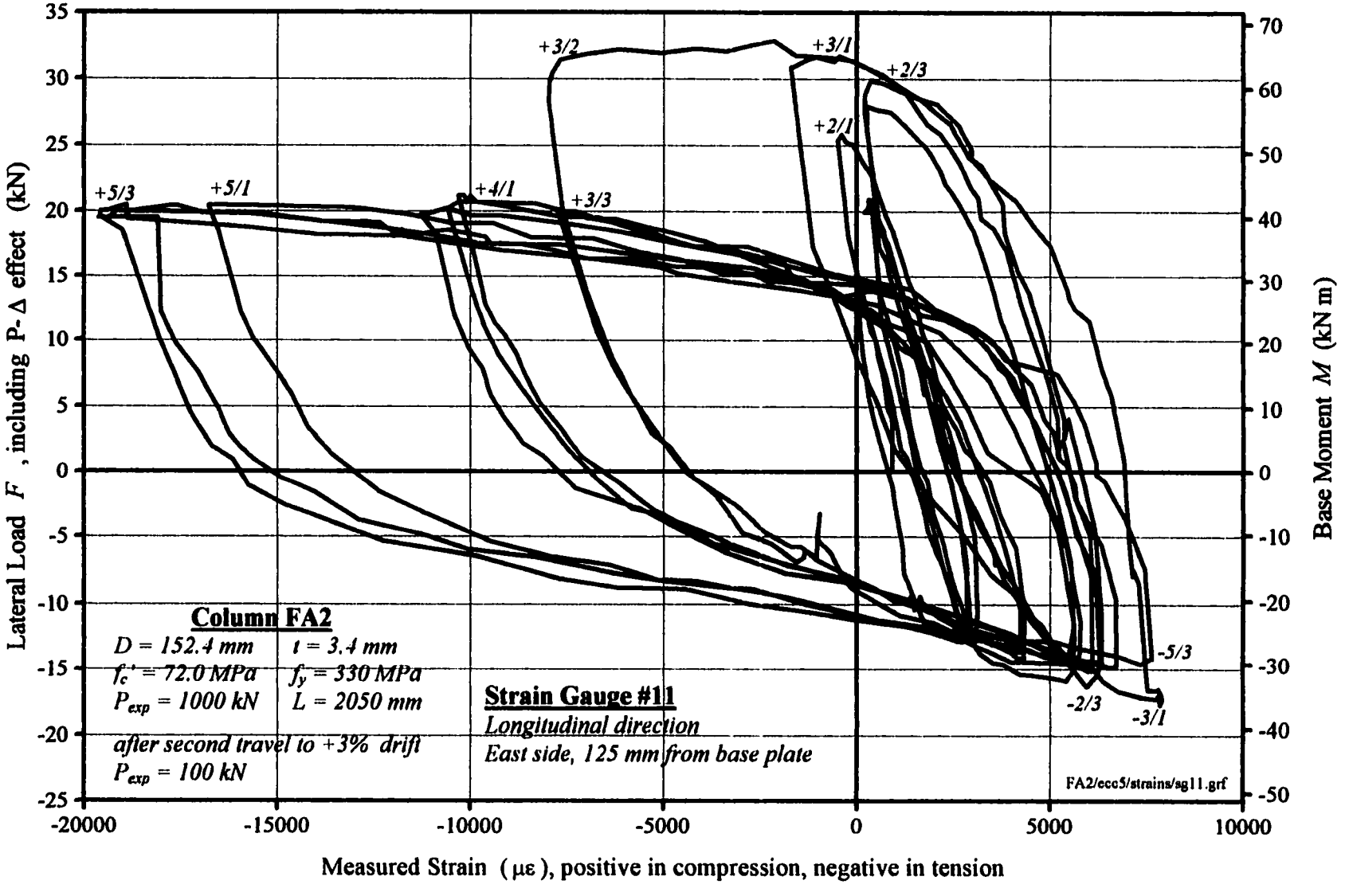

Figure A.18 : Strain Gauge #11 of Beam-Column Specimen FA2

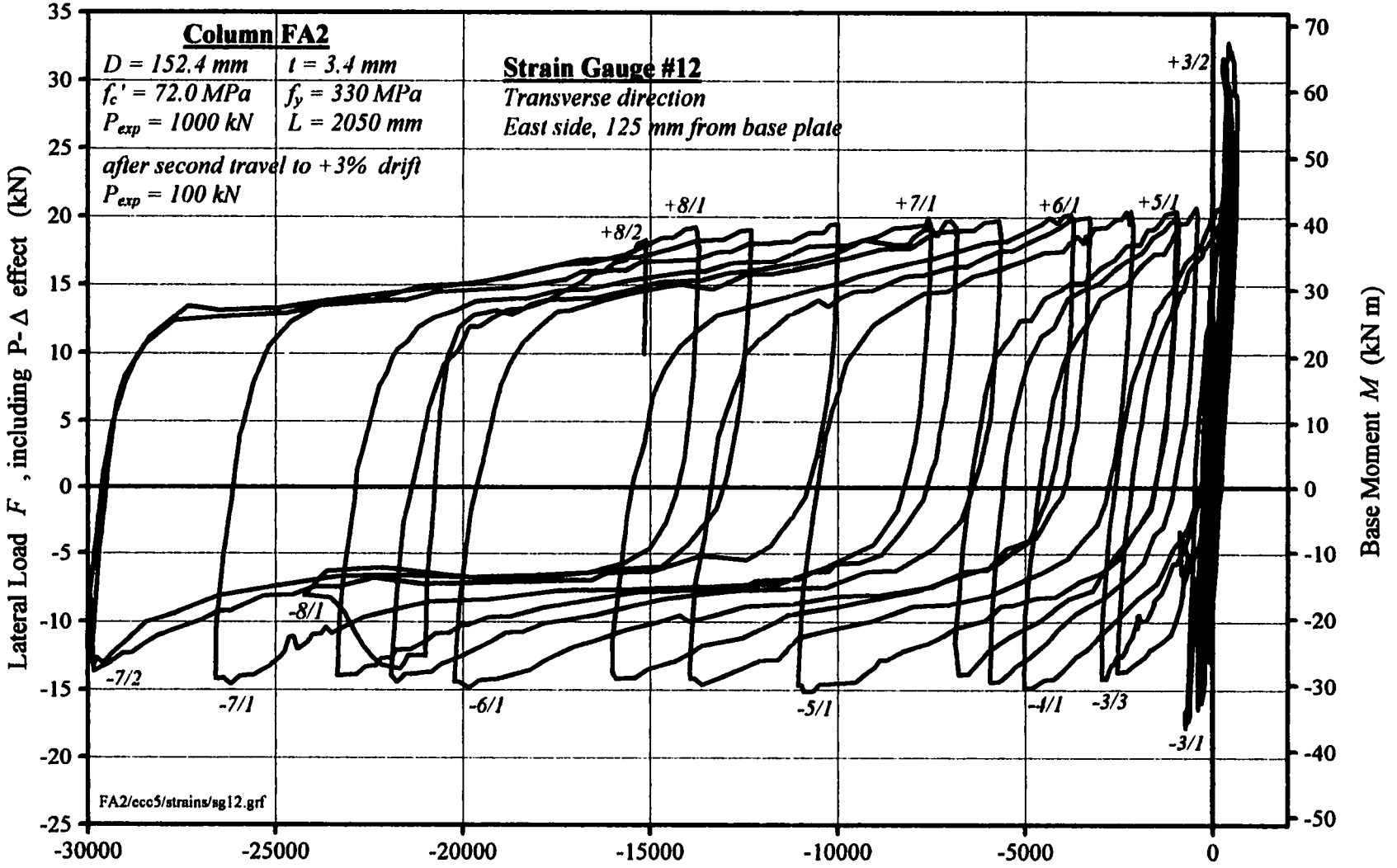

Figure A.19 : Strain Gauge #12 of Beam-Column Specimen FA2

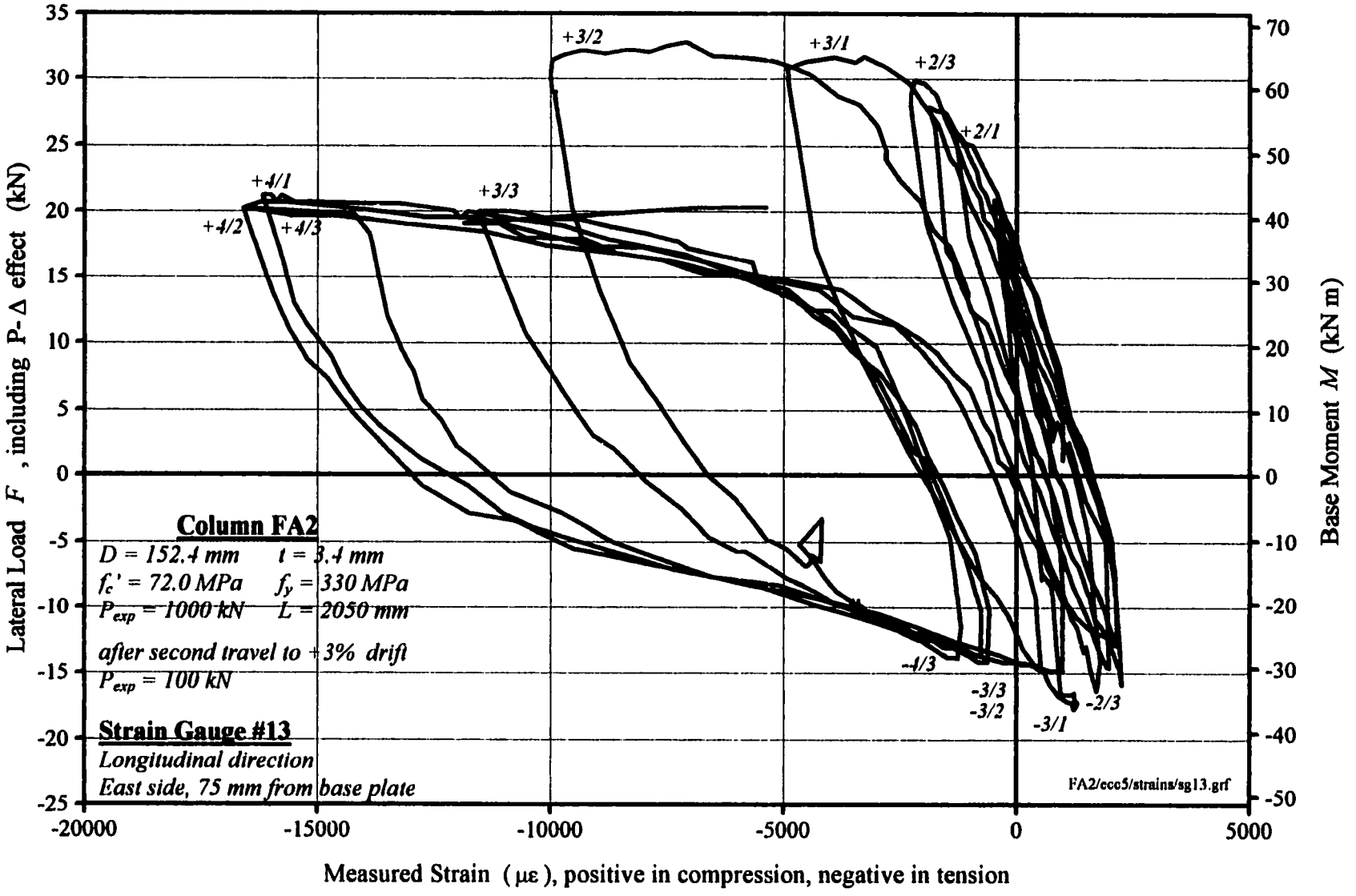

Figure A.20 : Strain Gauge #13 of Beam-Column Specimen FA2

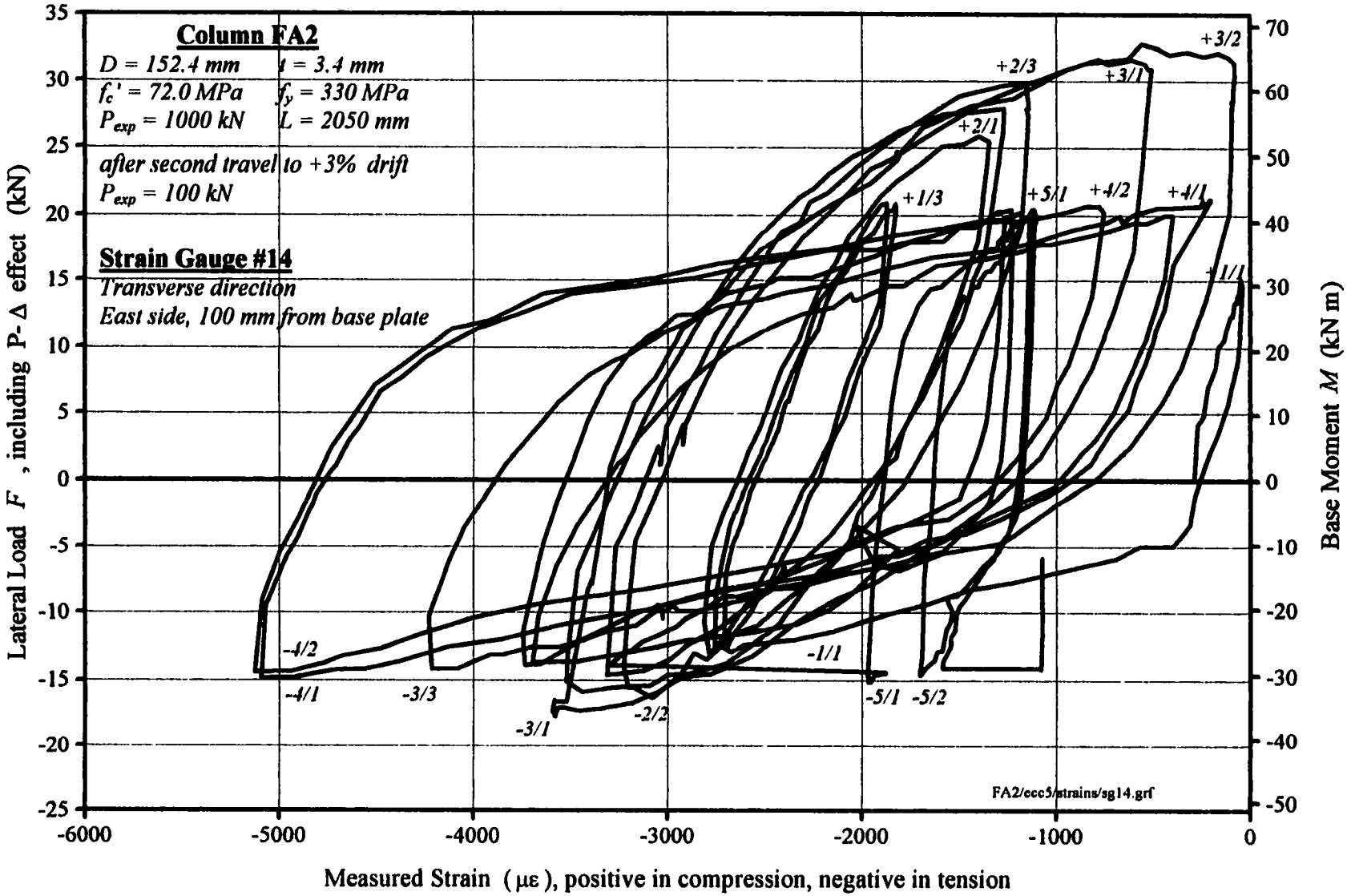

Figure A.21 : Strain Gauge #14 of Beam-Column Specimen FA2

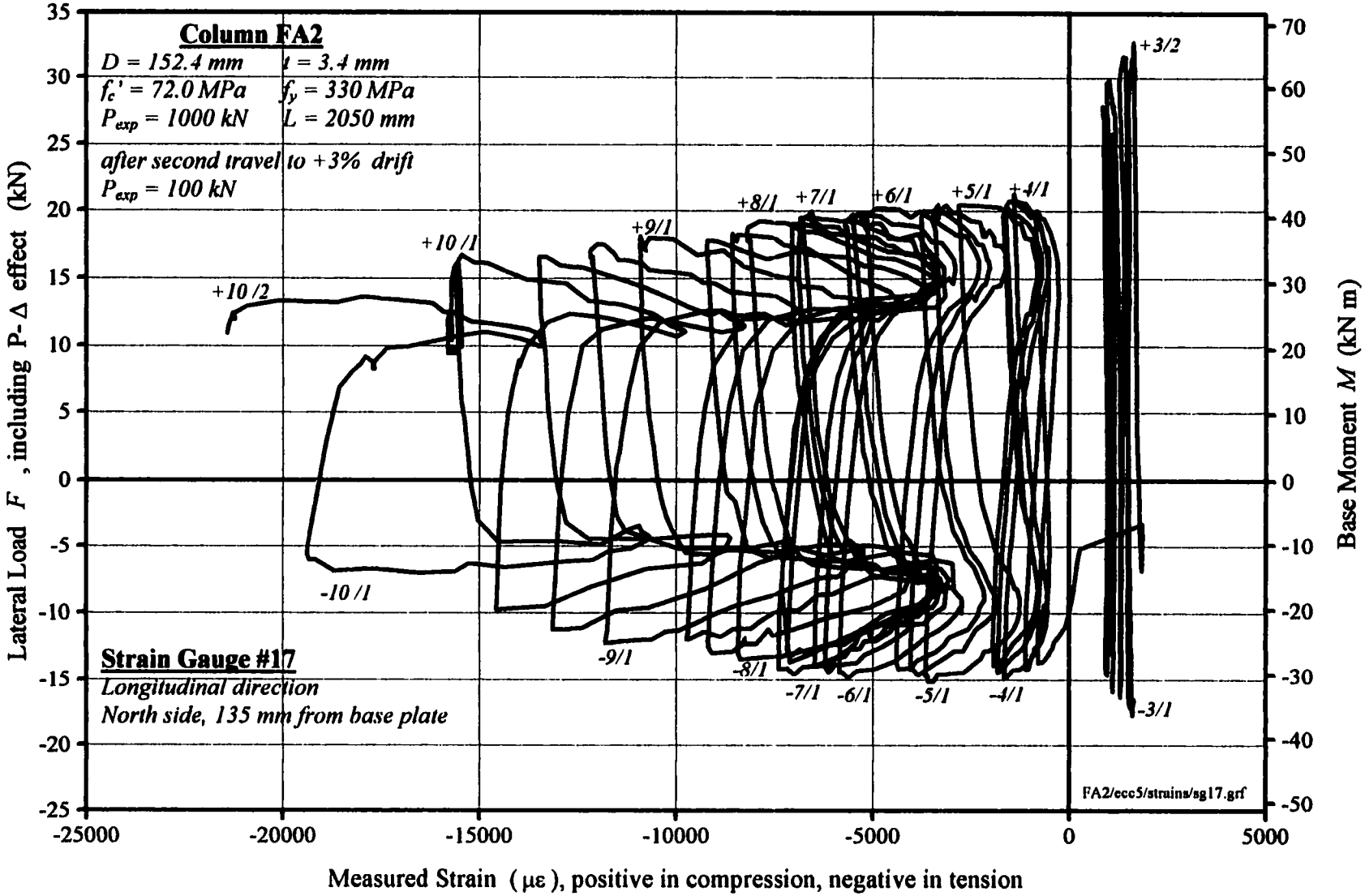

Figure A.22 : Strain Gauge #17 of Beam-Column Specimen FA2

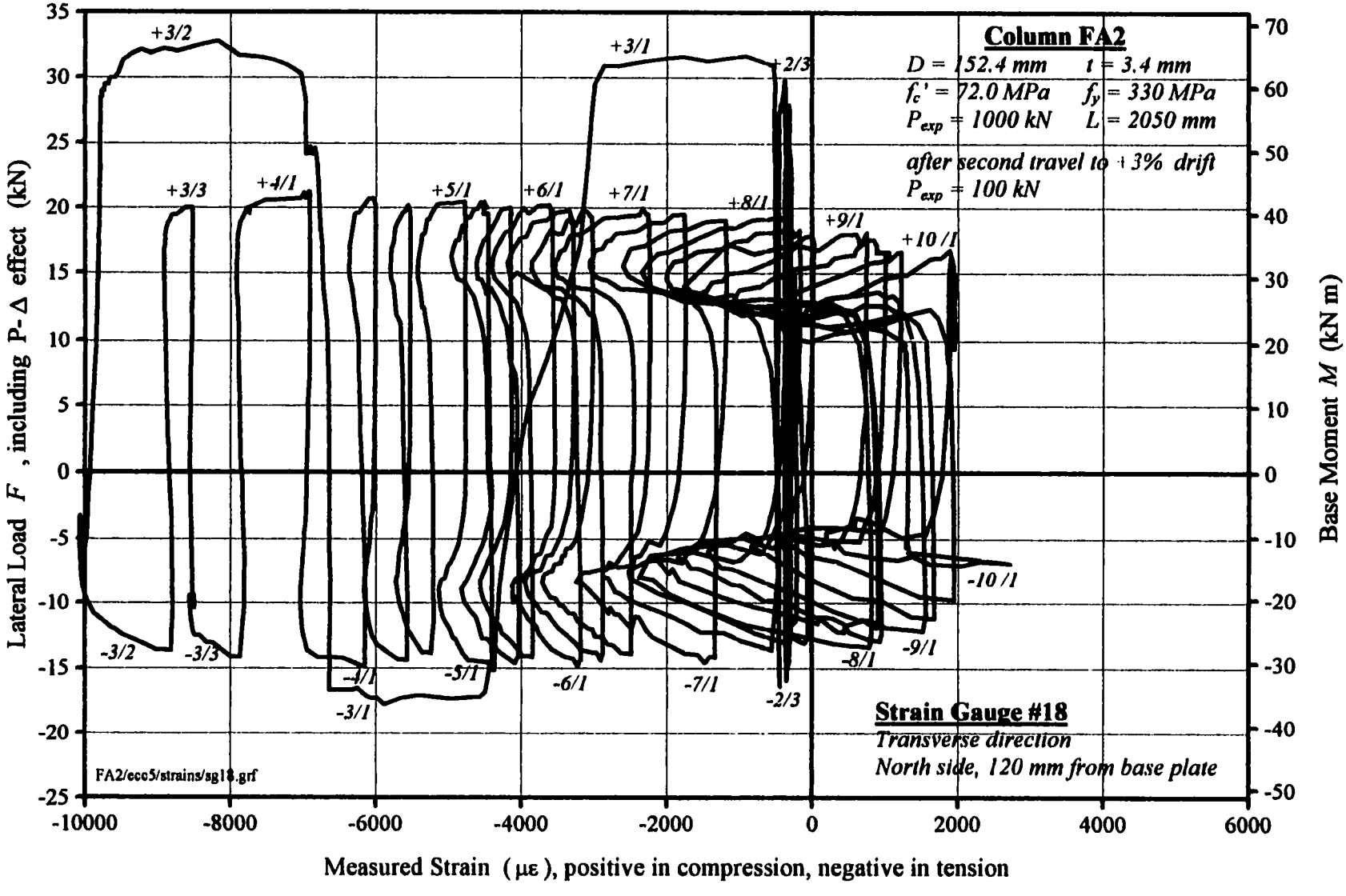

Figure A.23 : Strain Gauge #18 of Beam-Column Specimen FA2

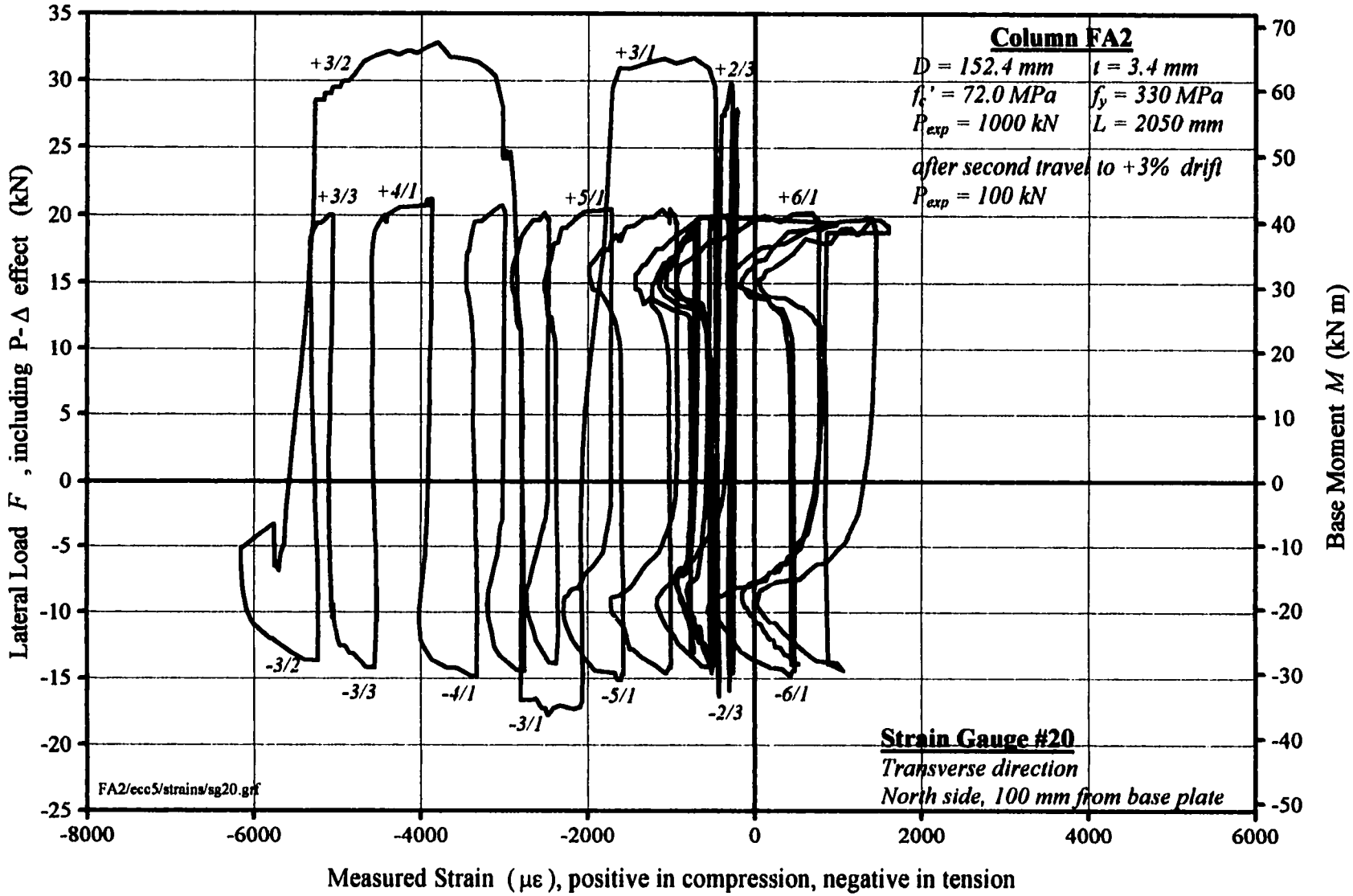

Figure A.24 : Strain Gauge #20 of Beam-Column Specimen FA2

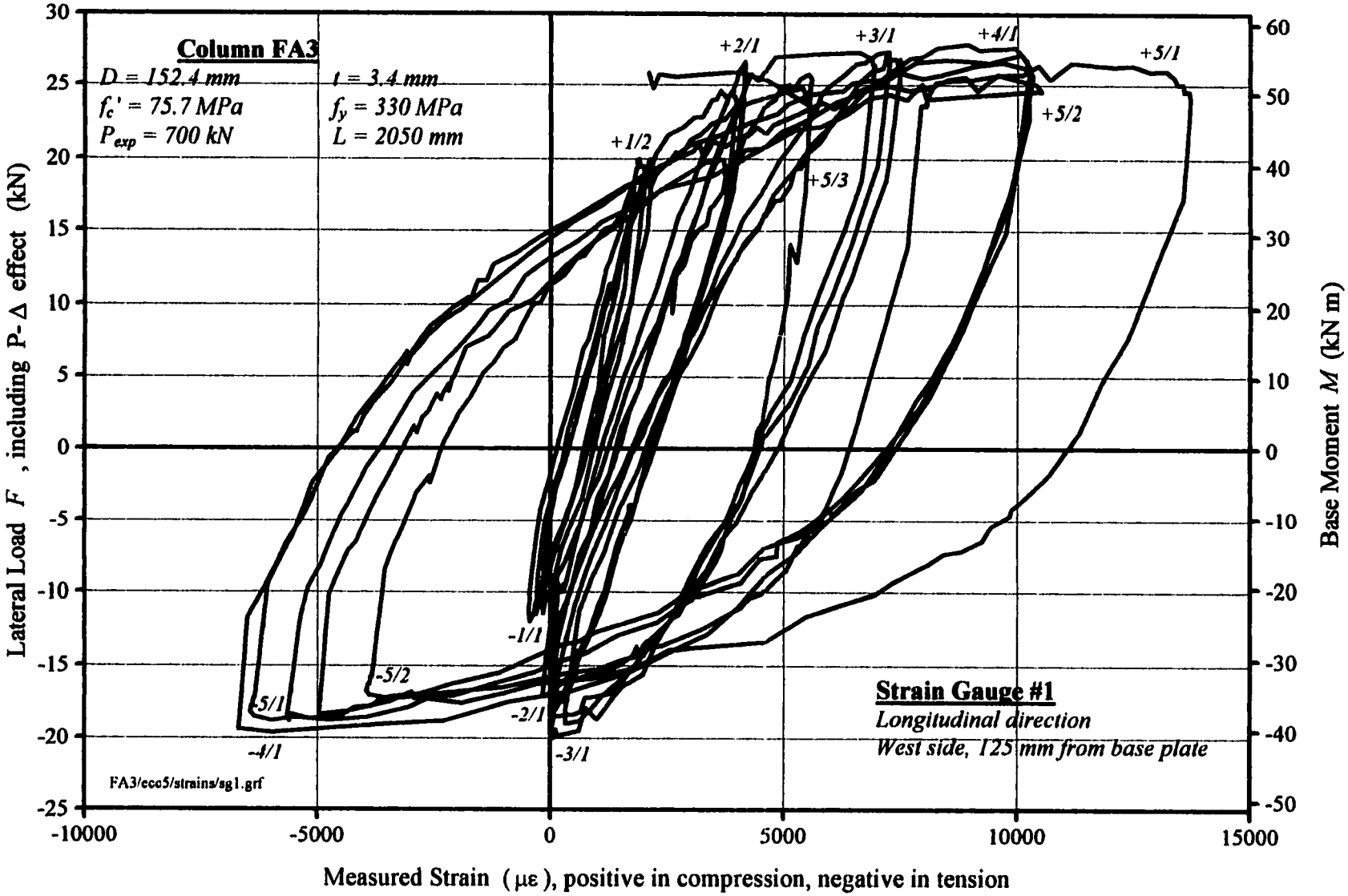

Figure A.25 : Strain Gauge #1 of Beam-Column Specimen FA3

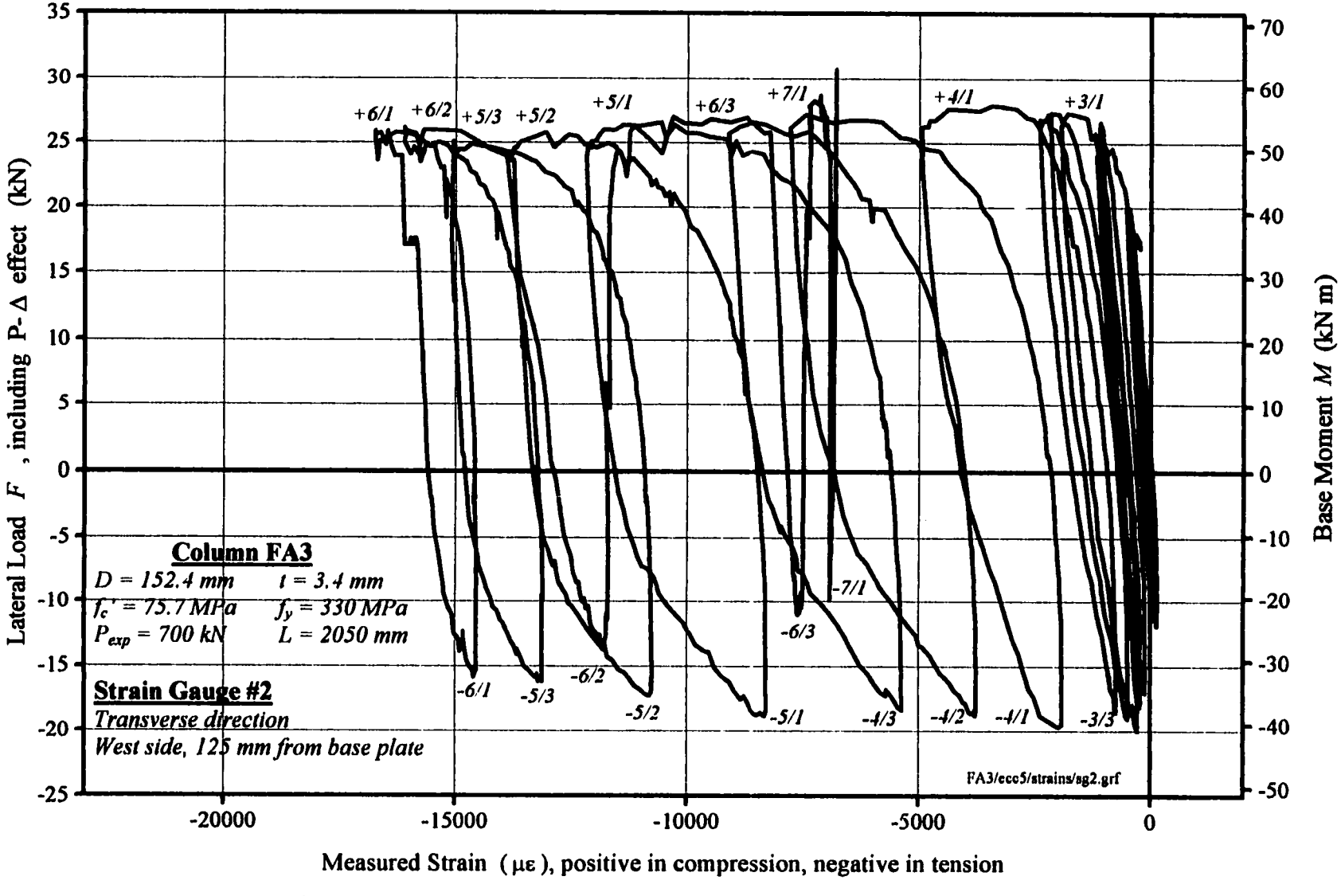

Figure A.26 : Strain Gauge #2 of Beam-Column Specimen FA3

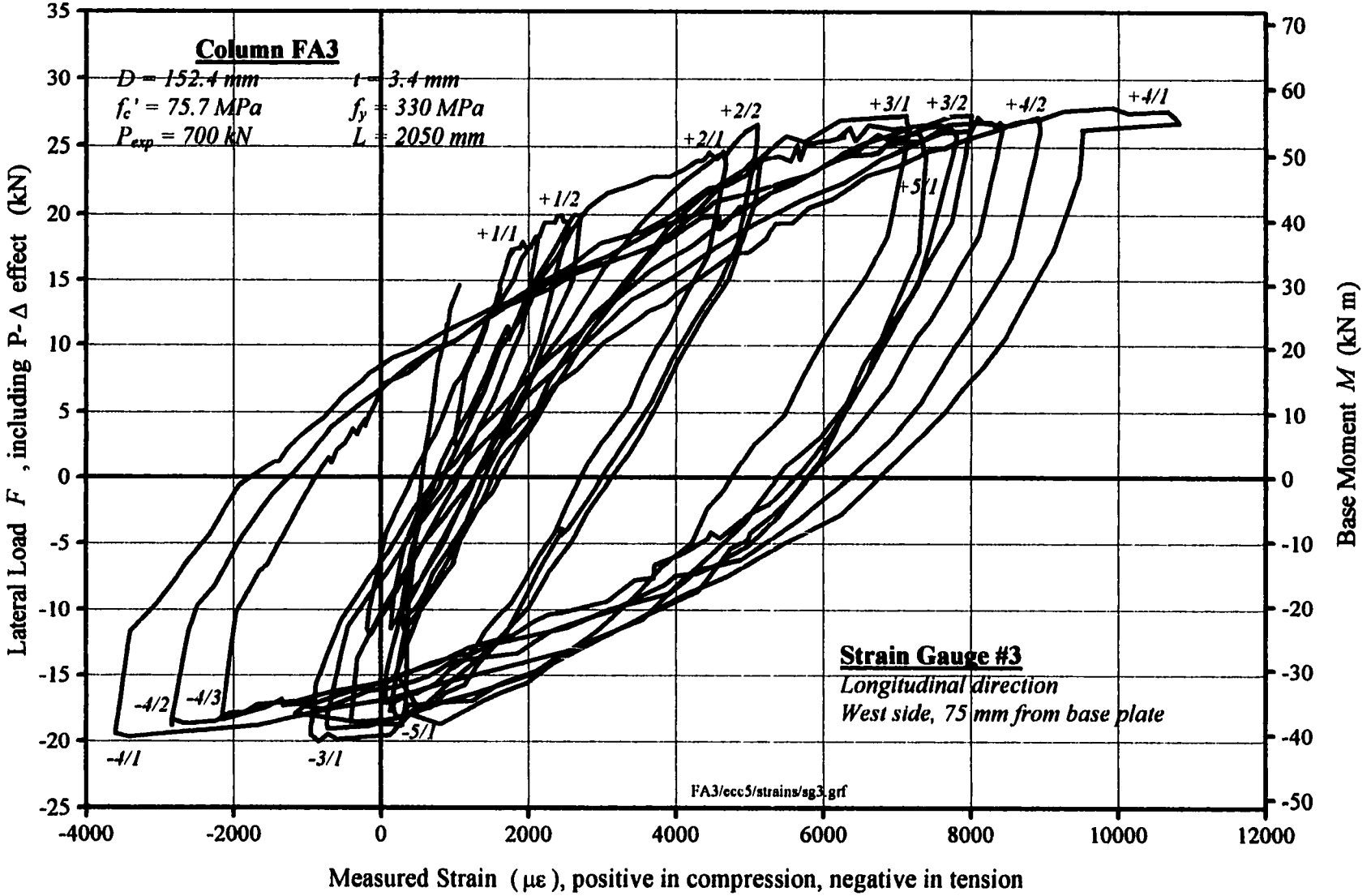

Figure A.27 : Strain Gauge #3 of Beam-Column Specimen FA3

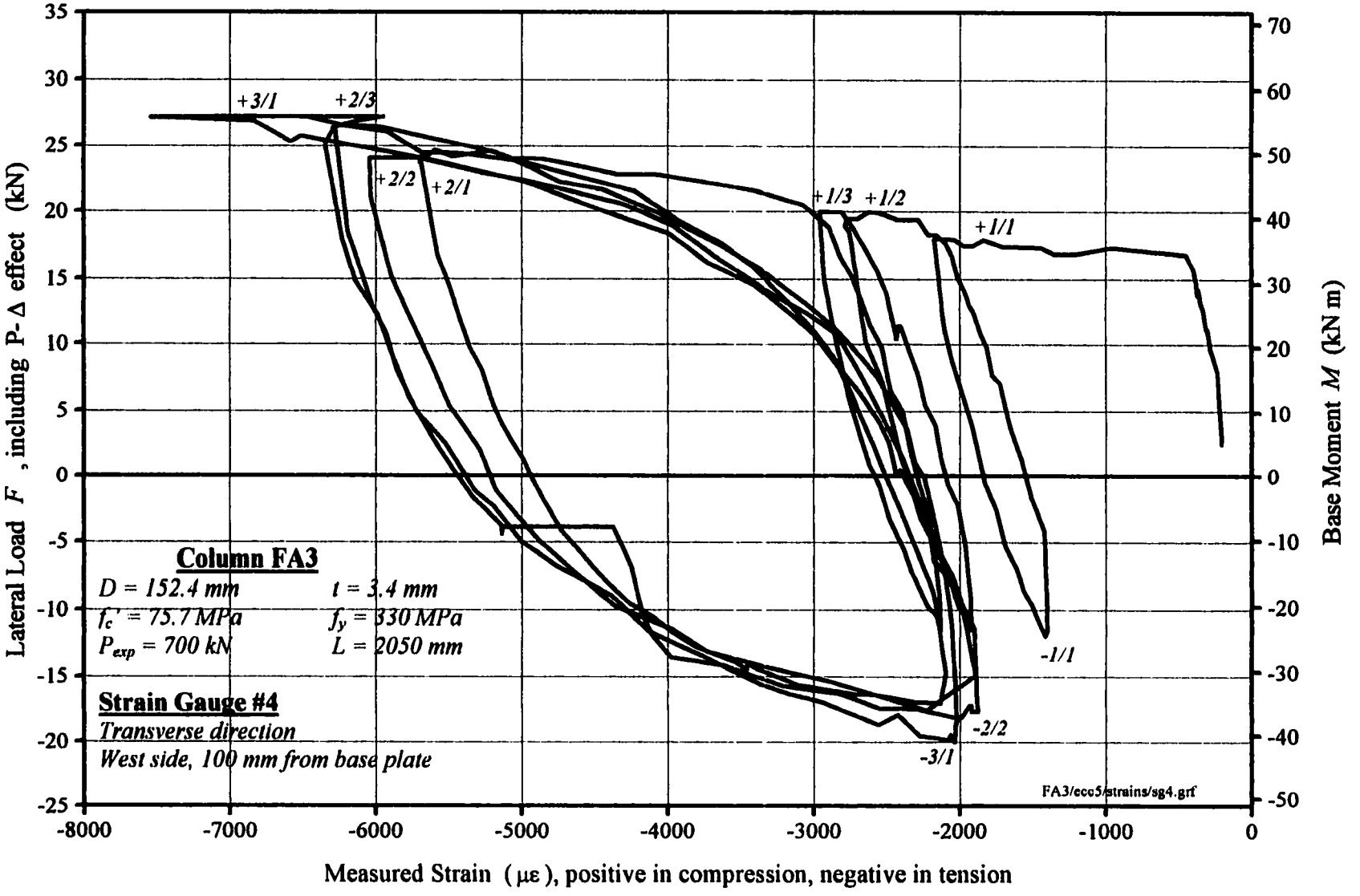

Figure A.28 : Strain Gauge #4 of Beam-Column Specimen FA3

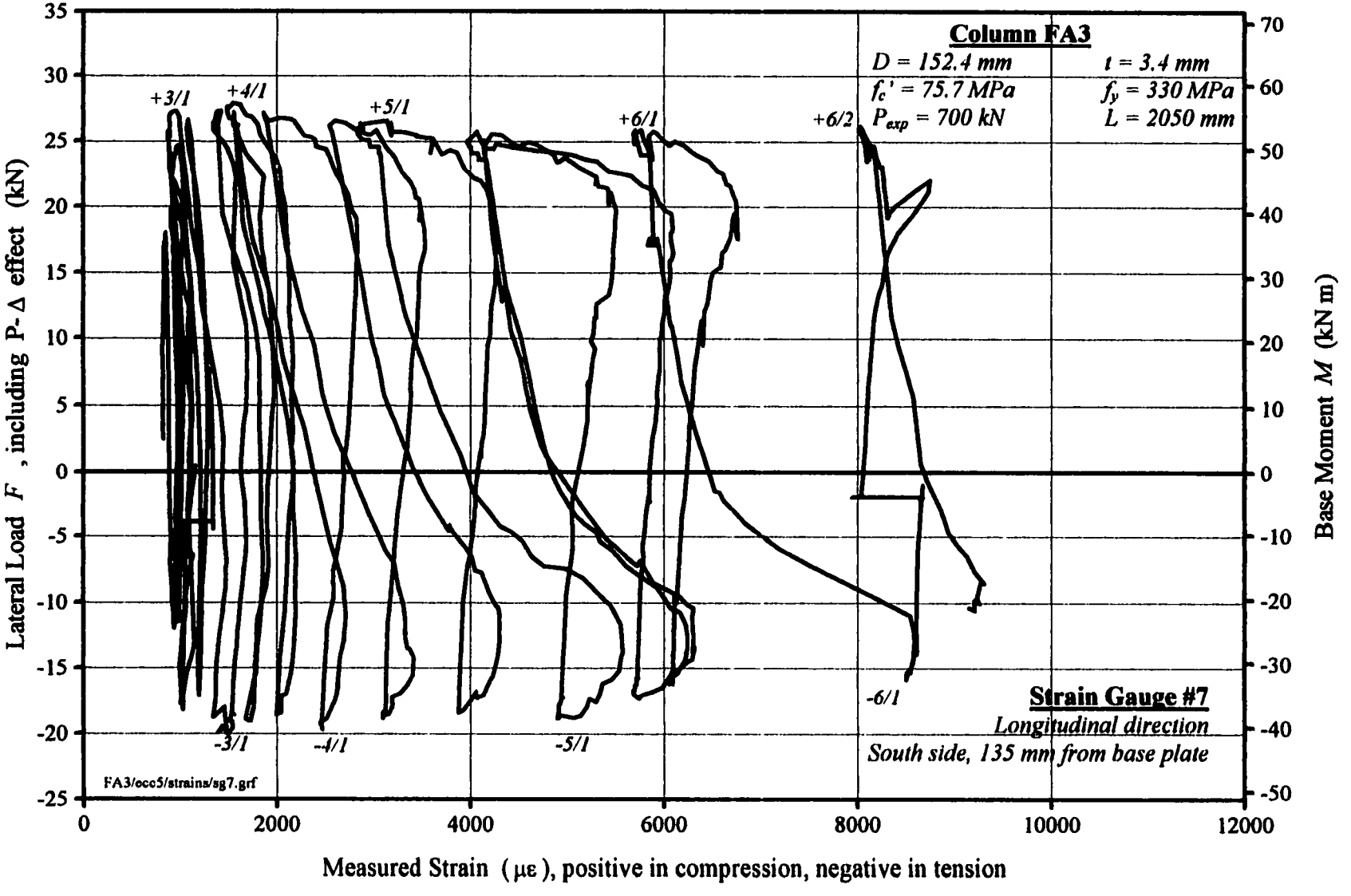

Figure A. 29 : Strain Gauge #7 of Beam-Column Specimen FA3

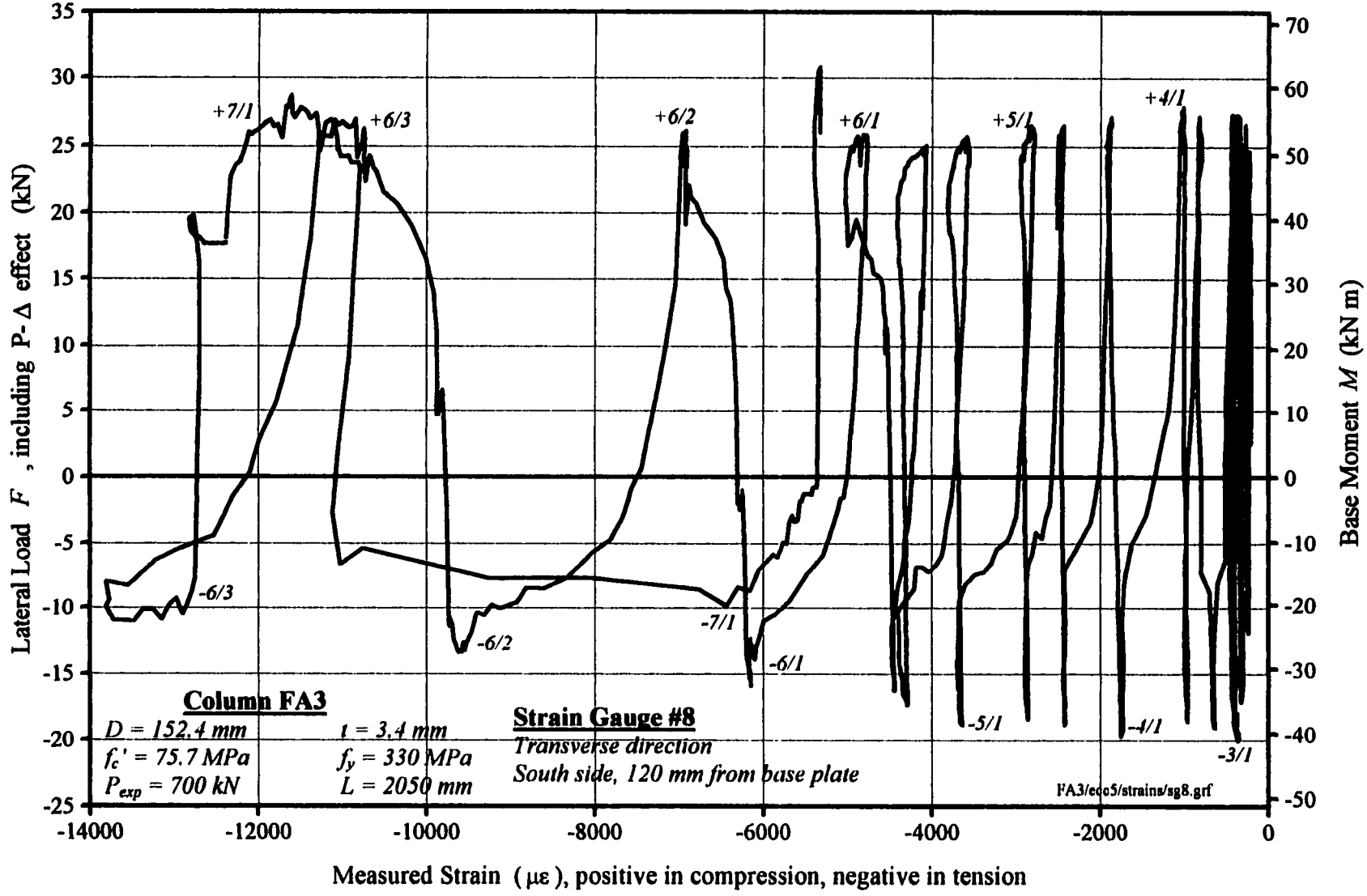

Figure A.30 : Strain Gauge #8 of Beam-Column Specimen FA3

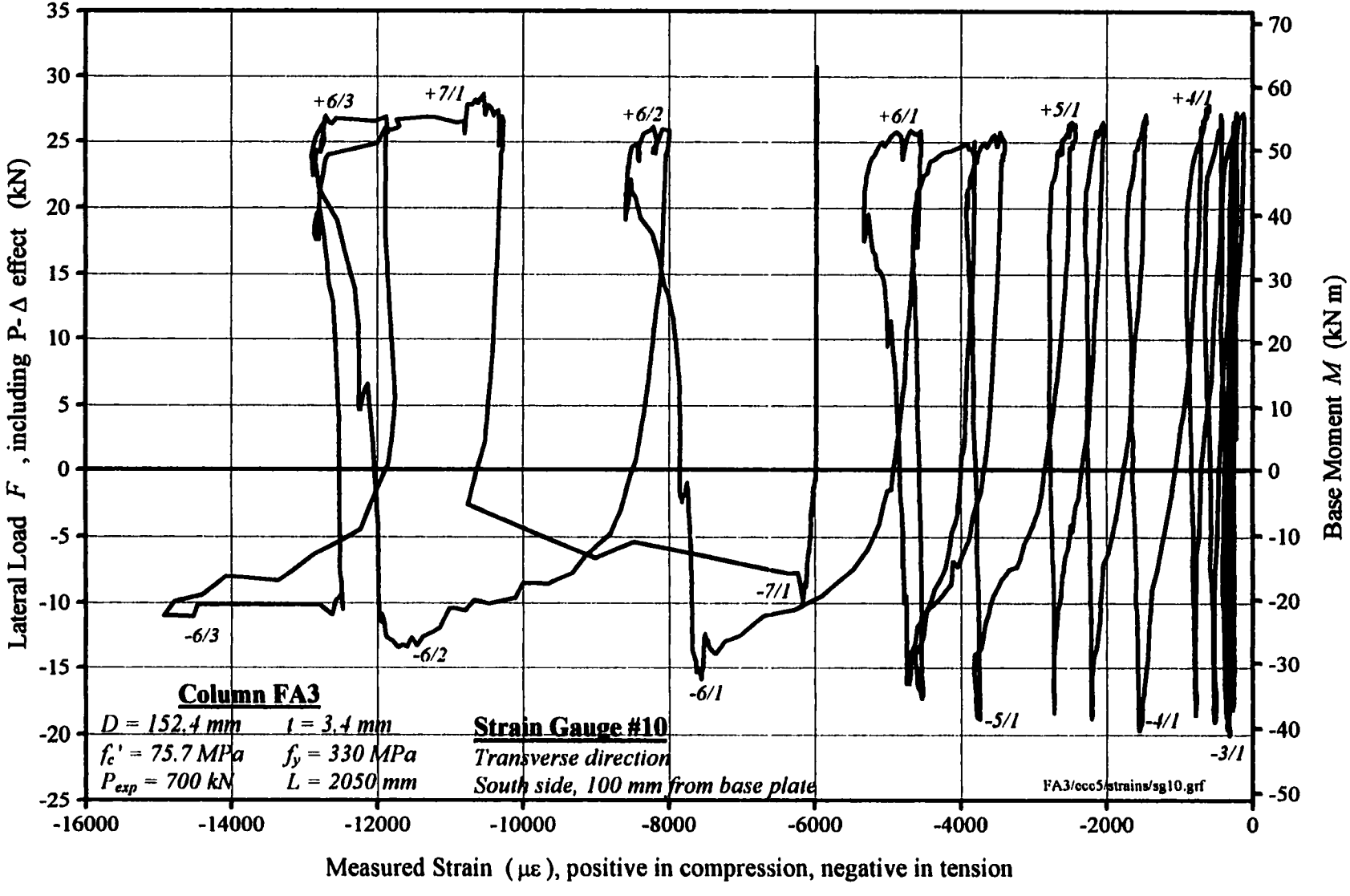

Figure A.31 : Strain Gauge #10 of Beam-Column Specimen FA3

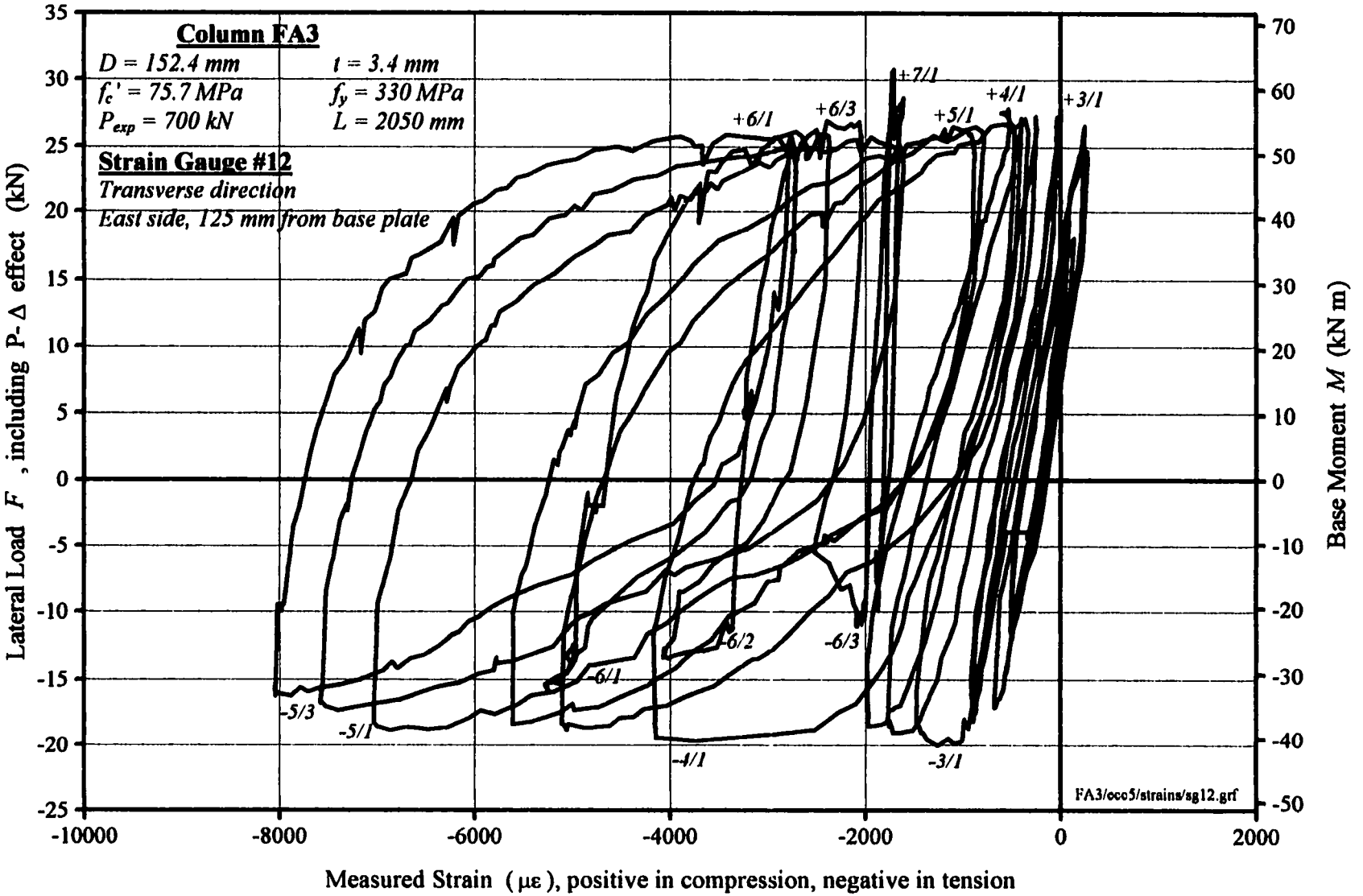

Figure A.32 : Strain Gauge #12 of Beam-Column Specimen FA3

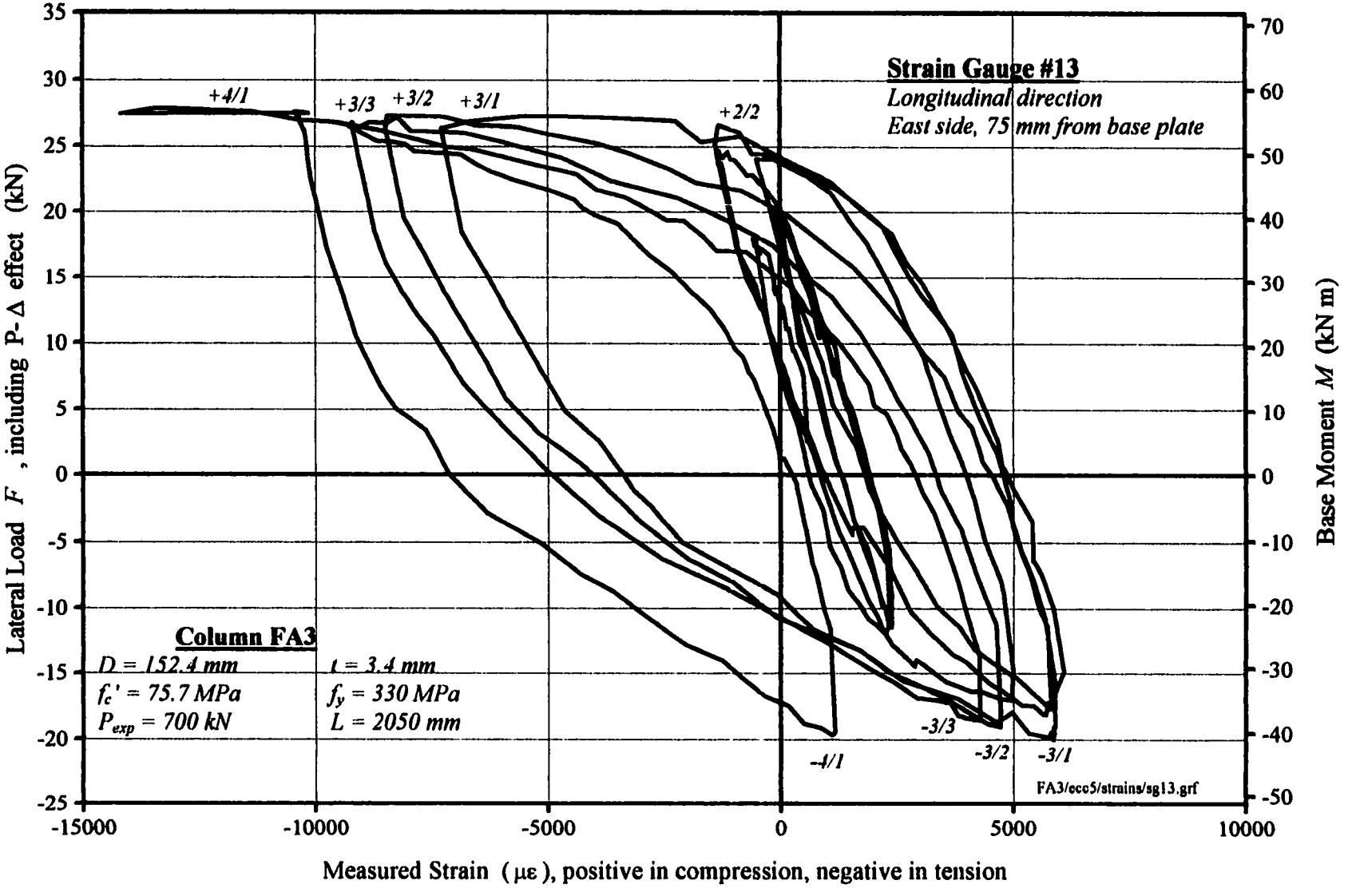

Figure A.33 : Strain Gauge #13 of Beam-Column Specimen FA3

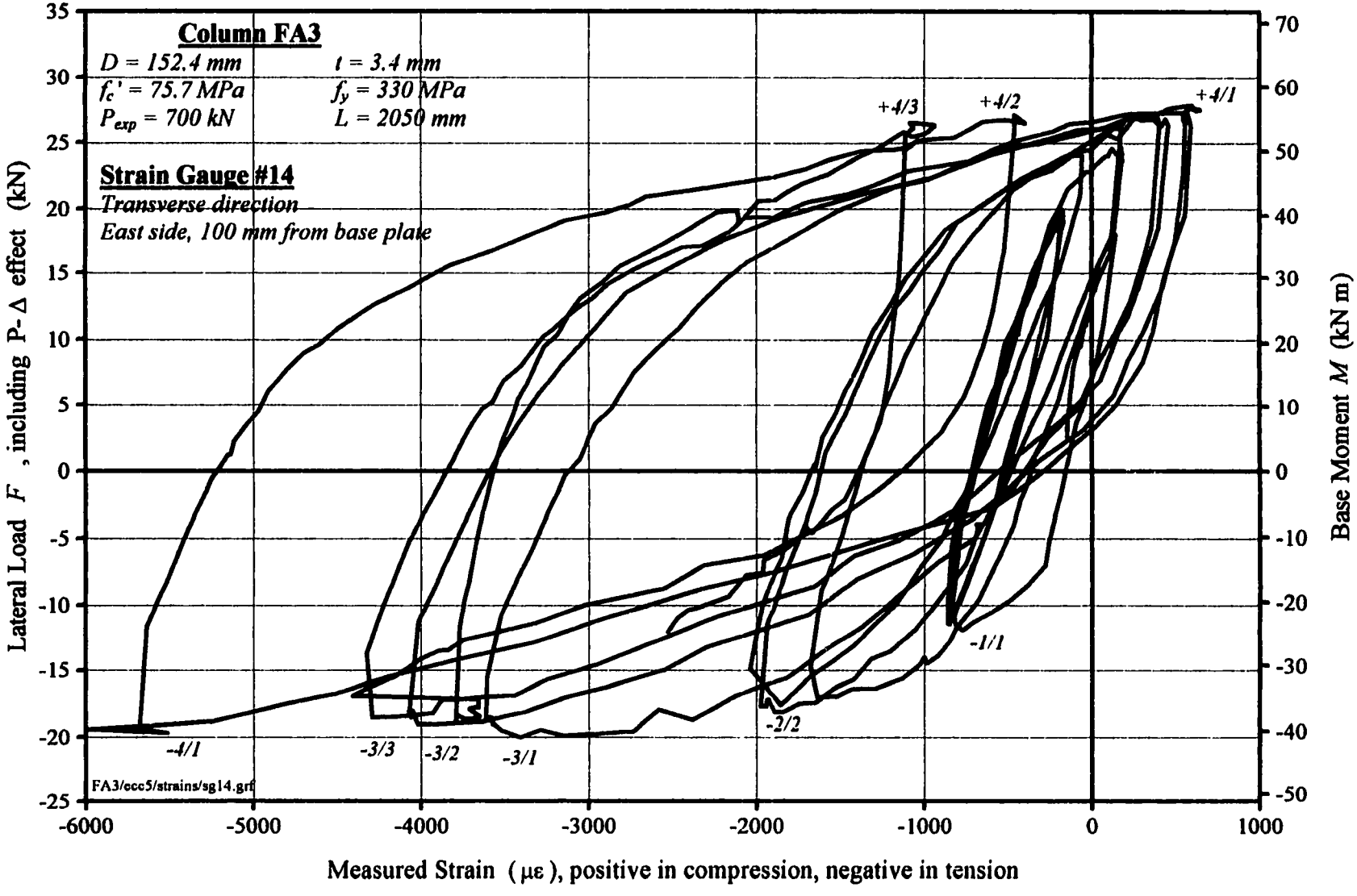

Figure A.34 : Strain Gauge #14 of Beam-Column Specimen FA3

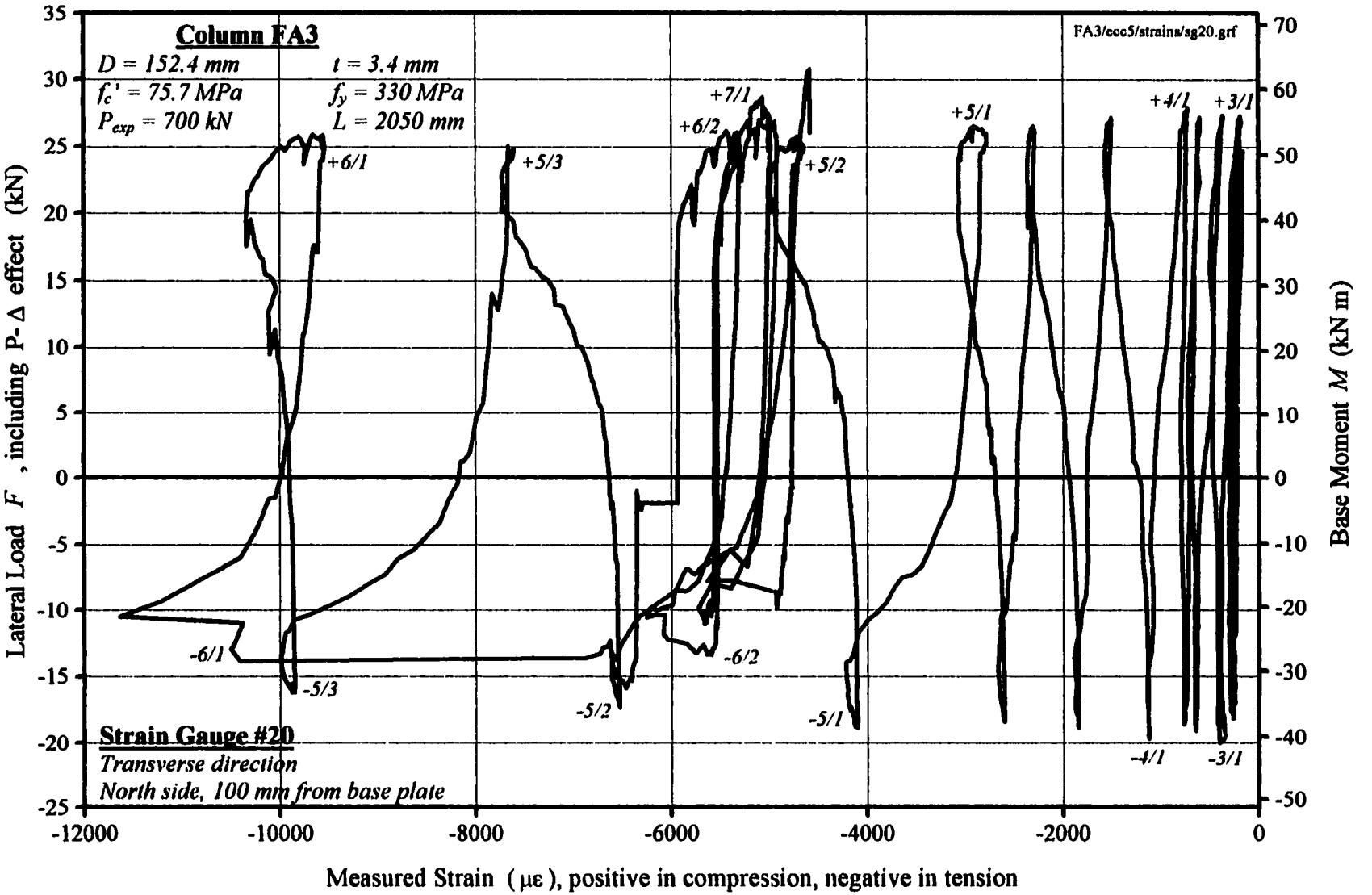

Figure A.35 : Strain Gauge #20 of Beam-Column Specimen FA3

Appendix B

Fortran Code for Program CFTACI

```
C   ***************************************************************
C   * CFTACI - PROGRAM FOR COMPUTING THRUST-MOMENT INTERACTION *
C   *        CURVES FOR CIRCULAR STEEL TUBES FILLED WITH     *
C   *        HIGH STRENGTH CONCRETE (>56 MPa) IN ACCORDANCE  *
C   *        WITH ACI 318-95 (COMPRESSIVE AXIAL LOAD ONLY).  *
C   *        ELASTIC-PERFECTLY-PLASTIC MODEL FOR STEEL.      *
C   *        NUMBER OF STEEL FIBRES - 2200.                  *
C   *        RECTANGULAR STRESS BLOCK FOR CONCRETE OF        *
C   *        INTENSITY 0.85 fc', a = 0.65 c.                 *
C   *        MAXIMUM CONCRETE COMPRESSIVE STRAIN 0.003.      *
C   *        NUMBER OF CONCRETE FIBRES - 2000.               *
C   *        OUTPUT EVERY 0.05 Po FROM 0 TILL 0.85 Po.       *
C   *    BY FARID ALFAWAKHIRI - LAST REVISED ON JULY 25, 1997 *
C   ***************************************************************
C
C
      IMPLICIT REAL*8 (A-H,O-Z)
      CHARACTER OUTPUT*80
      COMMON/SET1/AS(2200),AC(2200),ES(2200)
      COMMON/SET2/GS(2200),GC(2200)
      COMMON/SET3/Q(2200),SS(2200),SC(2200),Z(2200)
C
C     DATA INPUT
C
      WRITE (*,1000)
 1000 FORMAT (2X,'PROGRAM CFTACI - FOR ANALYSIS OF CIRCULAR COMPOSITE
     1 SECTIONS'/)
      WRITE (*,1001)
 1001 FORMAT (2X,'ENTER OUTER DIAMETER AND THICKNESS OF CURCULAR',/2X,
     1       'TUBE:',$)
      READ (*,*) D, TS
      WRITE (*,1002)
 1002 FORMAT (2X,'ENTER YIELD STRESS OF CIRCULAR STEEL TUBE,'/2X,
     1       'MODULUS OF ELASTISITY FOR STEEL,'/2X,
     2       'CONCRETE CILINDER STRENGTH,'/2X,
```

```
    3       'MAXIMUM NUMBER OF ITERATIONS PER STEP:',$)
      READ (*,*) FY, E, FC, ITMAX
      WRITE (*,1003)
 1003 FORMAT (2X,'ENTER THE NAME OF THE OUTPUT FILE:',$)
      READ (*,1004) OUTPUT
 1004 FORMAT (1A80)
C
C     COMPUTE SECTIONAL GEOMETRICAL PARAMETERS
C
      DM=D-TS
      DI=DM-TS
      R=D/2.
      RM=DM/2.
      RI=DI/2.
C
C     DIVIDE THE HALF-SECTION TO 1100 FIBRES (1000 FIBRES FOR CONCRETE
C     AND 1100 FIBRES FOR STEEL TUBE) AND CALCULATE THEIR AREAS,
C     DISTANCES TO SECTION CENTROID Z, AND DISTANCES TO THE COMPRESSED
C     EDGE Q
C
      STP1=TS/100.
      HSTP1=STP1/2.
      STP2=RI/1000.
      HSTP2=STP2/2.
      X=0.0
C
      DO 11 I=1,100
      X=X+STP1
      H=R-X
      Q(I)=X-HSTP1
      Z(I)=H+HSTP1
      WS=ACOS(H/R)
      YS=R*SIN(WS)
      GS(I)=WS*R*R-YS*H
   11 CONTINUE
C
      DO 12 I=101,1100
      X=X+STP2
      H=R-X
      Q(I)=X-HSTP2
      Z(I)=H+HSTP2
      WS=ACOS(H/R)
      YS=R*SIN(WS)
      GS(I)=WS*R*R-YS*H
      WC=ACOS(H/RI)
      YC=RI*SIN(WC)
      GC(I)=WC*RI*RI-YC*H
   12 CONTINUE
C
      AC(1)=0.
      AC(101)=GC(101)
      DO 13 I=102,1100
      AC(I)=GC(I)-GC(I-1)
   13 CONTINUE
```

```
C
      AS(1)=GS(1)
      DO 14 I=2,100
      AS(I)=GS(I)-GS(I-1)
      AC(I)=0.
   14 CONTINUE
C
      DO 15 I=101,1100
      AS(I)=GS(I)-GS(I-1)-AC(I)
   15 CONTINUE
C
C     COMPUTE THE FIBER PARAMETERS FOR THE OTHER HALF-SECTION
C
      DO 17 I=1,1100
      AS(1100+I)=AS(1101-I)
      AC(1100+I)=AC(1101-I)
      Q(1100+I)=D-Q(1101-I)
      Z(1100+I)=-Z(1101-I)
   17 CONTINUE
C
C     COMPUTE THE AREAS AND PLASTIC MODULI FOR
C     STEEL AND CONCRETE SECTIONS (FOR CHECK)
C
      ARS=0.0
      ARC=0.0
      WPS=0.0
      WPC=0.0
      DO 18 I=1,1100
      ARS=ARS+AS(I)
      ARC=ARC+AC(I)
      WPS=WPS+AS(I)*Z(I)
      WPC=WPC+AC(I)*Z(I)
   18 CONTINUE
      DO 19 I=1101,2200
      ARS=ARS+AS(I)
      ARC=ARC+AC(I)
      WPS=WPS-AS(I)*Z(I)
      WPC=WPC-AC(I)*Z(I)
   19 CONTINUE
      WRITE (*,1010) ARS, ARC, WPS, WPC
 1010 FORMAT (4E15.8)

C
C     COMPUTE THE DESIGN AXIAL LOAD STRENGTH OF THE COLUMN PN
C     AND THE AXIAL LOAD STEP FOR THE INTERACTION CURVE LSTP
C
      PN=0.85*(0.85*FC*ARC+FY*ARS)
      LSTP=PN/17.
C
C     OPEN THE DATA OUTPUT FILE
C
      CLOSE (7)
      OPEN (7,FILE=OUTPUT,STATUS='NEW')
C
```

```
C    COMPUTE THE BENDING MOMENT FOR EVERY LEVEL OF AXIAL LOAD
C    (START THE AXIAL LOAD STEP LOOP)
C
     CMAX=R
     CMIN=0.
     DO 20 L=1,18
     IL=L
     DUM1=L
     PFIX=LSTP*(DUM1-1.)
C
C    START ITERATIONS TO FIND THE RIGHT POSITION OF THE NEUTRAL AXIS C
C
     DO 21 ITER=1,ITMAX
     IITER=ITER
     C=(CMAX+CMIN)/2.
C
C    COMPUTE THE SECTION CURVATURE, FIBER STRAINS AND STRESSES
C    FOR THE TRIAL POSITION OF THE NEUTRAL AXIS C
C
     CURV=0.003/(C-TS)
     ESC=CURV*C
     DO 41 I=1,2200
     ES(I)=ESC-CURV*Q(I)
     SS(I)=E*ES(I)
     IF (SS(I).LE.FY) GO TO 42
     SS(I)=FY
     GO TO 41
  42 IF (SS(I).GE.-FY) GO TO 41
     SS(I)=-FY
  41 CONTINUE
C
     A=0.65*(C-TS)+TS
     DO 43 I=1,100
     SC(I)=0.0
     SC(2201-I)=0.0
  43 CONTINUE
     DO 44 I=101,2100
     IF (Q(I).GT.A) GO TO 45
     SC(I)=0.85*FC
     GO TO 44
  45 SC(I)=0.
  44 CONTINUE
C
C    COMPUTE AND CHECK AXIAL FORCE
C
     P=0.0
     DO 51 I=1,2200
     P=P+AC(I)*SC(I)+AS(I)*SS(I)
  51 CONTINUE
     PDIF=DABS(P-PFIX)
     IF (PDIF.LE.3000.) GO TO 70
  53 IF (P.LT.PFIX) GO TO 54
     CMAX=C
     GO TO 21
```

```
  54 CMIN=C
  21 CONTINUE
     WRITE (*,1020) IL,PDIF
1020 FORMAT (2X,'CONVERGENCE NOT ACHIEVED AT LOAD STEP',I3)
     GO TO 99
C
C    COMPUTE THE BENDING MOMENT
C
  70 CMIN=C
     CMAX=CMIN+0.5*D
     PE=0.
     DO 71 I=1,2200
     PE=PE+(AC(I)*SC(I)+AS(I)*SS(I))*Z(I)
  71 CONTINUE
C
C    WRITE THE RESULTS TO THE OUTPUT FILE
C
     WRITE (7,1021) P, PE, C
1021 FORMAT (3E15.8)
     WRITE (*,1022) IL,IITER
1022 FORMAT (2X,'LOAD STEP',I3,' COMPLETE AFTER',I3,' ITERATIONS')
  20 CONTINUE
C
  99 CONTINUE
     STOP
     END
```

Appendix C

Sample Calculations

Equations for M-P Interaction Curves for Column FA1

$D = 152.4\ mm$ $\quad t = 3.4\ mm$ $\quad A_c = 16650\ mm^2$ $\quad f_c' = 89.4\ MPa$

$A_s = 1591\ mm^2$ $\quad r_c = 36.4\ mm$ $\quad r_s = 52.7\ mm$ $\quad Z_s = 75497\ mm^3$

$I_s = 4418997\ mm^4$ $\quad f_y = 330\ MPa$ $\quad E_s = 200000\ MPa$

CAN/CSA-S16.1-94 , Clause 18.6.2 (Method 2)

$E_c = 5000 \times (89.4)^{0.5} = 47276\ MPa$

Case 1 : $\quad L = 0$

$\lambda_c = 0$; $\quad \lambda_s = 0$

$\rho = 0.02 \times 25 = 0.5$; $\quad \tau = (1 + 0.5 + (0.5)^2)^{-0.5} = 0.756$

$\tau' = 1 + (25 \times (0.5)^2 \times 0.756 \times 3.4 / 152.4) \times (330 / (0.85 \times 89.4)) = 1.458$

$P_c = 0.85 \times 89.4 \times 1665 = 1267\ kN$

$P_s = 330 \times 1591 = 525\ kN$

$P_u = 1.458 \times 1267 + 0.756 \times 525 = 2244\ kN$

$\tau' P_c = 1.458 \times 1267 = 1847\ kN$; $\quad U_1 = 1.0$

$\tau P_s = 0.756 \times 515 = 397\ kN$; $\quad \tau M_0 = 0.756 \times 75497 \times 330 = 18.835\ kN\ m$

The M-P interaction curve consists of 2 lines:

$M_u = 18.835$; $\quad$ *and*

$M_u = 18.835 \times (1 - (P - 1847) / 397)$

Case 2 : $K = 0.7$; $L = 2050$ mm

$\lambda_c = (0.7 \times 2050 / (3.14 \times 36.4)) \times (89.4 / 47276)^{0.5} = 0.546$

$\lambda_s = (0.7 \times 2050 / (3.14 \times 52.7)) \times (330 / 200000)^{0.5} = 0.352$

$\rho = 0.02 \times (25 - (2050 / 152.4)) = 0.231$; $\tau = (1 + 0.231 + (0.231)^2)^{-0.5} = 0.882$

$\tau' = 1 + (25 \times (0.231)^2 \times 0.882 \times 3.4 / 152.4) \times (330 / (0.85 \times 89.4)) = 1.114$

$P_c = 0.85 \times 89.4 \times 16650 \times (0.546)^{-2} \times ((1 + 0.25 \times (0.546)^{-4})^{0.5} - 0.5 \times (0.546)^{-2}) =$

$= 1172$ kN

$P_s = 330 \times 1591 \times (1 + (0.503)^{4.48})^{-0.446} = 523$ kN

$P_u = 1.114 \times 1172 + 0.882 \times 523 = 1767$ kN

$P_e = (3.14)^2 \times 200000 \times 4418997 / (2050)^2 = 2076$ kN

$\tau' P_c = 1.114 \times 1172 = 1306$ kN ; $U_1 = 0.6 / (1 - (P - 1306) / 2076)$

$\tau P_s = 0.882 \times 523 = 461$ kN ; $\tau M_0 = 0.882 \times 75497 \times 330 = 21.974$ kN m

The M-P interaction curve consists of 2 lines:

$M_u = 21.974$; *and*

$M_u = 21.974 \times (1 - (P - 1306) / 461) \times (1 - (P - 1306) / 2076) / 0.6$

AISC LRFD 1993

$KL = 0$ $\lambda_{ms} = 0$

$f_{my} = 330 + 0.85 \times 16650 / 1591 = 1125$ MPa

$P_u = 1591 \times 1125 = 1790$ kN

$M_0 = 330 \times 75497 = 24.914$ kN m

The M-P interaction curve consists of 2 lines:

$M_u = (1 - P / 1790) \times 24.914 / 0.89$; *and*

$M_u = (1 - P / 3580) \times 24.914$

Bibliography

1. ACI Committee 318; "Building Code Requirements for Structural Concrete (ACI 318-95) and Commentary (ACI 318R-95)"; American Concrete Institute, P.O.Box 9094, Farmington Hills, MI 48333; Second Printing, February 1996

2. American Institute of Steel Construction; "Manual of Steel Construction. Load and Resistance Factor Design. Volume I. Structural Members, Specifications, and Codes"; Second Edition, 1994

3. Barber, E.; Kennedy, S.J.; Kennedy, D.J.L.; MacGregor, J.G.; "Flexural Strength of Concrete-Filled Steel Hollow Structural Sections"; Proceedings of Canadian Society for Civil Engineering Centennial Conference, Montreal, May 1987, pp. 494-509

4. Barnard, R.; "Design and Use of Pipe Piles and Caissons in Deep Foundations"; Bulletin of Armco Drainage and Metal Products, Ohio, October 1954

5. Bauer, C.J.; "New Standards for Innovative Composite Construction"; The Construction Specifier, April 1988, pp. 84-89

6. Boyd, Philip F.; Cofer, William F.; McLean, David I.; "Seismic Performance of Steel-Encased Concrete Columns under Flexural Loading"; ACI Structural Journal, May-June 1995, Vol. 92, No. 3, pp. 355-364

7. Bradford, Mark A.; Gilbert, R. Ian; "Time-Dependent Analysis and Design of Composite Columns"; Journal of Structural Engineering, December 1989, Vol. 116, No. 12, pp. 3338-3357

8. Bridge, R.Q.; Ansourian, P.; Rotter, J.M.; Pham, L.; "Australian Standard for Composite Construction"; Composite Construction in Steel and Concrete, Proceedings of Engineering Foundation Conference, New England College, Henniker, New Hampshire, June 1987, Edited by Buckner, C.D. and Veist, I.M.; ASCE, New York, 1988, pp. 71-83

9. Bridge, Russell; Webb, John; "Thin Walled Circular Concrete Filled Steel Tubular Columns"; Composite Construction in Steel and Concrete, Proceedings of Engineering Foundation Conference, Potosi, MO, USA, 1992; Published by ASCE, New York, NY, USA, pp. 634-649

10. Committee No. 30; "Stresses and Strains in Open-Deck Beam Span Bridge on Concrete-Filled Pipe Pile Piers"; Bulletin of American Railway Engineering Association, June-July 1954, No.

11. Cai, Shao-Huai; "Chinese Standard for Concrete-Filled Tube Columns"; Composite Construction in Steel and Concrete, Proceedings of Engineering Foundation Conference, Potosi, MO, USA, 1992; Published by ASCE, New York, NY, USA, pp. 142-151

12. Cai, Shao-Huai; "Ultimate Strength of Concrete-Filled Tube Columns"; Composite Construction in Steel and Concrete, Proceedings of Engineering Foundation Conference, New England College, Henniker, New Hampshire, June 1987, Edited by Buckner, C.D. and Veist, I.M.; ASCE, New York, 1988, pp. 702,-727

13. Canadian Institute of Steel Construction; "Handbook of Steel Construction"; Sixth Edition, 1995

14. Chai, Y.H.; "Seismic Behavior of Steel Jacketed Circular Bridge Columns"; Proceedings of 10th Structural Congress, April 1992, ASCE, pp. 641-644

15. Chen, Wai-Fah; Atsuta, Toshio; "Theory of Beam-Columns. Volume 1: In-Plane Behavior and Design"; McGraw-Hill Inc., 1976

16. Chen, Wai-Fah; Atsuta, Toshio; "Theory of Beam-Columns. Volume 2: Space Behavior and Design"; McGraw-Hill Inc., 1977

17. Chen, Wai-Fah; Chen, C.H.; "Analysis of Concrete-Filled Steel Tubular Beam-Columns"; Proceedings of the International Association for Bridge and Structural Engineering (IABSE), September 1973, Vol. 33-II, pp. 37-52

18. Comite Euro-International du Beton; "CEB-FIP Model Code 1990"; Thomas Telford Services Ltd., 1993

19. Elnashai, A.S.; El-Ghazouli, A.Y.; Dowling, P.J.; "International Assessment of Design Guidance for Composite Columns"; Journal of Constructional Steel Research, 1990, Vol. 15, pp. 191-213

20. European Committee for Standardization; "Eurocode 4: Design of Composite Steel and Concrete Structures. Part 1.1: General Rules and Rules for Buildings"; Draft for Development DD ENV 1994-1-1, Brussels, 1994

21. European Convention for Structural Steelwork; "Composite Structures"; The Construction Press, 1981

22. Furlong, R.W.; "Strength of Steel-Encased Concrete Beam-Columns"; ASCE Journal of the Structural Division, 1967, Vol. 93, No. ST5, pp. 113-124

23. Furlong, R.W.; "Design of Steel-Encased Concrete Beam-Columns"; ASCE Journal of the Structural Division, 1968, Vol. 94, No. ST1, pp. 267-281

24. Furlong, R.W.; "Concrete Encased Steel Columns - Design Tables"; "; ASCE Journal of the Structural Division, 1974, Vol. 100, No. ST9, pp. 1865-1883

25. Furlong, Richard W.; "AISC Column Logic Makes Sense for Composite Columns, Too"; AISC Engineering Journal, 1st Quarter 1976, Vol. 13, No. 1, pp. 1-7

26. Furlong, Richard W.; "Composite Columns - A Bridge Between AISC and ACI Regulations"; Proceedings of the International Colloquium on the Stability of Structures under Static and Dynamic Loads, Washington DC, May 1977, ASCE, pp. 709-717

27. Furlong, R.W.; "Steel-Concrete Composite Columns"; Chapter 6 of "Handbook of Composite Construction Engineering" by Sabnis,G.M. (Ed.); Litton Educational Publishing, 1979, pp. 211-229

28. Furlong, Richard W.; "Column Rules of ACI, SSLC and LRFD Compared"; ASCE Journal of Structural Engineering, October 1983, Vol. 109, No. 10, pp. 2375-2386

29. Gardner, Noel J.; "Use of Spiral Welded Steel Tubes in Pipe Columns"; ACI Journal, November 1968, Vol. 65, No. 11, pp. 937-942

30. Gardner, Noel J.; "Design of Pipe Columns"; Transactions of the Engineering Institute of Canada, EIC-70-BR & STR 4, Vol. 13, No. A-3, March 1970

31. Gardner, Noel J.; Jacobsen, E.R.; "Structural Behaviour of Concrete-Filled Steel Tubes"; ACI Journal, July 1967, Vol. 64, No. 7, pp. 404-413

32. Ghosh, R.S.; "Strengthening of Slender Hollow Steel Columns by Filling with Concrete"; Canadian Journal of Civil Engineering, June 1977, Vol. 4, No. 2, pp. 127-133

33. Godfrey, K.A., Jr.; "Concrete Strength Record Jumps 36 Percent"; Civil Engineering, October 1987, pp. 84-88

34. Gong, C.-J.; Lin, X.; Cai, S.-H.; "Application of Concrete-Filled Steel Tubular Columns in Tall Buildings in Earthquake Area"; Proceedings of the 12th Structures Congress, Atlanta, April 1994, Vol. 1, pp. 146-151

35. Hass, R.; "Recent Developments in the Fire Engineering Design of Concrete Filled Hollow Section Columns"; Tubular Structures, by Wardenier, J. and Shahi, P.E. (Ed.); Proceedings of the 4th International Symposium on Tubular Structures, Delft, 1991, pp. 294-303

36. Itani, Ahmad M.; "Future Use of Composite Steel-Concrete Columns in High-Way Bridges"; Engineering Journal, AISC, 3rd Quarter 1996, Vol. 33, No. 3, pp. 110-115

37. Iyengar, H.S.; "State-of-the-Art Report on Composite or Mixed Steel-Concrete Construction for Buildings"; ASCE, 1977

38. Iyengar, H.S.; "Recent Developments in Mixed Steel-Concrete Systems"; ASCE, Composite and Mixed Construction, Edited by C.W.Roeder, December 1984, pp. 173-184

39. Jacobson, Eugene Ronald; "An Investigation Into the Structural Behaviour of Concrete-Filled Steel Tubes"; Thesis submitted in partial fulfillment of the requirements for the degree of Master of Engineering Science, The University of Western Ontario, March 1966

40. Johnson, R.P.; "Composite Structures of Steel and Concrete. Volume 1. Beams, Columns, Frames and Applications in Building"; Constrado Monographs, 1975

41. Johnson, R.P.; Buckby, R.J.; "Composite Structures of Steel and Concrete. Volume 2. Bridges, with a Commentary on BS 5400 : Part 5"; Constrado Monographs, 1979

42. Kenny, John R.; Bruce, Donald A.; Bjorhovde, Reidar: "Removal of Yield Stress Limitation for Composite Tubular Columns"; Engineering Journal, First Quarter 1994, Vol. 31, No. 1, pp. 1-11

43. Kerensky, O.A; Dallard, N.J.; "The Four-Level Interchange between M4 and M5 Motorways at Almondsbury"; Proceedings, The Institution of Civil Engineers, July 1968, Vol. 40, pp. 295-322

44. Kitada, Toshiyuki; "Ductility and Ultimate Strength of Concrete-Filled Steel Members"; article presented in "Stability and Ductility of Steel Structures under Cyclic Loading" edited by Fukumoto, Y. and Lee, G.; CRC Press, 1992

45. Klöppel, K.; Goder, W.; "Collapse Load Tests on Concrete-Filled Steel Tubes and Establishment of a Design Formula"; Translation from German, "Traglastversuche mit ausbetonierten Stahlrohren und Aufstellung einer Bemessungsformel"; Der Stahlbau, Berlin, January 1957, Vol. 26, No. 1, pp. 1-50

46. Knowles, R.B.; Park, R.; "Strength of Concrete Filled Steel Tubular Columns"; ASCE Journal of the Structural Division, December 1969, Vol. 95, No. ST12, pp. 2565-2587

47. Knowles, R.B.; Park, R.; "Axial Load Design for Concrete Filled Steel Tubes"; ASCE Journal of the Structural Division, October 1970, Vol. 96, No. ST10, pp. 2125-2153

48. Lahlou, K.; Aïtcin, P.-C.; Chaallal, O.; "Behaviour of High-Strength Concrete Under Confined Stresses"; Cement & Concrete Composites, 1993

49. Lally Column Company; "The Lally Column Handbook"; File 13-C, New York, 1962

50. Lohr, W.; "Concrete Columns Encased in Steel Shells Proposed"; Engineering News Record, December 1934

51. Lu, Yue Qing; Kennedy, D.J. Laurie; "The Flexural Behavior of Concrete-Filled Hollow Structural Sections"; Canadian Journal of Structural Engineering, 1994, Vol. 21, pp. 111-130

52. Magnusson, J.D.; Gouwerok, A.A.; Tschanz, T.; "Experience in the Design of Composite Buildings"; Proceedings of 10th Structural Congress, April 1992, ASCE, pp. 832-835

53. Mason, F.B.; "Concrete-Filled Steel Tube Bents"; Engineering News Record, March 1950

54. Matsui, C.; Tsuda, K.; Ishibashi, Y.; "Slender Concrete Filled Steel Tubular Columns under Combined Compression and Bending"; from "Structural Steel", by Shanmugam, N.E and Choo, Y.S. (ed.); Proceedings of 4th Pacific Structural Steel Conference (PSSC-95); October 1995, Vol.3, pp. 29-36

55. Narayanan, R.(editor); "Steel-Concrete Composite Structures"; Stability and Strength Series, Vol. 7, Elsevier Applied Science, New York, 1988

56. Neogi, P.K.; Sen, H.K.; Chapman, J.C.; "Concrete-Filled Tubular Steel Columns under Eccentric Loading"; Structural Engineer, May 1969, Vol. 47, No. 5, pp. 187-195

57. Orito, Y.; Sato, T.; Tanaka, N.; Watanabe, Y.; "Study on the Unbonded Steel Tube Concrete Structure"; Composite Construction in Steel and Concrete, by Buckner, D.C. and Viest,I.M. (Ed.); Proceedings of Engineering Foundation Conference, Henniker, New Hampshire, June 1987, ASCE, 1988, pp. 786-804

58. O'Shea, M.D.; Bridge, R.Q.; "Circular Thin Walled Concrete Filled Steel Tubes"; "Slender Concrete Filled Steel Tubular Columns under Combined Compression and Bending"; from "Structural Steel", by Shanmugam, N.E and Choo, Y.S. (ed.); Proceedings of 4th Pacific Structural Steel Conference (PSSC-95); October 1995, Vol. 3, pp. 29-36

59. Park, R.J.T.; Priestley, M.J.N.; Walpole, W.R.; "The Seismic Performance of Steel Encased Reinforced Concrete Bridge Piles"; Bulletin of the New Zealand National Society for Earthquake Engineering; June 1983, Vol. 16, No.2, pp. 123-140

60. Park, R.J.T.; Priestley, M.J.N.; Berril, J.B.; "The Seismic Performance of Steel-Encased Reinforced Concrete Bridge Piles"; Proceedings of Pacific Conference on Earthquake Engineering, New Zealand, August 1987, Vol. 2, pp. 23-34

61. Priestley, M.J.N.; Park, R.; "Strength and Ductility of Concrete Bridge Columns under Seismic Loading"; ACI Structural Journal, January-February 1987, Vol. 84, No. 1, pp. 61-76

62. Priestley, M.J.N.; Seible, F.; Xiao, Y.; Verma, R.; "Steel Jacket Retrofitting of Reinforced Concrete Bridge Columns for Enhanced Shear Strength. Part 1: Theoretical Considerations and Test Design"; ACI Structural Journal; July-August 1994, Vol. 91, No. 4, pp. 394-405

63. Prion, Helmut G.L.; Boehme, Jens; "Beam-Column Behavior of Steel Tubes Filled with High Strength Concrete"; Canadian Journal of Civil Engineering, April 1994, Vol. 21, No. 2, pp. 207-218

64. Ralston, M; Korman, R.; "Put That in Your Pipe and Cure It"; Engineering News Record, February 16, 1989, pp. 44-531

65. Randall, V.; Foot, K.; "High-Strength Concrete for Pacific First Center"; Concrete International, April 1989, Vol. 11, No. 1, pp. 14-16

66. Rangan, B.V.; "Design of Slender Hollow Steel Columns Filled with Concrete"; ICSAS-91, Proceedings of International Conference on Steel and Aluminium Structures, Singapore, May 1991, pp. 104-112

67. Rangan, B.V.; Joyce, M.; "Strength of Eccentrically Loaded Slender Steel Tubular Columns Filled with High-Strength Concrete"; ACI Structural Journal, November-December 1992, Vol. 89, No. 6, pp. 676-681

68. Richart, F.E.; Brandtzaeg, A.; Brown, R.L.; "A Study of the Failure of Concrete under Combined Compressive Stresses"; University of Illinois, Engineering Experimental Station, Bulletin No. 185, 1928

69. Richart, F.E.; Brandtzaeg, A.; Brown, R.L.; "The Failure of Plain and Spirally Reinforced Concrete in Compression"; University of Illinois, Engineering Experimental Station, Bulletin No. 190, 1929

70. Roik, K.; Bergmann, R.; "Composite Columns - Design and examples for Construction"; "Composite and Mixed Construction", by Roeder, C.W. (Ed.); Proceedings of US/Japan Joint Seminar, Seattle, July 1984, ASCE, 1985, pp. 267-278

71. Roik, K.; Bergmann, R.; "Composite Columns"; Chapter 4.2 of "Constructional Steel Design. An International Guide"; Dowling, Patrick J.; Harding, John E.; Bjorhovde, Reidar (ed.); Elsevier Science Publishers Ltd., 1992, pp. 443-469

72. Russell, W.A.; "Structural Properties of Light Gage Tubular Columns"; Paper No. 21; Housing and Home Finance Agency, Division of Housing Research, Washington D.C., October 1953

73. Saatcioglu, Murat; Razvi, Salim R.; "Strength and Ductility of Confined Concrete"; Journal of Structural Engineering, June 1992, Vol. 118, No. 6, pp. 1590-1607

74. Salani, H.J.; Sims, J.R.; "Behavior of Mortar-Filled Steel Tubes in Compression"; ACI Journal, October 1964, Vol. 61, No. 10, pp. 1271-1283

75. Sewell, J.S.; "Columns for Buildings"; Engineering News, October 1902, Vol. 48, No. 17

76. Shakir-Khalil, H.; "Bond Strength in Concrete-Filled Steel Hollow Sections"; ICSAS 91, International Conference on Steel & Aluminium Structures, Vol. 3, Composite Steel Structures, Singapore, May 1991, pp. 157-168

77. Shakir-Khalil, H.; "Push-Out Tests on Concrete-Filled Steel Hollow Sections"; International Symposium on Tubular Structures, Delft, The Netherlands, June 1991

78. Shakir-Khalil, H.; "Resistance of Concrete-Filled Steel Tubes to Pushout Forces"; Structural Engineer, July 6, 1993, Vol. 71, No. 13, pp. 234-243

79. Shakir-Khalil, H.; "Pushout Strength of Concrete-Filled Steel Hollow Sections"; Structural Engineer, July 6, 1993, Vol. 71, No. 13, pp. 230-233

80. Shakir-Khalil, H.; Boufennara, K.; "Columns of Concrete-Filled Concentric Steel Shells"; Structural Engineering Review, 1990, No. 2, pp. 31-44

81. Shakir-Khalil, H.; Illouli, S.; "Columns of Composite Cylindrical Shells"; Structural Engineering Review, 1988, No. 1., pp. 113-118

82. Shan-Tong, Zhong; Sumei, Zhang; "A New Method from China to Determine Load-Carrying Capacity for CFST Members"; Composite Construction in Steel and Concrete, Proceedings of Engineering Foundation Conference, Potosi, MO, USA, 1992; Published by ASCE, New

York, NY, USA, pp. 499-511

83. Shan-Tong, Zhong; Ruo-Yu, Miao; "Stress-Strain Relationship and Strength of Concrete Filled Tubes"; Composite Construction in Steel and Concrete, by Buckner, D.C. and Viest,I.M. (Ed.); Proceedings of Engineering Foundation Conference, Henniker, New Hampshire, June 1987, ASCE, 1988, pp. 773-785

84. Sherman, D.R.; "Inelastic Flexural Buckling of Cylinders"; Part 18 of "Steel Structures : Recent Research Advances and Their Approaches to Design" edited by Pavlovic, M.N.; Elsevier Applied Science Publishers, London, 1986, pp. 339-357

85. Sherman, D.R.; "Tubular Members"; Chapter 2.4 of "Constructional Steel Design. An International Guide"; Dowling, Patrick J.; Harding, John E.; Bjorhovde, Reidar (ed.); Elsevier Science Publishers Ltd., 1992, pp. 91-104

86. Stelco Inc.; "Hollow Structural Sections. Design Manual for Concrete-Filled HSS Columns"; Cidect Monograph #5, Canadian Edition, January 1981

87. Structural Stability Research Council; "Guide to Stability Design Criteria for Metal Structures"; 4th Edition, John Wiley, New York, 1988

88. Sugano, S; Nagashima, T.; "Seismic Behavior of Concrete Filled Tubular Steel Columns"; Proceedings of the 10th Structural Congress, April 1992, ASCE, pp. 914-917

89. Swain, F.W.; Holmes, A.F.; "An Investigation of the Strength and Elastic Properties of Concrete-Filled Pipe Columns"; Proceedings of the American Society for Testing and Materials, 1915

90. Task Group 20, Structural Stability Research Council; "A Specification for the Design of Steel-Concrete Composite Columns"; AISC Engineering Journal, 4th Quarter 1979, Vol. 16, No. 4, pp. 101-115

91. Tomii, M.; Yoshimura, K.; Morishita, Y.; "Experimental Studies on Concrete-Filled Steel Tubular Stub-Columns under Concentric Loading"; Proceedings of the International Colloquium on the Stability of Structures under Static and Dynamic Loads, Washington DC, May 1977, ASCE, pp. 718-741

92. Tomii, M.; Sakino, K.; Xiao, Y.; "Ultimate Moment of Reinforced Concrete Short Columns Confined in Steel Tube"; Proceedings of Pacific Conference on Earthquake Engineering, New Zealand, August 1987, Vol. 2, pp. 11-22

93. Uy, Brian; Patil, Sachin B.; "Concrete-Filled High Strength Steel Box Columns for Tall Buildings: Behavior and Design"; Structural Design of Tall Buildings, June 1996, Vol. 5, No. 2, pp. 75-94

94. Virdi, K.S.; Dowling, P.J.; "Bond Strength in Concrete Filled Steel Tubes"; IABSE Periodica 3/1980, International Association for Bridge and Structural Engineering, August 1980, Proceedings, P-33/80, pp. 125-139

95. Vögeli, R.; "New Transmission Lines with Concrete Filled Steel Tube Towers"; Proceedings of the International Conference on Large Electric Systems, June-July 1950, Vol. 2, Report No. 223

96. Vögeli, R.; "Steel Tube Pylons Filled with Concrete"; Proceedings of the International Conference on Large Electric Systems, 1948, Vol. 2, Report No. 220

97. Wakabayashi, M.; "A Historical Study of Research on Composite Construction in Japan"; Proceeding of the Conference on the Composite Construction in Steel and Concrete, 1991, ASCE, New York, pp. 400-427

98. Wakabayashi, M.; "A New Design Method of Long Composite Beam-Columns"; Proceedings of International Colloquium on Stability of Structures under Static and Dynamic Loads, Washington DC, May 1977, ASCE, pp. 742-756

99. Wakabayashi, M.; "Japanese Standards for the Design of Composite Buildings"; Composite Construction in Steel and Concrete, by Buckner, D.C. and Viest, I.M.; Proceedings of Engineering Foundation Conference, Henniker, New Hampshire, June 1987, ASCE, 1988, pp. 53-70

100. Yoshioka, Y.; "State of Art of Composite Steel Tube and Concrete Structures in Japan"; Proceeding of US-Japan Work Shop on Composite and Hybrid Structures. September 10-12. 1992, Berkeley, California, pp. 119-130

IMAGE EVALUATION TEST TARGET (QA-3)

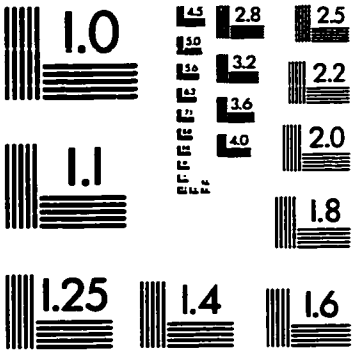

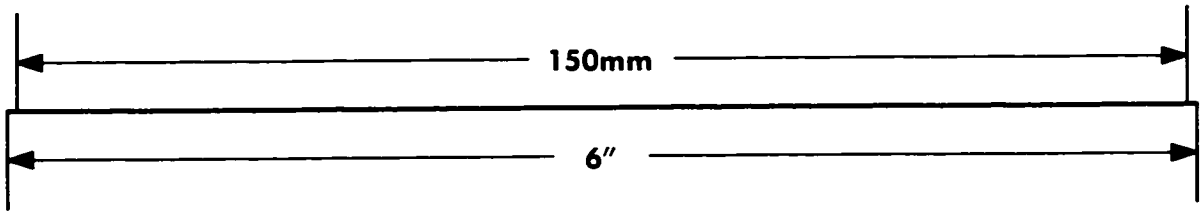

APPLIED IMAGE, Inc
1653 East Main Street
Rochester, NY 14609 USA
Phone: 716/482-0300
Fax: 716/288-5989